Numerical Weather Prediction over Antarctica

Neil Adams BSc, Dip Met., Dip Ed., MSc

Submitted in fulfillment of the requirements

for the degree of

Doctor of Philosophy

University of Tasmania

22nd April 2004

Declaration of originality

I certify that this thesis does not incorporate without acknowledgment any material previously submitted for a degree or diploma in any university; and that to the best of my knowledge and belief it does not contain any material previously published or written by another person except where due reference is made in the text.

Neil Adams.

Statement of authority of access

This thesis may be made available for loan and limited copying in accordance with the *Copyright Act 1968*.

Neil Adams

Abstract

Operations in Antarctica are very much at the mercy of the weather. From early explorations using skis and dogs sleds, through to modern large scale operations involving shipping, tractor trains, helicopters and large fixed wing aircraft, operating from modern facilities, all have been sidelined when the Antarctic atmosphere has become hostile. Since the earliest days of exploration, weather in Antarctica has been a critical issue in operations, and a focus of observational research. However, in comparison to mid and low latitude regions of the globe our knowledge of high southern latitude meteorology remains relatively poor. The dearth of conventional surface and upper air observations has limited observational studies and numerical modelling over the Antarctic region has not seen the same level of focus as modelling work over the more highly populated areas of the globe. Increasingly, operations are becoming more costly with the introduction of sophisticated scientific instrumentation and the use of larger aircraft, so timely and accurate forecasts are becoming more important. In order to decrease the time spent at sea by scientific and operational staff on crossing the Southern Ocean, the Australian Government has been studying the viability of operating an inter-continental air link between Australia and the Australian bases in East Antarctica. Such an operation is critically dependent on accurate medium to short term weather forecasts, both for on route weather, and most importantly for terminal area weather in Antarctica. Traditionally, only global numerical model output has been available to assist the forecaster in preparing the aviation forecasts. However, the temporal and spatial resolution of these models have been relatively poor, given only limited

support to forecasting operations.

The focus of this thesis was an analysis of the feasibility of employing a limited area grid point numerical model to operational weather forecasting in East Antarctica and the surrounding Southern Ocean, and using the model to investigate the dynamics associated with critical weather events experienced at Australian stations in East Antarctica.

Acknowledgments

Many people have helped me during this study and I wish to sincerely thank them all. Professor Bill Budd of the Antarctic CRC and Institute of Antarctic and Southern Ocean Studies at the University of Tasmania provided excellent guidance and encouragement throughout the lengthy study period. Dr. Kamal Puri of the Australian Bureau of Meteorology Research Centre for invaluable assistance in coming to grips with the LAPS model dynamics and physics, and Dr. Graham Mills of the Australian Bureau of Meteorology Research Centre for assistance in understanding the analysis and assimilation processes used in the model. I would also like to thank the Australian Antarctic Division Data Centre for access to meteorological data from the Aurora Australis cruises and to the digital map library for the detailed Antarctic maps used in this thesis. Dr. Jordan Powers, Dr. Kevin Manning and Dr. Michael Duda of the Meso-scale and Micro-scale Meteorology group at the NCAR Foothills Laboratory in Boulder Colorado, for their assistance in understanding some of the AMPS output, and for providing AMPS forecast output used for comparisons in this thesis.

Without the support of Hugh Hutchinson in his capacity as Regional Director of the Tasmania/Antarctic Regional Office this study would not have been possible. I would also like to thank Steve Pendlebury of the Tasmanian/Antarctic Regional Office for his valuable insights into Antarctic weather and weather forecasting.

Contents

List of Figures

1 Introduction

Meteorologists have been accompanying explorers and expeditioners to Antarctica since the inception of the Australian National Antarctic Research Expeditions (ANARE) in 1947. Weather forecasting has been of primary concern for all people venturing out into the Antarctic environment. The harsh conditions make working outdoors a chore at the best of times and impossible when the weather deteriorates into the cold and windy conditions that are all too often a part of Antarctic life. For many years single station forecasting techniques have had to be employed, with the forecaster relying on sketchy local knowledge from previous expeditions and "rules-of-thumb" forecast techniques using local surface and upper air observations. These forecasts were, at best, only good out to 24 hours and often provided little more than limited guidance out to a couple of hours. With the advent of global numerical models, and reasonable communications into Antarctica, it became possible to provide the Antarctic forecaster with basic meteorological fields upon which to prepare forecasts. The global forecasts, and availability of meteorological fields from the models, has gradually improved over the years (Adams 1997), yet the relatively poor model resolutions have proved a hindrance in forecasting many of the orographically induced weather phenomena that occur on the mesoscale, and generate adverse local weather.

The need for improved local area, or meso-scale, forecasting in the 12 to 48 hour time-frame over East Antarctica, and the surrounding Southern Ocean, has partially arisen out of the proposal to begin long range intercontinental flying between Hobart, in Tasmania, and Casey Station in East Antarctica, and provide fixed-wing commuter flights between the Australian

continental stations. With the potentially hazardous flying conditions around the Antarctic coast, such flights are weather critical, and access to accurate and timely weather forecasts essential. The inadequacies of the currently available global models surfaced some years ago when trying to support field operations and long range intra-continental helicopter flying in East Antarctica. Weather forecasters were having mixed results in trying to infer likely adverse weather from the broad-scale features depicted in the global model fields. The application of a high resolution, limited area model over the Antarctic domain has the potential to dramatically improve both the quality of short-term local area forecasts, and our understanding of the dynamics governing meso-scale weather phenomena in the Antarctic environment. The Australian Bureau of Meteorology has had the Limited Area Prediction System (LAPS) under development for some years, and running operationally in the Australian region since July 1996, and this model was chosen to assist in the Antarctic study because of it's proven operational performance, it's ability to employ full data assimilation and the fact that it was globally relocatable and able to run over the Antarctic coastal fringe where the majority of Australian operations occur. The model is not suited to very high latitude use because of the singularity in a latitude-longitude grid at the South Pole, but as will be seen in the following chapters, placing the model southern boundary at 80^{o}S provided a domain in which the model output provided useful forecast guidance for Antarctic stations around the coastal fringe between 65^{o}S and 70^{o}S, and over the Southern Ocean. The following thesis expands on the problems associated with Antarctic forecasting, describes the high resolution model employed, including modifications made to better

adapt the physics to the Antarctic environment and presents verification of the model performance through skill indicators, sensitivity studies and several case studies. The thesis not only advances the applicability of the high resolution limited area model to Antarctic weather forecasting, but provides a framework for applying both limited area, and global Numerical Weather Prediction (NWP) systems, along with surface and upper air observations to the Antarctic weather forecasting problem.

Since beginning the research into Antarctic weather forecasting using high resolution NWP systems in 1996, the National Science Foundation (NSF) of the United States of America (USA) has begun sponsoring a research program into improving the forecasting support available to weather forecasters stationed at the American base of McMurdo, who are tasked with the provision of forecasts for McMurdo and South Pole stations, and for the flights between the McMurdo and the Italian Base at Terra Nova Bay, and for the inter-continental flights from New Zealand to McMurdo. The research has been in the form of a collaborative effort between the Ohio State University and the National Center for Atmospheric Research (NCAR), with the development of the Antarctic Mesoscale Prediction System (AMPS), which is a polar version of the Penn State University (PSU)-NCAR version 5 Mesoscale Model (MM5). AMPS researchers, such as Bromwich et al. (2001) and Cassano et al. (2001) identified problems facing NWP development over Antarctica where model physics developed for mid-latitude applications where not necessarily appropriate at higher latitudes. AMPS has been run operationally at NCAR, in Boulder Colorado, in support of summer operations, starting with the 2000-01 summer season. A description of the model, with a case

study from the first field season can be found in Bromwich et. al. (2003) and Powers et al. (2003), with a further evaluation of the model described in Guo et. al. (2003). The AMPS system, along with the United States Air Force Weather Agency (AFWA) limited area Antarctic system, are currently the only other real-time operational limited area NWP systems being employed over Antarctica with AMPS providing a unique source of comparative information upon which to assess the ALAPS output.

1.1 Antarctic weather

Several landmark studies and volumes have been published over the last 50 years attempting to define the weather and climate of Antarctica. The International Geophysical Year (IGY) of 1957-58 saw significant advances in the collection of *in situ* Antarctic data (King and Turner 1997), and provided a data-set that contributed greatly to furthering the understanding of Antarctic weather, forming the basis of many published studies on the meteorology of Antarctica. Climatological studies such as those by Taljaard and van Loon (1964) and Taljaard (1967) based on the IGY data still provide a useful reference to high southern latitude meteorology. Schwerdtfeger (1984) attempted to provide an up-to-date description of and understanding of Antarctic weather systems based on surface and upper air observations taken throughout Antarctica over the preceding decades and King and Turner (1997) provide an excellent overview of Antarctic weather based on both *in situ* observations from the previous 50 years and employing the relatively new fields of remote sensing and numerical modelling. The following descriptions of broad-scale flow, the katabatic regime and mesoscale phenomena draw

heavily on the work of the authors mentioned above.

1.1.1 Broad-scale flow

Antarctica is the highest, driest and windiest continent on the planet. The plateau rises from a steep coastal escarpment and then with a gentle slope to heights in excess of 4000m in the interior (Figure 1.1). The continent is

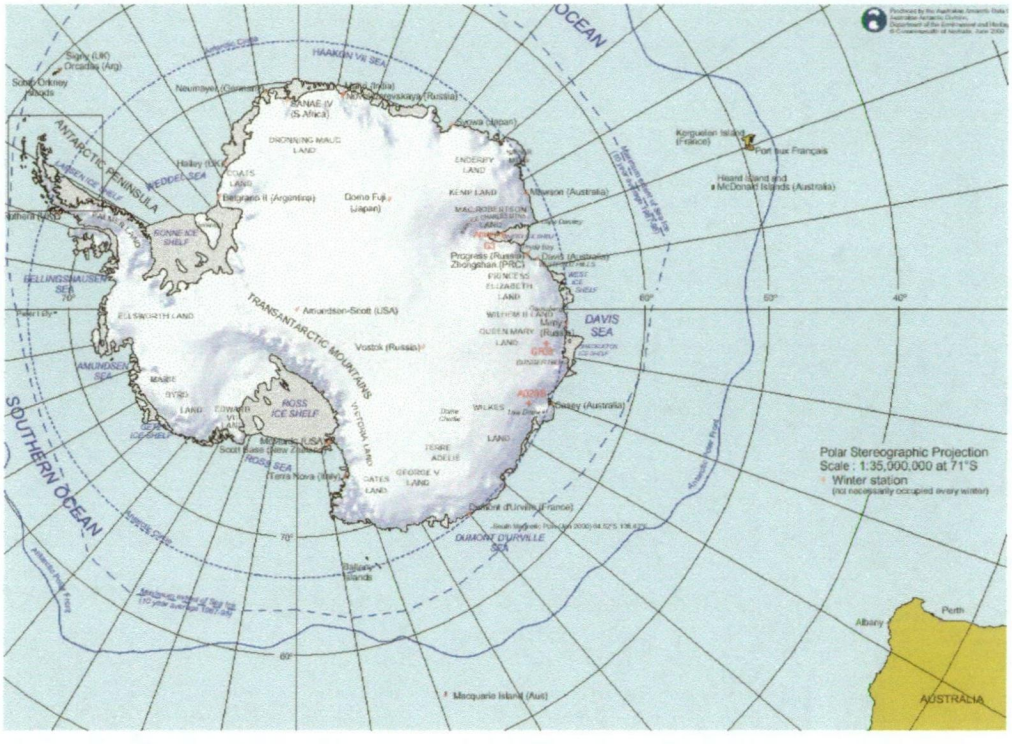

Figure 1.1: Map of Antarctica and the Southern Ocean, showing Australian Antarctic stations and orographic relief.

predominantly ice covered with less than 3% being exposed rock, and with the ice dome reaching depths of over 4000m inland, and holding over 70% of the worlds fresh water. Being located in the high southern latitudes, Antarctica receives significantly less radiation than the extra-polar regions and the high albedo of the predominantly ice and snow covered surface results in a significant portion of the already reduced incoming solar radiation being

reflected back into space. The continual radiative cooling of the surface that is observed over the continent, and is strongest inland and during winter, is only partially balanced by turbulent flux of heat from the atmosphere downwards through the planetary boundary layer, giving rise to cooling of the boundary layer relative to the free atmosphere. The strong surface inversions that arise are a significant meteorological phenomena of Antarctica. The existence of a thin cold and stable air-mass over the sloping terrain of the continent gives rise to a density current and the formation of what is known as katabatic flow. Ball (1960) provided one of the earliest theoretical studies of the Antarctic katabatic flow which will be discussed in more detail below. The katabatic plays a significant role in forcing the large scale flow of the high southern latitudes as the low level flow over Antarctic is dominated by this density current, resulting in broad-scale low level out-flow from the continent. With the long length and time scales a balance is set up between the katabatic forcing, Coriolis and surface friction resulting in a turning of the out-flow to the left and the setting up of an anti-cyclonic low level vortex. The predominantly easterly wind that results from this balance between the density current and Coriolis is often known as an inversion wind.

The radiation balance is such that over most of the year the surface of Antarctica is cooling, with the radiative cooling rates not balanced by the surface energy exchanges (King and Turner 1997). The maintenance of an energy balance then must be through atmospheric transport of heat from the mid-latitudes. This transport can also be seen in the conservation of mass. As the surface cools air is transported off the continent and out to the coast through the katabatic forcing; subsidence of air over the high

plateau results. In response to the subsiding air in the middle troposphere convergence results and a cyclonic vortex is established. In reality the three dimensional flow is somewhat more complicated than this simplified model, as Egger (1985) noted. The generation of mid level cyclonic vorticity will continue to grow with the maintenance of steady low level divergence in the katabatic flow. However, as the cyclonic vorticity increases the low pressure in the centre of the vortex would continue to deepen and act to oppose, and eventually stifle, the katabatic out-flow. Modelling studies by Egger (1992) showed that the excess cyclonic vorticity could be removed through the interaction with mid latitude cyclones. It has been known for some time that mid-latitude systems have a preponderance of tracking into the Antarctic coast and decaying (Jones et al. 1993), with a number of preferred areas of cyclolysis. From the modelling studies Egger (1992) showed that as these mid-latitude cyclones were modified by the sloping terrain of Antarctica they were able to remove progressively more cyclonic vorticity from the upper vortex, weakening the westerly flow and permitting the maintenance of a katabatic flow in reasonable agreement with that observed.

1.1.2 Katabatic regime

As mentioned above the low level katabatic flow dominates the circulation in Antarctica and can also significantly impact, on a day to day basis, the local weather. However, despite the katabatic out-flow driving the low level arm of the broad-scale circulation of the high southern latitudes, there is remarkable variability displayed in the katabatic observed around the Antarctic coast, both in the temporal and spatial sense. Coastal stations such as Casey (Fig-

ure 1.1), in East Antarctica, display only a light katabatic signature, yet Mawson (Figure 1.1) displays a very strong and persistent katabatic signal. Yet even Mawson can have extended periods of time were little or no katabatic is evident. Despite the katabatic being a dominant component of the broad-scale Antarctic climate, at the scales of local weather forecasting it can pose real problems to the meteorologist. During the summer months where the persistence of the katabatic sometimes fails, forecasting the onset and cessation of the strong wind is problematic, yet a high priority for aviation forecasting. Much work has been done on describing the katabatic with the study by Ball (1960) frequently cited in Antarctic literature, the considerable efforts of Parish and Bromwich (1987), and several observational studies including Bromwich (1989), Bromwich et al. (1996, 1997) and Gallee et al. (1998). The dynamics of the katabatic forcing have also been investigated through the application of modelling studies with good agreement being found between the model-defined surface flow and that defined from observational studies. Modelling studies by Parish (1984) over Adelie Land (Figure 1.1), revealed significant channeling of the surface flow, highlighting the importance of the continental topography in shaping of the coastal katabatic flow. Parish (1992, 1994) also extensively modelled the katabatic flow to highlight it's importance in defining the meridional circulation in the high southern latitudes. Modelling studies have also been undertaken to better understand the dynamics of localised katabatic flows with Murphy and Simmonds (1993) studying strong wind in the Casey area, Liu and Bromwich (1997) studying the Siple Coast katabatic, Gallee and Pettre (1998) the Adelie Land katabatic and Dare and Budd (2001) the katabatic flow at Mawson Station. In

all these studies the models performed well in defining the surface flow.

1.1.3 Mesoscale meteorology

With the introduction of advanced very high resolution radiometry (AVHRR) aboard polar orbiting satellites such as the NOAA series of craft remarkably detailed images of the polar trough and coastal regions of Antarctica (eg. Figure 1.2) have been possible. From these images it has been possible to

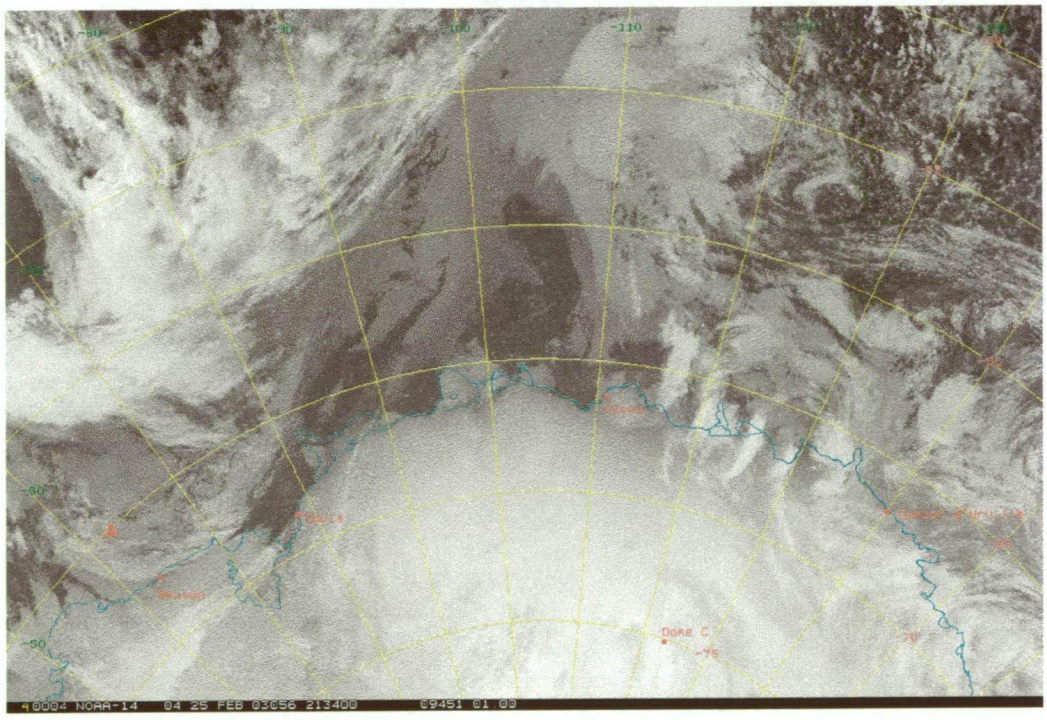

Figure 1.2: AVHRR band-4, infra-red mosaic covering East Antarctica and the Australian Antarctic stations, valid 2134UTC 25 February 2003.

identify small scale cloud features that can have a strong impact on the local weather, such as the mesoscale low, and the associated cloud band, to the northwest of Mawson in Figure 1.2. These features range from well formed vortices in the low level cloud formations to amorphous clumps of cloud that appear to have no discernible structure and are often missed entirely

by the coarse observational network and have life times that on occasions mean their development was missed even between the morning and afternoon passes of the polar orbiting satellites. This situation often leads, not only to the non-forecast of adverse weather, but often to the situation where the forecaster was entirely unaware of how the system developed and where it came from. Complete forecast failure due to meso or micro-scale weather system development has been a common occurrence around the Antarctic coastal environment and several factors need to be addressed to alleviate the problem. The first is the introduction of meso-scale observational networks around the Antarctic stations and the second is adequate meso-scale numerical modelling to attempt to better define and capture these systems. The introduction of meso-scale networks in Antarctica is logistically difficult and expensive. However, the proposed long range inter-continental flights between Hobart in Tasmania and Casey in East Antarctica has provided the impetus for the re-introduction of a meso-scale network in the Casey area, with 4 new automatic weather stations (AWS) already installed around Casey, and with another 2 to be installed within the next 12 months, bringing the number of observing sites within 120 km of Casey to 8 units. These sites have been chosen to assist in the real-time identification of meso-scale events that may lead to adverse weather conditions affecting the new runway site to the southeast of Casey. The glaciology group within the Cooperative Research Centre (CRC) for Antarctic and Southern Ocean Studies at the University of Tasmania has established a significant number of AWS's around East Antarctica for the support of the glaciological program and a number of these AWS's are located around the Lambert Basin from which a climatology

has been established (Allison et al. 1993). Although the AWS's only provide wind measurements up to 4m, rather than the standard 10m measurement expected under the World Meteorological Organisation (WMO) guidelines, they do provide an excellent source of meso-scale data. This network, and the new Casey network, will provide valuable meso-scale data from which to verify the accuracy and usefulness of the high resolution grid point NWP model under study and if the model proves successful, and becomes operational, these data will also provide extremely useful data for inclusion in the high resolution analysis system.

1.1.4 Australian stations

Australia maintains three stations on the Antarctic continent (Figure 1.1), at Mawson (67.6°S, 62.87°E), Davis (68.58°S, 77.97°E) and Casey (66.28°S, 110.54°E) and one station on Macquarie Island in the sub-Antarctic (54.5°S, 158.95°E). Each of these stations has a unique climatology defined by the local topography and latitude.

Mawson is a coastal station sitting on the edge of a very steep coastal escarpment (Figure 1.3) with the plateau rising southward to a height in excess of 3500 m. The Lambert Basin lies some 200 km to the east, with the Napier Mountains of Enderby Land 400 km to the west. It would be fair to say that Mawson's weather is dominated by a southeasterly katabatic out-flow from the high interior evidenced in the wind roses (Figure 1.4) taken from the aviation climatology of Australian Antarctic stations (Shepherd 1999), where the persistent southeasterly flow is pronounced. It is also apparent that Mawson experiences enhanced storm-force southeasterly wind, associ-

Figure 1.3: Topographic map of the Lambert Basin, including Davis and Mawson stations.

ated with the passage of polar cyclones to the north of the station. Mawson is the windiest of the three continental stations and the coldest. However, the cold out-flow regime results in Mawson also being the clearest with the lowest occurrences of low cloud and white-out conditions.

Davis station lies in the Vestfold Hills to the northeast of the Lambert Basin (Figure 1.3). The gentle sloping terrain results in Davis being the least windy of the three stations with the wind predominantly from the northeast and less than 15 knots. In general Davis is a sunny location with a low percentage of adverse weather conditions (Shepherd 1999). There appears to be little enhancement of cyclonic wind with the passage of lows, and the main forecasting difficulties experienced at Davis result when meso-scale cyclonic vorticies form in Prydz Bay (Figure 1.3) and move over the station causing

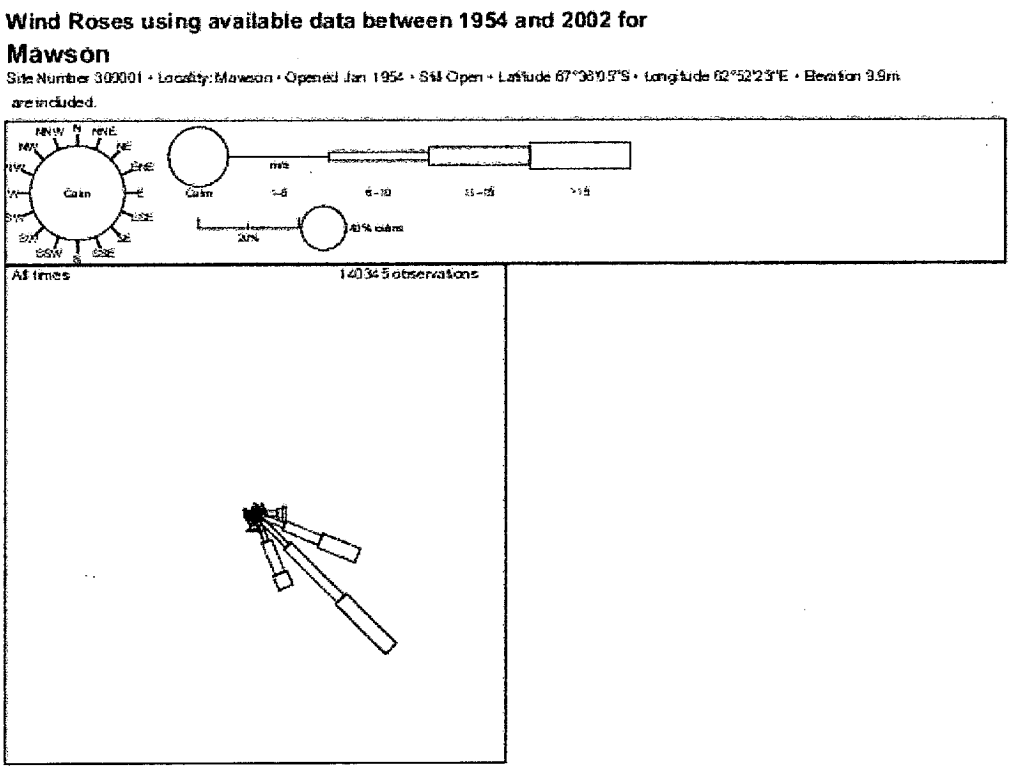

Figure 1.4: Wind-rose for Mawson station, based on data from 1954 until 2002.

a deterioration in the weather in the form of low cloud and reduced visibility with snow. Inland of Davis, close to the plateau escarpment, at Platcha (a temporary meteorological instrument site) much stronger wind is often observed and reports of hydraulic jumps moving across the area have been documented (Ball 1960). On rare occasions these jumps have been observed moving westward and over Davis station (Targett 1998).

Casey is a coastal station lying on the western side and in the lee of Law Dome, a regularly shaped dome rising to near 1395 m some 120 km to the east southeast of Casey (Figure 1.5). In general Casey does not experience

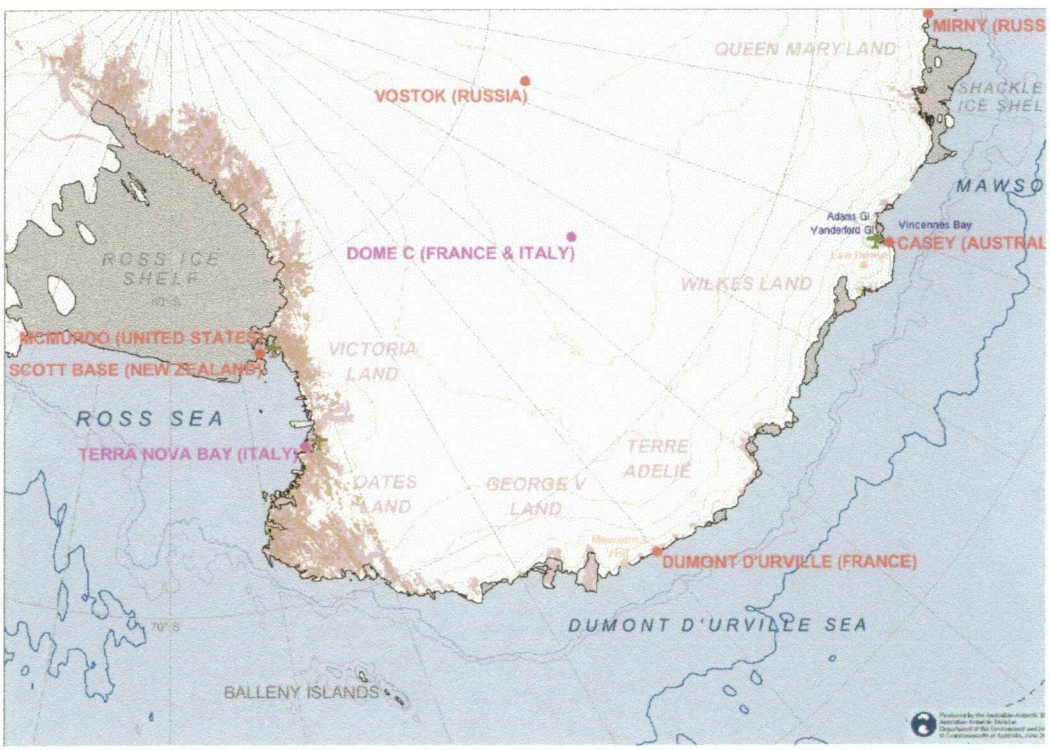

Figure 1.5: Wilkes Land, including Casey Station and Dome C.

a strong katabatic flow although a light (less than 15 knots) southerly wind from the glaciers to the south may be persistent during the autumn and winter months (Shepherd 1999) as evident in the wind roses (Figure 1.6),

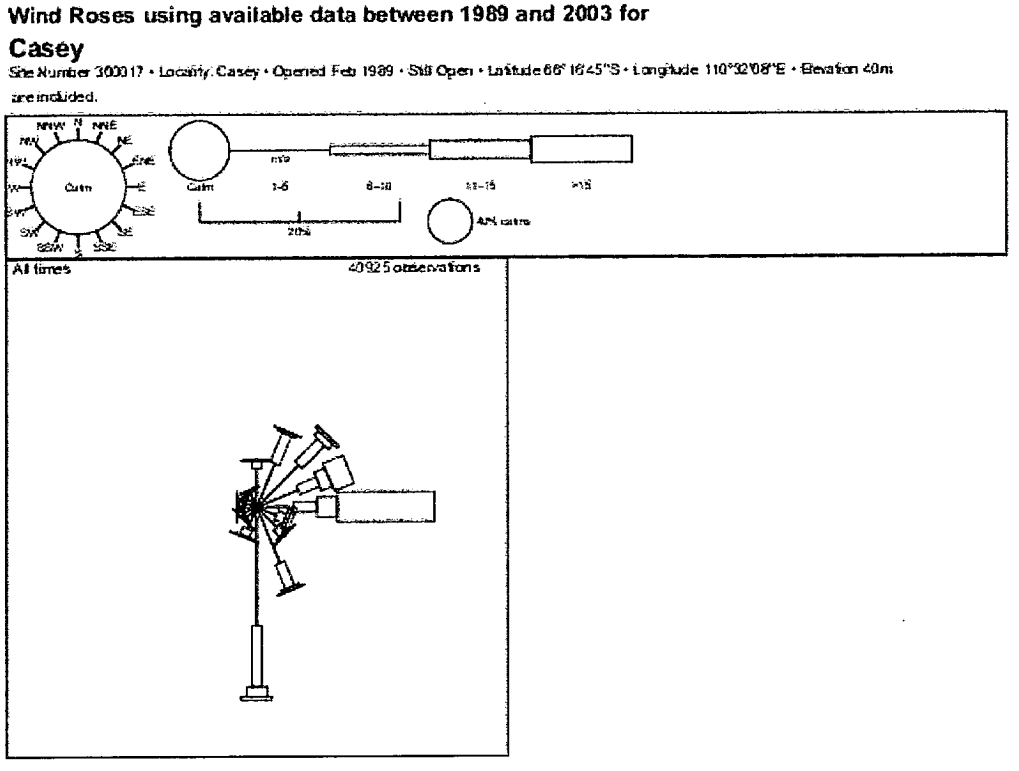

Figure 1.6: Wind-rose for Casey, based on data from 1989 to 2003.

as is the northeasterly flow turning off Law Dome. The dominant adverse weather conditions at Casey are the storm to hurricane strength easterlies that regularly affect the station during the autumn, winter and spring months and to a lesser extent during summer. The severity of these storms has been the focus of both modelling and observational studies from as early as Wilson (1992) through Murphy et al. (1993), Adams (1996) and most recently Turner et al. (2001) and Murphy (2003). What has been poorly understood is why cyclonic systems off-shore with gradient winds of around 40 to 50 knots often result in a mean surface wind in the Casey area averaging in excess of 70 knots with gusts recorded over 130 knots. The role Law Dome plays in controlling the local Casey weather is not limited to strong wind events, as it would seem that the eddy in the low level wind that forms around Law Dome also leads to Casey being the cloudiest of the three continental stations and most prone to poor visibility and white-out conditions (Shepherd 1999).

Macquarie Island lies in the prevailing westerly stream near 54.5^{o}S, 159^{o}E (Figure 1.1), and is oriented almost north-south. The island is about 30 km long, with a width around 3 km and rises to an average height of near 300 m. It is situated just to the north of the Antarctic Convergence, where cold northward moving Antarctic surface water has sunk below the warm sub-Antarctic surface water. The climate is dominated by moist westerly flow under a procession of cold fronts. Snowfall is common during the winter months but since the island is relatively low, and north of the convergence, snow tends not to persist for very long. Adverse weather at the island tends to be associated with very active cold fronts where gale force westerly wind

batters the island. However, operations at the island, particularly helicopter flying, may also be adversely affected when the air-stream is from the north-east, under the influence of a blocking high that is a common feature of the Tasman Sea region (Pook 1995) and results in the advection of relatively warm and moist air off the Tasman Sea over the island.

1.1.5 Weather forecasting

The number of surface and upper air observational sites over the Antarctic continent and surrounding Southern Ocean is very low when compared to the observational networks in place through the mid and low latitudes, and in particular those networks currently in place in the northern hemisphere. Figure 1.7 33 shows the surface and upper air observations that were avail-

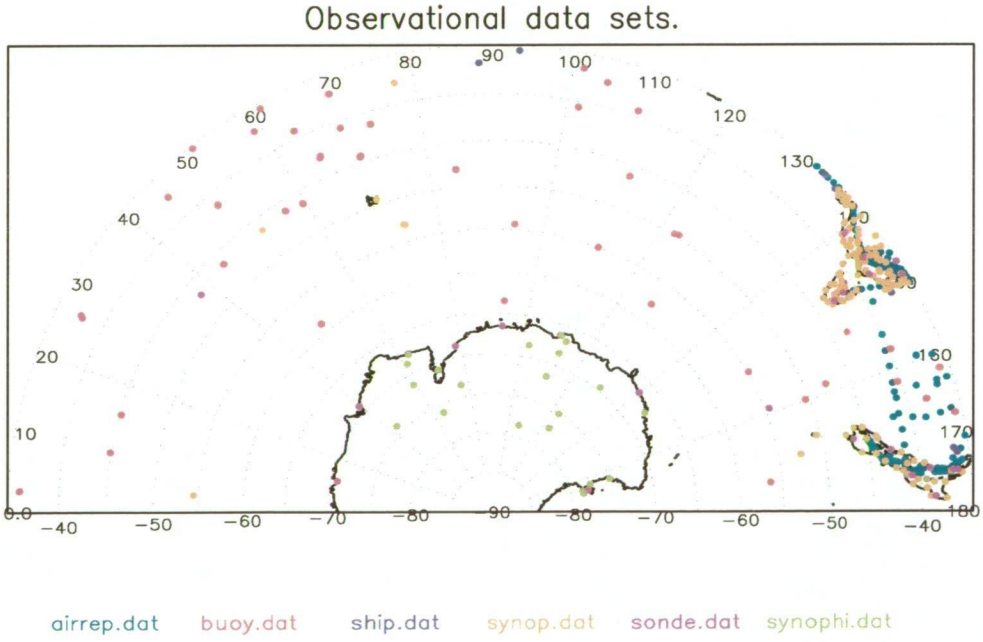

Figure 1.7: Surface and upper air observations valid over a 6 hour period during September 2001.

able for one 6 hour period in September of 2001. Apart from the relatively

large number of observations over southeastern Australia and New Zealand, in the far northeastern sector of the domain, data over the the area remains sparse. Attempting to sample the high latitude atmosphere and associated adverse weather events from routine surface based observations is severely limited, reducing the ability to adequately define, and hence, forecast the structure and time evolution of high latitude systems (Reeder and Smith 1998). With the advent of remote sensing from satellite platforms the amount of data available to the forecaster has improved and the manual surface analyses prepared at the Antarctic Meteorological Centre (AMC), at Casey, as part of the summer forecast program proved to be superior to the numerical products (Adams 1997). However, it was apparent that the severely limited amount of routine upper air data made the 500hPa geopotential height analyses prepared at the AMC inferior to the numerical products. Techniques for reducing AWS surface data on the high plateau to the 500hPa surface, for example Philpot (1991) and Radok and Brown (1996) proved over the summers between 1992 and 1999 to be of only marginal use. Over 5 summer periods during the mid to late 1990's, the author applied one, or other, of the above 2 techniques to the inland AWS stations in an attempt to increase the available data for the analyses. As a verification of the technique, the surface data from the American South Pole station was used to generate a 500 hPa height and then compared with the value obtained from the routine radiosonde flight. The results of the reduction techniques were disappointing and limited faith given to the values obtained from the remaining high plateau AWS sites.

Robust local forecasting techniques typical of Australian regional fore-

casting centres have not been available to the Antarctic forecaster due to the sparsity of observational networks around the Australian stations, coupled with the fact that forecasting has typically been carried out only over the summer months and by forecasters seconded from Australian forecasting centres typically for one summer season only. This has led to the situation where forecasting "rules-of-thumb" for each of the stations have been slow to develop and never robustly tested. Recent research and development has used data collected at the Australian stations over the last 40 to 50 years to implement a computer based analogue forecast system in an attempt to provide short to medium range forecast guidance. The system, designed by the author was implemented over the 1997/98 season in a test mode but the verification was disappointing, with the analogue system providing only fair guidance for temperature forecasts and poor results for wind speed and direction. The system was presented to the First International symposium on operational weather forecasting in Antarctica as reported by Turner et al. (2000). The most likely reasons for the poor results of such single station forecasting techniques was the inability of the technique to take into account the 3-dimensional structure of the atmosphere. Given a reasonable density of observations around each of the stations or access to almost instantaneous RADAR data, local forecasting techniques based on current and past observations may very well provide extremely useful short term forecasting guidance. However, it seems apparent that until adequate meso-scale networks are installed around the Antarctic stations to adequately define the local flow and provide the forecaster with meaningful data upon which to base a forecast and acquire detailed local knowledge, numerical model out-

put will continue to be the major source of meteorological information upon which to base weather forecasts.

1.2 Meteorological units.

In general, SI units prevail within the weather forecasting community, with 2 major exceptions. The first is in measuring wind speed, where both the aviation and marine industries expect speed to be given in knots, where a knot is defined as one nautical mile per hour, and 1 knot is equal to 0.5146 ms^{-1}. The second exception also arises from the aviation industry where aircraft altitude is still tied to the imperial units of feet, where 1 foot is equal to 0.3117 m. Within this thesis wind speeds and altitudes will continue to conform to industry standards and be given in units of knots and feet, respectively. All other units within the thesis conform to SI standards.

2 Current NWP models

2.1 The Australian global model

The Australian Bureau of Meteorology routinely runs a global assimilation and prediction system (GASP) to service forecasting and research activities both in the Australian region and more generally around the globe. The model has been the mainstay of high southern latitude meteorology in the Australian region for some years. GASP is a spectral model with vertical coordinates on sigma levels ($\sigma = \mathrm{p}/\mathrm{p}_{sfc}$) During the study period GASP was run at wave number 239 (triangular truncation) giving a nominal horizontal resolution of approximately 75 km. There were 29 sigma levels in the vertical with the lowest level at $\sigma = 0.991$ (approximately 70m around coastal Antarctica) and the upper boundary at $\sigma = 0.010$. Multivariate statistical interpolation (MVSI) was employed in the objective analysis cycle with analyses performed every six hours and forecast runs initiated every 12 hours at 1100UTC and 2300UTC through the first few months of the trial period, and 0000UTC and 1200UTC for the later part of the period. A semi-implicit, semi-Lagrangian time stepping algorithm was employed to maintain a relatively large time step (currently 600 seconds) to reduce computing time. For a more complete discussion of both the assimilation and forecast systems see Seaman et. al. (1995) and Bourke et. al. (1995) with an additional discussion on model improvements and upgrades by Bourke et al. (1999).

2.1.1 GASP performance

GASP model performance statistics are routinely collated by staff in NMOC and published quarterly in the Australian Meteorological Magazine (Skinner et. al. 2001). These statistics generally take the form of S1 skill scores of mean sea level pressure (MSLP) and 500hPa height and root mean square (RMS) errors of MSLP and 500hPa height over the Australasian region. For a full description of the Australian verification methods see Skinner (1995) but briefly, the S1 skill score has been used for some time to quantify model performance in Australia and is formulated by taking points from a synoptic chart (for example, MSLP or 500hPa heights) and using the gradient of the difference field corrected by a difficulty parameter defined as the maximum of either the observed or forecast gradient (Equation 1). In equation 1 Δx is the east-west grid-spacing, Δy the north-south grid-spacing, X_f the forecast value and X_O the observed value.

$$S1 = 100 * \frac{\sum e_g}{\sum G_L} \tag{1}$$

where

$$e_g = \left|\frac{\Delta(X_f - X_o)}{\Delta x}\right| + \left|\frac{\Delta(X_f - X_o)}{\Delta y}\right|$$

and

$$G_L = max\left(\left|\frac{\Delta X_f}{\Delta x}\right|, \left|\frac{\Delta X_o}{\Delta x}\right|\right) + max\left(\left|\frac{\Delta X_f}{\Delta y}\right|, \left|\frac{\Delta X_o}{\Delta y}\right|\right)$$

The resulting number, or skill score, provides a measure of how well the fore-

cast chart models the analysis, or reality. A small S1 skill score implies very good fit between the forecast and verifying analysis whilst a large skill score implies poor performance. For a more comprehensive description of the S1 skill score the reader is directed to the original work by Teweles S. and Wobus H. (1954). Over the years a general downward trend has been note in the S1 score for the GASP model in the Australasian region. For example, Bourke et al. (1995) highlighted the steady improvement in the GASP performance since the early 1990's where the S1 skill score for the +36 hour forecast fell from around 45 in 1990 to near 34 by late 1994. In this time period the model had progressed from a rhomboidal wave number 31, 9 level model, employing univariate methods of objective analysis, to a rhomboidal wave number 53, 19 level model employing multivariate statistical interpolation in the objective analysis. Indeed, steady improvements have continued to be observed over the last few years with the +36 hour forecast skill for the period April to June 1996 being approximately 28 (Skinner et. al. 1996) and for the April to June 2000 period further falling to near 26 (Skinner et al. 2000). The downward trend in skill for the latter period was also attributable to continual improvements to the model assimilation and forecast systems, with the major change over the above period being the move in December 1998 from the T79L19 system (triangular truncation, wave number 79 with 19 levels) to the T239L29 system currently employed.

As mentioned above, the skill scores for the GASP model have been calculated over the Australasian region and do not give any indication of the model performance over the high southern latitudes where observational data are significantly more sparse and weather systems possibly different in their

dynamics to the mid-latitude regions of Australia. To address the question of model performance the author (Adams 1997) took the S1 skill score methodology employed by the Australian Bureau and constructed a domain covering from 70°S to 50°S and 80°E to 160°E upon which to calculate the S1 skill scores. The domain had a resolution of 2.5^{o} of latitude by 5.0^{o} degrees of longitude, giving a total of 153 grid points. The domain was chosen because it covered the area of responsibility taken on by the AMC, at Casey, for high seas forecasts. The aim of the study was in fact to ascertain whether manually prepared prognostic charts were adding any skill to the numerical model charts they were based on but the study also highlighted the differences in skill from the mid-latitudes of Australia to the higher latitudes of the East Antarctic coastal regions. For the period late November 1993 through until February 1994 the average skill of the manually prepared +24 hour forecasts over the Antarctic region was 56.6 as compared to 37.6 for the manually prepared NMC prognoses. As these manual prognoses were prepared from the global model output it may be inferred that model performance at high latitudes was poorer than at mid latitudes. A direct comparison of GASP performance over Australia with GASP performance over the Antarctic domain for the period October through December 1995 also highlighted the poorer forecast skill at high latitudes with an S1 skill of 23 over the Australian domain (Skinner et al. 1995) and a skill of 25 over the Antarctic domain (Adams 1997). The study by Adams (1997) also highlighted the fact that changes to the GASP assimilation and prediction systems were also reflected in an improvement of the GASP skill at high latitudes from around 33 in June of 1994 down to around 21 by January 1996.

2.2 International global models

Meteorologists in the Australian Bureau of Meteorology also have access to data from global models run by international agencies. The European Centre for Medium range Weather Forecasting (ECMWF) and the National Center for Environmental Prediction (NCEP) both provide model output that are routinely available to Antarctic weather forecasters. It is not the aim of this thesis to go into any depth describing these models, other than to say that only gridded data at a latitude-longitude resolution of 5.0^{o}x 5.0^{o}for the MSLP and 500hPa height data were available from the ECMWF model, making the model of only limited use in providing weather forecasting support. NCEP provided the full model output from their aviation run (AVN) of the global model and these data were routinely processed and made available to the Antarctic forecasters. The next two sub-sections briefly describe the performance of both the ECMWF and NCEP output.

2.2.1 ECMWF performance

As mentioned above, ECMWF only made available fields of MSLP and 500hPa geopotential height on a 5.0^{o}x 5.0^{o}latitude- longitude grid. The model resolution was significantly higher than this and a full suite of dynamic and diagnostic fields available, but not to Australian Antarctic forecasters. However, it is interesting to note that the model MSLP forecasts significantly out-performed the GASP model over the period June 1994 through until January 1996 (Adams 1997) with an average S1 skill score of 28.6 as compared with 37.3 for GASP over the same period. For this reason, the AMC routinely used the ECMWF MSLP forecasts as the basis for the man-

ual prognostic charts that were broadcast on HF metfax for reception by mariners in the high southern latitudes and for other international stations able to receive the broadcast charts (Adams 1997).

2.2.2 NCEP performance

The NCEP model has proven to be the most popular of the global models available to Australian forecasters, and has also been the mainstay of Antarctic forecasting for a number of years. The popularity of the model has arisen out of the, anecdotally, better performance of the model in the Australian region and around the Antarctic coast. Although the resolution of the NCEP AVN model was marginally coarser than that of GASP (around 100 km as opposed to 75 km for GASP), the lowest sigma level of the NCEP model is set at $\sigma = 0.9950$ rather than $\sigma = 0.9910$, as is the case for GASP. This means the NCEP first sigma level around the coastal fringe of Antarctica was at about 39 m as opposed to 70 m in GASP and, anecdotally, appeared to perform significantly better than GASP in defining the observed low level flow. The improved surface flow definition from the NCEP AVN model, over GASP, has been observed both around the coast of Antarctica and in the mid-latitudes, where Australian forecasters routinely access low level wind data from both models. Little verification work has been done on the NCEP model although the quarterly model performance statistics provided by the National Meteorological Operations Centre (NMOC) in Melbourne consistently show S1 skill score performances for a range of international global models with the ECMWF spectral model consistently the best performer followed by the NCEP AVN model (Skinner et al. 2001). These statistics

were valid only for the Australasian domain, however a limited comparison of S1 skill scores over the Antarctic domain provided some substantive evidence for the better performance of NCEP over GASP, in the Antarctic context. A comparison of S1 scores for the period late November 2001 through until the end of June 2002 (Figure 2.1) showed NCEP with a marginally worse S1

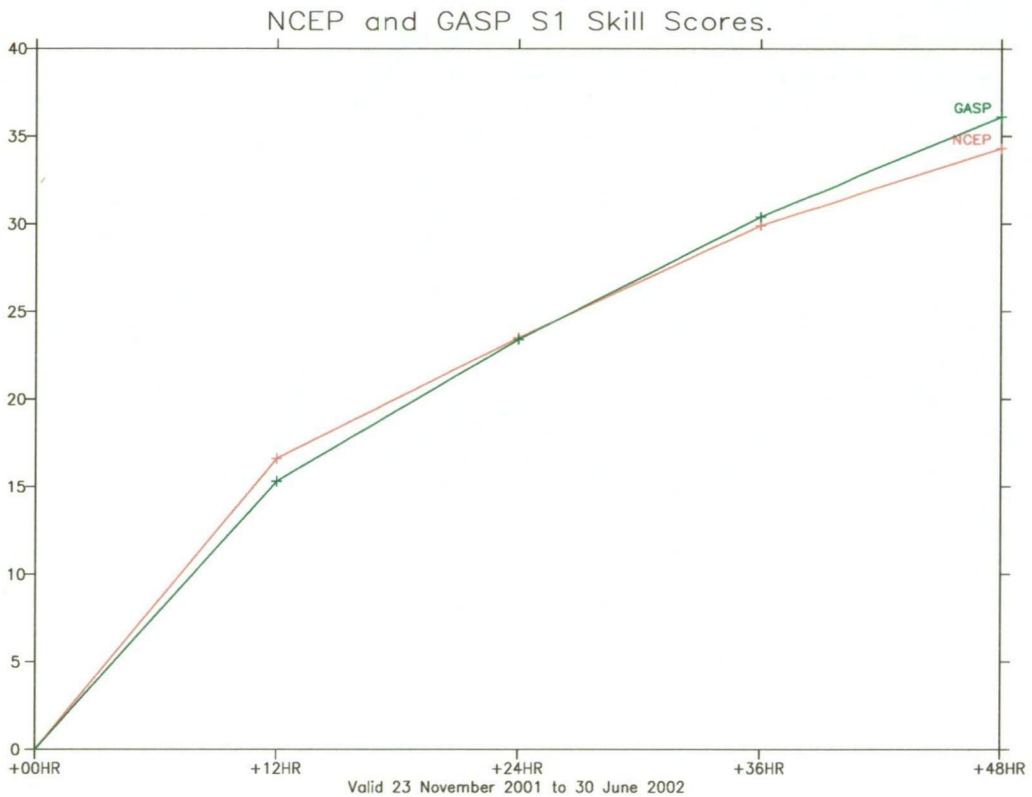

Figure 2.1: Comparison of S1 skill scores from GASP and NCEP from November 2001 to June 2002 over the domain 70°S to 50°S and 80°E to 160°E.

score in the first 12 hours of the model integration, but equaling GASP by +24 hours, and outperforming GASP in the 24 to 48 hour time period. In the chapter discussing ALAPS performance using single station verification techniques some NCEP data will also be presented, highlighting the solid performance of the global model.

2.3 International regional models.

As of 2004, the United States of America (USA), was using the Antarctic Mesoscale Prediction System (AMPS) in support of the USA Antarctic program. AMPS is a limited area NWP system based on version 3.6 of the PSU-NCAR MM5 model with modifications made for use over polar regions. The model has been implemented as an operational limited area Antarctic model in support of US operations between New Zealand and the US bases of McMurdo and South Pole. A general description of MM5 may be found in Dudhia (1993) and Grell et al. (1994) with a detailed discussion of the polar modifications made to the standard version of MM5 found in Bromwich et al. (2001) and Cassano et al. (2001). Details of the model will not be discussed here, other than to note that the model has a non-hydrostatic formulation of the primitive equations, running on a staggered grid in the horizontal with a vertical terrain following σ-coordinate system. The model included three-dimensional prognostic equations for the horizontal and vertical components of the wind, temperature, and pressure perturbation, which refers to a prescribed pressure reference state (Guo et al. 2003). Three dimensional prognostic equations for the water vapour, cloud water (ice), and rainwater (snow) mixing ratios are also part of the model equations with parameterisations for moist physics, radiative transfer, and turbulence included. For the polar version of MM5, moist physics were simulated with explicit cloud and precipitation prediction schemes (Guo et al. 2003). As of the 2002-03 season the operational version of AMPS, was running a 2-way nesting system with a full Antarctic domain at a resolution of 30 km, nested within a 90 km resolution hemispheric version of the polar MM5, which in turn was nested within

the NCEP AVN global model. The 30 km resolution domain provided output comparable in resolution to the ALAPS model (nominally 27.5 km horizontal resolution around the Antarctic coast). However, the evaluation described in Guo et al. (2003), and cited below, was based on a complete annual cycle of the model, producing 72 hour forecasts at a resolution of only 60 km, using a square horizontal grid centred on the South Pole, and so was somewhat coarser than the data available from ALAPS. The assessment of the polar MM5 simulations concluded that the model agreed well with the observed synoptic variability in pressure, temperature, wind speed and direction and water vapour mixing ratio, as well as agreeing well with the observed diurnal cycles of temperature, mixing ratio and wind. On the annual timescale the model appeared to be too cold in the near-surface temperatures and showed a deficit in total cloud cover, and a deficit in net precipitation over the interior of Antarctica. Over all time scales the polar MM5 simulations appeared to be most skillful in predicting surface pressure, temperature, water vapour mixing ratio and wind direction, with less skillful predictions of wind speed, with many strong wind events being missed (Gou et al. 2003).

In the case study presented by Bromwich et al. (2003), the AMPS system used 2-way nesting with a 90 km resolution outer domain, covering most of the Southern Hemisphere south of 40^{o}S, nested within the NCEP AVN model. Nested within the 90 km domain was a 30 km resolution AMPS domain, covering all of the Antarctic continent. A 10 km resolution domain centred on McMurdo and covering the western Ross Sea, and eastward over the Trans Antarctic Mountains, was nested within the 30 km domain. From this study, it was concluded that the AMPS system did show skill in resolving

many small-scale surface features common to the region around McMurdo and the Ross Sea, including katabatic winds and lows and highs induced by wind and topography. However, it was also noted by Bromwich et al. (2003) that AMPS forecasts were limited by errors in the atmospheric analyses used as the AMPS initial conditions.

Although no ALAPS model output was available for the 1993 annual time period discussed in Guo et al. (2003), the analysis of the AMPS performance by both Guo et al. (2003) and Bromwich et al. (2003) provides a valuable data source upon which to make useful comparisons of the ALAPS performance and as the verification statistics for ALAPS are presented below, comparisons with AMPS performance will be made, where applicable.

3 LAPS

3.1 General

LAPS was developed by the Bureau of Meteorology Research Centre (BMRC) to provide high resolution limited area forecast guidance to assist Australian forecasters in the provision of weather services. It has been in operation since July 1996 providing medium resolution output over the entire Australian domain and high resolution output over several smaller local domains. LAPS is a globally relocatable limited area grid point model employing full data assimilation. The system uses a latitude-longitude horizontal grid and sigma coordinates in the vertical, with the domain in this study having a resolution of 0.25^o of latitude by 0.50^o of longitude, with boundaries from 0^oE to 180^oE and 80^oS to 35^oS. 29 vertical sigma levels are used, ranging from 0.9988 near the surface (approximately 8 m over Antarctica), to 0.05 (approximately 50 hPa) at the model upper boundary, with a concentration of levels in the planetary boundary layer. A full description of the model is given by Puri et al. (1998) but in essence the governing equations are the multi-level primitive equations for momentum, mass, temperature and moisture, written in advective form, except for the mass equation which is in flux form. The model runs on an Arakawa A grid and in the current study employs fully explicit Miller-Pearce time differencing. High order spatial differencing is used where ever possible to ensure accuracy to at least that of second order C grid models. The ECMWF land surface, boundary layer and vertical diffusion schemes were used in the model and are described by Puri et al. (1998). The analysis system used in the assimilation cycle is a limited area

adaptation of the global multivariate statistical interpolation (MVSI) used in the GASP system as described by Seaman et al. (1995). The assimilation cycle typically employs a cycle starting either 12 or 6 hours prior to the model start time, with an analysis performed on either GASP data (cold start) or LAPS data from a previous model run (warm start). The resulting analysis is then integrated forward 6 hours to the next analysis cycle. Once the last analysis has been performed the model is integrated forward 48 hours. Each invocation of the model is typically initialised prior to integrating forward in time, in an attempt to reduce the effects of spurious gravity waves and in LAPS this is performed using the digital filter scheme of Lynch and Huang (1992). Nesting files, needed to provide boundary conditions for the LAPS model run, are provided from the GASP global model forecast. Prior to integrating LAPS out the full 48 hours a mass flux adjustment scheme may also be employed to ensure that within the GASP nesting files the domain averaged surface pressure tendency exactly matches the mass flux through the lateral boundaries. Within the Australian region the LAPS forecasts are initiated with a two hour data cut-off, which means the first guess field and boundary conditions are supplied from the previous GASP model run (a cold start) which are already over 12 hours old. This is known to have a negative impact on model performance (Puri et al. 1998) but by performing the cold start off the previous GASP model data with a very short cut-off period and performing the three analyses within the assimilation cycle (-12 hours, -6 hours and 0 hour) means the LAPS model output data are available for operational use within about three hours of the synoptic hour providing very timely forecast support.

3.2 Adaptation to Antarctica (ALAPS)

In general the ALAPS system is little different to the Australian version, with the core model code remaining unchanged. Figure 3.1 shows the domain used

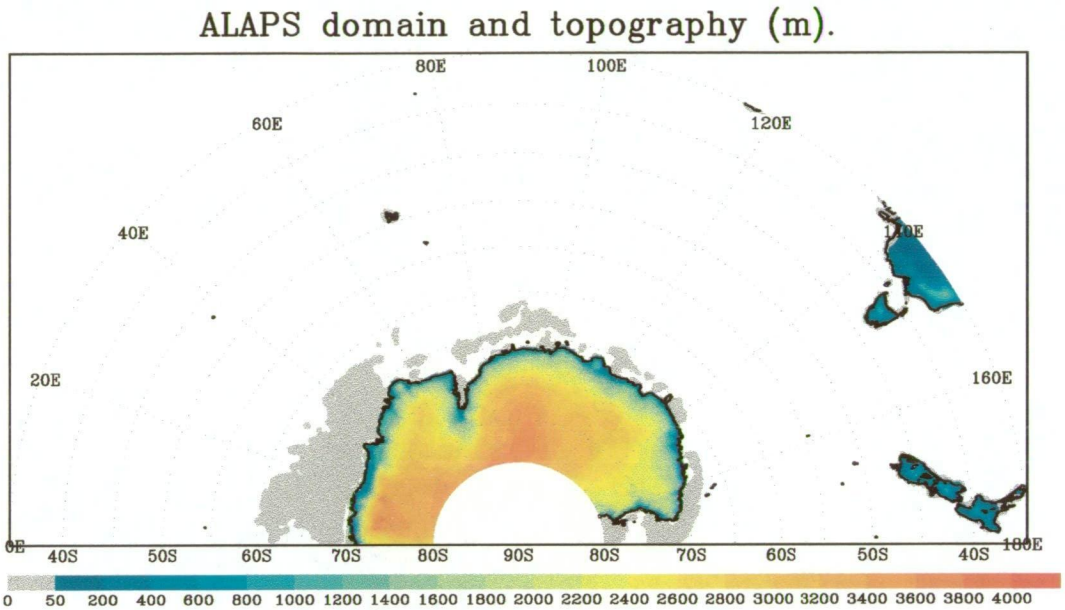

Figure 3.1: ALAPS domain and model topography.

by the current ALAPS system, and also shows the model topography, which was generated from a high resolution, 30 second data set. However, several minor changes have been made to the pre-processing stages of the ALAPS system, in order to better represent the Antarctic environment. Daily sea ice concentration data, at a 0.5 degree resolution, were imported from NCEP to improve the land-sea-ice mask used in LAPS, and to also alter the surface temperature field, depending on concentration values. If the sea ice concentration was higher than 95% then the surface was treated as land, and the topographic data updated accordingly (with a height value set at 2.0 m). If the sea ice concentration was less than 30% then the surface was set back to water with a sea surface temperature of 271.66K (-1.5^{o}C). For areas in

the sea-ice zone with concentrations between 30% and 95% the surface was treated as a simple "slab" of 2 m thick ice. No fractional sea-ice coverage within an individual model grid cell was used, as is the case in AMPS.

The albedo field generated in the Antarctic version of LAPS also differed from the Australian version. As with the Australian version the field was generated following the work of Hummel and Reck (1979) but with more accurate setting of albedo values over the Antarctic continent and sea-ice zone in the high resolution domain. The entire continent was set to the seasonal continental value from Hummel and Reck (1979), with 82% used for January through until June, and 88% for July through until December, except for a small zone near the coast where values reduced uniformly to a set coastal fringe value of 65%. Albedos were kept at 65% for high sea ice concentrations but reduce to the seasonal open ocean values as the ice concentration reduced to zero. Ocean albedos also reduced as the latitude decreased, as per seasonal values described by Hummel and Reck (1979). Alterations to the ALAPS albedo values were only performed south of 50°S, with Figure 3.2 highlighting the affect of the altered albedo field used by ALAPS.

Changes were also made to the initialisation of surface temperature south of 45°S, in the pre-processor stage of the ALAPS system. In the Australian version, an extrapolation was made from the air temperature values found at the lowest 2 sigma levels of the first guess model data. This had the adverse effect of generating winter time surface temperatures over the high Antarctic plateau significantly warmer than was observed, resulting in a substantial weakening of the strong Antarctic surface inversion, that is an important

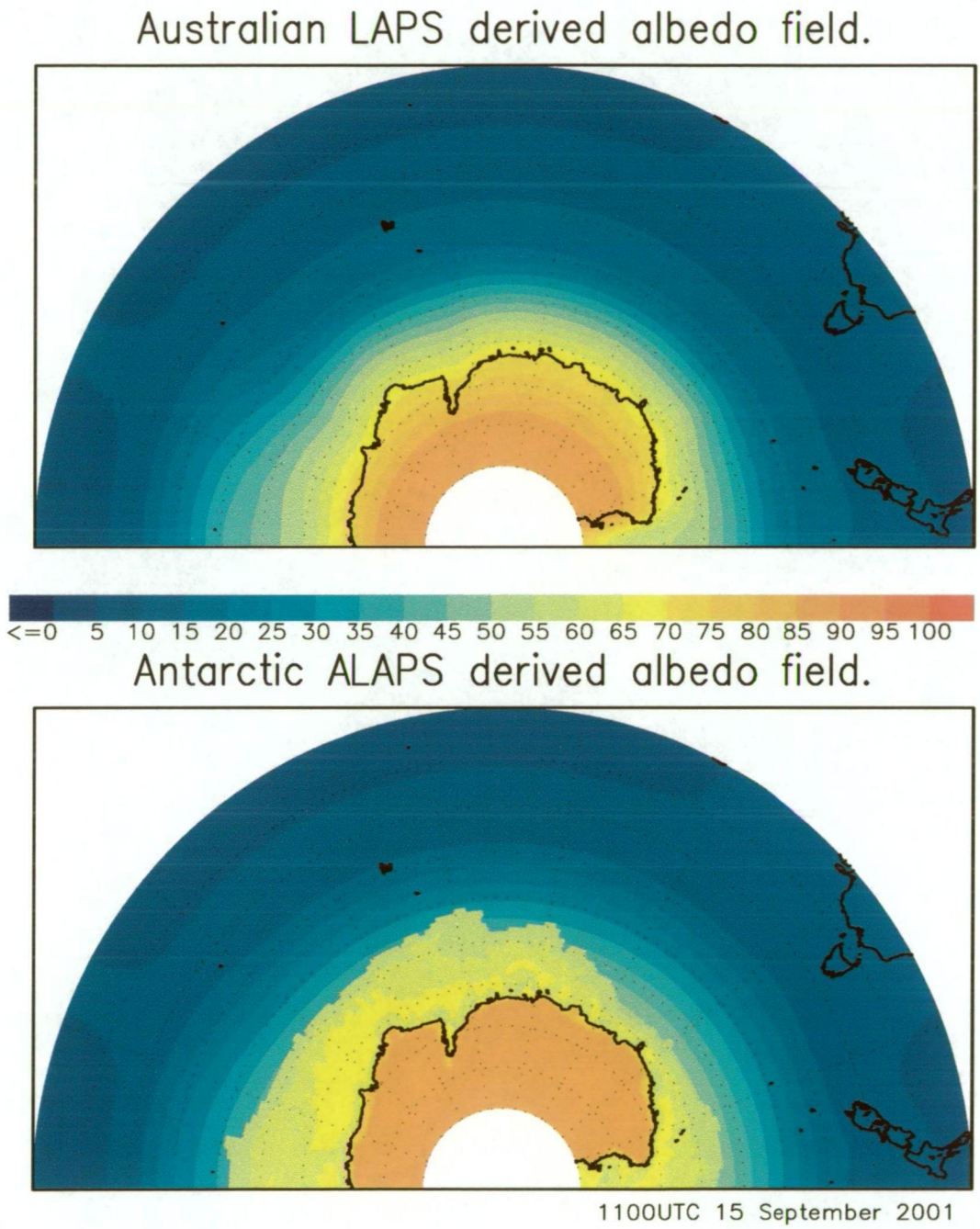

Figure 3.2: Top panel shows the unaltered albedo field generated within the LAPS pre-processor, with the lower panel showing the albedo used within ALAPS.

feature of the Antarctic planetary boundary layer, (Schwerdtfeger 1984). To overcome this shortcoming of the original LAPS pre-processor system, actual surface temperature data from the first guess field (either ALAPS in a warm start, or GASP for a cold start), were ingested and used from the outset. This also necessitated modifying the physics sub-routines within the LAPS model code itself since, despite the pre-processor generating new fields of surface temperature, and masked surface temperature, the physics sub system re-generated these fields during the initialisation phase of the model run, using a weighted mean of the lowest 2 sigma level air temperature fields. Similarly, the initialisation of sub-soil temperatures was also modified to use a weighted mean of the surface temperature and first sigma level air temperature, rather than a weighted mean of the first 2 sigma level air temperature fields. The modified initialisation of surface and sub-soil temperatures in the pre-processor and physics code was designed to improve, substantially, the treatment of surface temperature by the model. The effect on analysed and forecast surface temperature and surface inversion strength was obvious with Figure 3.3 showing the mean inversion strength for September 2001, which compares favourably with the long term winter time inversion strength detailed by Phillpot and Zillman (1970) and shown in Figure 3.4.

The Surface roughness was also treated differently in the ALAPS runs. Rather than using the effective roughness implementation of Wood et al. (1993), as used in the Australian LAPS code, a fixed roughness length of 0.001m was applied to the entire Antarctic continent. Early studies by Dalrymple et. al. (1966) measured roughness lengths of around 0.2 mm at the South Pole, with Weller et. al. (1968) measuring values from as

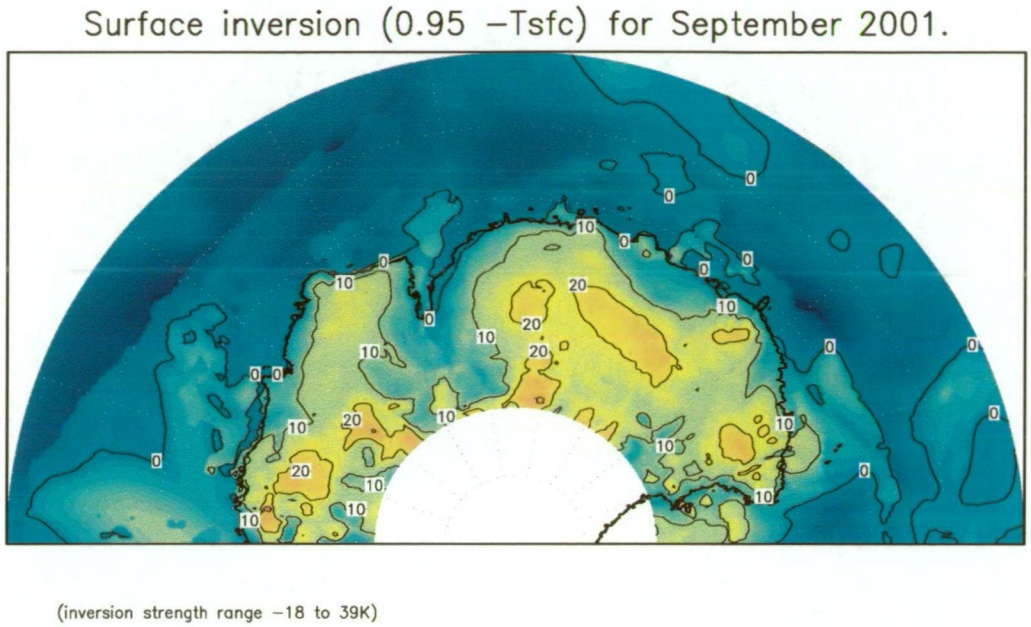

Figure 3.3: ALAPS +24HR forecast mean surface inversion strength ($T_{0.95}$-T_{sfc}) for September 2001.

low as 0.14 mm over gentle snow covered slopes, and up to 2.6 mm over the coastal ablation zone. Budd et al. (1964) measured values of around 0.18 mm at Byrd and Bintanja et. al. (1995) measured values ranging from 0.08 to 0.75 mm over smooth sites, with larger values at sites with sastrugi. The value of 1 mm used by ALAPS may have been on the high side for smooth gentle slopes, however, was considered a reasonable value for the steep coastal escarpment of East Antarctica, where sastrugi and snow dunes are common, and the Australian Antarctic stations are located. This implementation avoided the problem seen over Australia of unrealistically low wind speeds in the surface layer, which over Antarctica manifest itself in the almost complete destruction of the Antarctic katabatic flow. The use of a fixed roughness length has introduced a degree of simplification, in that a single surface type has been assumed for the entire continent, however, the

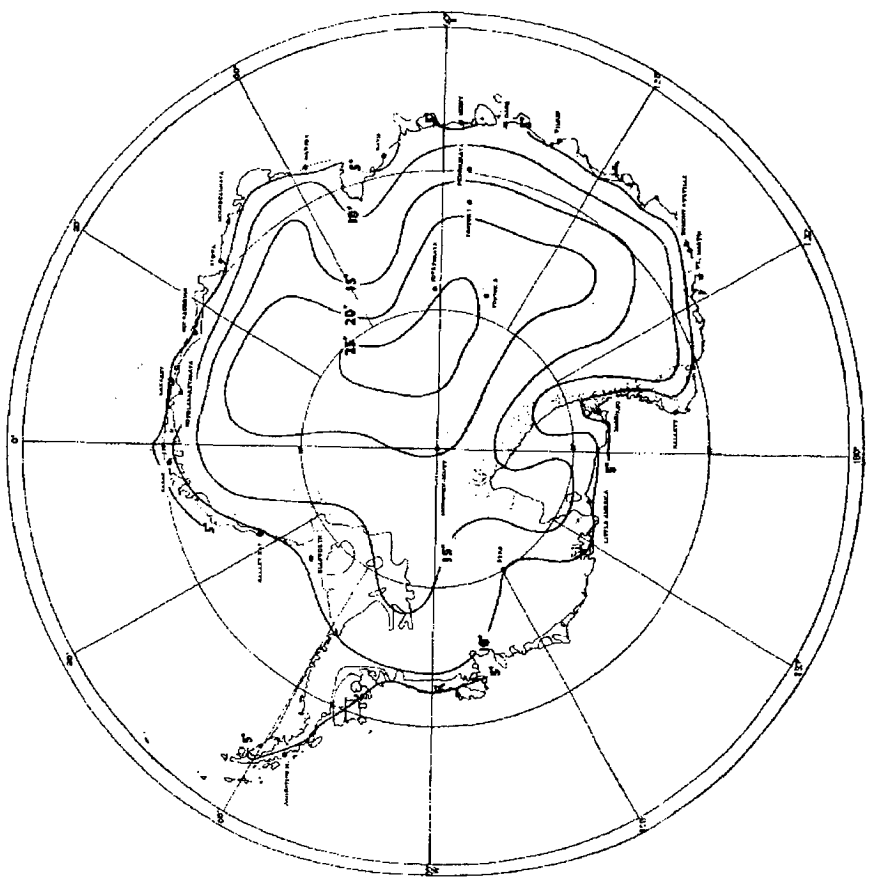

Figure 3.4: Estimated long term winter-time inversion strength from Phillpot and Zillman (1970).

sensitivity of the model to the chosen roughness length will be discussed in a later chapter.

The implementation of the assimilation cycle within ALAPS has also been altered to that of the Australian version of LAPS. Many trial runs were undertaken to ascertain the performance effects attributable to the analysis scheme, the digital filter initialisation, the mass flux adjustment process and to the differences between performing either a cold start directly off the GASP model data or a warm start off the +6 hour ALAPS forecast from the previous (12 hour old) ALAPS run. Each of the above components of the assimilation cycle have the potential to significantly impact on the starting analysis used by the model, and errors introduced by any one of them have the potential to produce a "shock" to the model, that may take some integration time to dampen out, or may simply result in poor model performance throughout the model simulation. Results from the trial runs are presented below, but in essence it was decided that the best model performance was likely to be produced when the assimilation cycle was initiated at -6 hours using a warm start off the +6 hour forecast from the previous ALAPS run, if it was available. If the previous ALAPS model output was not available, then the GASP -6 hour analysis from the latest GASP run was used as the first guess field for the initial -6 hour analysis. The initial analysis was then initialised using the digital filter initialisation scheme, described above, then integrated forward 6 hours, with a second analysis then performed using the new +6 hour ALAPS forecast as a first guess. The digital filter initialisation was again applied to the analysis, then the ALAPS model integrated forward 48 hours, with model output generated every 3 hours. For the 12

months of ALAPS output generated for this study, no mass flux adjustment was used at either the -6 hour or 0 hour analysis times, and boundary conditions for both the initial 6 hour model run and the full integration were provided from the latest GASP model run. By waiting for the latest run of GASP, a long data cut-off period was available, allowing appreciable time for all of the available synoptic and remotely sensed data to be collected prior to assimilation. Generally this cut-off period was around 8 hours with the system, running in research mode rather than operational mode, completing the assimilation cycle after about an hour, and the +48 hour model integration some 3 hours after this. Hence, model guidance was available some 12 hours after the synoptic hour. This was significantly poorer than in the Australian operational system where guidance was typically available about 3 hours after the synoptic hour. However, a more complete observational data set was utilised by ALAPS, and the latest GASP output available for use as boundary conditions. It's worth noting that despite the first 12 hours of model data not being available in real time to Antarctic forecasters, there was still 36 hours of useful model guidance available, from the +12 hour time step out to the +48 hour time step, and the first 6 to 12 hours of model integration was often suspect anyway, with spin-up problems associated with "shocks" from the assimilation cycle generally damping out within the first 12 hours of model integration.

With the southern boundary of the ALAPS domain located high on the Antarctic plateau, and considerably far south, the convergence of the meridians reduced the longitudinal resolution of the ALAPS domain to around 9.6km, necessitating the use of a small time-step in the integration scheme

of the model. After initial trials, a time-step of 5 seconds was chosen to minimise the risk of model failure due to violation of the Courant-Friedrichs-Lewy (CFL) condition (Krishnamurti and Bounoua 1996). However, on rare occasions during the 12 month trial the model did "crash", either during the assimilation cycle or during the main model integration. If a failure occurred during the full model integration then the assimilation cycle was restarted using a cold start, whereby GASP data valid at -6 hours, was used as the first guess field for the initial analysis and then a 6 hour model run invoked to provide the first guess field for the analysis at the zero time step. Similarly, if the model integration failed during the 6 hour assimilation run, then a cold start of the latest GASP data was performed. In original trial runs, when the assimilation failed, only a single analysis was performed, at the synoptic hour, and directly off the latest GASP analysis. However, this was found to lead to significant problems, generated from the digital filter initialisation. Very large corrections to the starting analysis were being generated by the digital filter, with these large corrections, or errors, taking some 3 to 6 hours to dissipate from the model run, and producing adverse S1 skill scores right out to +48 hours. It was found that if the assimilation model run failed then it was better to invoke a cold start off GASP data at -6 hours, as described above, as running the model for 6 hours produced significantly better first guess fields for the zero hour analysis, with the subsequent digital filter initialisation producing only minor, and generally positive, impacts to the initial conditions for the model run. If the full model run crashed, subsequent to performing a cold start, then no model run was performed, but as stated above, this was a very rare occurrence, with only 4 failures out of 12

months of twice daily runs (a 0.55% failure rate).

It should also be noted that the output from both analyses, at -6 hours and 0 hours, were modified to remove all super-adiabatic lapse rates. Due to the methodology employed by the analysis scheme, often significant super-adiabatic lapse rates were generated in the lower atmosphere, and it was considered prudent to remove these prior to running the model code. However, when the code was invoked at the start of the 12 month trial period the super adiabatic lapse rates were removed by integrating up from the first sigma level temperature field, rather than down from upper levels, due to the ordering of the multi-level data in the files. This had the unfortunate side effect, on those occasions when the lowest temperature was too warm, of increasing the depth of the warm surface layer and increasing the negative impact of the starting analysis. On rare occasions the analysis scheme produced a first sigma level temperature field with excessively warm temperatures, which on closer inspection were the result of the interpolation scheme used in moving from the analysed increment field to the new sigma levels used in the updated analysis, and probably attributable to the interpolation scheme not handling strong surface temperature inversions. The very warm temperatures were only present at the first sigma level, but the adiabatic adjustment code deepened the very warm layer by correcting the upper sigma level temperature to force an adiabatic lapse rate. The resulting increase in temperature through a reasonable depth of the lower troposphere caused the initialisation system to force surface pressure low, generating a deep, unrealistic low pressure system. Figure 3.5 highlights the errors propagating from the analysis field through to the initialised state of the model. The analysed

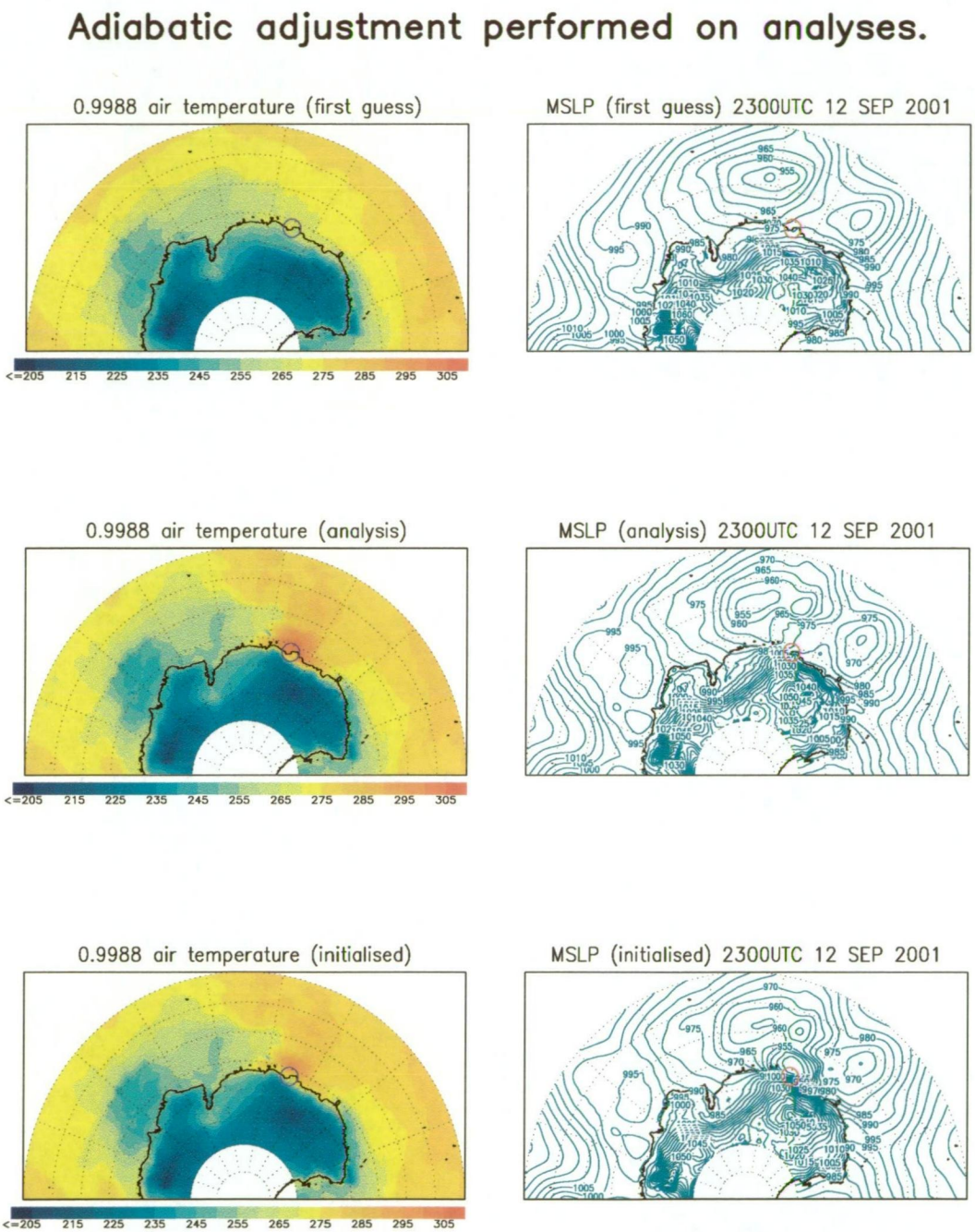

Figure 3.5: Near surface temperature and pressure from the first guess field (top panels), analysis scheme (middle panels), and after digital filter initialisation (lower panels), where adiabatic adjustment has been performed.

surface temperature was in excess of $+25^{o}$C offshore and around the Casey coast (panel 2 temperature in Figure 3.5), and even after the digital filter initialisation was run, temperatures remained very warm (panel 3 temperature in Figure 3.5). However, the significant error introduced by the digital filter initialisation was in the pressure field where a significant "bomb" in mean sea level pressure was generated in response to the excessively warm region (panel 3 MSLP, Figure 3.5). Very strong wind speeds (not shown) were also generated around the mesoscale low pressure system, but the system was fictitious, and not in balance with the broad-scale synoptic situation, and the model took some hours of integration to removed the system, resulting in very poor forecast skill out to +48 hours. Re-running the system with the super-adiabatic adjustment code turned off still resulted in the analysed and initialised first sigma level temperature values being significantly too warm (temperature fields in panels 2 and 3 of Figure 3.6) around the Casey coast, however the response in the surface pressure, and MSLP field after initialisation (panel 3 MSLP in Figure 3.6) was insignificant, as the very high temperatures from the analysis were confined to only the first sigma level temperature. Current ALAPS runs no longer use the adiabatic adjustment code in this manner, but integrate down through the temperature data and hence force any excessively warm surface temperatures back to an adiabatic laps rate. Unfortunately, the 12 months worth of data that the following verification analysis is based on has the wrong adjustment code in effect. Large errors as described above were rare, but it was probable that a component of the relatively poor performance of the ALAPS analysis system was attributable to this problem, with perhaps a small error propagating through

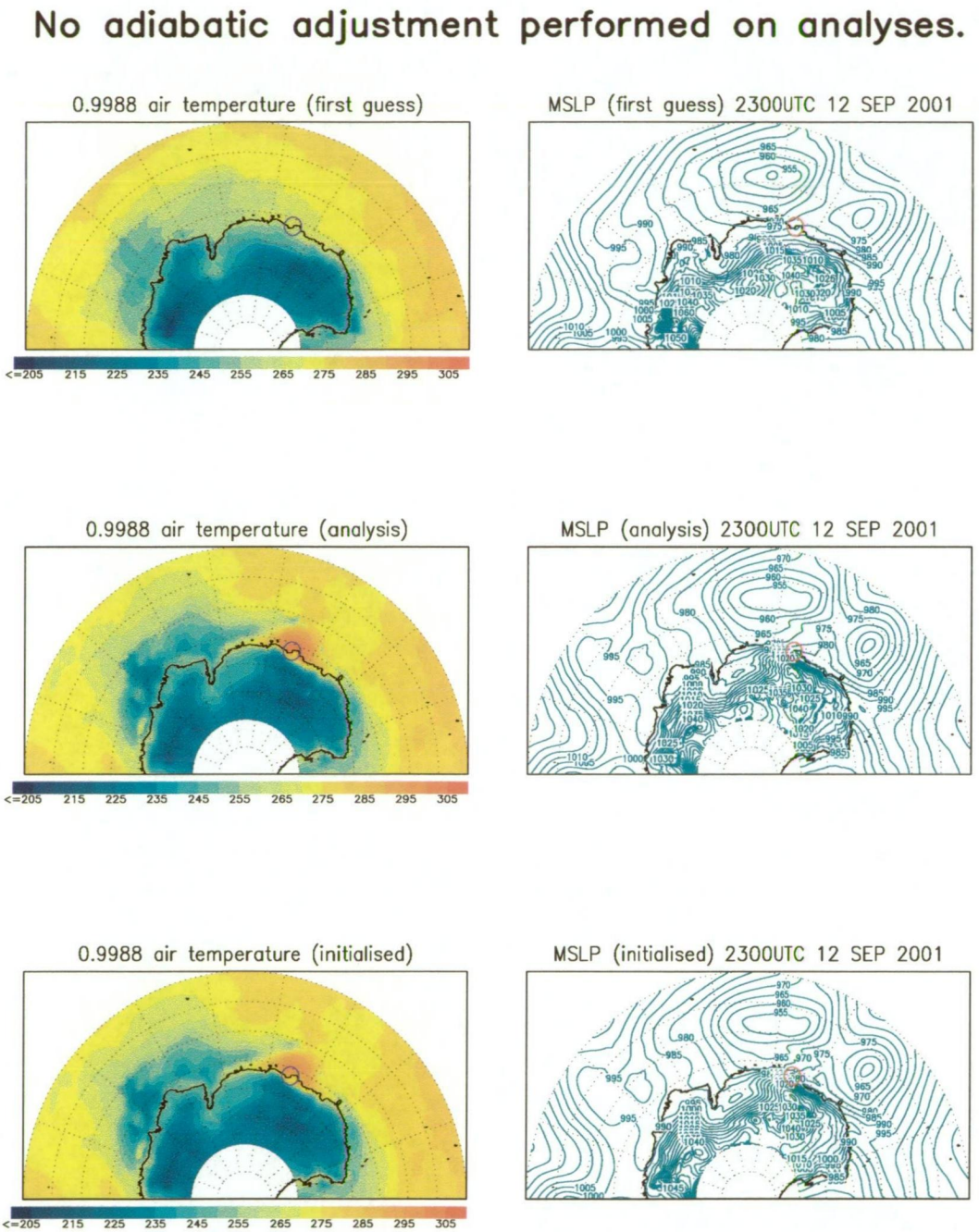

Figure 3.6: Near surface temperature and pressure from the first guess field (top panels), analysis scheme (middle panels), and after digital filter initialisation (lower panels), where adiabatic adjustment has not been performed.

to the +48 hour forecasts. For the following chapter on ALAPS performance the model was re-run over the first 3 weeks of January 2001 using the correct adiabatic adjustment process and results of the correct scheme are discussed there.

3.2.1 Issues over the Antarctic domain.

Through the life of the study several problems were encountered while testing and adapting LAPS to the Antarctic environment. LAPS is a complex system, incorporating a pre-processing stage, full data assimilation, high order numerics, and multiple choices for defining physical parameters and schemes. In developing ALAPS, it was decided to make minimal changes to the LAPS system in order to identify whether the system had the potential to provide useful short term weather forecasting support for Antarctic operations. However, it became apparent during the 12 month trial phase that some changes were necessary in order to have some degree of faith in the model's ability to properly simulate the Antarctic environment. The first major problem encountered was in the method of initialising surface temperatures. As mentioned in the previous section, LAPS used a simple interpolation of the lowest two air temperature values as an estimate of surface temperature. During the Antarctica winter, this approximation led to the almost complete destruction of the winter-time surface temperature inversion, necessitating a change to the initialisation scheme to ensure that the surface temperature data from the initial conditions file was carried through into the new model run, and so maintaining a more realistic surface temperature field. To test the modifications the ALAPS system was then re-run for the entire 12 month

period to validate the modification.

The second problem encountered was in the manner in which albedo data and, again, surface temperature data were initialised. An unforeseen problem with the changes made to the initialisation of surface temperature, coupled with the move to warm starting the model, was that albedo and surface temperature data were directly read from the initial conditions file which meant that daily and seasonal changes in albedo and SST, coupled with the changing sea-ice conditions, were never carried through to the new model run, unless the warm run system failed and a cold run was initiated. In the cold run system, where the latest GASP data were used for the initial conditions, the new albedo data and SST data were incorporated into the GASP initial condition file during the pre-processor stage. However, this was not the case in the warm run system, where forecast data from the previous ALAPS run were used without being modified by the newly created climate data. The problem was not identified until late in the analysis, when sensitivity studies were being carried out on climatological albedo values. Throughout the 12 month trial period, there were several warm start failures, resulting in a cold start, and the subsequent updating of sea-ice concentration and SST data. Hence, a substantial period of the 12 month trial still had valid albedo, SST and sea-ice cover information in the initial conditions file, but the transition months of December 2001 through January, and into February of 2002, were a problem, as the warm start running carried excess sea-ice cover, and associated higher albedo, and lower surface temperature data, through into the summer months. As will be discussed in chapter 6, on model sensitivities, model cloud and precipitation are sensitive to the sea-ice

cover, so it was deemed prudent to re-run the model over the December 2001 to February 2002 period. An analysis of the sea-ice and SST data carried through the other months of the trial suggested that results would not have been unduly affected by the problem, so the re-run was limited to three months of the summer period. The re-run of the model also incorporated the corrected adiabatic adjustment code and applied the mass flux correction to the analysis field (a discussion of the relative merits of different model configurations is discussed in chapter 4). Figure 3.7 shows a comparison of the mean S1 skill scores (see chapter 4 for details), for the three month period from 1 December 2001 to 28 February 2002, where scores for the model run with the incorrect surface specifications are shown in red, and for the correct surface scheme, including mas flux adjustment shown in green. The corrected surface specification resulted in an improvement of nearly 2 skill score points from +12 hours to +36 hours of the model integration, although with the improvements decreasing by +48 hours. The 12 months of data used in the following chapters on model performance, case studies and sensitivity studies include the modified summer month data.

The last problem was identified during the study of diurnal variations in temperature at Dome C (Chapters 4 and 6), where the model was significantly under-estimating the amplitude of the summer-time near surface and surface temperature variations. Sub-soil temperatures were being initialised correctly within the model, however, on further investigation of the model code, it was found that the model had been configured with an unrealistically high deep-soil temperature. The ECMWF scheme as implemented in ALAPS (Puri et al. 1998), assumed a single value deep-soil temperature for the entire

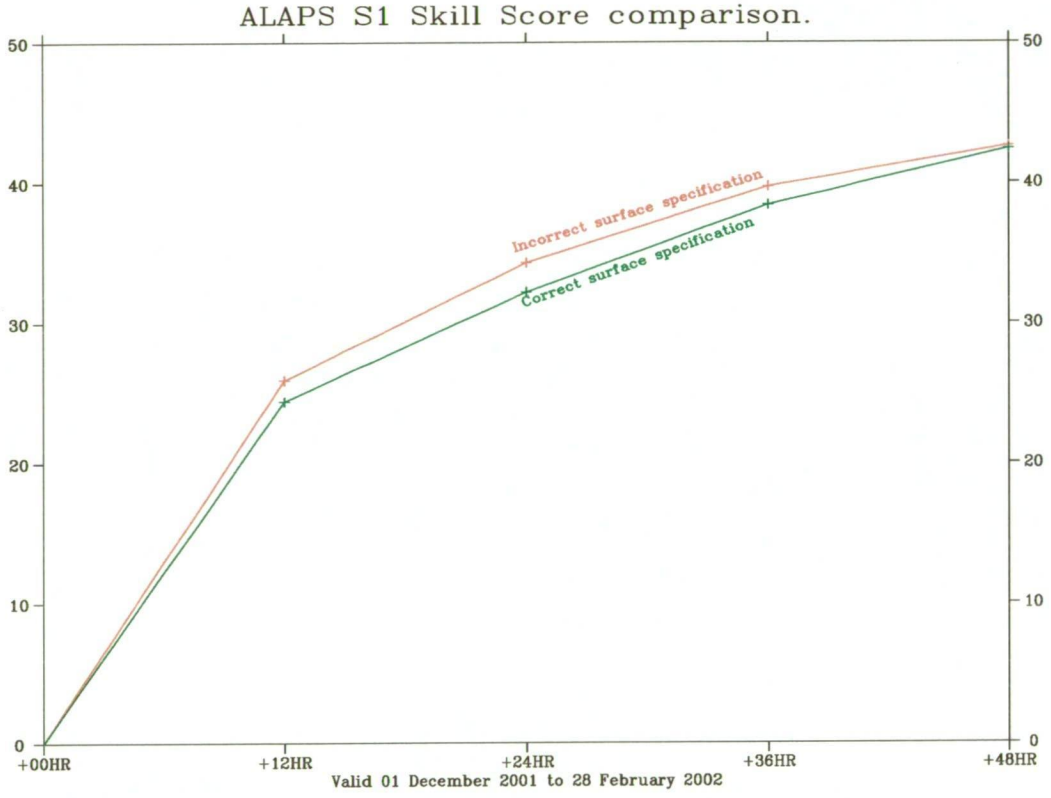

Figure 3.7: Comparison of S1 skill scores for December 2001 to February 2002, for the corrected (green) and uncorrected (red) surface scheme over the domain 70°S to 50°S and 80°E to 160°E.

Antarctic continent with the value set at 280K. This value would be realistic for coastal regions during summer and the transition months, but completely inadequate for defining deep-ice temperatures over the high plateau, particularly during winter. Having a single value definition for the entire continent was an inadequate approach and an area for further development. The sensitivity results presented in Chapter 6 showed that decreasing the deep-soil temperature to 220K produced better over-night minimum temperatures at Dome C, although day-time maximum temperatures were adversely affected. Given that the predominate use of the model was for forecasting at coastal sites, were the deep-soil value of 280K was not necessarily significantly in error, it was decided that re-running the model to assess the impact over the entire 12 month trial period was not warranted. Refinements to the boundary layer physics, and in particular, the surface fluxes of heat is certainly required in the ALAPS code to properly address continental Antarctic processes, but outside the scope of this thesis.

4 ALAPS performance

The following analysis of the performance of ALAPS will cover several techniques. Within the Australian Bureau of Meteorology, model output has traditionally been verified using the S1 skill score (Teweles and Wobus, 1954), generated from either mean sea level pressure or 500hPa geopotential height data, and verified against a control analysis, typically the model analysis used in initialising the model run. However, this method of forecast verification has several shortcomings. Firstly, using the model's own analysis as a measure of model performance may lead to questionable results, especially in the high southern latitudes where few data are available during the analysis phase to modify the model first guess field used in the assimilation process. Secondly, the S1 score is not ideal in trying to compare models of varying resolution, since the score is based on the forecast of gradients and a high resolution model, such as ALAPS, may perform well in forecasting a tight meso-scale gradient but have the gradient marginally misplaced in either space or time, resulting in a poor S1 skill score. A lower resolution model, such as the coarser global models traditionally used in high latitude forecasting, may not forecast the tight gradient at all, yet score well on the S1 score against their own analysis. With the advent of high resolution models, such as ALAPS, forecasters now have the ability to assess direct model output, where atmospheric variables from a single model grid point, coincident with the site for which forecast are being written, may be used directly as a forecast for the weather conditions at that location. Assessment of the model performance can then be directly related to how well data from selected grid points correlates with the observed weather from the coincident

real sites. This style of test is quite severe because, even at the relatively high resolution of ALAPS, the model topography is only a proxy of reality, with steep coastal slopes smoothed, and coupled with the errors associated in using a discrete numerical solution to a set of partial differential equations, that have also been simplified through such approximations as hydrostatic balance, and parameterised moist processes. However, in the context of using the numerical model as a weather forecasting tool, such validation processes are necessary as the S1 skill score does not provide the weather forecaster with a meaningful assessment of the veracity of one model over another. Also, by providing single station verification statistics, useful information on model biases, strengths and weaknesses, can be obtained and used by the weather forecaster to enhance the integration of the NWP product into the forecast process. Temperature, moisture, precipitation and wind are of primary concern to weather forecasters, and the spatial resolution now available from ALAPS, makes single station verification against actual synoptic observations of these parameters possible. Bromwich et al. (2001), Cassano et al. (2001) and Guo et al. (2003) all include single station verification techniques in presenting results of AMPS model performance. Within this study, numerical model data at 3 hourly intervals from the analysis out to +48 hours were extracted at several key sites around Antarctica and the Southern Ocean, coincident with, or very close to, synoptic and upper air stations. Time-height profiles of temperature, wind, moisture, vertical motion and geopotential height were saved from each run of the model for comparison with surface and upper air observations. Similarly, GASP model data, at 6 hourly intervals were also collected for the key sites for comparison with

the ALAPS output. Basic bias and root-mean-square error statistics will be presented along with an analysis of the forecasting success of the ALAPS model at significant locations around Antarctica and the Southern Ocean.

Before discussing the single station verification results for the 12 month ALAPS verification period, an analysis of S1 skill scores, and single station verification results, are presented for a short sequence of model runs over the first three weeks of January 2001. The short analysis was undertaken in order to assess the optimum assimilation cycle to use in the ALAPS running, and to also provide a reference performance data-set for assessing future improvements to both the ALAPS analysis and prediction cycles. The S1 skill score assessment of ALAPS was performed over the same high seas domain described in chapter 2, (70^{o}S to 50^{o}S, 120^{o}E to 160^{o}E), and compared against GASP S1 skill scores for the same time period, and over the same domain. A comparison is also made of LAPS and GASP S1 skill scores over the Australasian region, for the same time period.

4.1 Analyses

In the study of numerical model performance over Antarctica, Adams (1997) concluded that one of the obstacles to acceptable numerical model performance was the relatively poor performance of the model analysis and assimilation systems. With very little data to assimilate the analyses were often not far removed from the first guess field used, resulting in acceptable skill scores when the models were verified against their own analyses but with poorer skill evident when compared to manual analyses which had the benefit of a more complete observational data set, and the inclusion of analysis

techniques employing visible and infrared satellite imagery. In a more recent study, Pendlebury et al. (2003) concluded that in a broad sense the analyses from the numerical models had reached a level that provided useful representations of synoptic scale systems over high latitudes. However, improvements were needed in the temporal and spatial resolution of observational data available to the analysis and assimilation cycle before numerical model output at high southern latitudes was as effective as in the mid and low latitude areas of the world. Pendlebury et al. (2003) also noted that model performance over the interior of Antarctica was of limited operational use, highlighting that the most probable cause for the model deficiencies was a lack of observational data, and the difficulties in adequately representing the orography.

With the introduction of the medium (27.5 km) resolution ALAPS limited area model, the influence of a poorly defined model orography, to a major extent, has been removed, and the analysis-assimilation cycle ought to be able to better resolve dynamical forcing attributable to orographic effects, and so have a positive impact on the quality of the starting analyses. However, the analysis-assimilation process is complex, and deciding on how best to initialise NWP systems is a difficult task. When this study began the model was initialised using an assimilation process employing two analyses (at -6 hours and 0 hours), and with a digital filter initialisation, as described in chapter 3, invoked. However, on occasions the starting analyses prepared by the ALAPS assimilation system were obviously poor when assessed against surface observations from around Antarctica, and despite those same surface observations being used in the analysis. Trying to assess

whether the analysis code was at fault, whether the digital filter initialisation was introducing errors, or whether some observation types were causing the problems was difficult. Mass flux adjustment was touted as a possible cause, as was the initial employment of cold starts off the GASP data, rather than warm starting off the previous ALAPS output. This conundrum was best highlighted by assessing both the S1 skill scores and single station time-series model forecasts for several different assimilation methods. By running the model in several different modes it was hoped that the problems associated with analysis and forecast errors could be isolated, and the optimum assimilation cycle defined. To do this the model was re-run using the different assimilation methods over the first 3 weeks of January 2000, providing 42 model runs. The different assimilation methods included;

1) Full use of the analysis and digital filter initialisation,

2) Employment of the analysis system but with the digital filter initialisation switched off,

3) The analysis switched off and only the digital filter initialisation performed,

4) Analysis and digital filter initialisation used and with mass flux adjustment turned on.

The above four methods were employed using a cold start off the GASP forecast data whereas the following two schemes employed a warm start off ALAPS data from the previous model run with the following methods employed;

5) Analysis and digital filter initialisation used but with no mass flux adjustment,

6) Analysis and digital filter initialisation used with the mass flux adjustment system on.

Although the run of 3 weeks was short the differences between the six model runs were significant. A comparison of S1 skill scores (Figure 4.1) showed

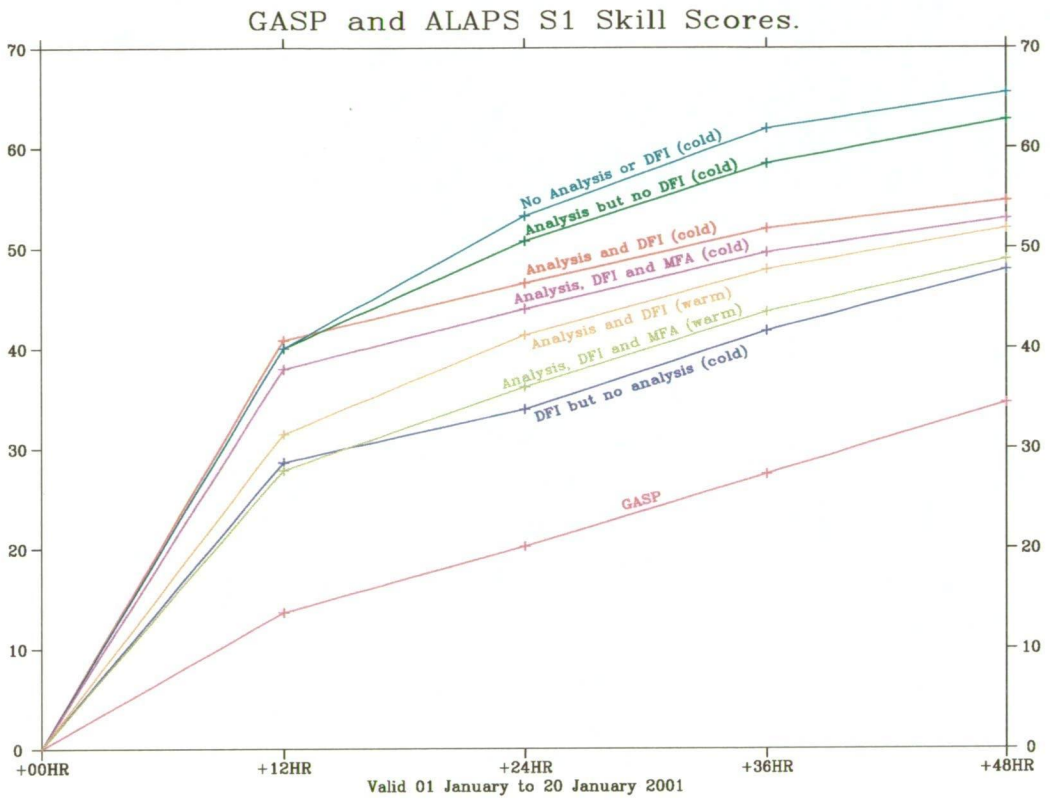

Figure 4.1: Mean S1 skill scores for the first 3 weeks of January 2001 for the 8 different model configurations over the domain 70^{o}S to 50^{o}S and 80^{o}E to 160^{o}E.

that when applying cold starts, the model runs using the analysis but no digital filter initialisation (scheme 2) , produced forecasts at 24 hours significantly poorer than when no analysis was performed and only the digital filter initialisation was used (scheme 3) to modify the first guess field for the model run. Similarly, scheme 1, in which both the analysis and initialisation were performed did not produce forecasts of better skill than simply run-

ning the digital filter initialisation, without any analysis performed (scheme 3), although from Figure 4.1 it would appear that the S1 scores of scheme 1 and scheme 3 were converging as the forecast was integrated forward in time. Employing the mass flux adjustment code did slightly improve the skill of the cold start model runs when running both the analysis and digital filter initialisation code. The S1 score comparison between cold start runs with and without analyses would suggest that the extra computational time expended in performing the analysis was not warranted. However, this conclusion was not justified when single station verification statistics were scrutinised. The comparison of model data with surface observational data from Casey, for this period offered a quite different interpretation. A comparison of output from ALAPS starting analyses with observational data from Casey, where the model had used only the digital filter initialisation, and no analysis, (scheme 3) showed a poor fit of model analysis output to surface observations (Figure 4.2). The storm that occurred between 14 and 18 January 2001, where wind speeds exceeded 40 knots was poorly represented in the scheme 3 analyses, with model winds only reaching 20 knots. However, the ALAPS fit of scheme 2 output, where only the analysis was performed and no digital filter initialisation used was far better, with the late January storm modelled well (Figure 4.3). The starting analyses where both the analysis and digital filter initialisation were performed (scheme 1) performed as well as scheme 2 for the storm event, and overall were more accurate in the fit to both wind speed and direction (Figure 4.4). Applying the mass flux adjustment scheme appeared to have little effect on the starting analysis near Casey (not shown). By +12 hours, the output provided by the differ-

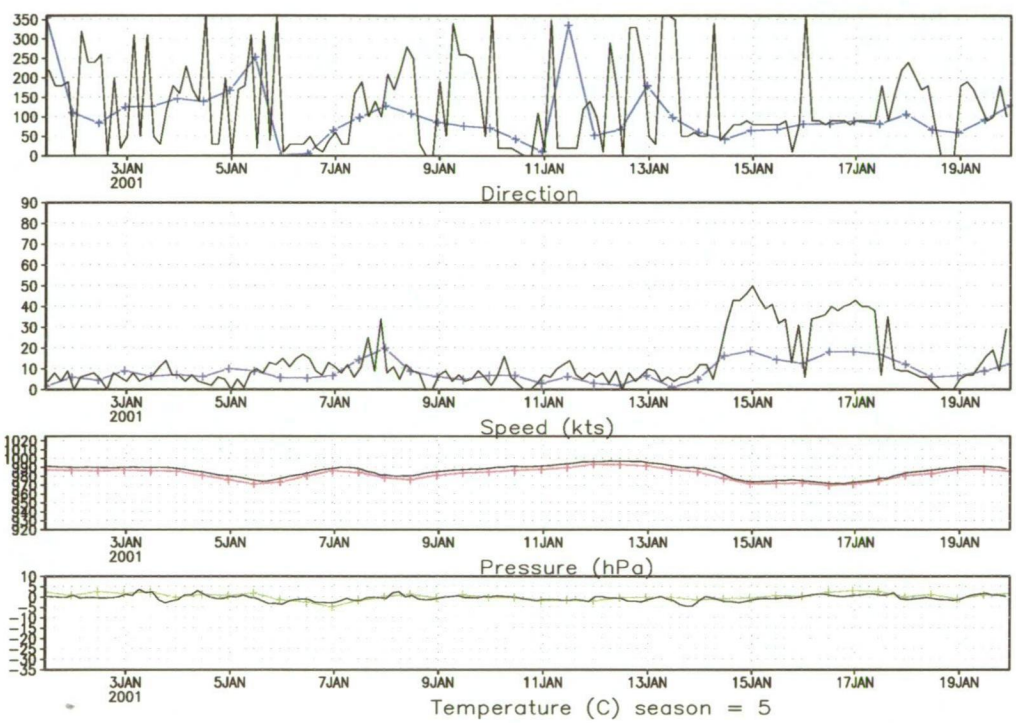

Figure 4.2: Comparison of ALAPS analysed surface data (coloured time-series) with observations from Casey Station (black time-series), for the first 3 weeks of January 2001, where no analysis was performed but the digital filter initialisation was used.

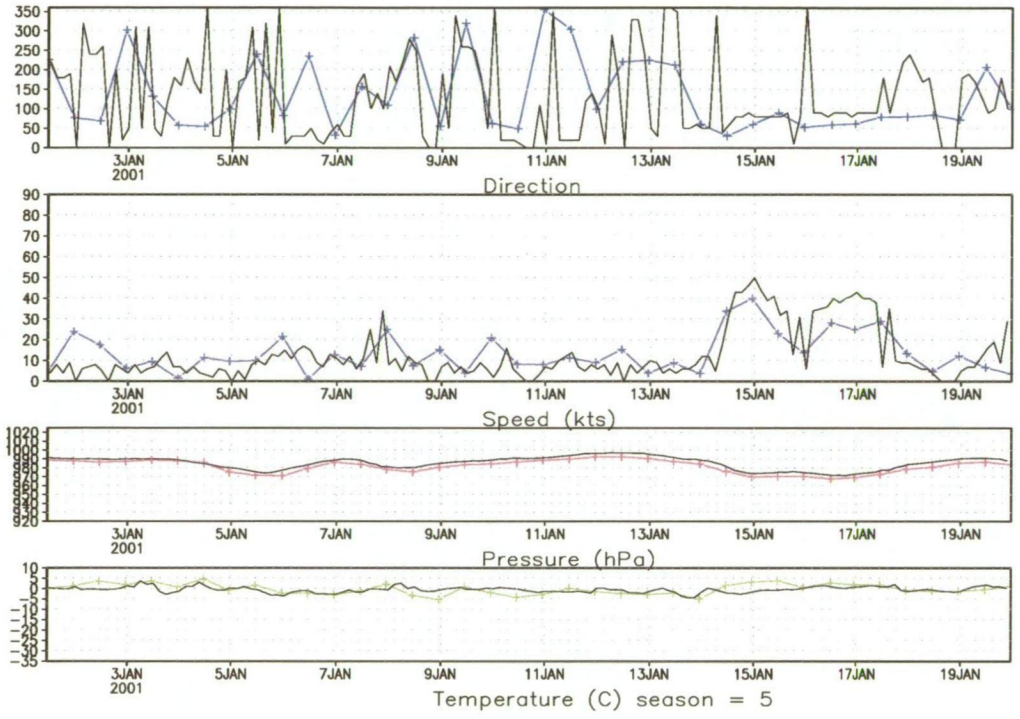

Figure 4.3: Comparison of ALAPS analysed surface data (coloured time-series) with observations from Casey Station (black time-series), for the first 3 weeks of January 2001, where an analysis was performed, but no digital filter initialisation.

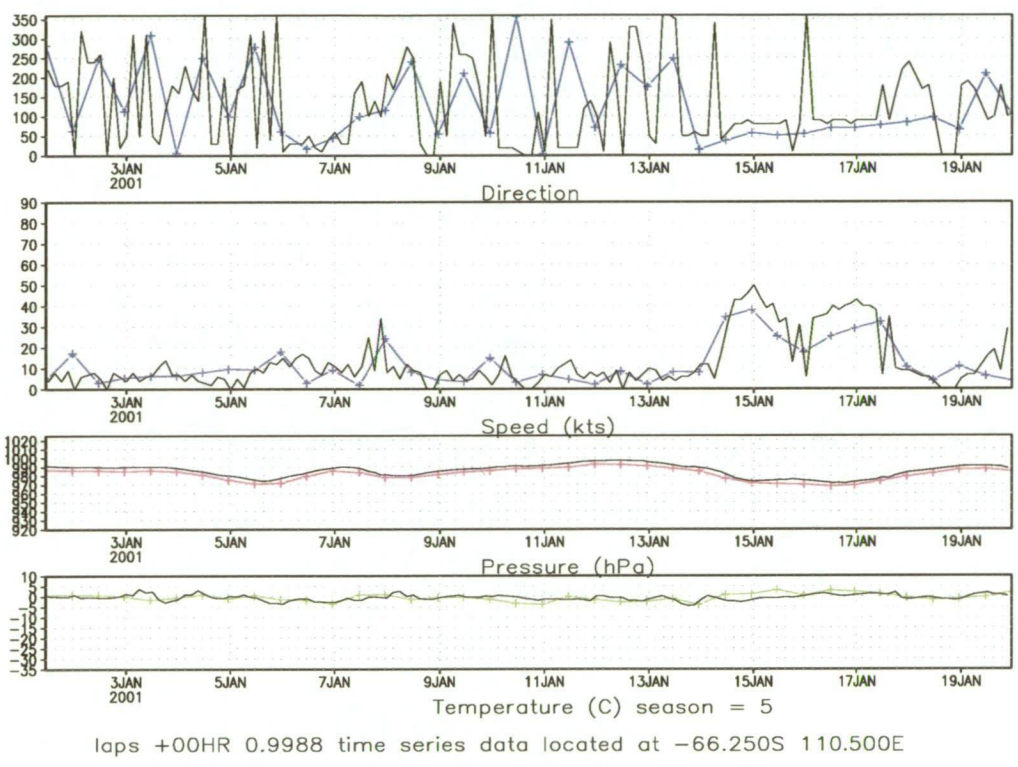

Figure 4.4: Comparison of ALAPS analysed surface data (coloured time-series) with observations from Casey Station (black time-series), for the first 3 weeks of January 2001, where an analysis and digital filter initialisation were performed.

ent schemes suggested that scheme 1, (analysis and initialisation), runs were providing better forecasts, although not significantly better than the scheme 2 forecasts, where no digital filter initialisation was performed. Similarly, running the mass flux adjustment scheme appeared to make little difference to the ALAPS Casey wind forecasts at +12 hours. However, by +48 hours, the scheme 3 forecasts, where only the digital filter initialisation was used, and no analysis, were performing better than other schemes (Figure 4.5),

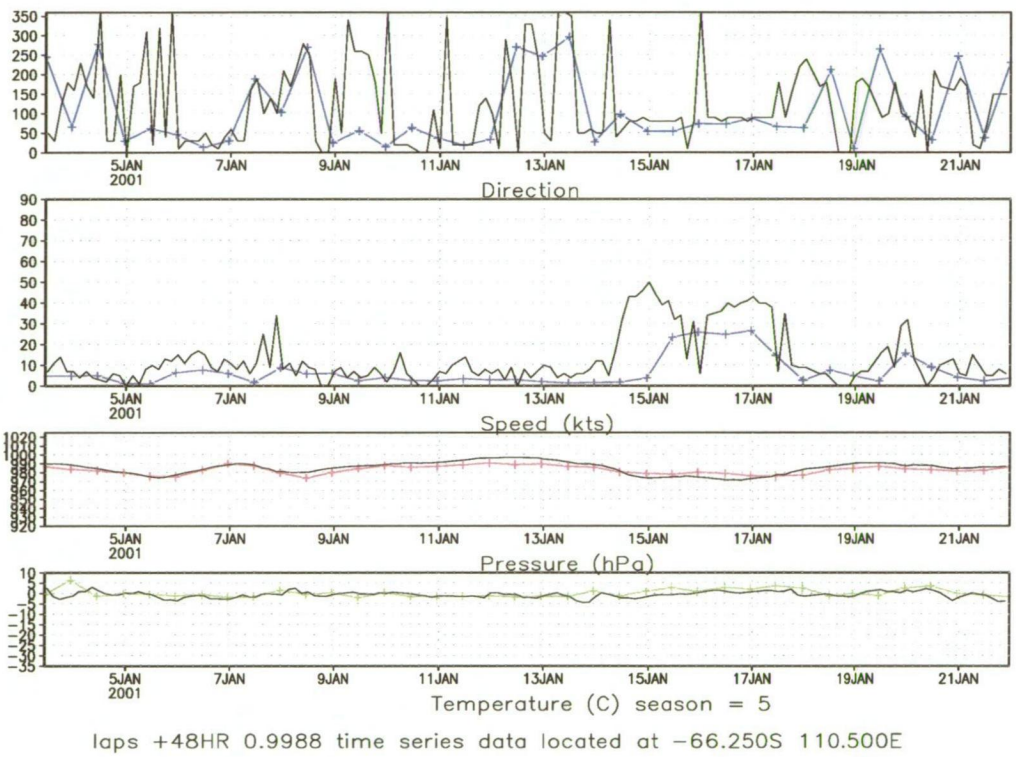

Figure 4.5: Comparison of ALAPS +48 hour surface data (coloured time-series) with observations from Casey Station (black time-series), for the first 3 weeks of January 2001, where no analysis was performed.

with scheme 1 forecasts (full analysis and digital filter) providing the next best wind forecasts (not shown). By +48 hours the mass flux adjustment scheme had significantly degraded the cold start forecasts (Figure 4.6), with the storm late in January effectively non-existent in the model. The mass flux

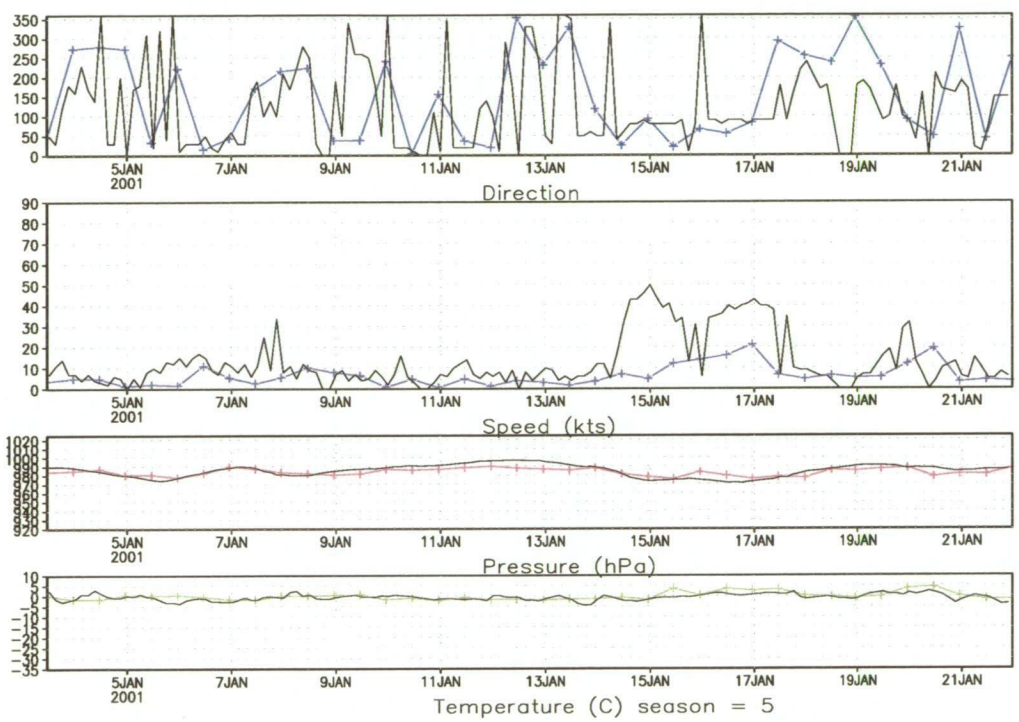

Figure 4.6: Comparison of ALAPS +48 hour surface data (coloured time-series) with observations from Casey Station (black time-series), for the first 3 weeks of January 2001, where the mass flux adjustment was performed.

adjustment scheme when applied to the cold start method appeared to only produced better model output from the analysis out to around +24 hours, with the last 24 hours of model output significantly degraded by the process. It is worth noting that over the 3 week period during January of 2001, the GASP +48 hour forecasts of near surface wind for Casey (Figure 4.7),

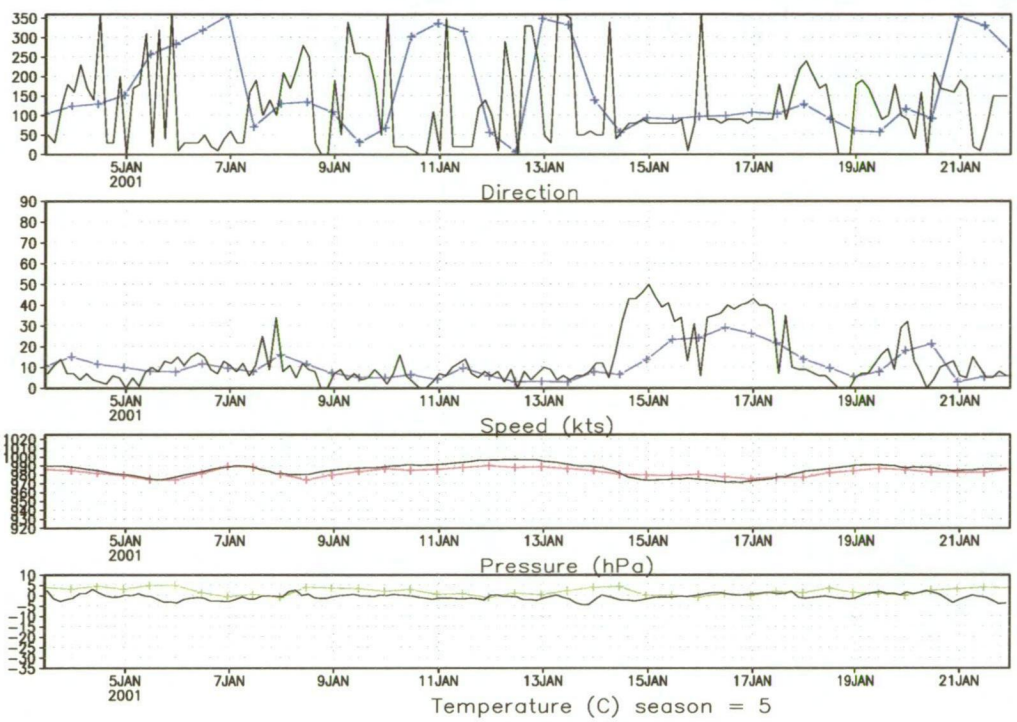

Figure 4.7: Comparison of GASP +48 hour surface data (coloured time-series) with observations from Casey Station (black time-series), for the first 3 weeks of January 2001.

provided better guidance than any of the cold start ALAPS forecasts.

The warm start method, without mass flux adjustment performed better, when considering S1 skill scores, than the cold start scheme 1 method (analysis and digital filter initialisation, but with no mass flux adjustment), although did not perform as well as the cold start method where only the digital filter initialisation was performed (Figure 4.1). Comparison of the

Casey time series data using the warm start method, without mass flux adjustment, indicated that the starting analyses of the scheme (not shown), although much better than GASP (not shown), were not as good as the cold start ALAPS analyses, with several instances of higher than expected wind speeds. However, by +24 hours, the forecasts of wind speed and direction from the warm start method were better than GASP, and all of the cold start schemes, and similarly, at +48 hours the warm start scheme was out-performing the other cold start model runs (Figure 4.8).

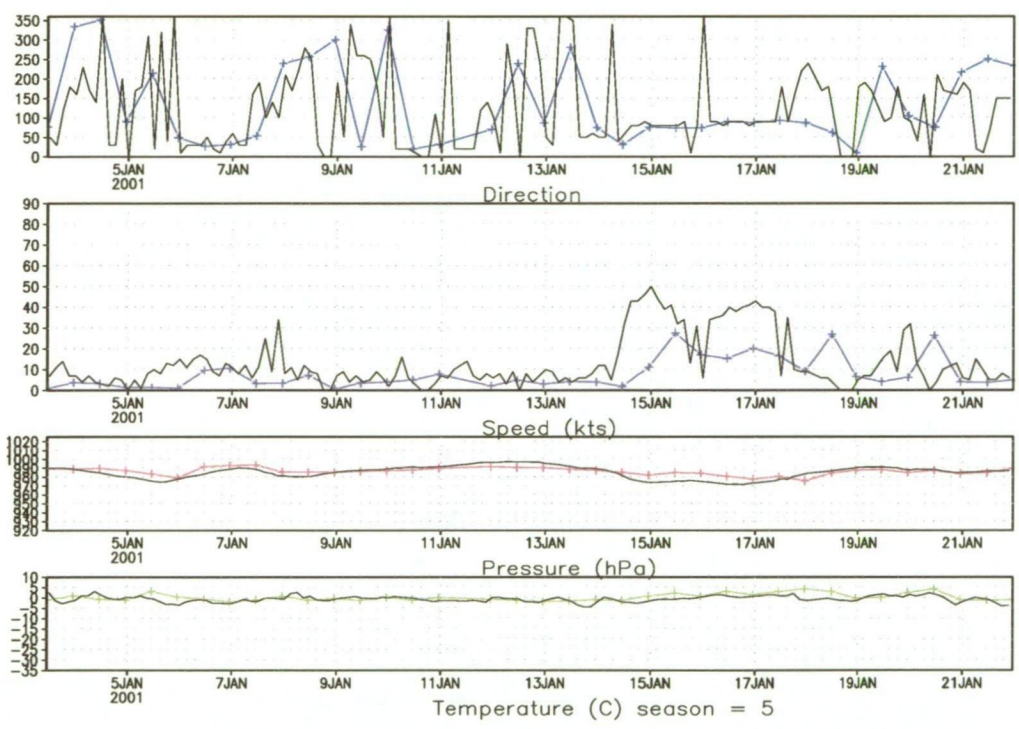

Figure 4.8: Comparison of ALAPS +48 hour surface data (coloured time-series) with observations from Casey Station (black time-series), for the first 3 weeks of January 2001, where a warm start was performed.

On the basis of the performance of the different schemes, the 12 month trial run of the ALAPS system was set up to employ a warm start analysis cycle, including use of the digital filter initialisation scheme, but with the

mass flux adjustment scheme turned off. During the pre-trial runs over the first three weeks of January a test of the warm start method with the mass flux adjustment scheme included was not made, due to the degradation of forecasts beyond +24 hours seen in the cold start runs. Subsequent to the 12 month trial, the warm start system was re-run over the first three weeks of January 2001, with the mass flux adjustment code used, and in fact the adjustment code not only contributed to an improvement in the S1 skill scores, of around 4 skill score points over the 48 hour forecast run (Figure 4.1), but also produced an improvement in the wind forecasts at Casey over the 3 week period, right out to +48 hours (Figure 4.9), with the late January

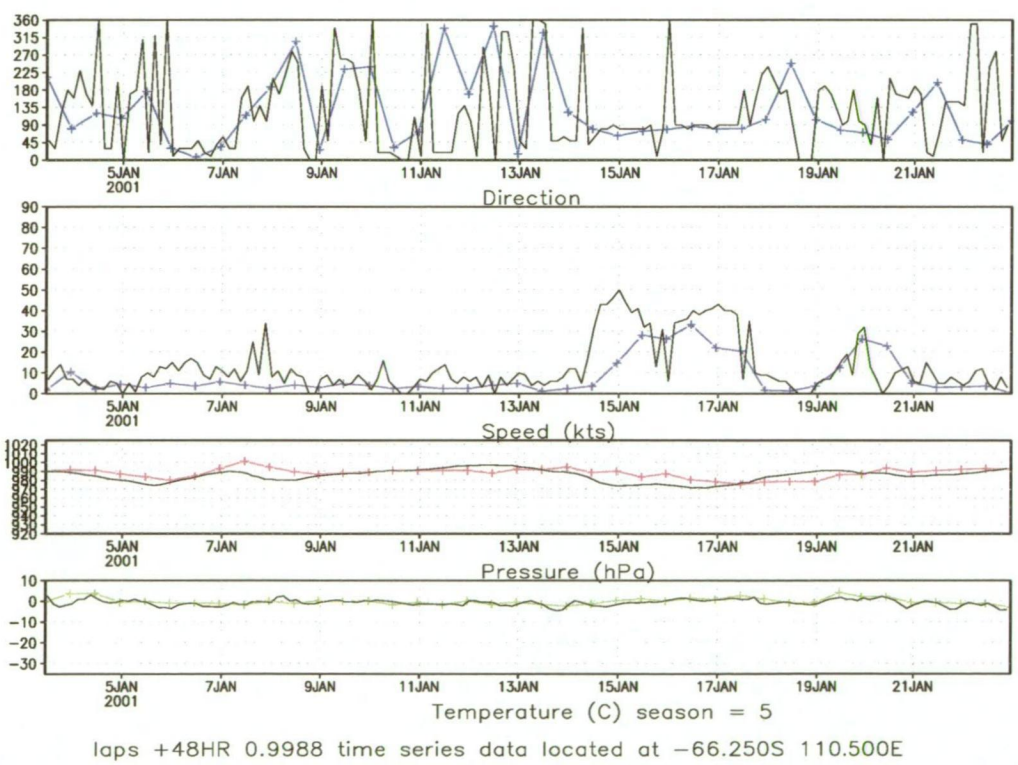

Figure 4.9: Comparison of ALAPS +48 hour surface data (coloured time-series) with observations from Casey Station (black time-series), for the first 3 weeks of January 2001, where a warm start and mass flux adjustment were performed.

storm better forecast in both strength and duration, and also with a far better forecast of the strong wind event that occurred on 20 January 2001.

Trying to assess the best assimilation cycle to use in the forecast system was complex. Quite different starting analyses appear, after some time (> +24 hours) to make little difference to the forecast output, but in the short term (0 to 12 hours), had a significant impact on the forecast quality. Given, that model output from the ALAPS system was not likely to be available in the first 12 hours of model integration, due to run-time considerations, it was decided that the assimilation cycle most appropriate would be a warm start, using output from the previous ALAPS run, with two analysis cycles (-6 and 0 hours), and with the digital filter initialisation performed on both the short 6 hour model integration and the full 48 hour model run. As mentioned above, at the time it was decided that the mass mass flux adjustment scheme would not be used, however in future operational implementations of ALAPS the scheme should be used.

Throughout the trial running of ALAPS it became apparent that regular, significant errors in the analysis of surface pressure and wind were occurring over the Antarctic continent. These errors would present themselves as high-low pressure couplets over the continent, in the analysis that would then generate spurious wind fields during the digital filter initialisation, and first few hours of the model integration. Further investigation focused on the relative impact of different observation types, and in particular the observations from the Antarctic interior. Automatic weather station (AWS) data and pseudo observations (PAOBS), generated by the National Meteorological Operational Centre (NMOC) Melbourne, from mean sea level pressure

(MSLP) analyses, were found to have a large negative impact on the starting analyses. The PAOB MSLP data were causing major problems, due to the very high topography and large errors generated when the inferred MSLP was reduced to surface level pressure (SLP) over the continent. The analysis scheme only assimilated surface level pressure data from the AWS network, with the AWS pressure data hydrostatically reduced from the actual topographic height of the AWS to the coincident height of the model topography. Although differences between the actual topographic height of the continent, and model topographic heights were small, the AWS pressure data often produced significant, non-physical increments (observation - first guess). The most likely cause of the errors was the hydrostatic approximation not adequately accounting for the often, very large surface inversions that exist over the continent for significant portions of the year. It was also possible that the pressure sensors used by the AWS were not properly calibrated, or the assigned height of the AWS station was in error. Investigation of the AWS locations, and best known altimeter heights for the assigned locations suggested that AWS height assignment wasn't a problem, leaving pressure sensor error, or pressure reduction problems associated with a strong surface inversion as the most likely cause. What ever the error source, the magnitude of the increments to the surface pressure field were often as much as +/- 6 hPa. Once the digital filter initialisation had been performed, the resulting balance between the wind and mass field resulted in gross and unrealistic surface wind fields over the continent and coast fringe. In light of the problems associated in locating the errors it was decided to exclude high continental surface observations (AWS and PAOBS) from the analysis scheme.

4.2 Forecasts

As mentioned in the previous section, one of the key problems of the S1 skill score is in deciding what is the best analysis against which to verify the forecasts under investigation. Also, differing starting analyses can, after a short period of time (~24 hours), end up producing similar forecast guidance. So it becomes difficult to assess whether the S1 skill score measures the performance of the forecast, or is a measure of the quality of the starting analysis. Detailed analyses of MSLP, on the the scale of the ALAPS domain are not routinely prepared, so quality, independent, verifying analyses were not available upon which to calculate the S1 skill scores and so reasonably assess model performance. There is also the added problem of comparing S1 skill scores between models of different resolutions. Figure 4.10 shows the annual average S1 skill scores, over the period July 2001 until June 2002, for the +12, +24, +36 and +48 hour forecasts, over both the Australian and Antarctic S1 skill score domains. The skill of a persistence forecast, over both domains, has been added as a relative measure of how well the models performed. Over the Australian domain the GASP model consistently outperformed LAPS by 1 to 2 skill points, which was most probably due to the lower resolution of the GASP model, and not necessarily indicative of GASP providing superior forecasts over LAPS. High resolution models are able to forecast tighter pressure gradients, but small errors in the location of tight gradients are penalised in the S1 score, leading to the possibility of higher S1 values than models of a lower resolution. Over the Antarctic domain the comparison between GASP and ALAPS was not so simple. Persistence forecast skill over the Antarctic domain was comparable to that of

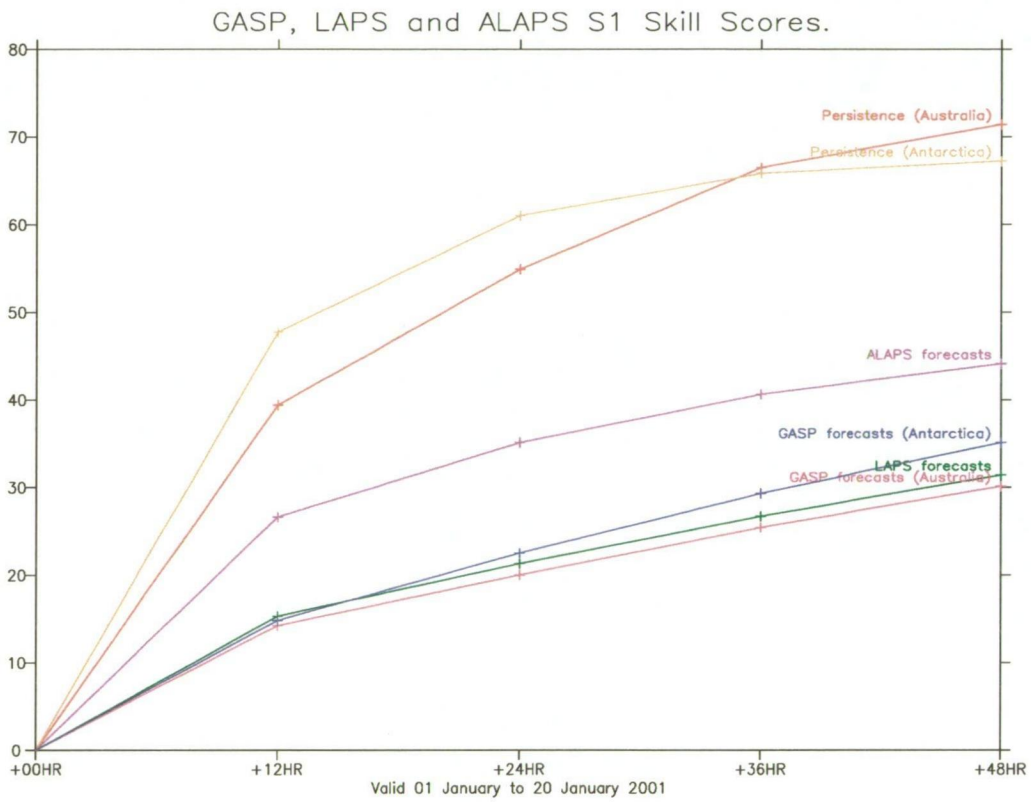

Figure 4.10: A comparison of S1 skill scores over the first 3 weeks of January 2001, for GASP and ALAPS over the Antarctic domain, and GASP and LAPS over the Australian domain. Persistence scores are also shown over the 2 domains.

the Australian domain, suggesting that weather complexity and variability was comparable between the two regions, and significantly, the GASP S1 scores at +48 hours were only, on average, 5 points worse than over the Australian region. However, the ALAPS skill was some 10 points worse than GASP over the Antarctic domain, a considerably larger difference than that seen between GASP and LAPS over the Australian region. It is unlikely that the difference can be entirely attributable to the differences in model resolution as such a large difference is not seen over the Australian region. Given that the ALAPS S1 scores are calculated using the ALAPS analyses it would seem that the starting analyses are a likely source of error. In fact, it is worth noting that the performance of the ALAPS forecasts improved dramatically, with a 10 skill score point reduction at +24 hours , when verified against GASP analyses, rather than the ALAPS analyses. Similarly, the GASP +24 hour forecasts suffered about a 15 point skill score increase when verified against the ALAPS analyses, which placed the ALAPS and GASP forecast on a nearly even score, provided ALAPS analyses were considered "perfect".

If optimising the S1 skill score was considered a key factor in providing the best forecast support, then the ALAPS analyses and resulting forecasts would be questionable, and the GASP model would be considered a superior product to the higher resolution ALAPS, and the computational expense of running ALAPS would not be justified. However, the chief role of NWP, in the context of this study, is in providing both single station forecasts for key locations around East Antarctica, and local area forecasts on a scale of 50 to 2000 km, and model performance needs to be assessed on this basis.

The following sections provide an analysis of the ALAPS performance for each of the Australian Antarctic stations and for the French coastal station of Dumont d'Urville and inland station at Dome Concordia.

4.2.1 Casey

For the single station verification study, numerical model data at 3 hourly intervals, from the analysis out to +48 hours, were extracted from several grid points coincident, or very nearly coincident, with synoptic observation sites around East Antarctica. Time-height profiles of all model fields were saved from each GASP and ALAPS model run for the 12 month period from July 2001 to June 2002. Figure 4.11 shows the time series plot of +24 hour

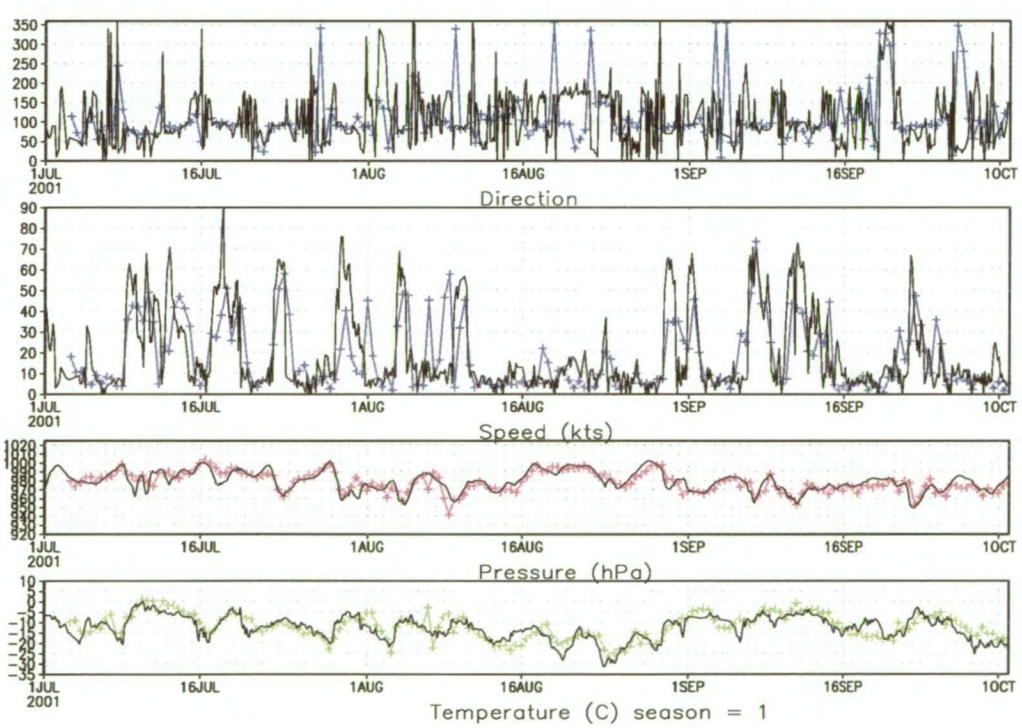

Figure 4.11: Comparison of ALAPS +24 hour surface data (coloured time-series) with observations from Casey Station (black time-series), for the 3 month period from 1 July 2001.

ALAPS forecast first sigma level data (σ=0.9988) at 66.25^{o}S, 110.5^{o}E, overlaid with observational data from Casey Station (66.279^{o}S, 110.536^{o}E) for the 3 month period from 1 July 2001 to 1 October 2001. Casey observational data are plotted as the black lines, with the ALAPS model data plotted in colour. The top panel is of wind direction, in degrees true, the second panel wind speed, in knots, and the third panel mean sea level pressure, in hPa, with the ALAPS forecast surface pressure, and the bottom panel shows air temperature (^{o}C). Figure 4.12 shows the same plot, but comparing out-

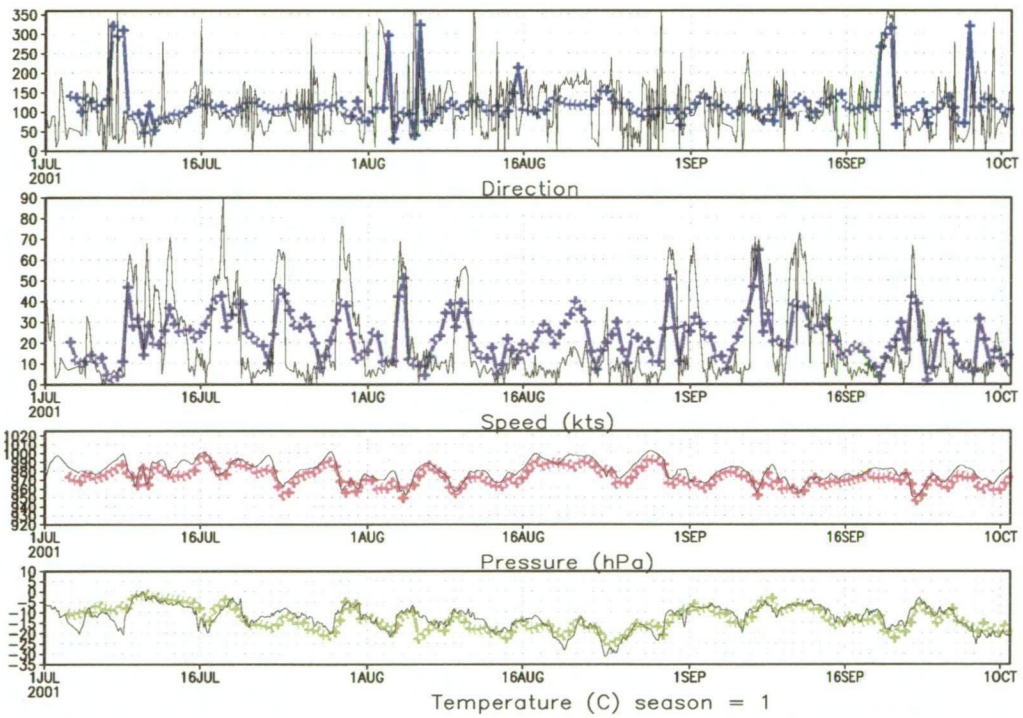

Figure 4.12: Comparison of GASP +24 hour surface data (coloured time-series) with observations from Casey Station (black time-series), for the 3 month period from 1 July 2001.

put from the GASP first sigma level fields (σ=0.991), with Casey surface observational data (observational data in black and model data in colour). Both Figure 4.11 and Figure 4.12 are only a sub-set of the full 12 months

of data, however, statistics from the entire 12 months have been calculated with biases, root mean square errors (RMSE), and bias corrected RMSE errors generated for near surface temperature, dew-point and wind speed, and surface pressure. Figure 4.13 highlights the errors for ALAPS, with Fig-

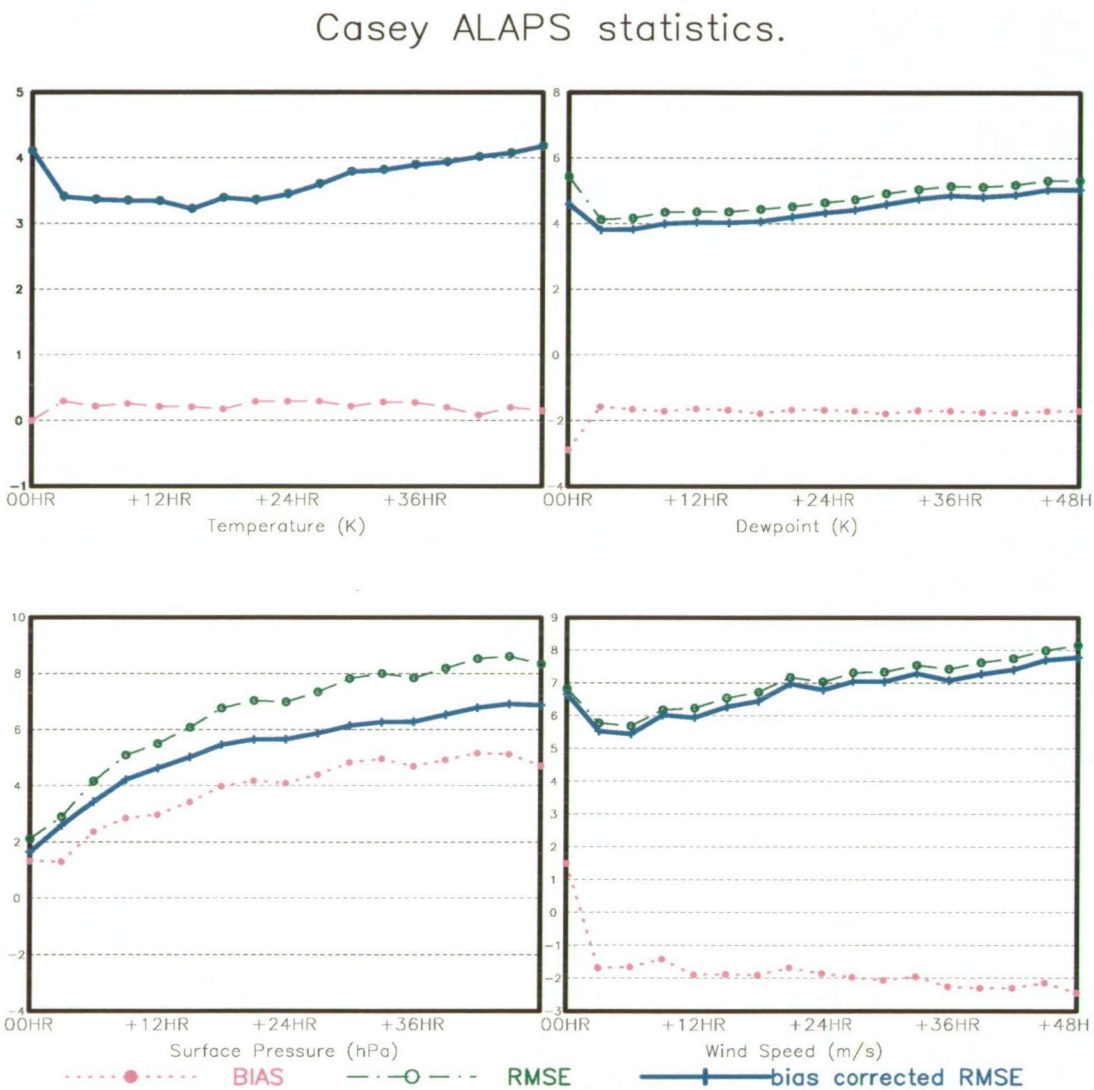

Figure 4.13: Bias, RMSE, and bias corrected RMSE statistics for ALAPS forecasts of Casey near surface weather parameters.

ure 4.14 those for GASP. In general, both GASP and ALAPS were good in forecasting temperature with both models showing a bias corrected RMSE of

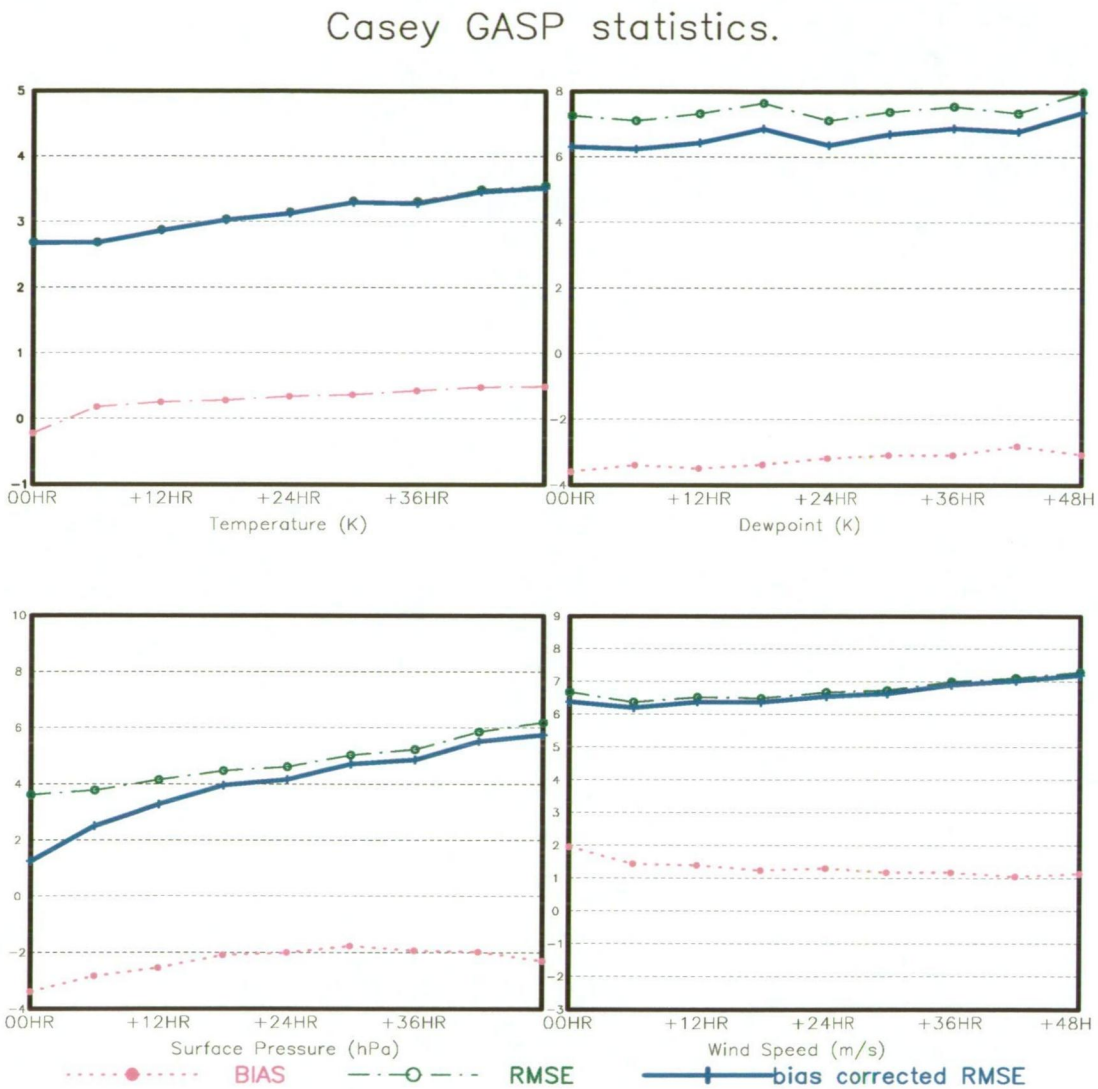

Figure 4.14: Bias, RMSE, and bias corrected RMSE statistics for GASP forecasts of Casey near surface weather parameters.

around 3K, ALAPS was however, better than GASP in forecasting moisture, with a lower bias and bias corrected RMSE 2K better than GASP. Surface level pressure forecasts were similar, with GASP marginally better but with the wind speed forecasts there were some significant differences. GASP displayed a positive bias of around 2 ms^{-1}, whereas ALAPS had a negative bias of around 2 ms^{-1}. Both models showed bias corrected RMSE values of around 6 to 7 ms^{-1} which were considered large. Perusal of the time series profiles (Figures 4.11 and 4.12), highlighted the fact that GASP in general, over-forecast the wind speed between storm events, whereas ALAPS did well in forecasting the general ambient flow at Casey. Both models generally under-forecast the strength of the storms, which resulted in the small negative bias seen with the ALAPS wind speed forecasts. The positive wind speed bias seen in the GASP data was despite the model under-forecasting wind speed during storm events. Figure 4.13 highlights significant problems associated with the ALAPS analysis scheme in the Casey area. In all fields, apart from surface pressure, there was a significant, large RMSE value at the analysis time-step, with the errors dropping in the first few hours of model integration and, not decaying back to the analysis level until well into the 48 hour run.

Comparison of the ALAPS and GASP model errors, showed similar results, with little in the way to suggest that the ALAPS output provided any enhanced forecast guidance. However, in the forecasting of significant weather at Casey, strong wind events are of primary importance as the often excessive wind speeds (in excess of 50 knots), coupled with reduced visibility in blowing snow adversely affects the majority of operations. To further

assess the ability of each of the models to forecast gale or storm force wind over the full 12 month period, the wind speed data were analysed and model output checked against gale or storm criteria. There were 28 storms identified during the 12 month period, where an event was classified as a storm if at least 2 consecutive 3 hour observations of the the 10 minute average wind speed equaled or exceeded the storm force lower limit of 48 knots. There were another 28 events in which 2 consecutive observations of the 10 minute average wind either equaled or exceeded the gale lower limit of 34 knots. Table 1 highlights the forecast ability of both GASP and ALAPS in forecasting storm

	GASP	GASP	ALAPS	ALAPS
Storms	Successes	False Alarms	Successes	False alarms
+12 hours	6/28	0	8/28	0
+24 hours	4/28	0	8/28	1
+36 hours	5/28	0	8/28	0
+48 hours	4/28	1	4/28	0

Table 1: Forecast success rate on predicting storm force wind events at Casey.

events over the 12 month period with both models showing a low success rate. GASP forecast about 18% of the storms and ALAPS about 28%, but with a very good (low) false alarm ratio for both models. In the case of the gale events (Table 2) both GASP and ALAPS forecast around 28% of events,

	GASP	GASP	ALAPS	ALAPS
Gales	Successes	False alarms	Successes	False alarms
+12 hours	10/28	4	11/28	0
+24 hours	8/28	4	7/28	7
+36 hours	5/28	7	4/28	5
+48 hours	8/28	9	7/28	5

Table 2: Forecast success rate on predicting gale force wind events (no storms) at Casey.

although the false alarm ratio was reasonable poor (high), with between 4

and 9 events forecast that did not occur. If the storm events were simply classified as gales and a forecast success defined if the model wind speed forecast equaled or exceeded 34 knots (Table 3) then the success rate for both

	GASP	GASP	ALAPS	ALAPS
All events	Successes	False alarms	Successes	False alarms
+12 hours	33/56	3	35/36	0
+24 hours	34/56	6	31/56	5
+36 hours	33/56	8	25/56	2
+48 hours	27/56	10	25/56	3

Table 3: Forecast success rate on predicting all wind events > 34 knots at Casey.

models increased substantially with GASP at around 56% and ALAPS at 52% although the false alarm ratio for GASP was significantly worse than for ALAPS. From the time-series of ALAPS and GASP wind speed (Figures 4.11 and 4.12), it was clear that the GASP model was, in general, forecasting wind speeds between storms that were too high, but under forecasting peak wind speeds during gale and storm events. The ALAPS model performed significantly better in capturing the background, between storm, wind regime and generally had a much better forecast of storm strength. The lowest sigma level in GASP was at 0.991, or around 75 m, and so somewhat higher than the 10 m observed wind used in the comparison, which may possibly explain why the model over-forecast the between storm wind speeds, but if the boundary layer wind profile was adequately capturing the dynamics then it would be expected that the GASP model would then also over forecast the storm wind strengths, or at least model the extreme wind speeds seen at Casey better than observed in Figure 4.12. GASP appeared to be capturing the dynamics adequately, as the modelled surface pressure

field was well correlated with the observed MSLP (Figure 4.12). Perusal of the ALAPS 0.9943 sigma level data (approximately 40 m above the surface) from the ALAPS model (not shown) highlighted a much better fit to the extreme wind events, with the wind speed values between storm events still well matched to the Casey observations. Table 4 details the storm statistics

ALAPS	Storms	Storms	Gales	Gales
σ=0.9943	Successes	False alarms	False alarms	False alarms
+12 hours	17/28	0	19/28	2
+24 hours	23/28	3	14/28	5
+36 hours	17/28	2	10/28	6
+48 hours	11/28	2	11/28	8

Table 4: Forecast success rate for predicting gales and storms at Casey.

for ALAPS 0.9943 sigma level data, highlighting the significant improvement in forecast success when comparing Casey observations with ALAPS model wind at around the 40 m level. Table 5 highlights the model success rate

$\sigma = 0.9943$	Successes	False Alarms
+12 hour	44/56	3
+24 hour	39/56	6
+36 hour	33/56	10
+48 hour	29/56	8

Table 5: Forecast success rate on predicting all wind events $>$ 34 knots at Casey.

when a storm event was defined as any wind speed over 34 knots (as per Table 3). As can be seen, ALAPS 0.9943 sigma level forecast wind showed considerable forecast success with an increase in +24 hour forecast skill from 55% to 70%. In the above classification of forecast success, the model had to have forecast either gale or storm force wind, yet in a predictive sense this may be too stringent a measure. For example, if the model were to forecast

a jump in wind speed from around 5 knots to 30 knots, or even 25 knots, the forecaster would be alerted to the potential of a significant wind event and be in a position to assess the likelihood of the actual wind exceeding the model forecast, knowing that the model was biased toward under forecasting wind strength. With the above statistics recompiled with a model success defined as forecasting wind speed to within 15% of the actual strength, then the forecast success of ALAPS improved dramatically, making ALAPS output significantly better than that from GASP. It is also worth noting that wind direction was better modelled in the ALAPS system, with the high resolution model better simulating the variability in wind direction between storms, and more accurately predicting the true storm wind direction. Both GASP and ALAPS performed well in predicting surface pressure and temperature.

4.2.2 Davis

Error statistics of bias, RMSE and bias corrected RMSE data were also collated from GASP and ALAPS forecast data for Davis Station. The ALAPS grid point closest to Davis (68.58°S, 77.97°E) was at 68.5°S, 78.0°E, with the closest GASP grid point at 68.25°S, 78.0°E. Figure 4.15 shows the error statistics from the ALAPS forecasts, with GASP error statistics shown in Figure 4.16. The results for Davis were similar to those for Casey, although the errors in forecast wind from both GASP and ALAPS were somewhat less, which was probably indicative of the more benign wind conditions that are experienced at Davis, where very large storms are less frequent, and not so heavily modified by the local terrain, as they are at Casey. The errors in the ALAPS analysis, noted with the Casey statistics, were also quite ev-

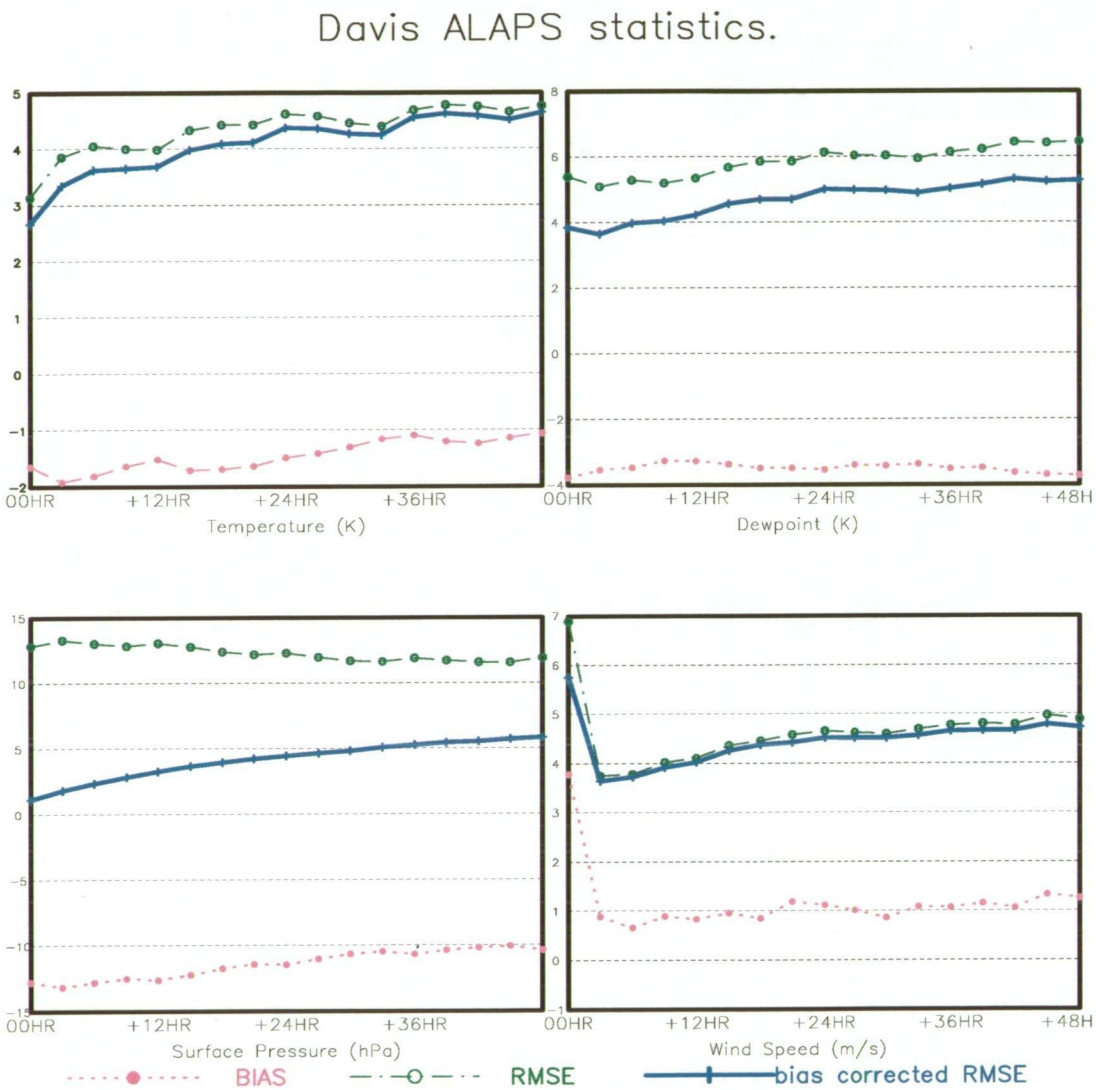

Figure 4.15: Bias, RMSE, and bias corrected RMSE statistics for ALAPS forecasts of Davis near surface weather parameters.

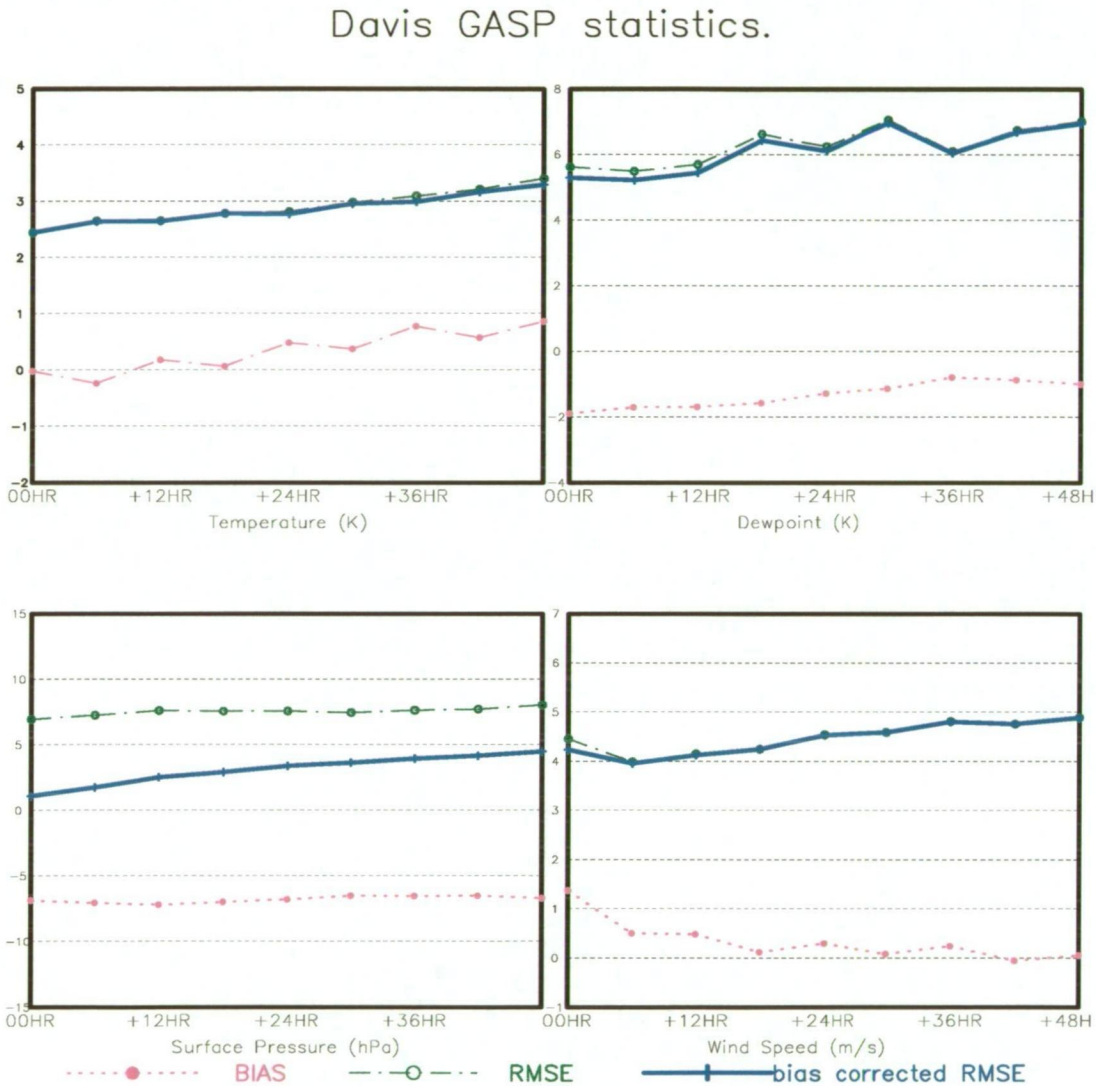

Figure 4.16: Bias, RMSE, and bias corrected RMSE statistics for GASP forecasts of Davis near surface weather parameters.

ident in the surface wind speed errors at Davis, where the bias corrected RMSE dropped from nearly 6 ms^{-1} at the analysis down to below 4 ms^{-1} by +3 hours into the model integration.

Tables 6, 7 and 8 highlight the comparison between GASP and ALAPS

	GASP	GASP	LAPS	LAPS
Storms	Successes	False alarms	Successes	False alarms
00 hours	1/3	3	3/3	22
+12 hours	1/3	0	3/3	2
+24 hours	1/3	0	3/3	4
+36 hours	1/3	0	2/3	3
+48 hours	1/3	0	2/3	3

Table 6: Forecast success rate on predicting storm force wind events at Davis.

Gales	Successes	False alarms	Successes	False alarms
00 hours	14/20	5	17/20	34
+12 hours	10/20	3	9/20	6
+24 hours	6/20	3	10/20	7
+36 hours	7/20	6	9/20	9
+48 hours	6/20	3	9/20	10

Table 7: Forecast success rate on predicting gale force wind events (no storms) at Davis.

All events	Successes	False alarms	Successes	False alarms
00 hours	17/23	5	20/23	34
+12 hours	13/23	3	12/23	6
+24 hours	8/23	3	13/23	7
+36 hours	9/23	6	11/23	9
+48 hours	8/23	3	11/23	9

Table 8: Forecast success rate on predicting all wind events > 34 knots at Davis.

forecasts of gale and storm force wind events at Davis, in an identical fashion to the analysis described above for Casey (Tables 1, 2 and 3). Davis had a

significantly lower number of storm events and also fewer gale events. In general, both GASP and ALAPS performed well in forecasting the strong wind events, with GASP slightly under-estimating the peak strengths and ALAPS over-estimating peak strengths. The ALAPS analyses were particularly prone to significantly over-estimating wind strengths with an excessive number of false alarms, although by +12 hours into the ALAPS run the model had settled down and by +24 hours was out-performing GASP, although still with a slightly higher false alarm ratio. Perusal of the time series graphs for GASP and ALAPS forecasts at the grid point closest to Davis, overlaid with Davis surface observations (not shown), also highlighted the fact that both models performed well in forecasting surface weather conditions at Davis, although GASP did a better job with forecasting surface pressure and also near surface temperature, especially during the winter months. Closer inspection of the two model orographic representations of the Davis area (Figure 4.17), in comparison to the real orography, highlighted the fact that the closest ALAPS grid point used in the above study, was in fact located inland, within the model, on a reasonably steep slope, and at an altitude of near 130 m. The GASP grid point used in the study, was also slightly inland, within the GASP model orography, but further north than the ALAPS point and at an altitude of only 80 m. Both model versions of the Davis orography where subtly incorrect, as Davis is in fact, located on the coast and very near mean sea level (Figure 4.17). The GASP version of conditions, for the chosen grid point, was more closely consistent with reality, while the dynamics associated with ALAPS grid point appeared to have more of an inland signature than is typically not experienced at Davis and would account for the large neg-

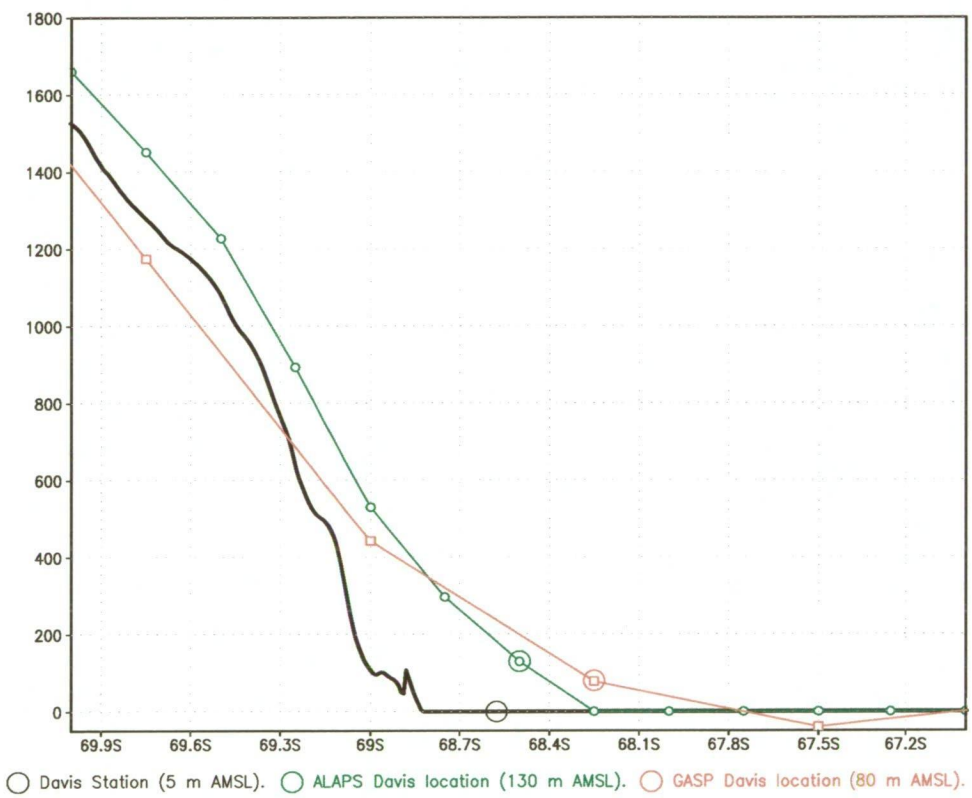

Figure 4.17: North-south orographic details along 78°E, near Davis, from high resolution orography (black), ALAPS model orography (green), and GASP model orography (red).

ative bias observed in the surface pressure and temperature. For example, the ALAPS temperature forecasts displayed a significant diurnal signature during the summer months, which was not evident within the Davis temperature record (lower panel Figure 4.18), and the ALAPS forecast wind

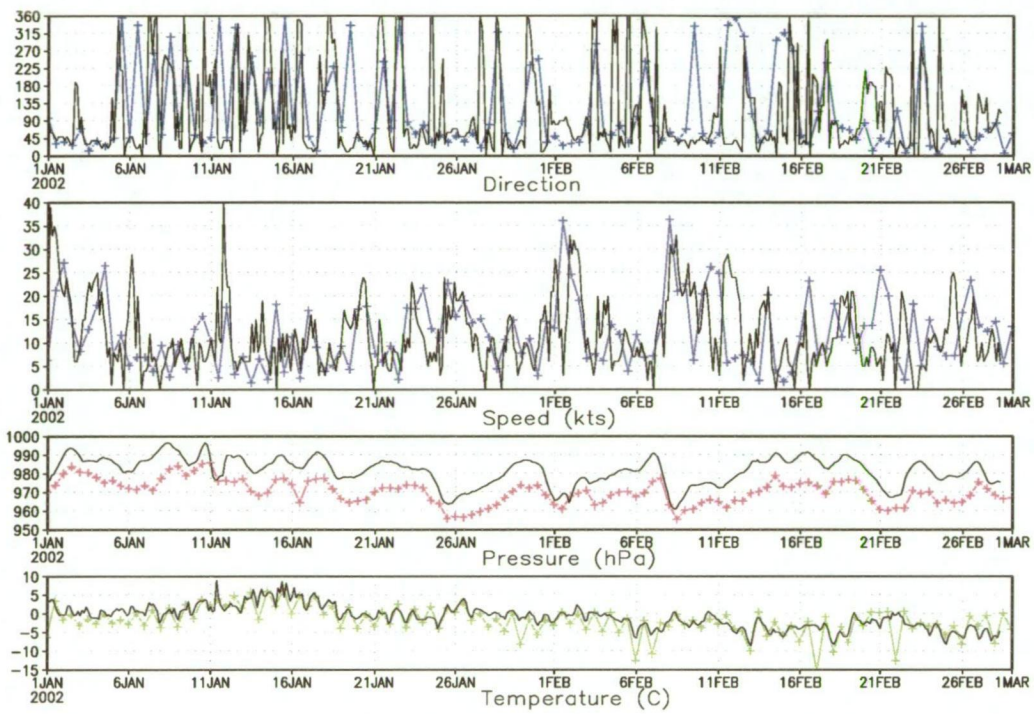

Figure 4.18: Comparison of ALAPS +24 hour surface data (coloured time-series) with observations from Davis Station (black time-series), for the 2 month period from 1 January 2002.

speeds, between strong wind events, appeared to be too high (Figure 4.18), which was also evident in the ALAPS wind speed bias of 1 ms^{-1}. To see if the ALAPS output was unduly affected by the chosen grid point, ALAPS data were extracted from the grid point directly to the north, at 68.25^{o}S, 78.0^{o}E, and coincident with the GASP grid point used in the study. At this location the ALAPS orography was closer to reality, with the point being at mean sea level in the model, although still close to a reasonable slope

(Figure 4.17), which is not the case at Davis. Perusal of the time-series data from the northern ALAPS point (not shown), highlighted several problems with the model data, as a proxy for Davis weather. Although there was a better fit to the station level pressure in the early forecast period, due to the model grid point being at mean sea level, and a better fit to the near surface temperature, the wind data was not well represented. The northerly location experienced onset of strong wind during storm events, on average, some 12 hours prior to the more southerly grid point closer to Davis. This phase shift in the wind speed signal resulted in poorer bias and RMSE values for wind speed and out past 24 hours into the model integration bias corrected RMSE errors for surface pressure were worse. However, the prevailing wind at Davis is from the east northeast so the grid point immediately down wind, to the west of the grid point closest to Davis, was considered a more likely proxy for Davis weather. Figure 4.19 shows the actual and model orographies in the east-west plane through the latitude of Davis and shows the ALAPS grid point immediately to the west to be at sea level, although still with the inland slope in the ALAPS orography non-zero, and not representative of the near zero slope in the actual Davis environs. Bias, RMSE and bias corrected RMSE values for the westerly point showed values very similar to those for the northern point, although with the grid point closest to Davis still having better error statistics for wind speed and surface pressure. The better fit of the temperature and dew-point data for the grid points to the west and north of Davis, suggest that perhaps interpolating surrounding model grid point data may have provided a better fit.

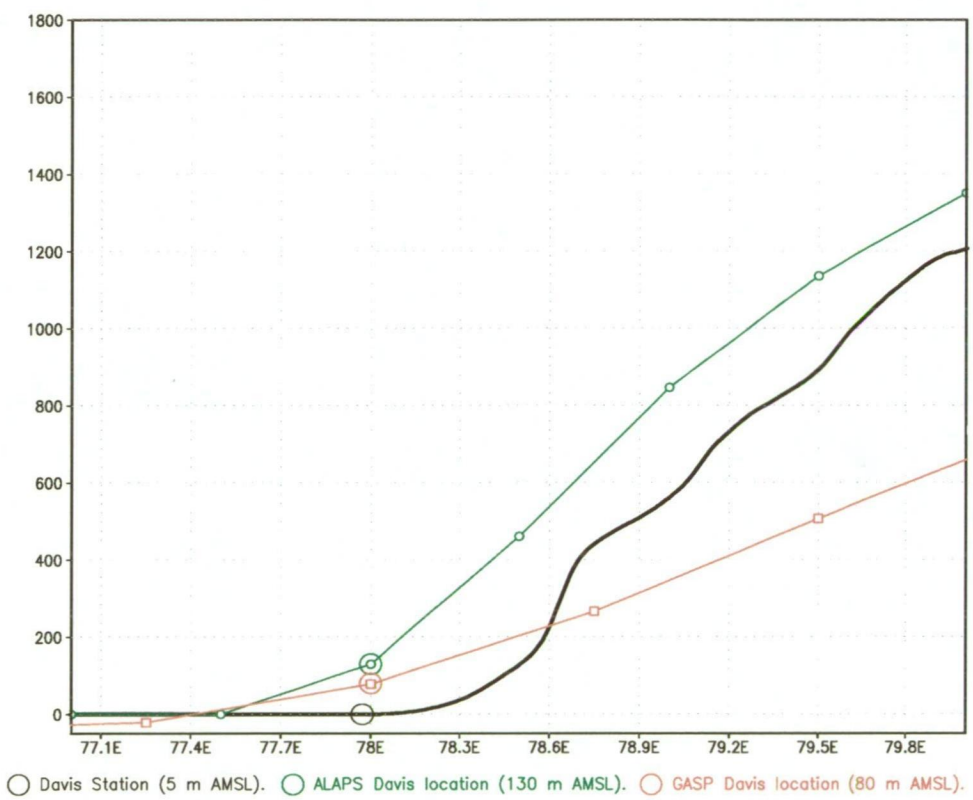

Figure 4.19: East-west orographic details along 68.5°S, near Davis, from high resolution orography (black), ALAPS model orography (green), and GASP model orography (red).

4.2.3 Mawson

A comparison of the bias, RMSE and bias corrected RMSE statistics from ALAPS (Figure 4.20), and GASP (Figure 4.21), for Mawson, shows results

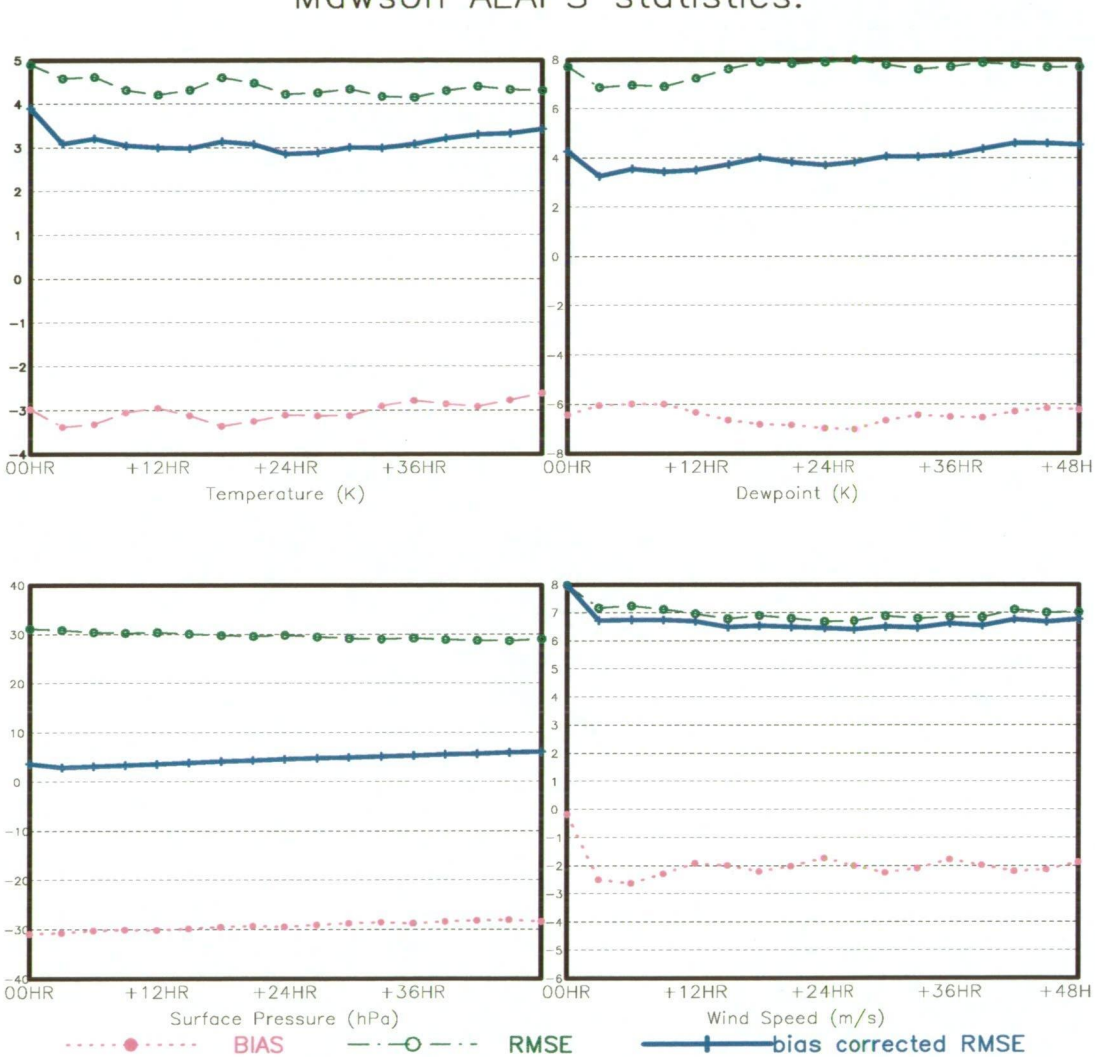

Figure 4.20: Bias, RMSE, and bias corrected RMSE statistics for ALAPS forecasts of Mawson near surface weather parameters.

very similar to Davis and Casey. Very large negative biases in surface pressure for both ALAPS and GASP were a result of the very steep orography in the Mawson area, coupled with both the closest GASP (67.5^{o}S, 63.0^{o}E),

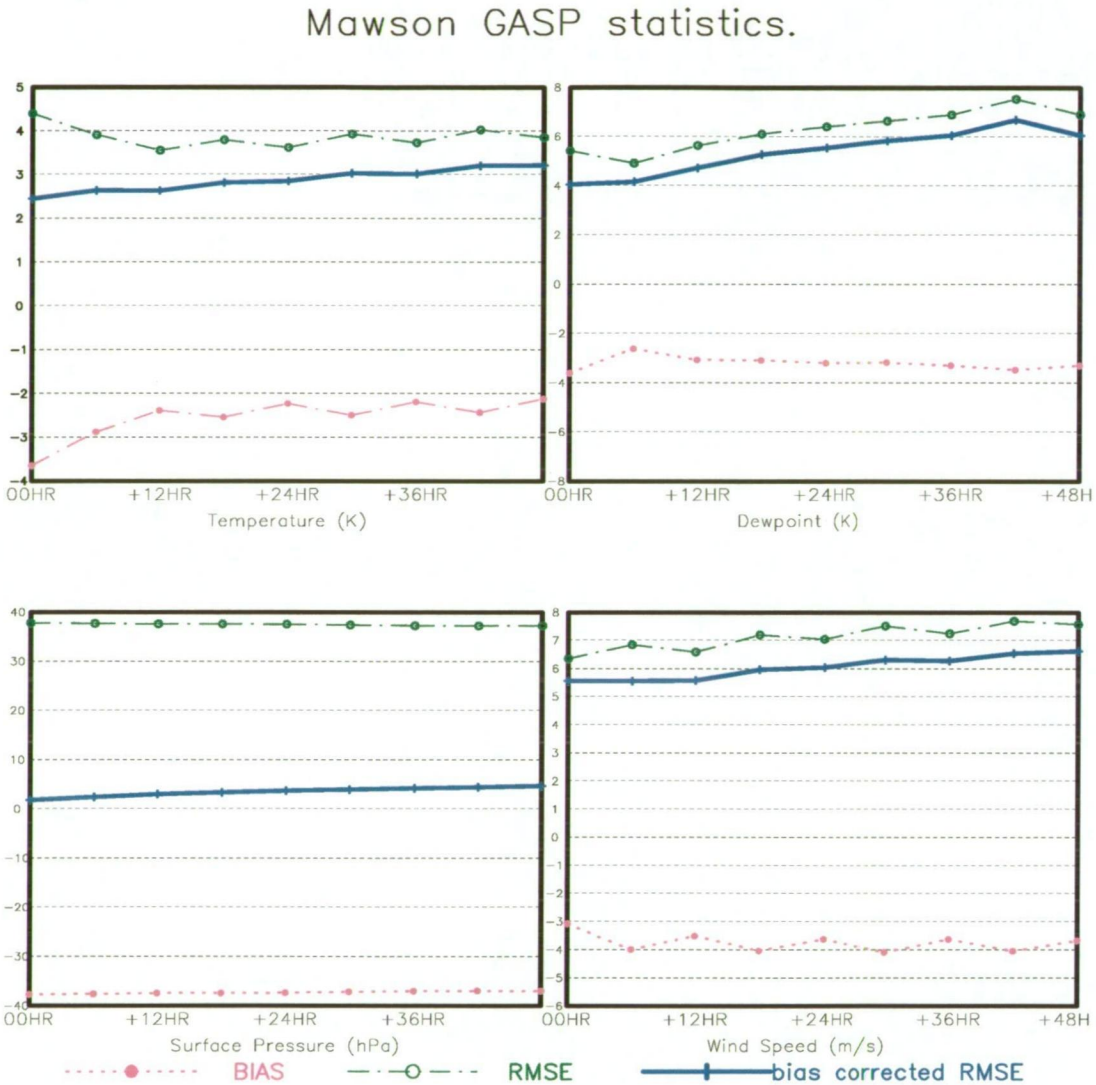

Figure 4.21: Bias, RMSE, and bias corrected RMSE statistics for GASP forecasts of Mawson near surface weather parameters.

and ALAPS (67.5°S, 63°E), grid points lying on steep slopes within their respective model domains, and at some altitude, and distance, from the actual location of Mawson (67.6°S, 62.87°E). However, bias corrected RMSE values for Mawson were similar to the other two Australian stations, although, the bias corrected RMSE values for wind speed were larger than at Davis, and comparable to those at Casey. Mawson, like Casey, is prone to very strong wind events, and forecasting the actual wind speeds during these events, and getting the timing of such events correct is a severe test of any NWP system, and magnitude and timing errors of the model forecasts were reflected in the larger RMSE values.

Perusal of the time series data at Mawson from both the ALAPS and GASP models (not shown) highlighted the fact that differences between GASP and ALAPS forecasts were not so marked as at Casey, with GASP performing better on wind speed and direction in the early forecast period but with little difference out past 24 hours. Table 9 shows the success rate

	GASP	GASP	ALAPS	ALAPS
Storms	Successes	False alarms	Successes	False alarms
00 hours	2/25	0	11/25	9
+12 hours	1/25	0	1/25	0
+24 hours	0/25	1	1/25	1
+36 hours	0/25	1	4/25	1
+48 hours	2/25	0	2/25	0

Table 9: Forecast success rate on predicting storm force wind events at Mawson.

and false alarm statistics for both GASP and ALAPS in forecasting storm force wind events. Although ALAPS analyses significantly more of these events than GASP, the very high false alarm value underscores the problems ALAPS has with the analysis process. From 24 hours out to +48 hours

ALAPS forecasts more of the storm events, although still significantly fewer than were observed. If a wind speed of 40 knots was taken as a forecast marker of a storm event (Table 10) then both GASP and ALAPS perform

	GASP	GASP	ALAPS	ALAPS
>= 40 kt	Successes	False alarms	Successes	False alarms
00 hours	10/25	1	17/25	16
+12 hours	4/25	1	7/25	3
+24 hours	6/25	2	4/25	1
+36 hours	7/25	2	7/25	1
+48 hours	4/25	1	6/25	1

Table 10: Forecast success rate on predicting storm force wind events at Mawson using a model forecast of 40 knots.

somewhat better in forecasting such events, but still miss a significant number of storms. The weather at Mawson is dominated by the surface katabatic flow, with the katabatic signature adding to synoptically forced storm events, to significantly increase observed wind speeds during the passage of deep polar lows. The very steep topography in the local Mawson environs is thought to be the chief driving force of the local wind and even at a resolution of 27.5 km, the ALAPS model does not adequately capture the steepness of the local Mawson terrain. A further discussion of the Mawson terrain and katabatic flow may be found in chapter 5.

4.2.4 Dome C.

Dome Concordia is a joint French-Italian station located located on the high eastern plateau of East Antarctica, on Dome C, some 1080 km inland from the coast and at an elevation of 3280 m above mean sea level. The station is located at 74.5^{o}S, 123.0^{o}E, although, currently, no observations are

available from the station. However, an AWS is located some 70 km away at 75.12^{o}S, 123.37^{o}E. The AWS is one of a series of units located around Antarctica, belonging to the University of Wisconsin (Stearns et al. 1993), with sensors located approximately 3 m above the ice surface. Data from the closest ALAPS grid point, (75.0^{o}S, 123.5^{o}E), was extracted for comparison with the AWS data, with the model wind speed data corrected from a model average first sigma level height of 8 m to the 3 m AWS height, assuming a logarithmic speed profile (Garrat 1992), and using the roughness length employed in the ALAPS model (0.001 m). In the following discussion, temperature data were not corrected to 3 m, so a small bias, due to the disparate heights, was expected. The magnitude of the error ought to be relatively small, following the micro-meteorological study of temperature profiles at Plateau Station (Schwerdtfeger 1984), located at 79.2^{o}S, 40.5^{o}E, and at an elevation of 3625 m. The diurnal variation in temperature over a 25 day period in February 1967 was monitored, with temperatures measured at 0.25 m, 2 m, 8 m and 32 m above the surface. Daily maximum temperatures were almost identical at 2 m and 8 m, with the minimum temperature at 2 m being approximately 2.5^{o}C lower than at 8 m (Fig. 2.6, Schwerdtfeger 1984). Diurnal variations of the 3 m temperature at Dome C, some 4^{o} of latitude further north than Plateau Station, were observed during January 2002, to be around 4^{o}C greater than shown in the Plateau Station data. It would be expected that the 8 m ALAPS temperatures would correlate well with the observed 3 m temperatures, although during summer perhaps be somewhat warmer during the cooler part of the day with the lower 3 m temperature cooling through conduction with the surface. Figure 4.22 shows a comparison

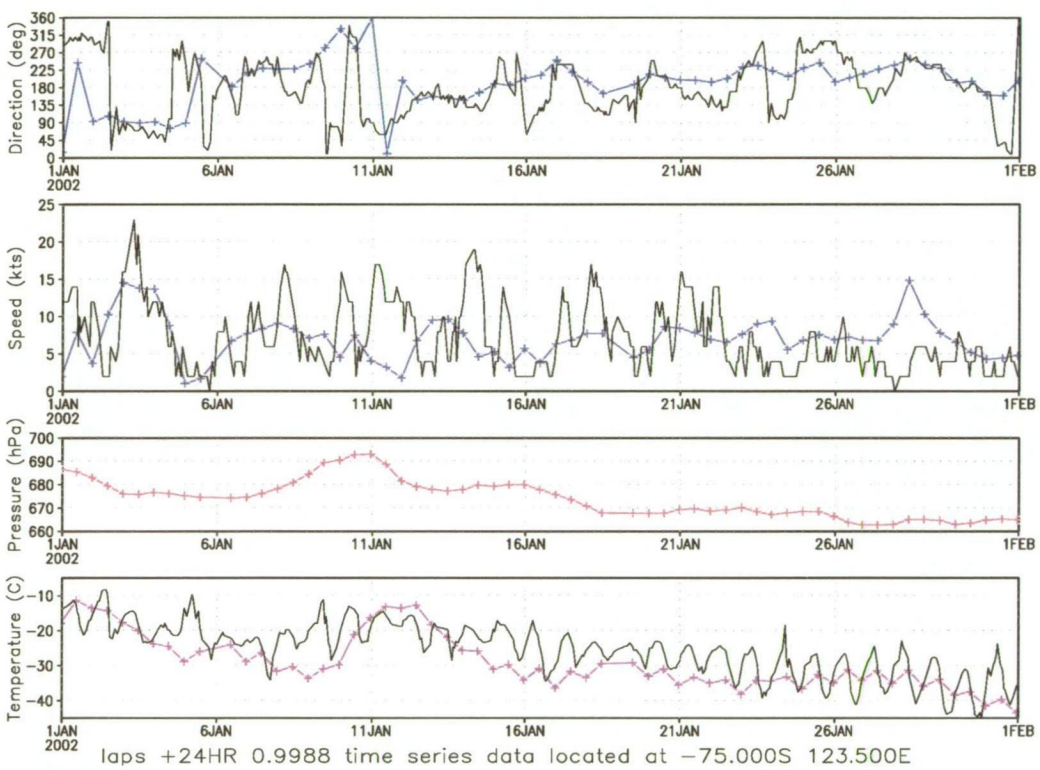

Figure 4.22: Comparison of ALAPS +24 hour surface data (coloured time-series) with observations from the Dome C AWS (black time-series) , for January 2002.

of the observed data from the Dome C AWS (black time-series data), with 12 hourly ALAPS +24 hour near surface forecast data (coloured time-series data) for January 2002, where the ALAPS wind speed has been reduced to 3 m. A strong diurnal signal was evident in the observed temperature data, although the wind speed and direction appeared to be dominated more by synoptic scale features. The ALAPS +24 hour forecast data did a reasonable job of forecasting the wind, although peaks in the wind speed, associated with synoptic scale features were under-forecast. Where the ALAPS forecasts did not perform well, was in capturing the amplitude of the diurnal temperature signal. To further investigate the diurnal attributes of the ALAPS output, time-series data encompassing the full 48 hours of model integration were studied. Figure 4.23 again shows the January 2002 time-series data from Dome C but with 3_hourly model output data out to +48 hours from both the 1100UTC initialised runs (red time-series data), and 2300UTC initialised runs (green time-series data) displayed. In late January Dome C observations showed a diurnal variation of nearly 15^{o}C in temperature, but the ALAPS model forecasts, at best, showed only a 5^{o}C amplitude. It is also worth commenting on the obvious bias between the 2300UTC and 1100UTC initialised runs, with a clearly warmer signal, of over 1^{o}C, in the 1100UTC runs, compared to the 2300UTC runs. Careful perusal of Figure 4.23 highlights the fact that at the time the 2300UTC runs were being initialised, near surface temperatures were approaching the diurnal minimum, with the 6 hour assimilation cycle introducing a further slight cooling to the 2300UTC initial temperature, rather than beginning to warm as would be expected after the diurnal minimum had been reached. Conversely, at the time the 1100UTC

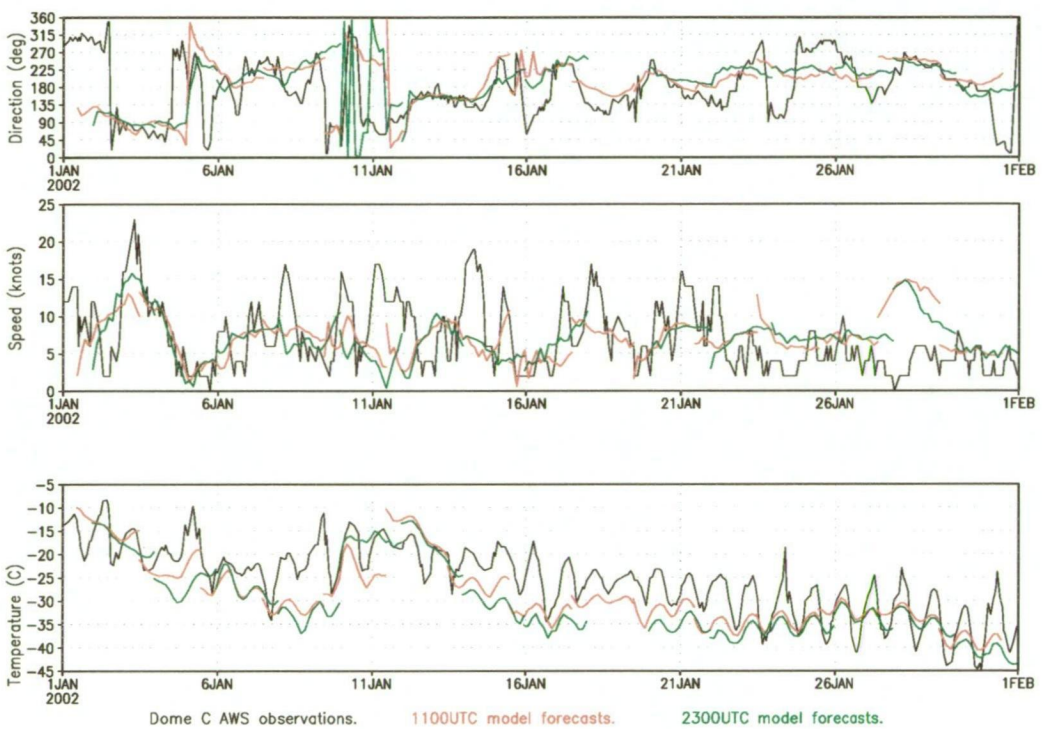

Figure 4.23: Comparison of ALAPS 3 hourly surface data out to +48 hours, from the 1100UTC runs (red time-series), and 2300UTC runs (green time-series), with observations from the Dome C AWS (black time-series) , for January 2002.

runs were being initialised, near surface temperatures were reaching a maximum, and the assimilation cycle continued the warming process rather than beginning to cool near surface temperatures as would have been expected. The radiation code was being called every three hours so should have been adequately handling radiative processes, so it would appear that the 6 hour model integration from the -6 hour analysis forward to the synoptic hour of the model initialisation was not adequately handling the diurnal variation in near surface temperature, suggesting that perhaps a longer assimilation cycle might have been warranted. The temperature discrepancy between 2300UTC and 1100UTC initialised runs was also evident at Mawson during January of 2002 (Figure 4.24) with temperature forecasts from 1100UTC

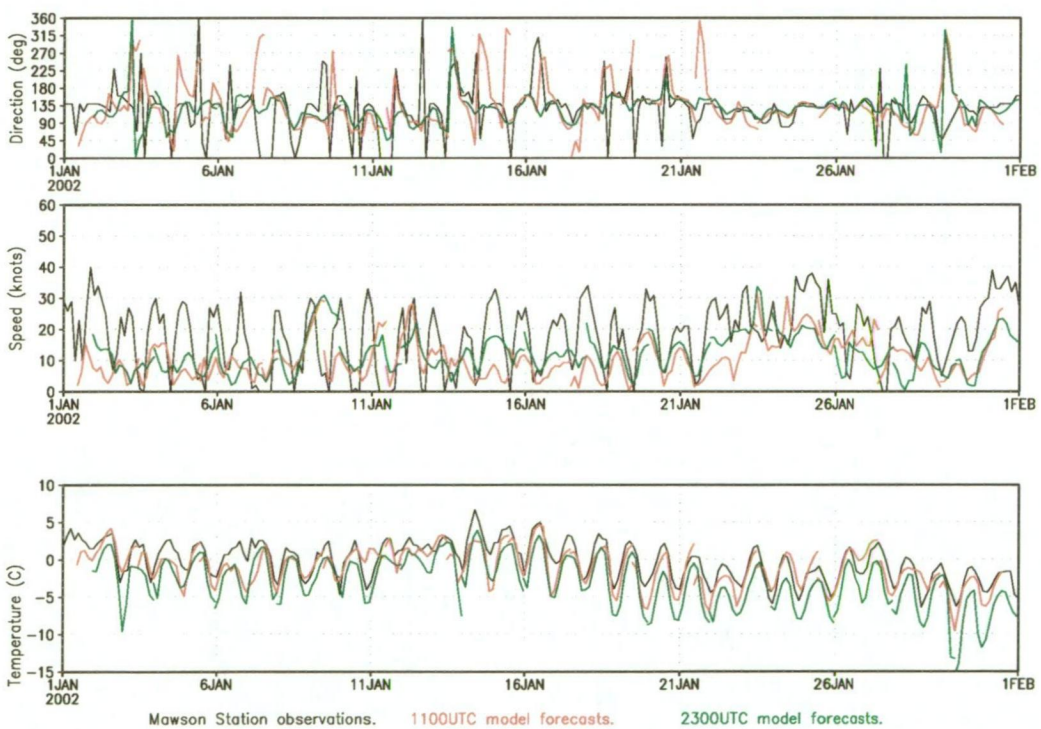

Figure 4.24: Comparison of ALAPS 3 hourly surface data out to +48 hours, from the 1100UTC runs (red time-series), and 2300UTC runs (green time-series), with observations from Mawson Station (black time-series) , for January 2002.

initialised runs distinctly warmer than runs initialised at 2300UTC. However, it is worth noting that the diurnal variation in temperature forecast by ALAPS, from both the 1100UTC and 2300UTC initialised runs, for Mawson, was, if anything, slightly greater than the magnitude of the observed diurnal variation in temperature, suggesting the problem at Dome C was a function of the high plateau site.

Discrepancies in near surface temperature between the 2300UTC and 1100UTC initialised model runs was not so pronounced during winter-time runs (Figure 4.25), although what was obvious was the model failure to

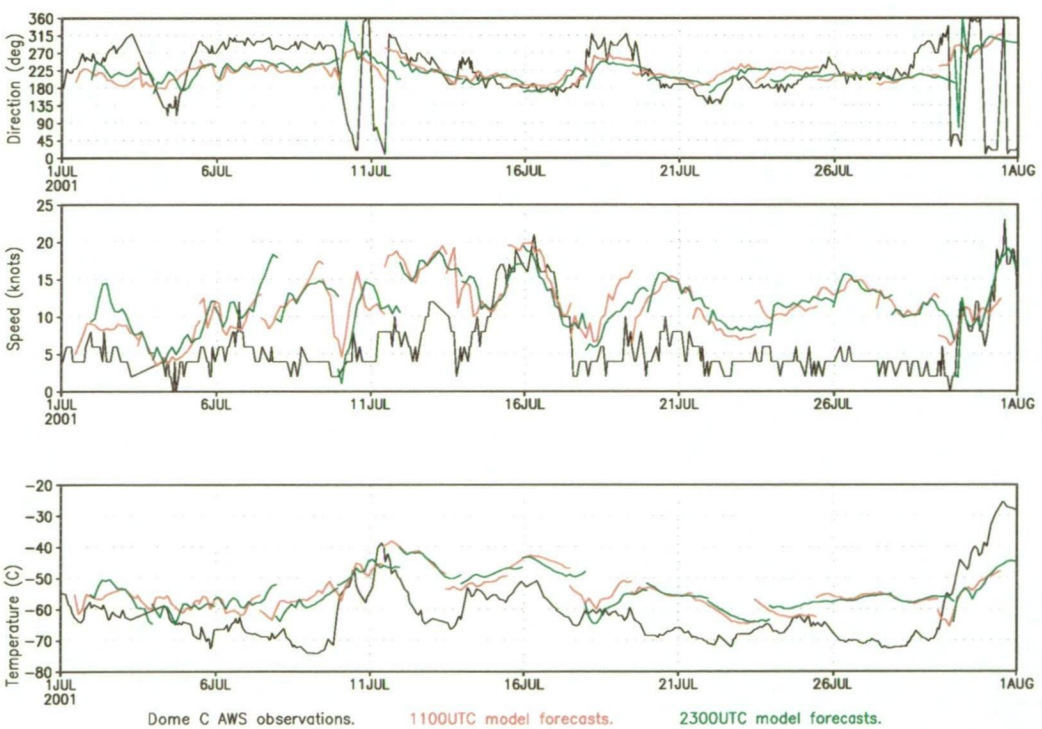

Figure 4.25: Comparison of ALAPS 3 hourly surface data out to +48 hours, from the 1100UTC runs (red time-series), and 2300UTC runs (green time-series), with observations from the Dome C AWS (black time-series) , for July 2001.

replicate the very low temperatures observed during July of 2001. At the time of the very low temperatures, for example, around 27 July 2001, where

the observed temperature was around -70^{o}C, the observed surface wind was less than 5 knots, but the model forecasts actually increased the wind speed during this period, with a subsequent rise in the modelled near surface air temperature, most probably through turbulent mixing of the very strong near surface temperature inversion, experienced over the plateau during the winter months.

There were obvious ALAPS model failures occurring over the high plateau, both during winter and summer. Boundary issues may have played a part in the forecasts out past 24 hours, as the southern boundary of the model was only 5^{o} of latitude to the south, and a southerly wind at 10 knots would take only 30 hours to have an impact at 75^{o}S. A further complication to the boundary problem was the fact that GASP nesting data was blended with ALAPS model data over a 4^{o} latitude edge along the southern boundary. The blending was a linear trend from full GASP data on the boundary at 80^{o}S to full ALAPS data by 76^{o}S, with possible contamination from GASP boundary data even more likely near Dome C. Investigation of the GASP model output, however, suggested that the global model forecasts near Dome C were adequately capturing the surface flow, and in fact the GASP wind forecasts were performing better than ALAPS. Figure 4.26 shows the GASP +24 hour forecasts of near surface variables for January 2002, and when compared with the ALAPS +24 hour forecasts (Figure 4.22), it appeared that GASP out-performed ALAPS in forecasting the synoptic variability in near surface wind direction. GASP wind speed values were reduced to 3 m using a simple logarithmic reduction, and as with the ALAPS forecasts, did not manage to forecast the peak wind speeds particularly well, but overall,

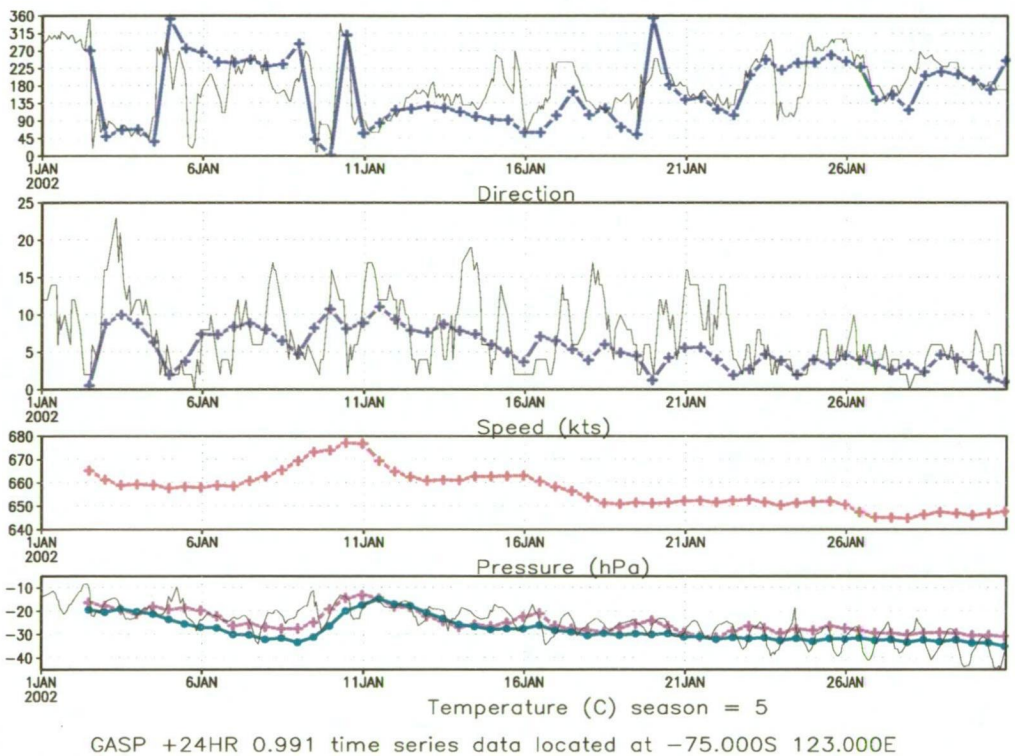

Figure 4.26: Comparison of GASP +24 hour surface data (coloured time-series) with observations from the Dome C AWS (black time-series) , for January 2002.

GASP performed better than ALAPS in the lighter wind regimes. Similarly, during July of 2001, GASP +24 hour output (not shown) provided better surface flow forecasts than ALAPS. Where GASP did not perform better was in the forecast of the diurnal variation in near surface temperature. Both the σ=0.991 air temperatures and surface temperatures from the GASP model are plotted in the last panel of Figure 4.26, with only a very low amplitude diurnal signal evident in the GASP surface temperature values, and significantly lower than observed in the ALAPS data, despite both models running the radiation code every three hours. Little diurnal signal would be expected at the first sigma level from the GASP model, as the average height of the level was around 75 m above the surface, however the surface temperature ought to have responded to diurnal forcing. Overall, given the relatively good performance of the GASP surface flow, it was unlikely that boundary conditions were entirely responsible for the relatively poor performance of ALAPS at Dome C, and further investigations of the ALAPS physics was warranted. Figure 4.27 further highlights the discrepancies between modelled and observed temperatures during summer, showing a comparison of observed temperature, (blue), with near surface temperature, (black), from the ALAPS run initialised at 1100UTC on 26 January 2002, clearly demonstrating the significantly damped diurnal oscillation forecast by the model. The ALAPS skin temperature is also plotted (green line) showing only a marginally stronger diurnal amplitude than the ALAPS near surface air temperature. Given the fact that the amplitude of the diurnal variation in skin temperature in the model near Dome C was not comparable to the observed near surface air temperature values suggests a surface

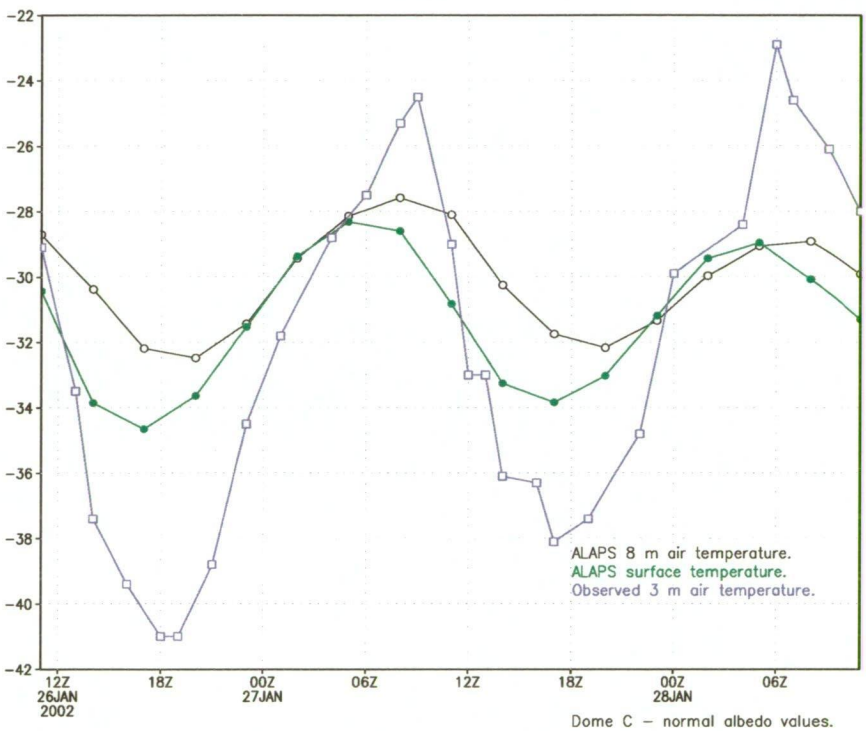

Figure 4.27: ALAPS 3 hourly output of surface (green) and near surface (black) temperature from the model run initiated at 1100UTC 25 January 2002, compared with observations from the Dome C AWS (blue).

energy balance problem in the model, with either incoming solar radiation being affected by too much model cloud, the surface albedo values being too high, or sub-surface temperature gradients not being adequately handled by the model. Radiation issues within the model are also a likely cause of the poor model performance during winter. These issues will be further discussed in the following sections on precipitation and cloud forecasting and in the chapter on sensitivity studies.

4.3 Precipitation forecasts.

This section on the performance of ALAPS precipitation forecasts forms the basis of a paper now published in Weather and Forecasting (Adams 2004a), with the hope of fostering further collaborative work on addressing the verification and improvement of model precipitation forecasts, to both assist weather forecasting and address the increasingly important question of Antarctic mass balance.

In Antarctica precipitation plays an important role in both defining the local weather, and as a major component of the continental mass budget, where establishing an accurate measure of the total precipitation over the continent is essential in assessing whether the continental mass budget is in equilibrium or whether the Antarctic ice cap is evolving. Measuring precipitation *in situ* is fraught with problems, mainly as a result of the difficulty in differentiating between whether snow accumulated in a gauge had actually fallen at the site or been transported there as blowing or drifting snow. As a result of these difficulties routine measurements of precipitation are not made, and those observations that are available, are generally consid-

ered unreliable (Bromwich 1988). Precipitation output from NWP models provide a proxy data source from which mass balance measurements may be made, and local weather forecasts prepared. The focus of this section is on identifying the usefulness of NWP precipitation output in Antarctic weather forecasting, despite the stated problems of unreliable observations. The precipitation field stored within the ALAPS 3 hourly output files was the accumulated precipitation from model initialisation time but with a reset after every 24 hours. Hence the +24 hour ALAPS precipitation field held the full precipitation over the prior 24 hours (from model start time) and the +48hour field held the precipitation having fallen in the last 24 hours of the model run. To assess a more instantaneous precipitation rate, or at least the accumulated precipitation over the 3 hours up to a model output time-step, was simply a matter of subtracting the previous time-step precipitation. For example, the precipitation that had fallen in the 3 hours up to the +36 hour forecast would simply be the +36 hour forecast precipitation minus the +33 hour precipitation.

4.3.1 Model verification over Tasmania

Making a quantitative assessment of ALAPS precipitation forecasts over Antarctica is not possible with the current Antarctic observing systems, but in order to have some knowledge of the quantitative performance of the ALAPS precipitation output a comparative study of observed rainfall and ALAPS precipitation output over Tasmania, in southeast Australia was made. Both long term and daily rainfall records are maintained for several sites around Tasmania, and to assess the quantitative accuracy of the model,

both a comparison of model annual rainfall against long term observational statistics, and single station verification have been made. Before presenting results of ALAPS precipitation forecasts over Tasmania it is worth noting that precipitation events over the state appear to be significantly modified by the local orography. The top panel of Figure 4.28 shows the orography of Tasmania, with Figure 4.29 detailing the average annual rainfall over the state, compiled from data between 1961 and 1990. A comparison of both figures highlighted the fact that maxima in precipitation occurred on the high peaks of the west coast ranges where a predominant westerly wind prevails, with generally high precipitation rates on the western slopes of the ranges. A peak in precipitation was also observed on the northeast highlands where onshore flow in northeasterly weather events would likely lead to orographically enhanced precipitation in this region, and with the ranges also capturing some of the moisture not precipitated on the western ranges during westerly events. There is, in general, a minimum in precipitation through the plains region of southeastern and central (Midlands) districts of the state. Figure 4.29 was derived from irregularly spaced observational data, using a sophisticated interpolation routine that took into consideration local orography. Figure 4.30 details the 12 month accumulated rainfall for Tasmania for the period 1 July 2001 to 30 June 2002, but where a cruder Barnes analysis has been applied to the observational data to produce the colour shaded plot. The time period in Figure 4.30 is coincident with the available ALAPS data and Figure 4.31 shows the ALAPS forecast rainfall accumulation over the same 12 month period. In broad terms the model output showed good agreement with the observed rainfall figures. Maxima

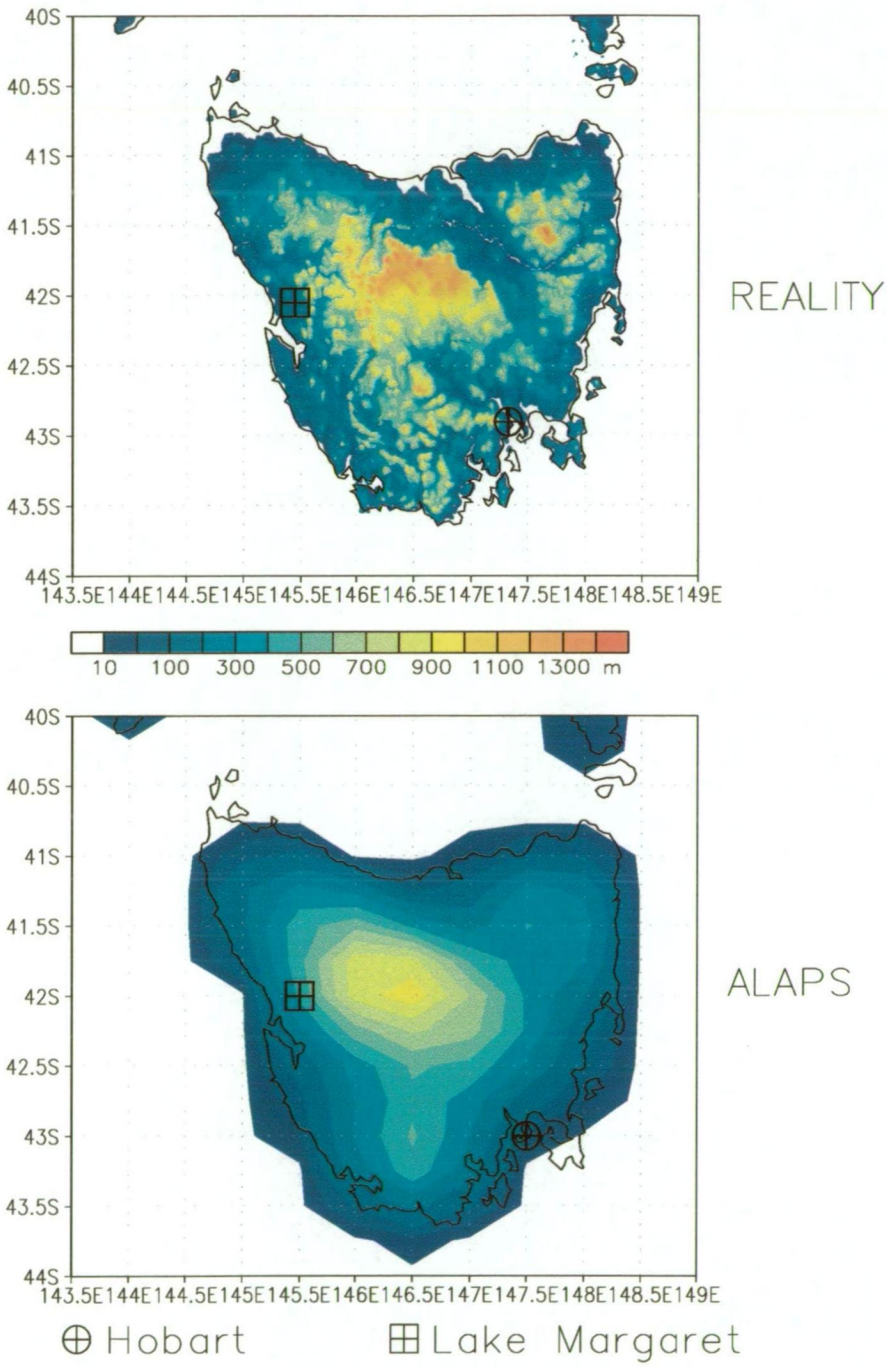

Figure 4.28: The orography of Tasmania, in reality (top panel), and as used in the ALAPS model (lower panel).

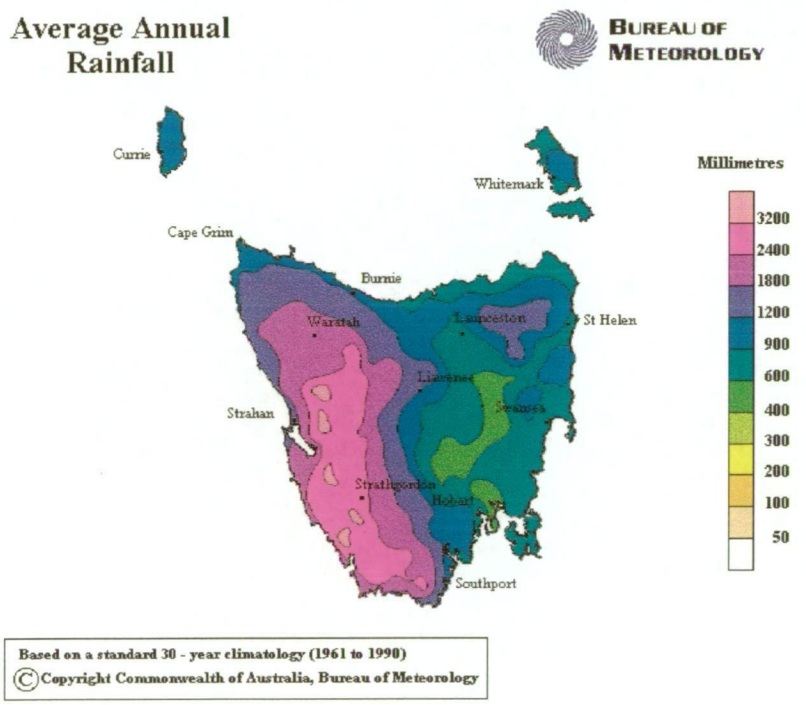

Figure 4.29: The average annual rainfall for Tasmania, compiled from data from 1961 to 1990.

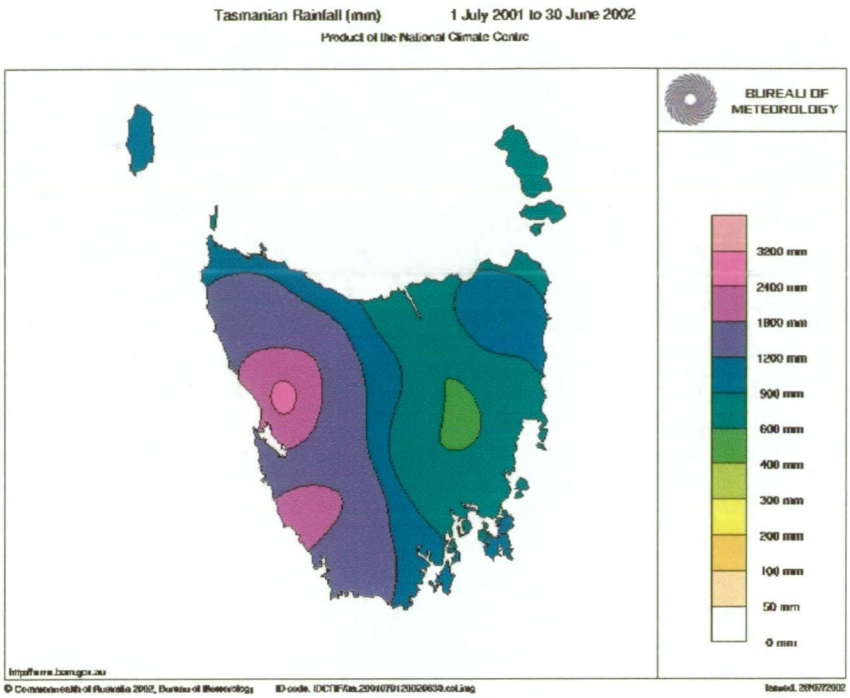

Figure 4.30: The 12 month accumulated rainfall for Tasmania for the period 1 July 2001 to 30 June 2002.

were slightly shifted and the minimum observed through the central north of the state was too extreme in the model output. These differences would seem to be linked with the differences between actual and model orography. The lower panel of Figure 4.28 shows the orography of Tasmania as "seen" by the ALAPS model. The west coast ranges are not well defined, with only a low ridge running north-south from the model version of the central highlands, which peaks at just under 1000 m rather than the actual peak heights of just over 1500 m. The northeast highlands are also significantly lower in the model orography than in reality. However, despite these discrepancies the model precipitation for the 12 month period is in good agreement with maxima in the west reaching around 3000 mm and consistent with the observed maxima slightly further to the west. One could argue that if the

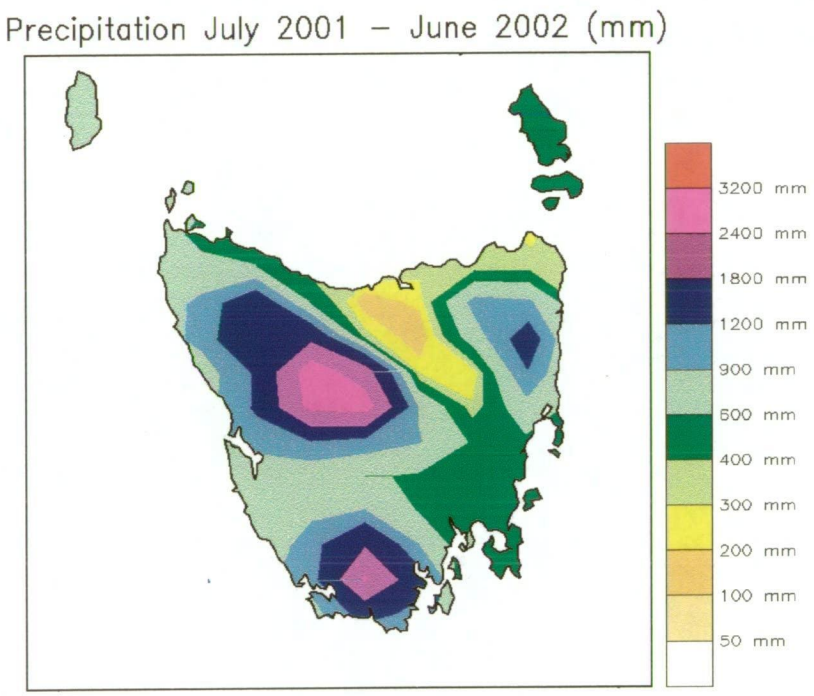

Figure 4.31: The ALAPS forecast of the 12 month accumulated rainfall for Tasmania for the period 1 July 2001 to 30 June 2002.

model was run at a higher resolution, with topography closer to reality, then the precipitation forecasts would not only be more accurate in quantity but maxima and minima would probably be better located.

Comparisons of long term accumulation figures suggest that the ALAPS forecasts were indeed modelling precipitation over Tasmania with some accuracy, but this presumption needs to be assessed at the time-scale of single precipitation events, and for specific locations within the model domain. Figure 4.32 shows a comparison of the +24-hour ALAPS forecasts, valid at 2300UTC, for the above 12 month period from the grid point closest to Lake Margaret, on the west coast of Tasmania, with the observed rainfall at Lake Margaret, over the same 12 months. Figure 4.33 shows a similar comparison, but of ALAPS forecasts at the closest grid point to Hobart, with observed 24 hour accumulated rainfall totals from Hobart in the southeast of the state. Both Lake Margaret and Hobart, and the closest ALAPS grid-points to the two sites, are marked on Figure 4.28, with the marks on the top panel showing the actual locations, and on the lower panel the closest model grid points used for each of the locations. In general, the ALAPS forecasts for Lake Margaret under-estimated the rainfall, with a bias of -4.7 mm for the year, although the model did perform well during January of 2002 (panel 3 Figure 4.32), picking each of the rainfall events and forecasting the intensities with some accuracy. Over the 12 month period 143 rainfall events were recorded in which the rainfall exceeded 5 mm. Of these 143 events ALAPS successfully forecast 59 events, in the process failing to capture 84 such events. ALAPS also forecast 12 events exceeding 5 mm in 24 hours for which there were no supporting observations. For Hobart, ALAPS output

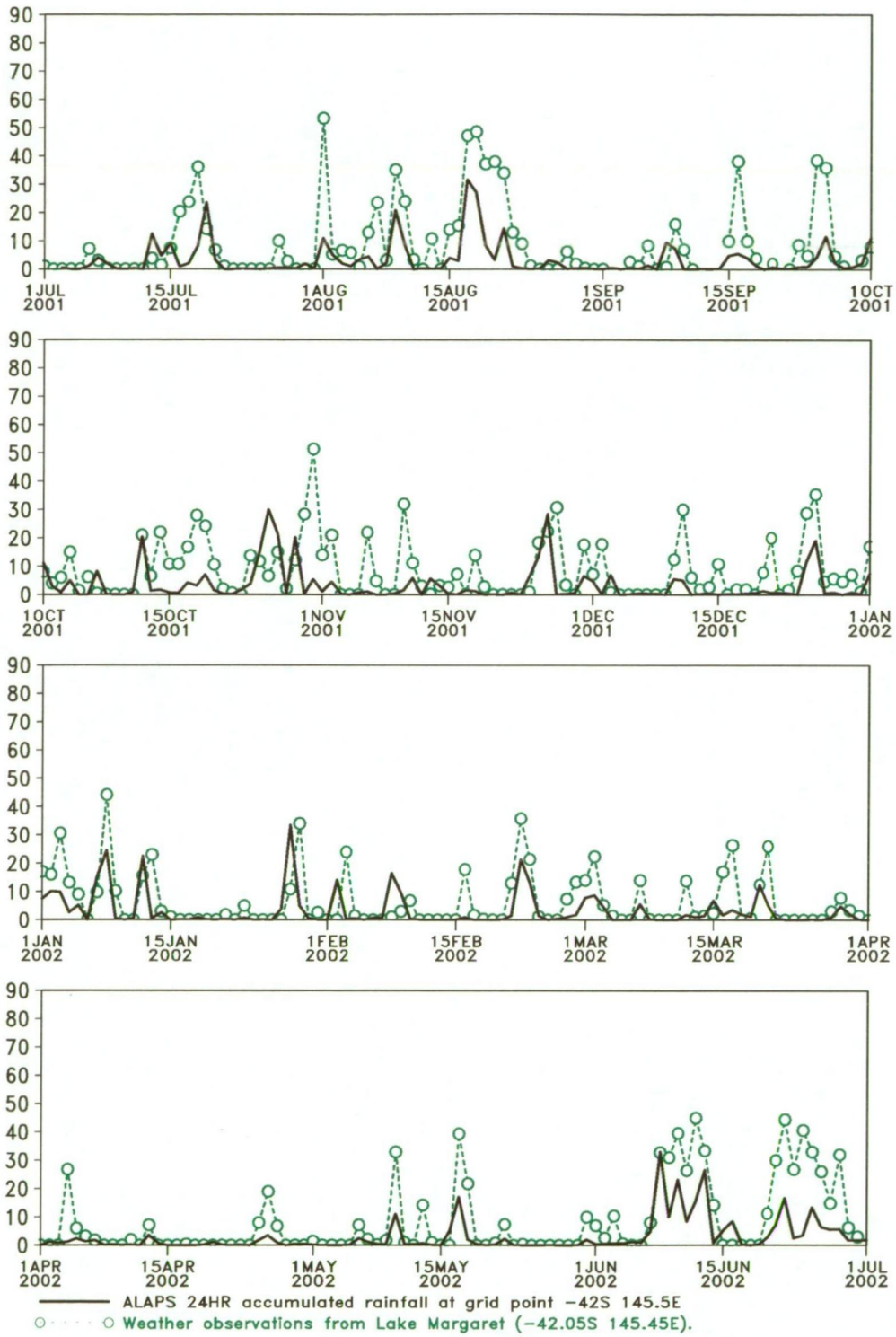

Figure 4.32: A comparison of ALAPS +24 hour forecasts of 24 hour accumulated precipitation (mm) valid at 2300UTC (black), with observations from Lake Margaret, for the period 1 July 2001 to 30 June 2002.

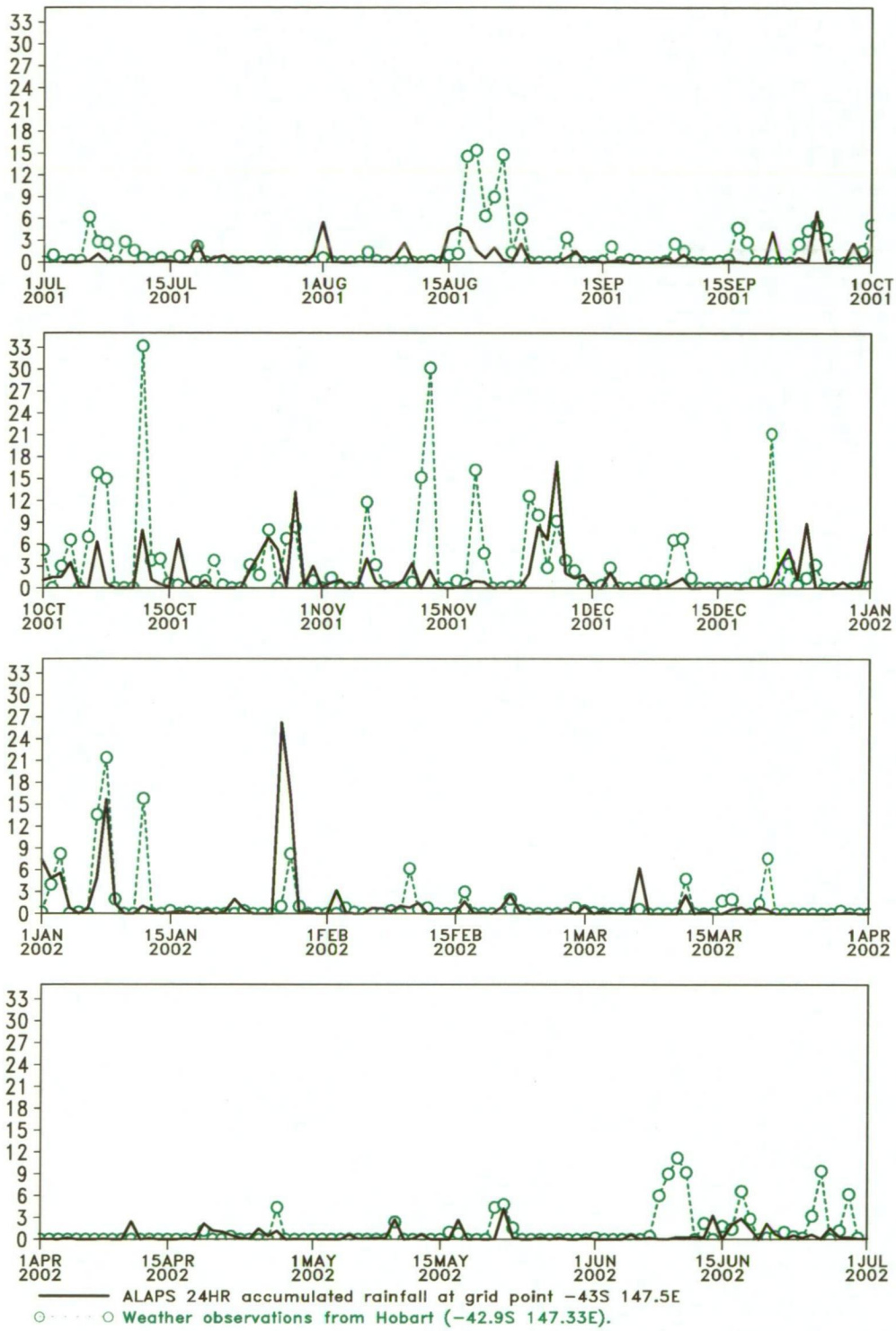

Figure 4.33: A comparison of ALAPS +24 hour forecasts of 24 hour accumulated precipitation (mm) valid at 2300UTC (black), with observations from Hobart, for the period 1 July 2001 to 30 June 2002.

at the closest grid point (43.0°S 147.5°E) also under-estimated the rainfall with a bias of -0.7 mm, which is somewhat better than on the west coast around Lake Margaret, although it should be noted that rainfall totals in the southeast of Tasmania are significantly less than on the west coast. ALAPS forecast statistics for Hobart are detailed in Table 11, along with the statistics

Precipitation > 5 mm	Successes	False Alarms	Failures
Lake Margaret	59/143 = 41%	69/128=54%	84/143 = 59%
Hobart	10/41 = 24%	37/47=79%	31/41 = 76%
Hobart (east)	12/41 = 29%	59/71=83%	29/41 = 71%

Table 11: Comparison of observed and forecast precipitation events of greater than 5 mm in 24 hours at Lake Margaret and Hobart for the period July 2001 until June 2002.

for Lake Margaret, mentioned above, and also with statistics from a comparison between the observed Hobart rainfall and ALAPS +24HR forecast rainfall for the grid point immediately to the east of Hobart (Figure 4.34) at 43.0°S 148.0°E. One problem with single station verification of NWP output is the fact that on occasions the closest model grid point to the observing site may not necessarily best represent the observing site because of the way the orography is smoothed and lowered in the model domain. Orographic forcing plays a significant role in the spatial variation of precipitation and it is worth considering a grid point within the model that may better represents the local terrain. In the case of the Hobart data the model grid point directly to the east, at 43.0°S and 148.0°E , appeared to better correlate with the observed data (Figure 4.34) with a bias of only -0.4 mm and an RMS error of 3.6 mm compared to the RMS error of 4.0 mm for the model grid point used in Figure 4.33. Although the forecast failure rate and false alarm ratio remained high, the results were better than from the grid point closest to

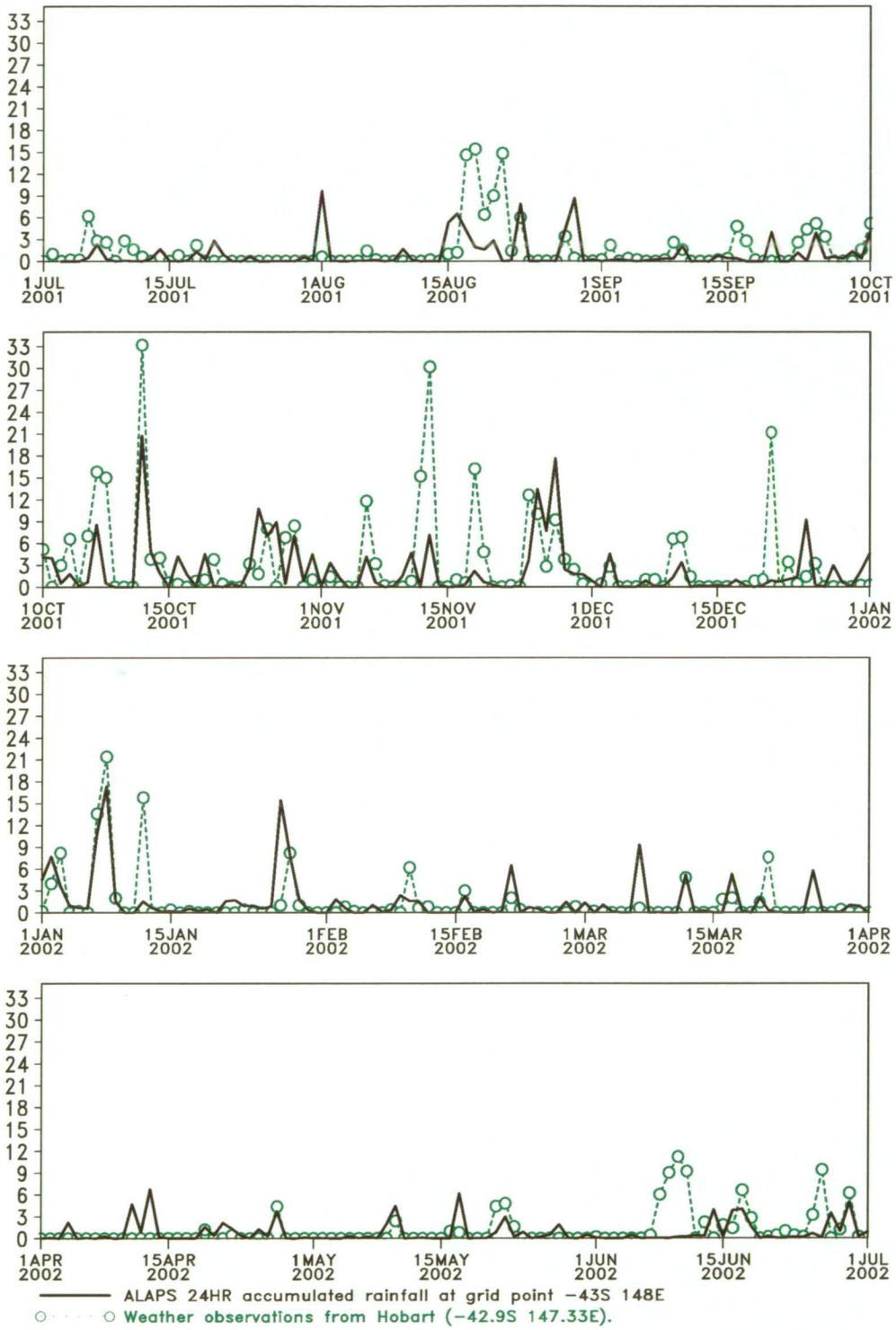

Figure 4.34: A comparison of ALAPS +24 hour forecasts of 24 hour accumulated precipitation (mm) valid at 2300UTC (black), from the grid-point to the east of Hobart, with observations from Hobart, for the period 1 July 2001 to 30 June 2002.

Hobart. Whether, this was simply chance or in fact related to local model orography producing a better Hobart prediction at this location would need further investigation.

The statistics in Table 11 don't reflect particularly well on the ability of the model to predict significant rainfall events accurately, with the success rate varying from 41% at Lake Margaret to only around 29% for Hobart. However, it would be argued that the model does perform better when simply used to forecast the likelihood of a rainfall event occurring. In Table 12 an

Precipitation > 0.5 mm	Successes	False Alarms	Failures
Lake Margaret	160/213 = 75%	33/193 = 17%	53/213 = 25%
Hobart	73/122 = 60%	46/119 = 39%	49/122 = 40%
Hobart (east)	80/122=66%	61/141 = 43%	42/122 = 34%

Table 12: Comparison of observed and forecast precipitation events of greater than 0.5 mm in 24 hours at Lake Margaret and Hobart for the period July 2001 until June 2002.

event has been defined as any situation in which more than 0.5 mm of rain fell, or was forecast to fall, in each 24 hour period to 2300UTC from July 2001 until June 2002. As can be seen from Table 12, the model performs well in forecasting rainfall events although the false alarm ratios remained high, as was the case for events in excess of 5 mm. Perusal of Figure 4.33 suggests that phase shifts in the +24HR forecast data may account for some of the reduced forecast success and relatively high false alarm ratios. If the 1100UTC ALAPS 24 hour rainfall totals are also considered, and a forecast success defined as an ALAPS forecast greater than 5 mm either concurrent with an observation of greater than 5 mm, or forecast 12 hours either side of the observation then the results do improve over those shown in Table 11, with the Lake Margaret forecast success rate rising from 41% to 64%, and

with the false alarm ratio falling from 54% to 28%. For Hobart the success rate rose from 24% to 44% with the false alarm ratio falling from 79% to 62%.

In absolute terms the ALAPS precipitation output fell short of providing quantitatively reliable forecasts over Tasmania. However, the rainfall patterns over the state of Tasmania, in the mean, were reasonable, and the forecasts of significant ($>$ 5 mm in 24 hours) precipitation events on the west coast, where onshore flow and orographic influences dominate, were considered good. Weather patterns around the Antarctic are also dominated by orographic influences and it would seem reasonable to expect precipitation events to be almost exclusively influenced by onshore flow.

4.3.2 Model verification over Antarctica

As discussed above, observations with which to verify forecast precipitation over Antarctica are not readily available. However, studies have been undertaken to estimate accumulation rates over the Antarctic continent using both numerical model output and glaciological, or meteorological, records. Budd et al. (1995) used the Australian global model, GASP, to demonstrate that net air-mass and moisture fluxes over the Antarctic from the numerical model produced annual mean net surface accumulations that closely resembled glaciologically observed distributions. Cullather et al. (1998) provided a good overview of the current state of accumulation estimates and also provided an analysis using data from the European Centre for Medium-Range Weather Forecasting (ECMWF) over an 11 year period, between 1985 and 1995, to assess model net precipitation (precipitation minus evapora-

tion/sublimation) against a variety of observational records. Cullather et al. (1998) used the accumulation compilation of Giovinetto and Bentley (1985) as the basis for their validation of ECMWF model precipitation estimates, with Vaughan et al. (1999) further improving on the Giovinetto et al. (1985) net (precipitation minus evaporation) annual accumulation distribution with the distribution from their work shown in the top panel of Figure 4.35. These studies were primarily aimed at assessing the moisture budget over Antarctica but also provided a good climatology of precipitation from which an assessment of the ability of the ALAPS NWP to forecast precipitation may be made. The lower panel of Figure 4.35 shows the annual accumulated precipitation field from the ALAPS run from July 2001 through to June 2002, and a comparison of the ALAPS annual accumulated precipitation with the Vaughan et al. (1999) net precipitation (P-E) distribution showed some consistency in the spatial pattern of the annual accumulation. The ALAPS data are purely precipitation, rather than precipitation minus evaporation of the Vaughan diagram so the zero areas (wind ablation) apparent in the upper panel of Figure 4.35 do not appear in the ALAPS data. It is also apparent from the ALAPS accumulated precipitation (lower panel Figure 4.35), that the coastal precipitation was much higher in the ALAPS year than would be suggested from the Vaughan et al. (1999) climatology. Evaporation losses and wind transport around the Antarctic coast would account for most of the discrepancies and also, given the high resolution of the ALAPS model and the significant orographic lift generated off the steep coastal escarpment, it is perhaps not unreasonable that the higher resolution of the ALAPS model may generate larger precipitation rates around the Antarctic coastal fringe.

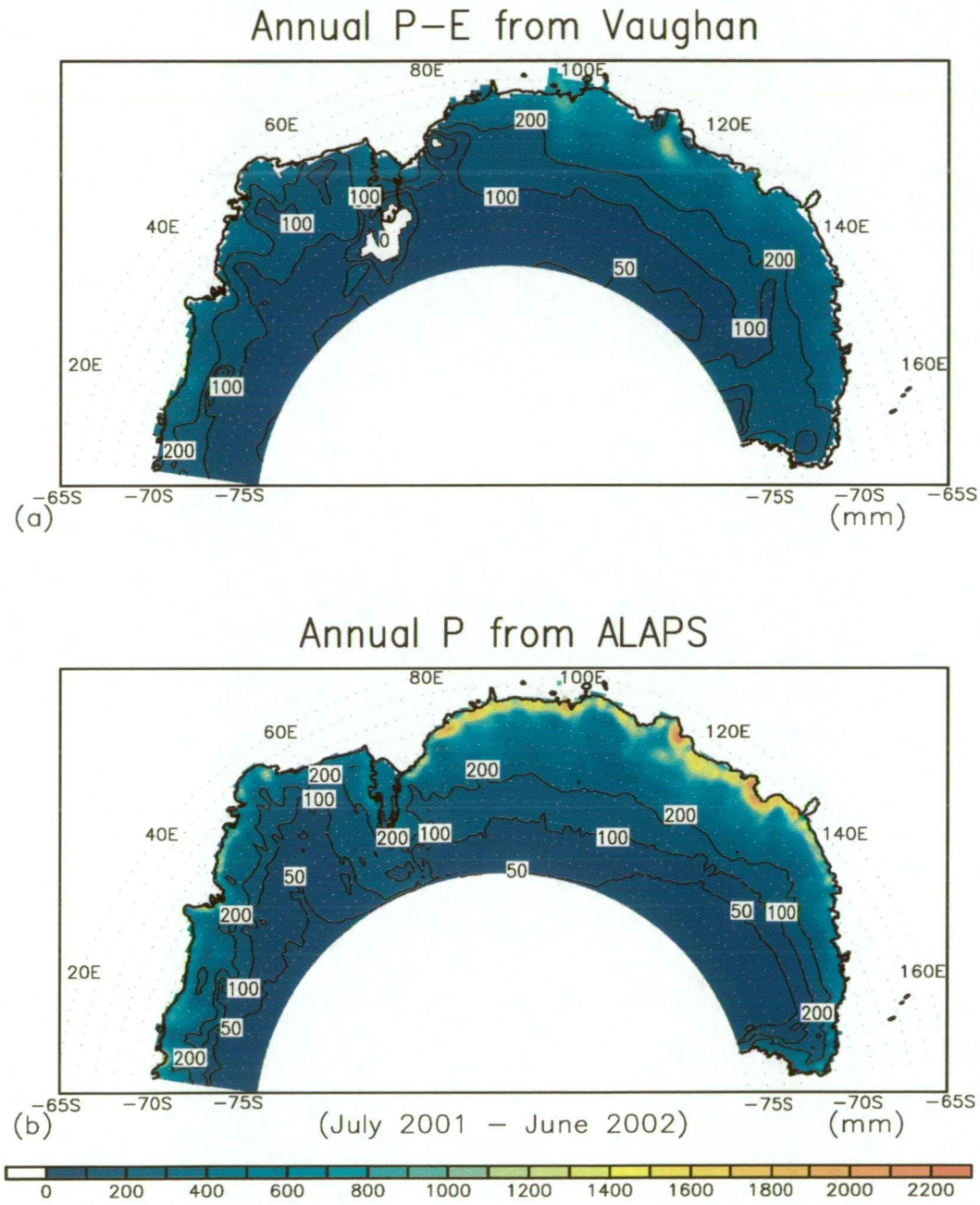

Figure 4.35: Annual precipitation minus evapouration from Vaughan (1999) (top panel), with the lower panel showing the annual precipitation from ALAPS over the period 1 July 2001 to 30 June 2002.

A direct comparison of ALAPS precipitation minus evaporation with the Vaughan data-set would have been more useful. However, due to a processing problem in the archiving system ALAPS evaporation data were lost.

The long term means, discussed above, give some indication as to the veracity of the ALAPS precipitation forecasts, but to be a useful forecasting tool the NWP scheme needs to demonstrate forecast accuracy on the local scale, and over time periods commensurate with the model forecast period (48 hours). Single-station verification of precipitation forecasts in an absolute sense isn't possible, for the reasons mentioned above. However, it was possible to assess forecast precipitation events against visual observations of precipitation. This will not verify the forecasts in a quantitative sense but will show whether the model is adequately capturing precipitation, and non-precipitating, events occurring over the Antarctic continent. The Australian stations of Casey ($66^{o}17$'S $110^{o}32$'E), Davis ($68^{o}35$'S $77^{o}58$'E) and Mawson ($67^{o}36$'S $62^{o}52$'E), (Figure 1.1) have staffed meteorological offices that provide visual observations of weather elements during staffing hours, (nominally 0000UTC to 1200UTC), and a comparison can be made between visual observations of falling or blowing snow and the ALAPS 24 hour accumulated precipitation rates at the +24 hour model time-step. Model predictions of an accumulation of precipitation, in a realistic model run, ought to be coincident with, or be slightly preceded by, visual observations of falling, or perhaps blowing snow. In attempting to define how well the model was performing, events in which ALAPS predicted 24 hour accumulations in excess of 5 mm were considered and the station observations studied to see whether the observed weather elements supported the model forecasts. The ALAPS

grid-point closest to Casey was at 66.25°S, 110.5°E, and at this point the model predicted 46 "events" in which the 24 hour accumulated precipitation exceeded 5 mm in the 12 month period of July 2001 through to June 2002. Observations of falling or blowing snow at Casey supported 43 of these events (Figure 4.36). The Casey observations were also scrutinised for those events where a reasonable number of continuous observations of falling, or blowing, snow were made but at which time the ALAPS forecasts were not predicting precipitation, and for the 12 month period in question, 6 such precipitation events were observed at Casey. Table 13 highlights the observed and forecast

Precipitation > 5 mm	Successes	False Alarms	Failures
Casey	41/47 = 87.2%	7/48 = 14.6%	6/47 = 12.8%
Davis	15/19 = 78.9%	4/19 = 21.1%	4/19 = 21.1%
Mawson	11/13 = 84.6%	2/13 = 15.4%	2/13 = 15.4%

Table 13: Comparison of observed falling or blowing snow events with forecasts of precipitation rates greater than 5 mm in 24 hours at Casey, Davis and Mawson for the period July 2001 until June 2002.

precipitation events, along with the number of false alarms and missed events for Casey and Davis and Mawson.

ALAPS provided excellent forecast guidance of the likelihood of precipitation events at the coastal stations of Casey, Davis and Mawson, with success rates significantly higher than those seen over Tasmania, and with significantly lower false alarm ratios. The analysis of precipitation at the Antarctic stations is somewhat less rigorous than the analysis over Tasmania, given the lack of quantitative observations. However, the reports of either falling or blowing snow related extremely well to to the ALAPS forecasts of precipitation. As has already been mentioned, the observations of precipitation in Antarctica are complicated in strong wind events where surface snow is

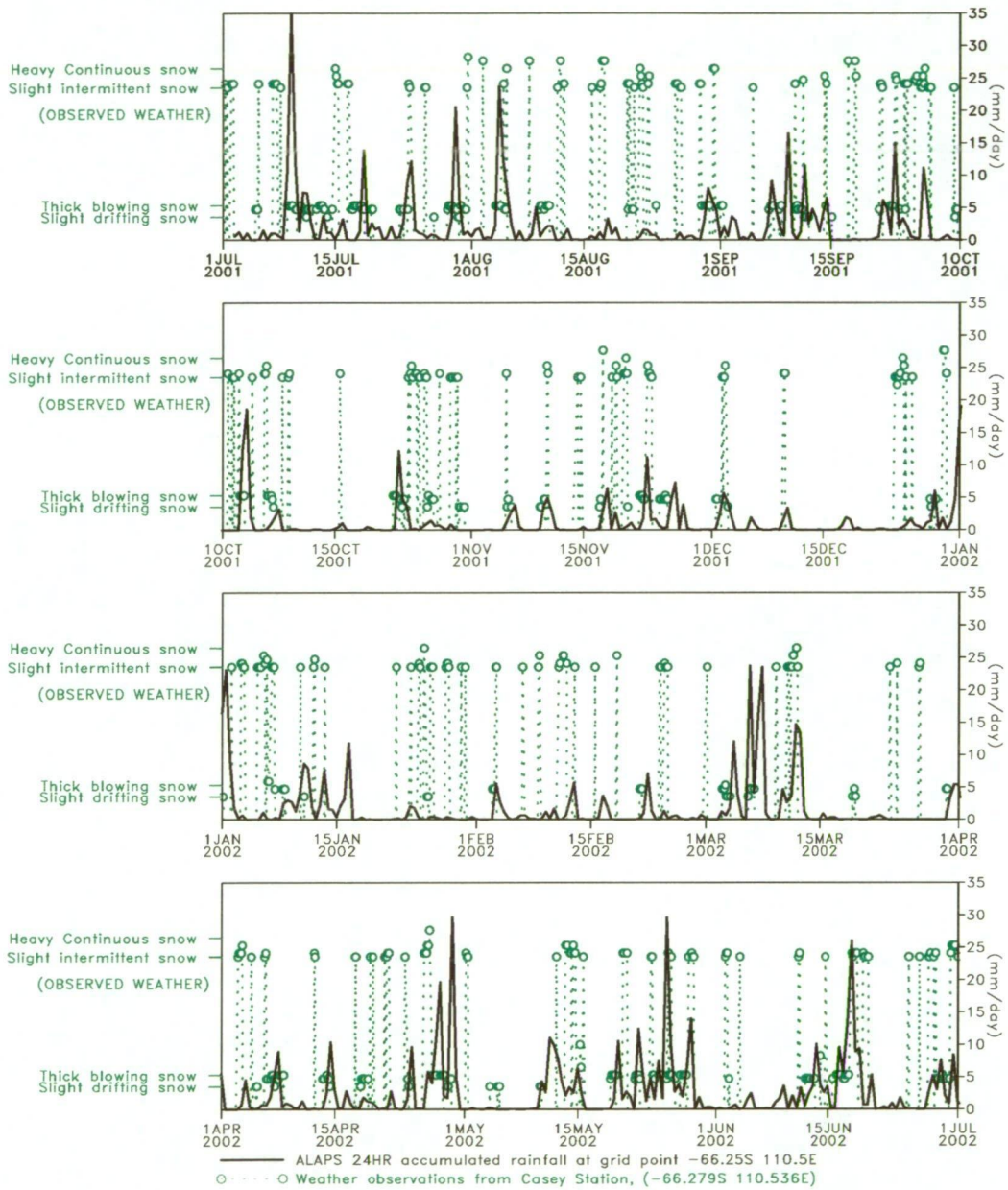

Figure 4.36: A comparison of the ALAPS +24 hour precipitation forecasts with observations of falling, blowing or drifting snow from Casey, for the period 1 July 2001 to 30 June 2002.

lifted and observations of blowing snow give no indication as to whether any of the snow was actually falling at the time of the observation. At Casey and Davis a significant number of blowing snow events occur in moist, maritime, air-masses (Shepherd 1999), so it is likely that observations of blowing snow did include a component of falling snow. This is not necessarily true at Mawson where windy conditions are often associated with dry continental air advecting off the plateau such that a significant number of observations of blowing snow were unlikely to include any falling snow. If only observations of falling snow are used in comparison with ALAPS forecasts of 5 mm or more of precipitation then the statistics are somewhat worse, as shown in Table 14, although still remarkably good.

Precipitation > 5 mm	Successes	False Alarms	Failures
Casey	26/32 = 81.2%	22/48 = 45.8%	6/32 = 18.8%
Davis	12/16 = 75.0%	7/19 = 36.8%	4/16 = 25.0%
Mawson	5/7 = 71.4%	8/13 = 61.5%	2/7 = 28.6%

Table 14: Comparison of observed falling snow events with forecasts of precipitation rates greater than 5 mm in 24 hours at Casey, Davis and Mawson for the period July 2001 until June 2002.

4.3.3 Snow accumulation

The three stations used in the comparison of ALAPS forecasts and observed weather, in the previous section, were all coastal stations (Figure 1.1) , where precipitation events are more regular and, in general, higher in value than would be expected at inland locations. Unfortunately, there are no staffed stations inland, within the ALAPS domain, providing observations of weather elements. However, the Australian Antarctic Division maintains a network of Automatic Weather Stations (AWS) around East Antarctica which are fitted

with sonic devices for measuring snow accumulation at the AWS site (Allison 2000 and http://www.antcrc.utas.edu.au/argos). Increases in accumulation recorded by these sensors, is in general, associated with precipitation events. Strong wind events may contaminate the signal, but a direct comparison of discrete positive jumps in the sensor accumulation data may provide a guide for the occurrence of precipitation events. Accumulation and wind speed data from AWS's located at GF08-A, Amery-G3, DSS and A028-B, (see Figure 1.1 for locations), were overlaid with the +24-hour forecast of 24 hour accumulated precipitation from ALAPS, and the +24-hour ALAPS wind speed forecast, using data from the closest ALAPS grid-point to each station. In Figures 4.37 and 4.38, snow accumulation and wind speed data from the AWS at A028-B (68.41^{o}S 112.22^{o}E) are displayed, along with the ALAPS data from the 68.5^{o}S, 112.0^{o}E grid point. Figure 4.37 covers the period from 1 July 2001 to 30 September 2001, with Figure 4.38 the period 1 October 2001 until 31 December 2001. Significant portions of the wind record are missing in Figure 4.36 due to the propensity for the wind sensors to freeze during the winter months. However, there is a good fit between the ALAPS +24-hour wind speed forecasts at the first sigma level (approximately 8 m above the ground) and the observed 4 m wind speed from the AWS during the second 3 month period (Figure 4.38) giving some faith in the ability of the model to capture, at least the time-series of the dynamics of the situation at the AWS site. Comparison of the snow accumulation record and forecast precipitation showed some measure of agreement although with notable differences. One of the difficulties with the accumulation record is the problem of altering surface conditions, as either sastrugi moves through the site or deflation occurs with

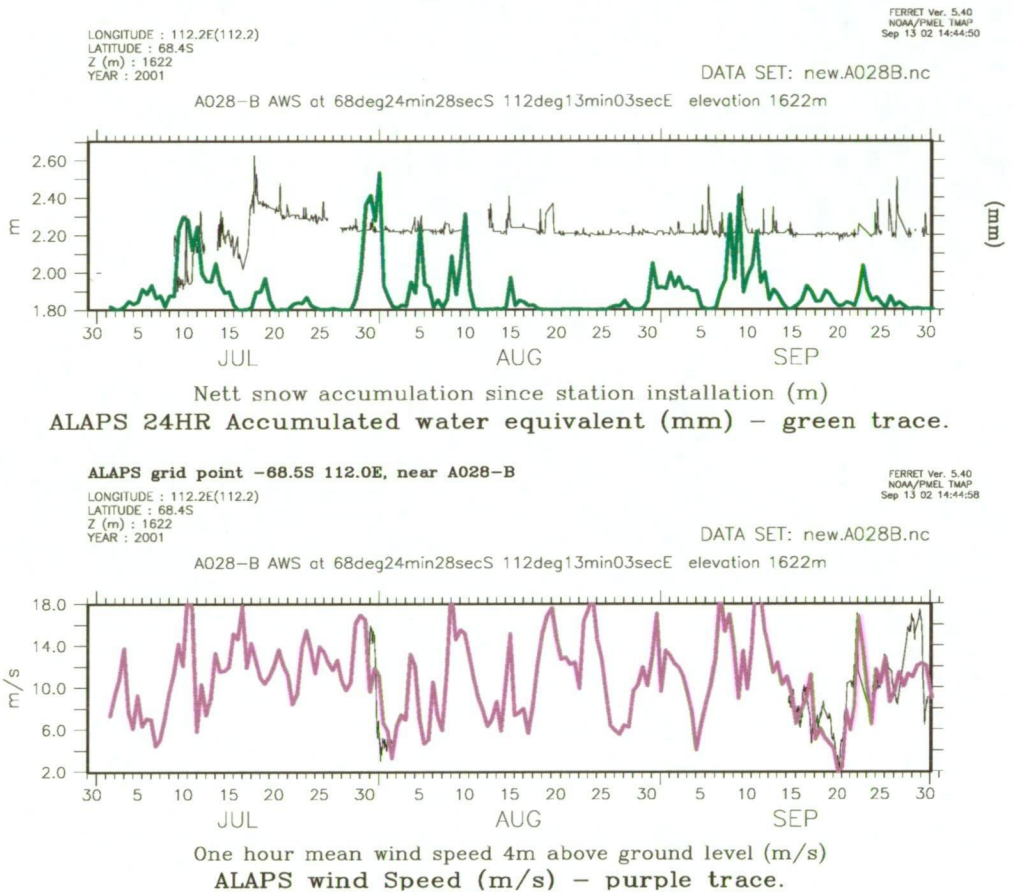

Figure 4.37: A comparison of ALAPS 24 hour accumulated precipitation forecasts (top panel, green), and ALAPS near surface wind speed (lower panel, purple), with observations of snow accumulation (top panel, black), and wind speed (lower panel, black) from the AWS at A028-B, for the period 1 July 2001 to 30 September 2001.

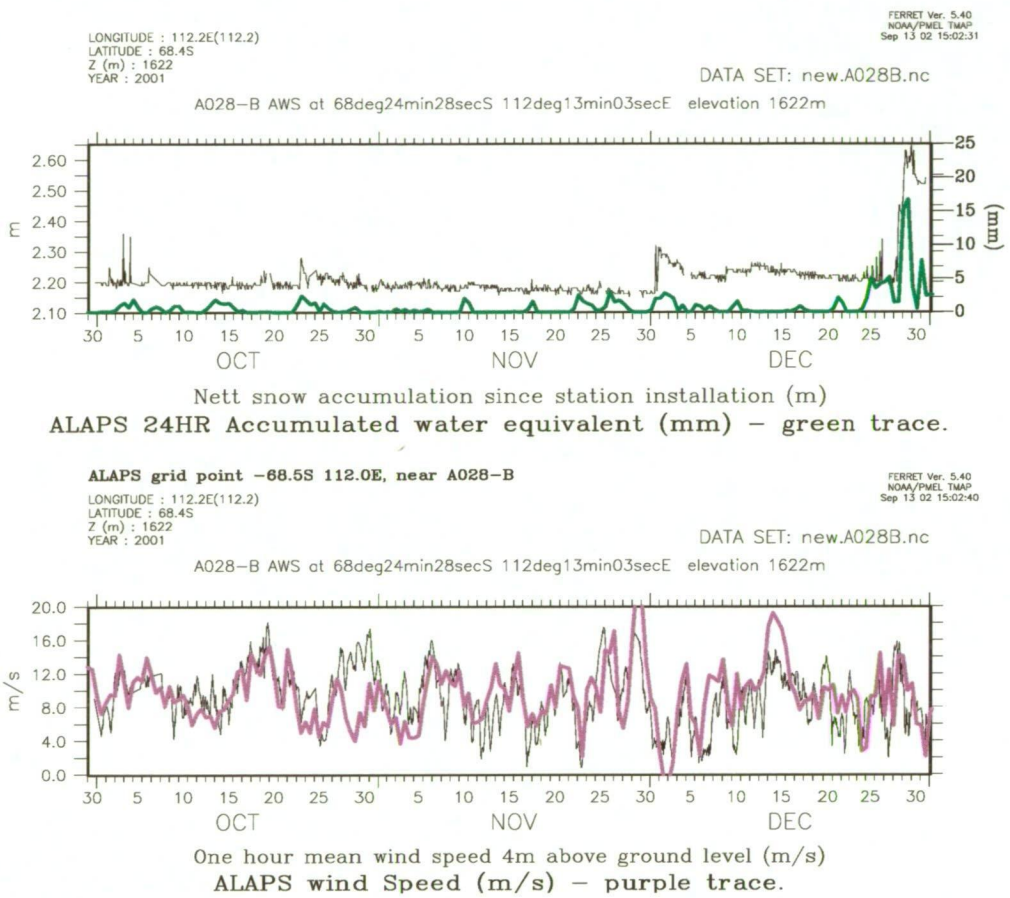

Figure 4.38: A comparison of ALAPS 24 hour accumulated precipitation forecasts (top panel, green), and ALAPS near surface wind speed (lower panel, purple), with observations of snow accumulation (top panel, black), and wind speed (lower panel, black) from the AWS at A028-B, for the period 1 October 2001 to 30 December 2001.

significant surface evapouration. The large precipitation event forecast in early July is seen in the AWS accumulation record with a significant jump during 9 July, and others on 10 and 12 July. However, the large spike in the AWS accumulation record on 18 July was not accompanied by any forecast precipitation from ALAPS. Wind speeds at this time were high and may have corrupted the AWS accumulation record, or resulted in sastrugi moving under the AWS accumulation sensor, but it is also possible that the ALAPS forecasts were deficient. On, and around, 31 July 2001 the ALAPS forecasts predicted a significant precipitation event with a peak of near 21 mm per day, yet only a minor spike in the AWS accumulation record was evident on 30-31 July. Wind speeds at this time were very high ($\tilde{}$ 15 ms^{-1}) so it is probable that an appreciable amount of the precipitation was advected across and away from the site. This poses a real problem in defining a relationship between the magnitude of the precipitation event and the amount of snow accumulated at a site. In all probability the ALAPS forecast did capture a significant precipitation event, since AVHRR infrared imagery from that time (Figure 4.39) showed a substantial cloud band over the area with a clearly visible feed of moisture from the northeast. However, coupling of strong wind with the precipitation event appears to have caused blowing snow, leading to a dampening in the spike in the AWS accumulation record. Perusal of the A028-B data and ALAPS forecasts does show reasonable agreement between forecast precipitation events and spikes in the AWS accumulation record. There were 19 ALAPS forecast precipitation events exceeding 3 mm/day over the 6 month period, with 11 of these events showing a corresponding AWS accumulation spike, suggesting 8 forecast events that did not occur. Similarly,

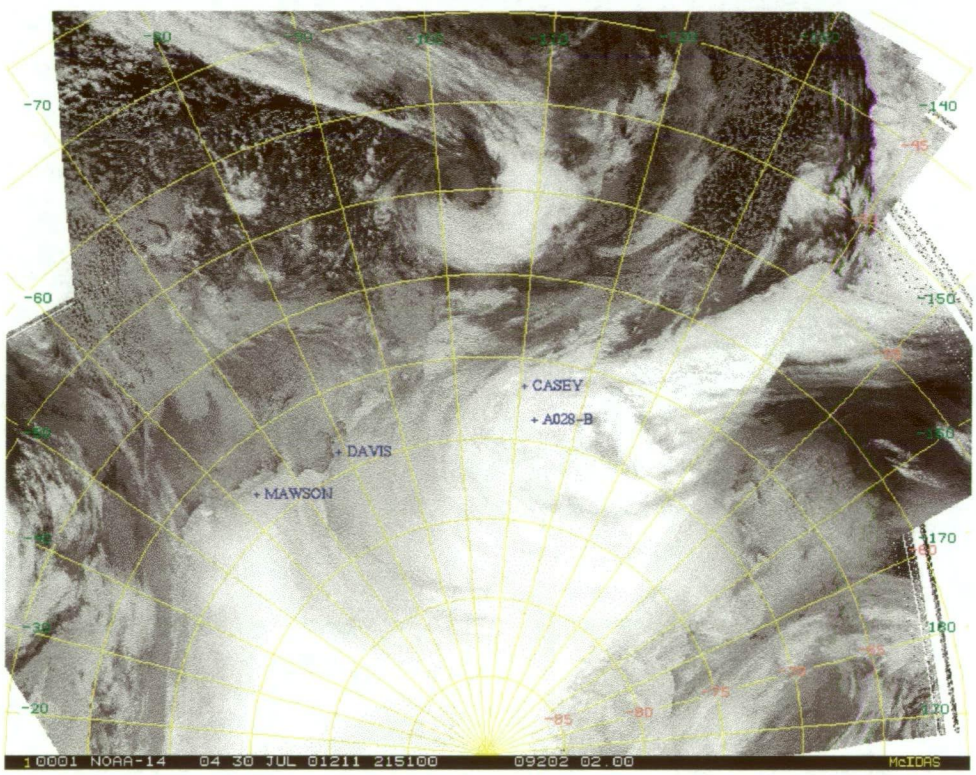

Figure 4.39: AVHRR band 4 thermal infrared mosaic of East Antarctica, valid at 2151UTC, 30 July 2001.

the AWS accumulation record shows around 12 spikes for which there was no corresponding ALAPS forecast precipitation event, although it was possible that these spikes were associated with dry wind events, where drifting snow accumulated at the site, as on most of the 12 occasions strong wind was either observed or forecast. Similar statistics show up in the analysis of observational and forecast data from the remaining three AWS sites of DSS, Amery-G3 and GF08-A.

4.3.4 Discussion

The performance of single-station precipitation forecasts from ALAPS probably fall short of what is ideally required by operational forecasting services. However, the forecasting of precipitation events and long-term averages seems good and may be considered useful in assisting the forecast process. One of the primary forecast concerns in Antarctica is reduced visibility and loss of surface and horizon definition, which is often caused by falling or blowing snow. At its worst, blowing snow, or very heavy falling snow, can lead to white-out conditions in which the horizon and surface definitions have completely disappeared. If significant precipitation rates are forecast and they are coincident with forecast strong wind then the forecasting of poor visibility, or blizzard conditions, is not difficult. However, if forecast precipitation rates are low or non-existent, yet strong wind is still expected, it is not an easy task to forecast poor visibility, or reduced surface and horizon definitions, in drifting snow without some knowledge of the availability of surface snow upstream of the forecast site. However, by maintaining an archive of accumulated precipitation, and strong wind events, it should be possible to

infer the availability of surface snow for such occasions and thus be able to make an educated assessment of the likelihood of surface snow being available and lifted to cause adverse conditions. Figure 4.40 (July to December 2001), and Figure 4.41 (January to June 2002), show the mean daily accumulation rates for each month through the 12 months that the ALAPS system was run, highlighting the seasonal variability in the coastal precipitation maxima. Ongoing maintenance of such charts would provide a useful tool in assessing the surface snow availability for visibility forecasting in strong wind events.

The ALAPS system has only been run for a 12 month period so long-term or climatological monthly mean charts of accumulated precipitation are not available, and a more formal assessment of model bias compared with other accumulation studies not possible. However, despite the problems associated with single-station forecasts it does appear that the ALAPS fields of precipitation, in the mean, do provide useful information on the spatial and temporal variation of precipitation around Antarctica. The physical parameterisations employed within the ALAPS model have not been altered from the mid-latitude version at all and it may well be possible to better tune the model to enhance and improve the Antarctic precipitation forecasts. Certainly the model forecasts of available moisture (mixing ratio) appeared to be accurate from the comparison of the +24-hour ALAPS forecasts of mixing ratio with data from the Casey, Davis and Mawson radiosonde flights, as shown in Figure 4.42. At each of the three stations the model showed a negative bias through the troposphere, with a small positive bias in the stratosphere. In the lowest 700 hPa of the troposphere the bias was between 0.1 and 0.2 g/kg for each of the three stations, with mean observed mixing

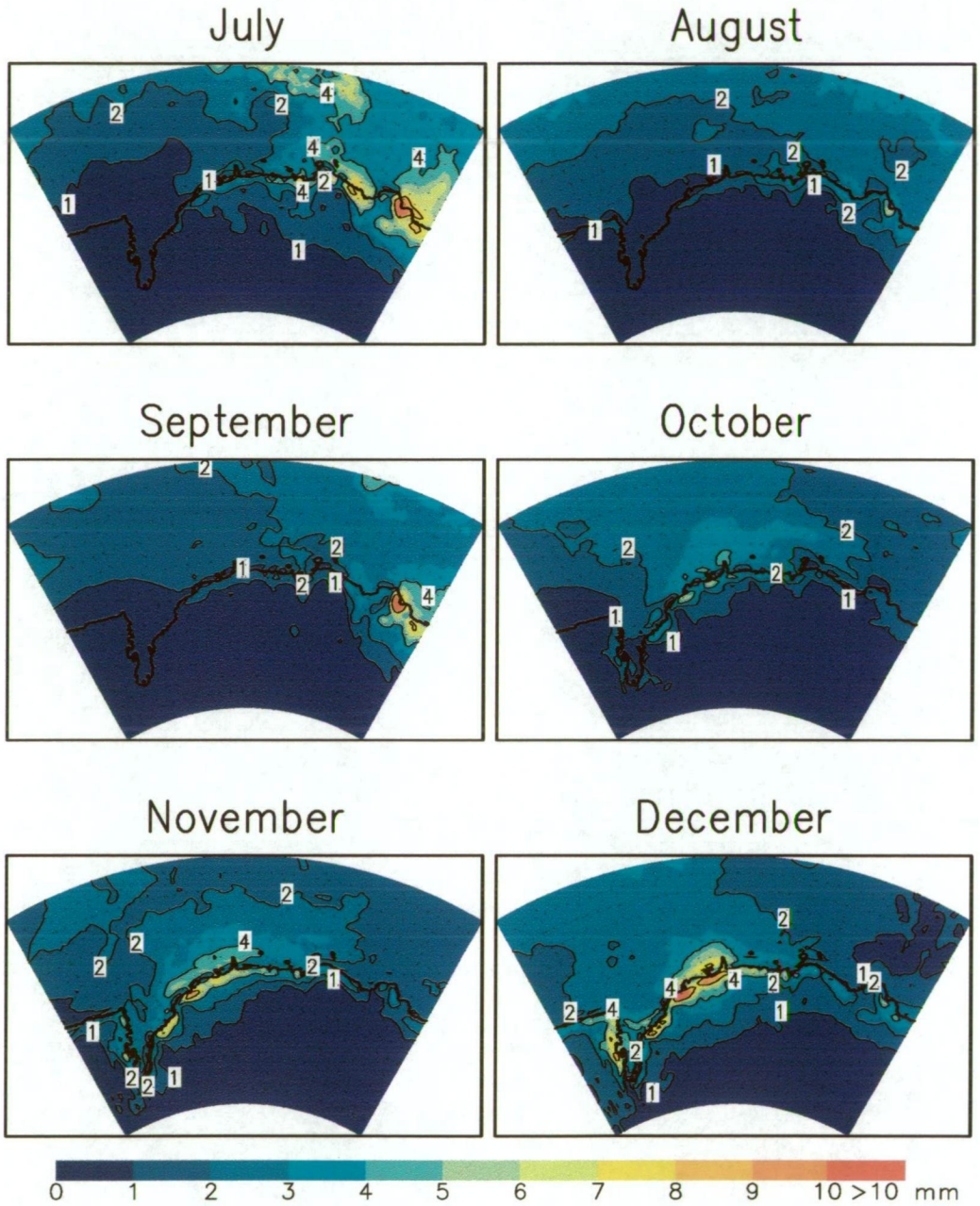

Figure 4.40: Mean daily accumulation (precipitation, mm) for each month from July until December 2001.

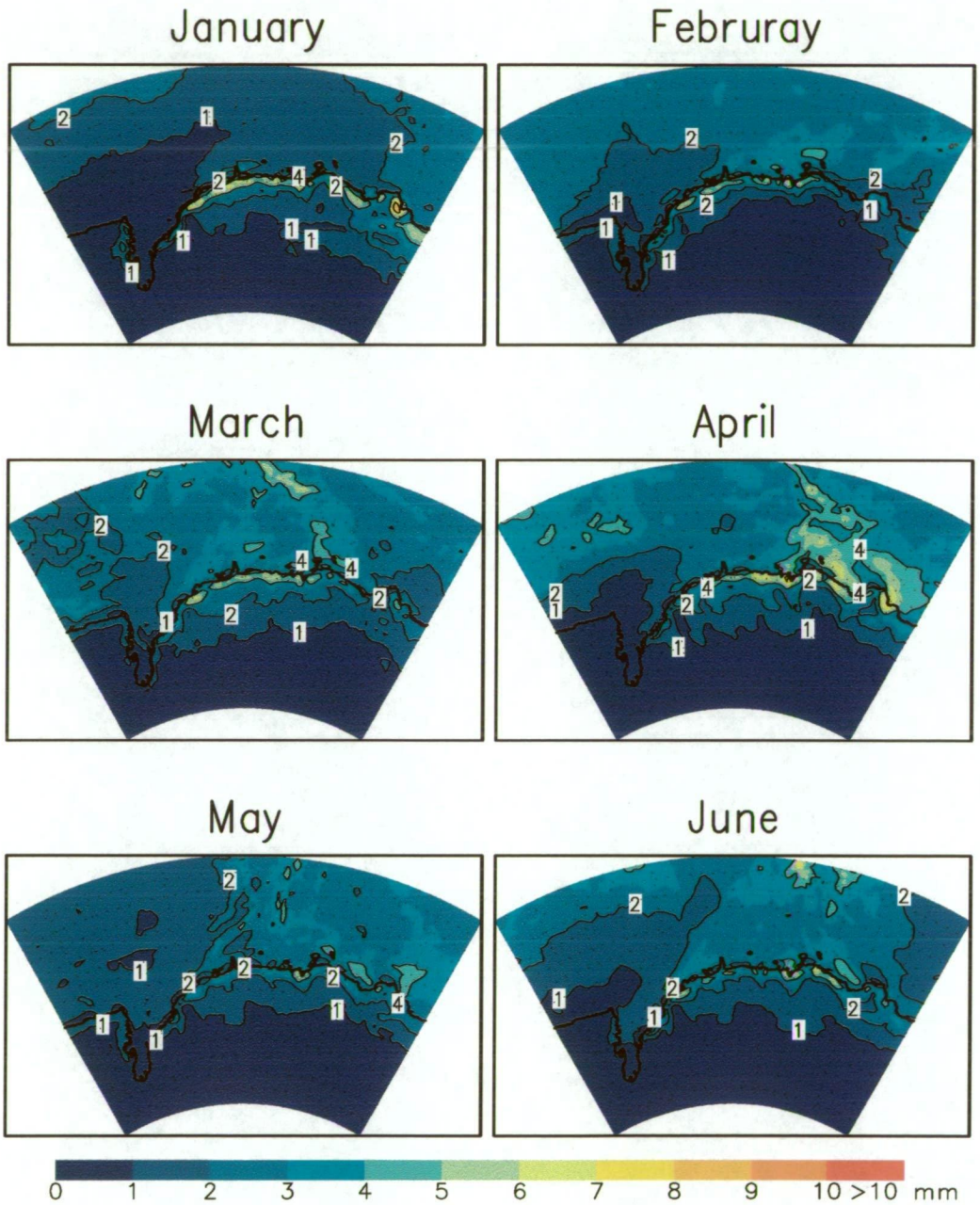

Figure 4.41: Mean daily accumulation (precipitation, mm) for each month from January until June 2002.

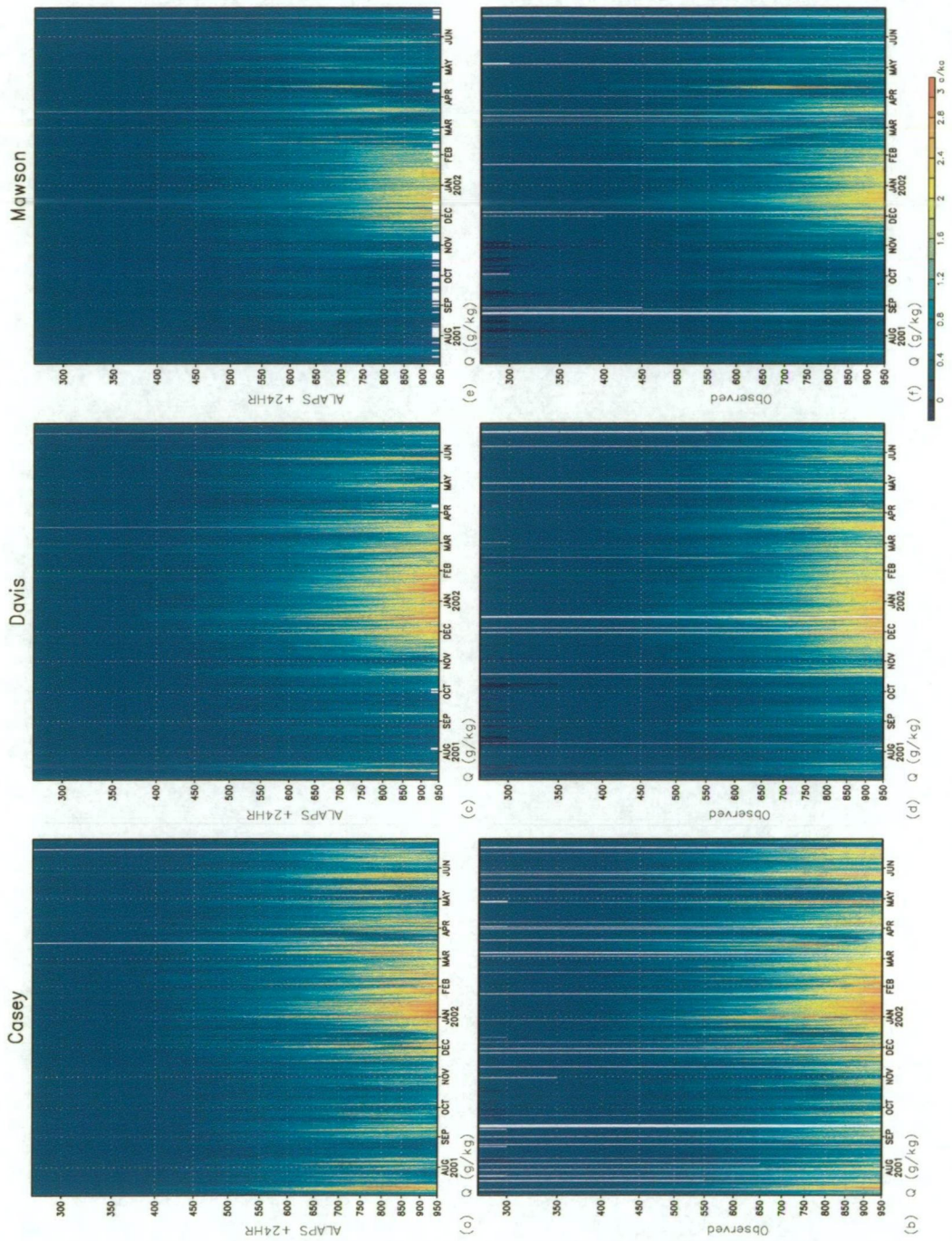

Figure 4.42: A comparison of ALAPS forecast mixing ratio (g/kg), (top three panels), with observed mixing ratio, (bottom three panels), from Casey, Davis and Mawson, for the period July 2001 to June 2002.

ratios varying from 0.7 g/kg at Mawson to 1.2 g/kg at Casey. In general, the RMS errors in the lowest 700 hPa were of the order of between 0.3 and 0.5 g/kg. Given the reasonable quality of the ALAPS moisture forecasts, and known biases, at high latitudes it should be possible to improve the precipitation parameterisation scheme as with the AMPS system (Bromwich et al. 2001 and Cassano et al. 2001) for use in the Antarctic environment and improve the precipitation forecasts.

4.4 Cloud forecasts.

Cloud cover is an important weather element in Antarctica from an aviation weather forecasting perspective where cloud has a negative impact on surface and horizon definition. Uniform layers of cloud, at any height, over the snow and ice cover of the continent, or extensive areas of unbroken fast-ice or pack-ice around the coast, have the potential to significantly reduce both the surface and horizon definitions, making visual flying operations unsafe, and at times impossible. Having reliable model guidance of cloud cover provides the potential for forewarning pilots of possible surface and horizon definition problems associated with cloud, and obviously warning of areas of low cloud that may impact on flying operations. The model cloud images described in the forecast systems chapter, and used in the auto-TAF generation for defining both cloud layers and surface and horizon definitions, were deduced from the model relative humidity profiles. The ALAPS physics code carried fields of low, middle and high cloud, but it was felt that the relative humidity values available at all model levels provided a better means of deducing a more detailed cloud structure. A problem with

this approach was deciding what threshold values of relative humidity were appropriate at each model level to decide whether cloud was present or not. The approach taken in this study was to assess observations of cloud base heights from the Casey Station surface observations against the upper profiles of relative humidity taken from the station radiosonde flights. Comparison of the observations highlighted the fact that cloud at high levels was associated with relative humidity values significantly less than 100%, in fact by the upper troposphere, cloud was being observed with relative humidity values as little as 60%, and in some cases lower. In the boundary layer relative humidity values between 90 and 100% were more typical. Model levels above the 0.275 sigma level (approximately the height of the tropopause) were not included in the generation of the cloud images, because inclusion of data from the model stratosphere resulted in a very cold, wave like signal, in the generated cloud field, which appeared to be like a gravity wave signal in the stratosphere, and probably associated with gravity wave energy reflecting off the upper boundary back into the model domain. Even capping the cloud field to levels below σ=0.275 resulted in some wave like signals evident in the model cirrus cloud around Antarctica. The threshold values were set at 99% for the lowest three σ-levels then falling away to 60% by σ=0.275. The scheme had threshold relative humidity values falling away rapidly from 99% at σ=0.9943 to 70% by the 0.85 sigma level (approximately 1200 m, or 4000 ft), and then linearly falling away to 60% by σ=0.275 (approximately 9000 m, or 30000 ft).

Verifying the model cloud images was difficult as there are very few observations of clouds made, apart from at the staffed stations, concentrated

around the Antarctic coast. The auto TAF system (chapter 7) included the model cloud within the body of the TAF, and also used the model cloud to deduce surface and horizon definition, making verification of model TAFS against surface observations one means of model cloud verification. It was also possible to build up statistics of model clouds from both the model derived cloud fields and the observations from staffed stations around the Antarctic coast. Table 15 shows a comparison of ALAPS cloud statistics

2001/02	Cloud days	Under 5000 ft	Under 1500 ft	Under 500 ft
Summer	Obs/Fcst	Obs/Fcst	Obs/Fcst	Obs/Fcst
October	77% / 59%	35% / 19%	0% / 0%	0% / 0%
November	73% / 59%	30% / 19%	3% / 2%	0% / 0%
December	71% / 52%	39% / 34%	10% / 9%	0% / 0%
January	94% / 82%	87% / 52%	39% / 20%	10% / 7%
February	86% / 77%	79% / 54%	14% / 14%	0% / 5%
March	77% / 67%	48% / 32%	6% / 0%	0% / 0%

Table 15: Comparison of observed cloudiness at Casey station and model derived cloudiness at +24 hours into the model integration.

from the grid-point at -66.25^{o}S, 110.5^{o}E, with the observed cloud statistics from Casey Station. A day was deemed to be cloudy if there were three observations during the day with more than 3/8 of cloud at any height. A day was considered to have cloud below 5000 ft if there were 3 observations during the day where there was more than 3/8 of cloud below 5000 ft, and similarly for 1500 ft cloud days and 500 ft cloud days. The results are presented as a percentage number of days in the month meeting the criteria. Overall, the forecasts of cloud amounts were low, which was consistent with the results from the ALAPS precipitation analysis, where it was found that the ALAPS bias in mixing ratio in the lowest 700 hPa was around -0.2 g/kg, reducing to near a zero bias in the upper tropopause. The negative model

bias in mixing ratio was equivalent to around -2 to -5% bias in relative humidity for typical temperatures in the lower troposphere. To test whether these biases had an impact on the cloud statistics shown in Table 15, the threshold values of relative humidity in the lower troposphere were reduced, with the lower levels reduced by 5%, tapering off to only a 1% reduction by the 0.6 sigma level, (around 4000 m or 13000 ft). The surface layer (first three sigma levels) were maintained with a 99% relative humidity threshold. Table 16 details the updated ALAPS cloud statistics using the lowered

2001/02	Cloudy Days	Under 5000 ft	Under 1500 ft	Under 500 ft
Summer	Obs/Fcst	Obs/Fcst	Obs/Fcst	Obs/Fcst
October	77% / 64%	35% / 28%	0% / 0%	0% / 0%
November	73% / 60%	30% / 28%	3% / 3%	0% / 0%
December	71% / 56%	39% / 44%	10% / 13%	0% / 5%
January	94% / 90%	87% / 63%	39% / 31%	10% / 11%
February	86% / 83%	79% / 54%	14% / 13%	0% / 6%
March	77% / 68%	48% / 40%	6% / 0%	0% / 0%

Table 16: Comparison of observed cloudiness at Casey station and model derived cloudiness at +24 hours into the model integration using the updated threshold relative humidity values.

tropospheric threshold values, and highlights the better agreement with the observations.

The geographic distribution of significant low cloud, such as that detailed in Table 16, provides very useful data for local flying operations. Figure 4.43 shows the monthly distribution of percentage cloudy days in the Casey area, with Figure 4.44 the percentage days with cloud below 5000 ft (1524 m) above the surface, Figure 4.45 percentage of days with cloud below 1500 ft (457 m) above the surface, and Figure 4.46 the percentage number of days with cloud below 500 ft (152 m) above the surface. What is significant

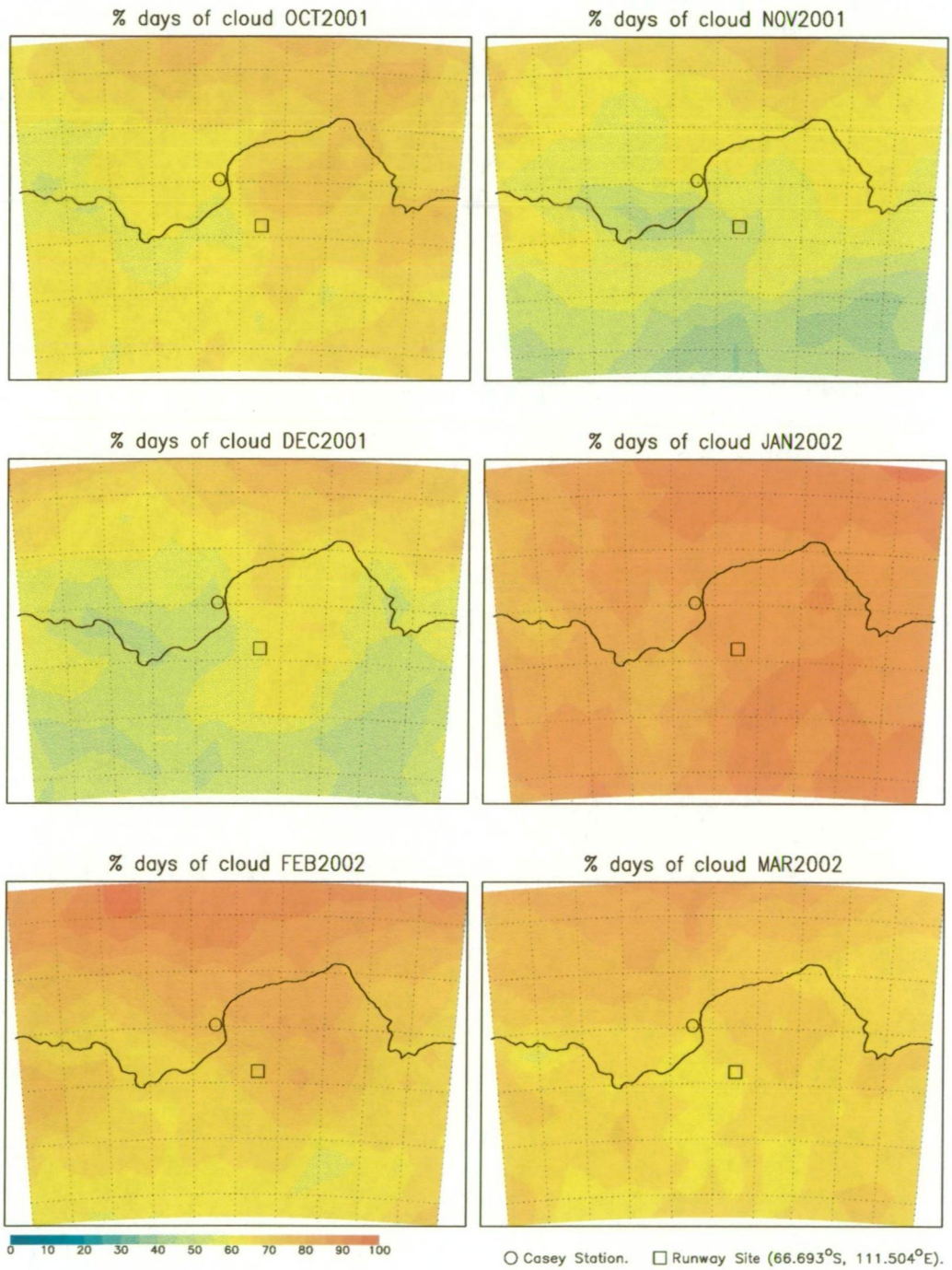

Figure 4.43: Percentage number of days in the month with cloud at any level in the Casey area, for the period October 2001 to March 2002 derived from the ALAPS +24 hour cloud forecasts.

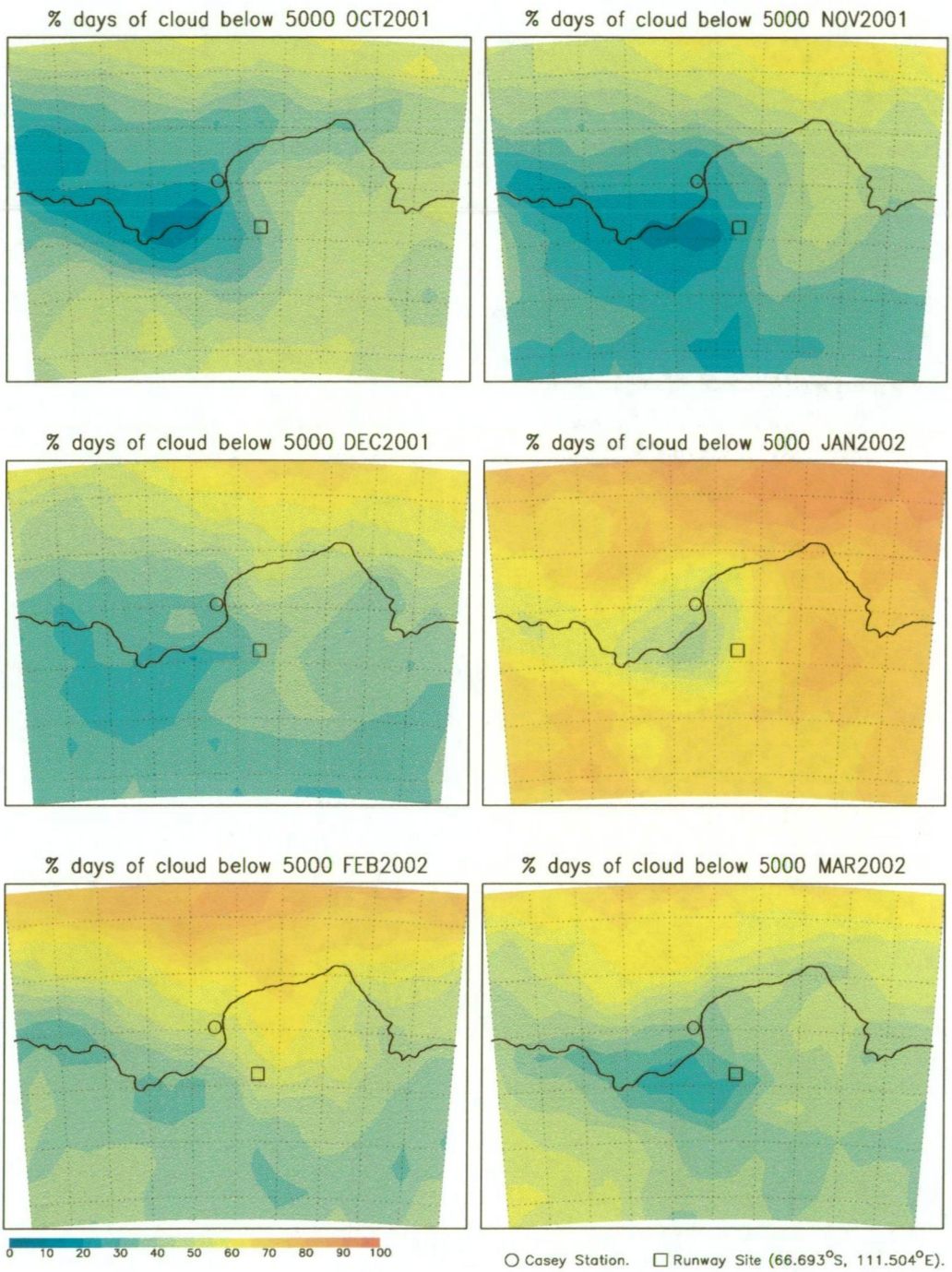

Figure 4.44: Percentage number of days in the month with cloud below 5000 ft in the Casey area, for the period October 2001 to March 2002 derived from the ALAPS +24 hour cloud forecasts.

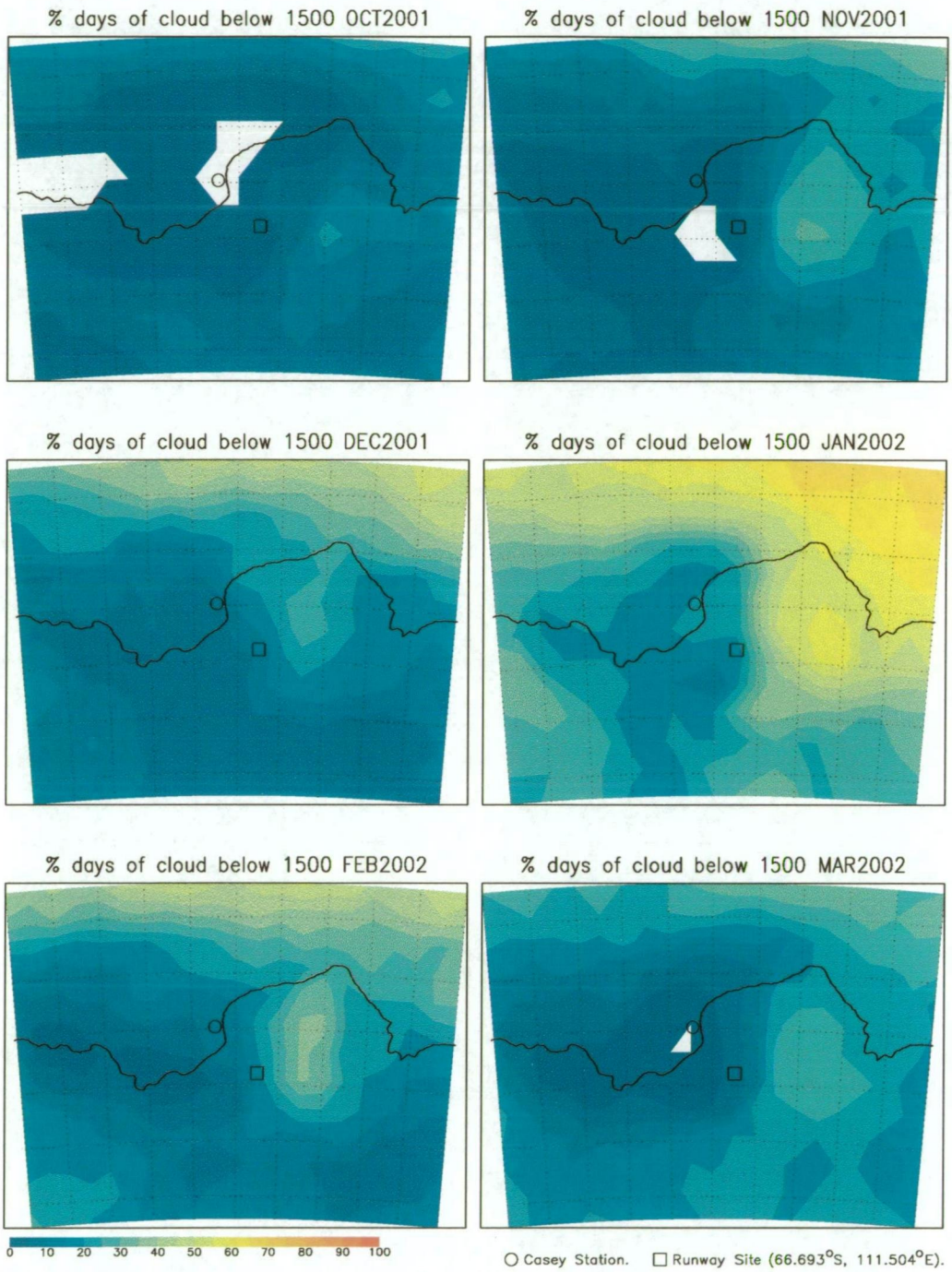

Figure 4.45: Percentage number of days in the month with cloud below 1500 ft in the Casey area, for the period October 2001 to March 2002 derived from the ALAPS +24 hour cloud forecasts.

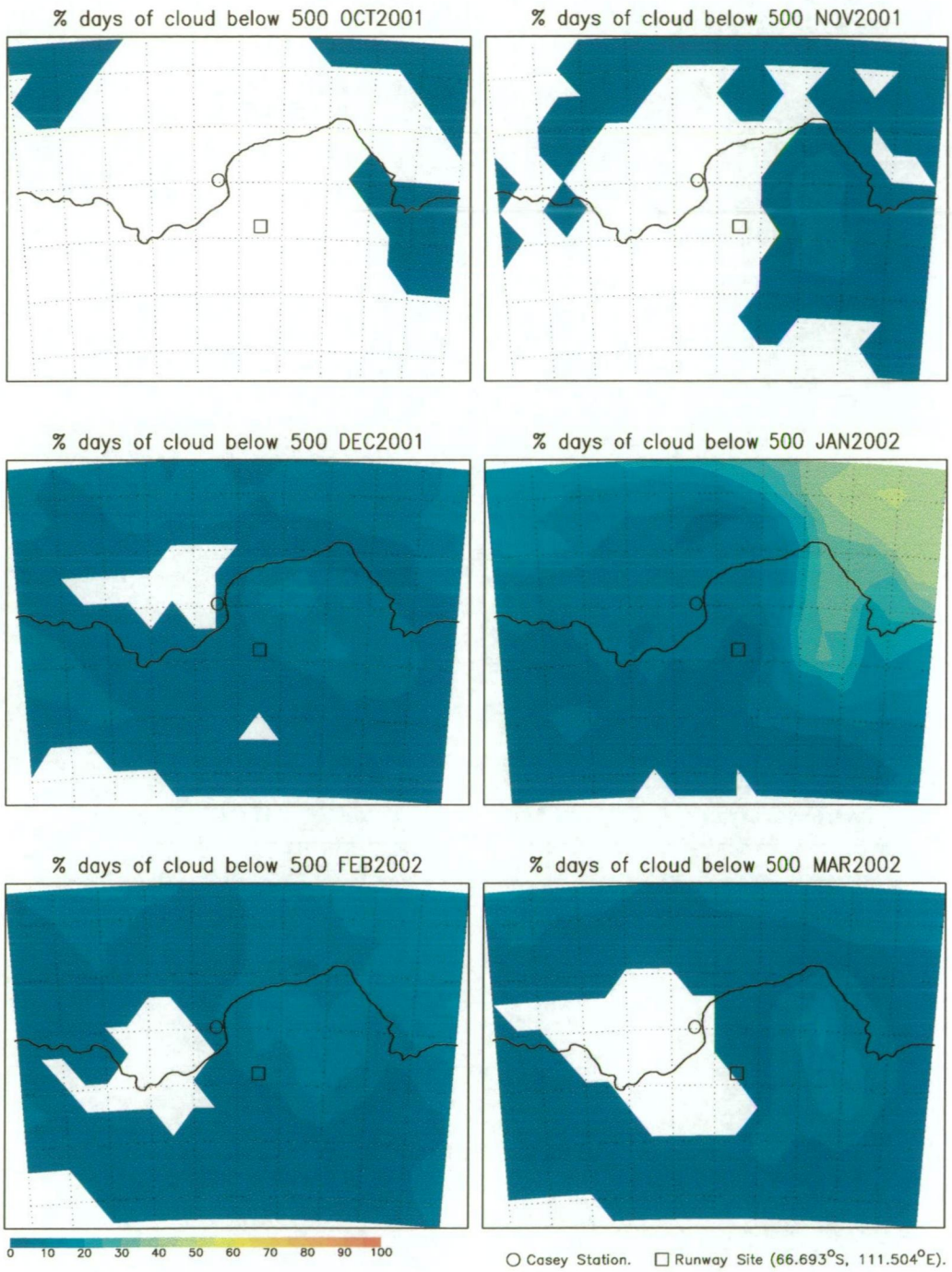

Figure 4.46: Percentage number of days in the month with cloud below 500 ft in the Casey area, for the period October 2001 to March 2002 derived from the ALAPS +24 hour cloud forecasts.

from these graphs is the distribution of cloud around Law Dome, to the east of Casey, and south-westward across Vincennes Bay to the Vanderford and Adams Glaciers (see Figure 1.5 for location details). The eastern side of Law Dome was significantly cloudier than the west and there was a distinct minima in low cloud southwest of Casey over the Adams Glacier. The open circle on each of the figures marks the location of Casey Station, while the open square marks the location of the proposed runway (as of March 2003), to be used for long range, inter-continental, flights from Hobart in Tasmania, to Casey. In general, low cloud events drop away in number to the south of Casey but with the runway at an elevation of around 727 m and located to the southeast of Casey the model statistics suggest that low cloud events would be slightly less than at Casey, although overall cloudiness very similar, if not slightly cloudier. Spring and autumn months (October, November and March) were relatively low-cloud free, but the summer months of December, January and February saw a rise in the number of days expected to be adversely affected by low cloud. Cloud below a nominal circling minima of 500 ft were still not common, at around 15% of days during January (about 5 days out of the month). However, the number of days with significant cloud below 5000 ft rose to a maximum during January of 70%, or about 22 days in the month, which may have a negative impact on surface and horizon definition. Independent data to verify the distribution of cloud around Casey was almost non-existent, however, from late October 2001 until mid December 2001 there was a surveying team located at -66.574^{o}S, 111.192^{o}E, some 2.6 km due north of the proposed runway site. Some observations of cloud were taken during the period, although not of the standard, or fre-

quency, expected of an established observing site. During November of 2001 there were 19 days on which observations were taken, and of these there were indications of 13 cloudy days (68%) , 6 of which were with "low" cloud events (32%). During December 2001 there were 10 days of observations, of which 9 were deemed cloudy (90%), with 8 of them "low" cloud days (80%). No definition of "low" was forthcoming but was assumed to be less than 5000 ft. Given the lack of definite cloud base heights and the very limited number of observations, the observed cloudiness values were not too dissimilar to those observed at Casey or predicted by ALAPS.

5 Case studies

Several unique forecasting problems are routinely faced by meteorologists working in Antarctica, and the usefulness of any NWP system may be gauged against how well the numerical guidance performs in forecasting these unique situations. The usefulness of the NWP may also be judged on the ability of the high resolution model output data to define the underlying meteorology associated with the unique aspects of Antarctic weather. This chapter presents four case studies of varying weather situations that challenge the Antarctic forecaster, with the first looking at the influence of low pressure systems and frontal bands in the Casey area that routinely cause the near surface wind speed to exceed storm force, and occasionally hurricane strength, with the severe wind conditions often lasting for several days. The second case study looks at the more unusual wind event at Casey Station, where a strong to gale force southerly wind reaches Casey, under clear sky conditions. The third case study is of the katabatic wind regime experienced in and around Mawson, and the last case study an assessment of the ability of the ALAPS system to provide useful oceanic forecasting guidance for ships plying the Southern Ocean, to the south of Australia. The bulk of this chapter is now in press (Adams 2004b), adding to the growing body of literature on high resolution numerical modelling of the Antarctic atmosphere, in support of weather forecasting.

5.1 Casey easterly storms

One of the key meteorological problems in the Casey area is forecasting the onset and strength of storm force wind events that are associated with either

the passage of extra tropical cyclones to the north of the station, or with very strong frontal systems generated from deep low pressure systems situated to the west-northwest of Casey. Despite being able to track the passage of such synoptic scale features with reasonable accuracy, and monitor the increasing gradient wind speed from data received from the AWS on the summit of Law Dome (Figure 1.5), forecasting the onset of what is often hurricane strength wind at Casey has been problematical. Nowcasting techniques, involving the monitoring of fluctuations in the local wind, and visually monitoring the drift tails of blowing snow caused by increasing wind speed on the steep coastal escarpment inland of Casey, can assist in onset timing to within an hour or so. However, reliably forecasting 12 to 48 hours in advance has not been possible. Several studies have been undertaken to assist in our understanding of the dynamics associated with these events, such as Murphy (1990 and 2003), Wilson (1992), Adams (1996) and most recently by Turner et al., (2001), but in all, no conclusive evidence has been found to categorically define the dynamics associated with the onset and maintenance of what is a significantly super-geostrophic flow at Casey, nor provide any forecasting rules for reliably predicting such events 12 to 24 hours in advance. The lack of a mesoscale network of surface and upper air data in the area has limited the effectiveness of the above observational studies and it is in this respect that a high resolution atmospheric numerical model may be able to assist in providing a detailed description of the dynamics associated with the enhanced flow and, more importantly assist in more accurately forecasting storm onset and duration.

The most popular current theory as to why Casey experiences a sig-

nificantly super-geostrophic, and indeed, super-gradient, wind speeds is described in the paper by Turner et. al. (2001) and it is this theory that the ALAPS model output appears to support. The Turner (2001) paper proposes a scenario in which the extreme wind at Casey develops as a response of: (1) a synoptic scale high-low pressure couplet, providing a strengthening pressure gradient; (2) entrainment of radiatively cooled air by the super critical synoptic gradient, leading to down-slope flow; (3) the acceleration of the wind down the lee slope of Law Dome, occurring primarily in response to an orographically induced, long period, vertically propagating gravity wave; and (4) sources of negative buoyancy, including pre-storm radiatively cooled air and, later in the storm, maritime air cooled by heat flux to the ice surface. The orographically induced gravity wave increases the horizontal temperature difference, thus increasing the negative buoyancy of the surface air-flow.

As discussed in the previous section, the performance of ALAPS in forecasting the onset of strong wind events was considered good, with the model able to forecast, with some accuracy, the surface storm force wind events over the 2001-2002 12 month period. A closer study of the model 4-dimensional evolution of the flow around Casey during such a storm may provide useful clues to understanding the dynamics of these extreme events. One such event, lasting 3 days, commenced on 6 September 2001 where the wind at Casey increased from around 8 knots to just over 60 knots within a three hour period, and persisted at over storm force (48 knots) until late on 7 September, and over gale force until 2100UTC on 8 September (Figure 5.1). Perusal of Figure 5.1 highlights the fact that, although the storm was a significant event, it was not unusual, with 4 other strong events during September alone.

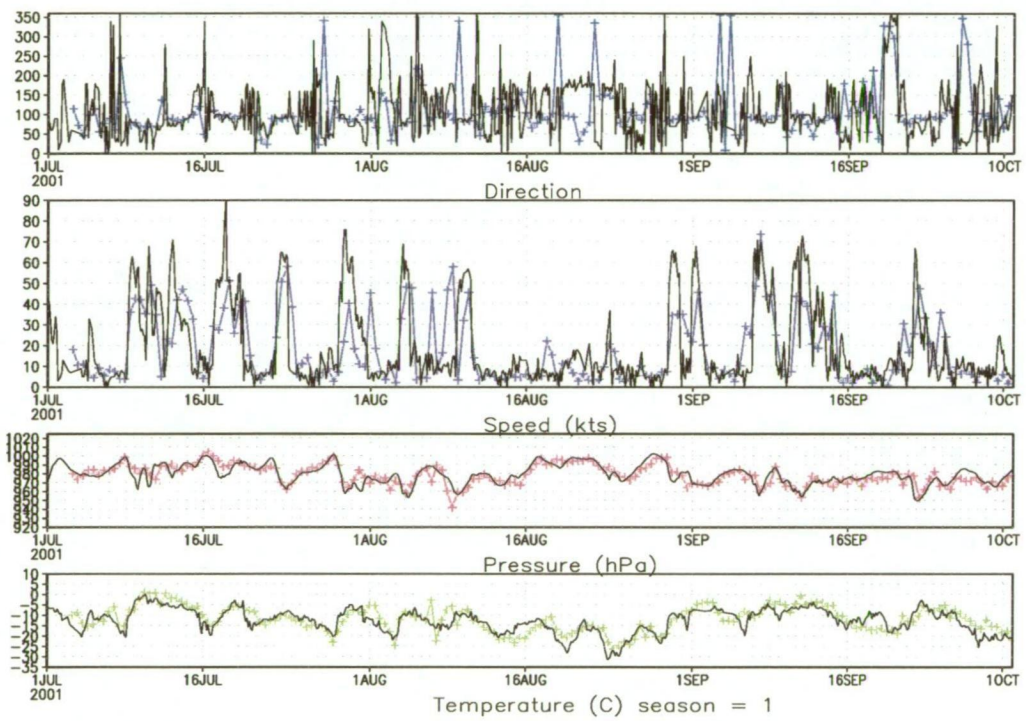

Figure 5.1: Comparison of ALAPS +24 hour surface data (coloured time-series) with observations from Casey Station (black time-series), for the 3 month period from 1 July 2001.

A comparison of the Casey surface observations with ALAPS model output from the run initiated at 2300UTC on 5 September (Figure 5.2) showed that

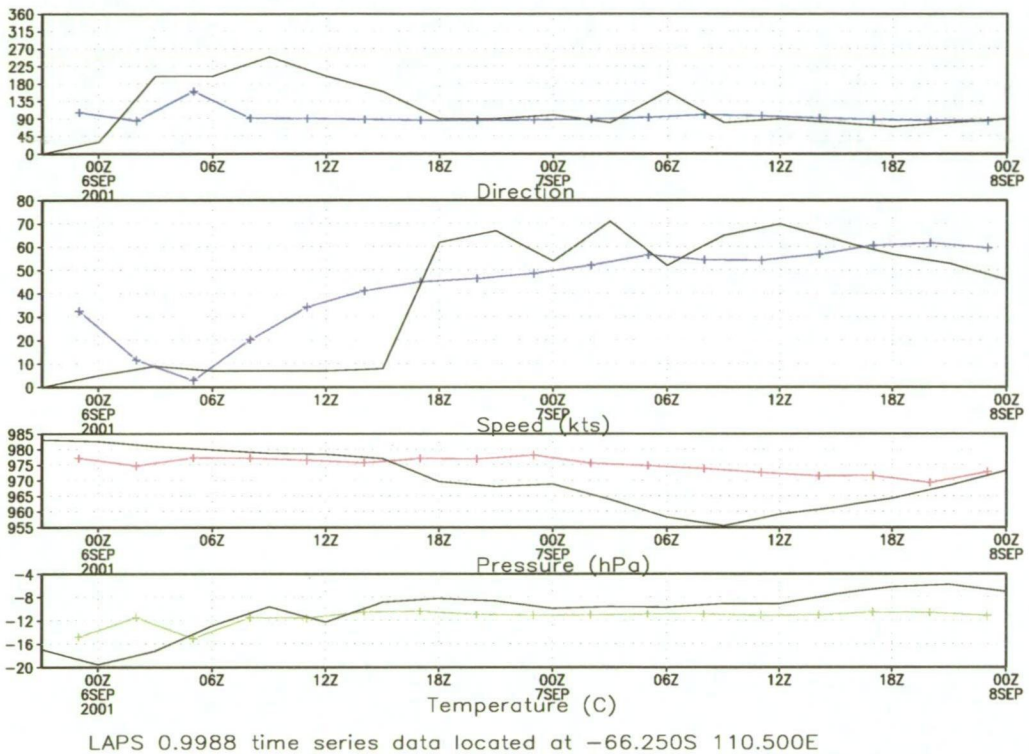

Figure 5.2: Comparison of ALAPS 3 hourly surface data (coloured time-series) with observations from Casey Station (black time-series), for the model run initiated at 2300UTC on 5 September 2001.

the model (coloured lines) gradually increased the wind from 0800UTC on 6 September, some 9 hours earlier than the actual onset (black lines denote Casey observations), but maintained storm force wind for the remainder of the model run. The +24 hour modelled surface flow around Casey and Law Dome (Figure 5.3), near the height of the storm (2300UTC 6 September 2001), showed a region of very strong wind on the western side of Law Dome (shaded area) with a tongue of very strong flow out to the northwest, and an area of relatively light wind over Vincennes Bay, also extending out to the northwest. The wind speed near the summit, and to the east, of Law Dome

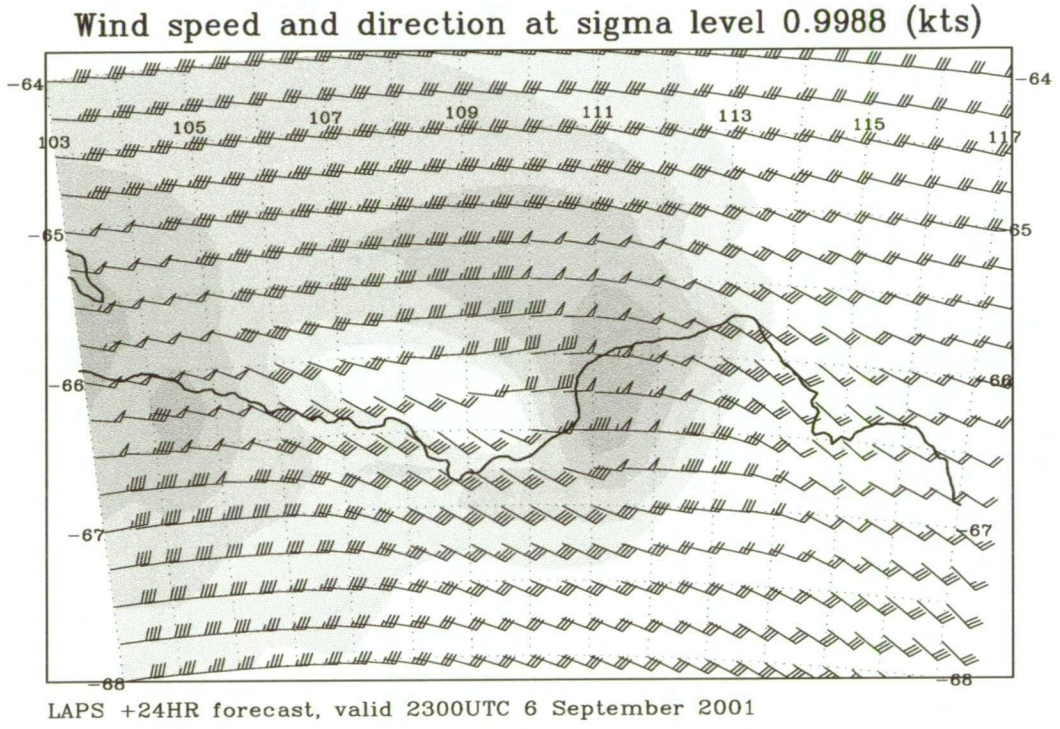

Figure 5.3: ALAPS +24 hour forecast near surface flow in the Casey area, valid at 2300UTC 6 September 2001.

was significantly less than that near Casey, with the summit wind consistent with the gradient wind speed observed off the coast of Casey. The modelled surface flow pattern shown in Figure 5.3 was consistent with the theory of an accelerated down-slope flow in the Casey area. Figures 5.4 and Figure 5.5

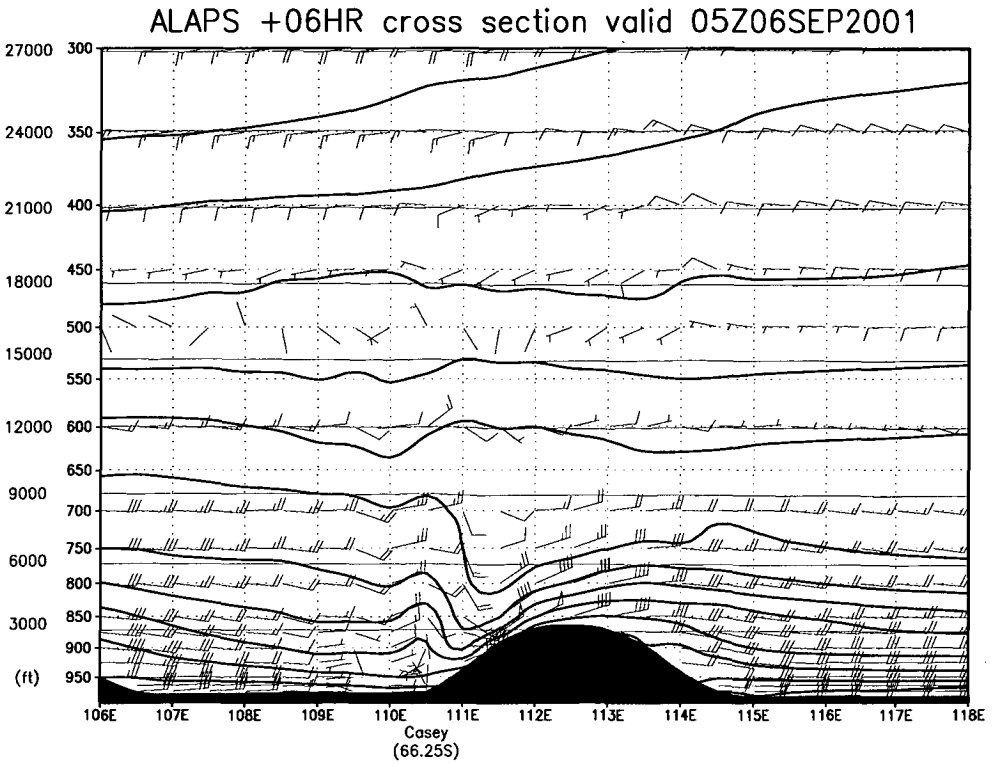

Figure 5.4: Vertical cross-section along the latitude of Casey, showing moist static energy (contours), and air-flow in the vertical plane (wind barbs), from the ALAPS +06 hour forecast valid at 0500UTC 6 September 2001.

show cross-sections along the latitude of Casey from well to the west of Vincennes Bay to well east of Law Dome, with the contour plot showing moist static energy, ($E_{ms} = C_pT + Lq$), a conservative quantity, and overlaid with the wind flow in the 2-dimensional plane (vectorised zonal and vertical velocities), displayed as wind barbs. Figure 5.4 was from the +06 hour model time-step, valid at 0500UTC 6 September, where the flow at Casey was almost calm, and Figure 5.5 at +24 hours (2300UTC 6 September), where the

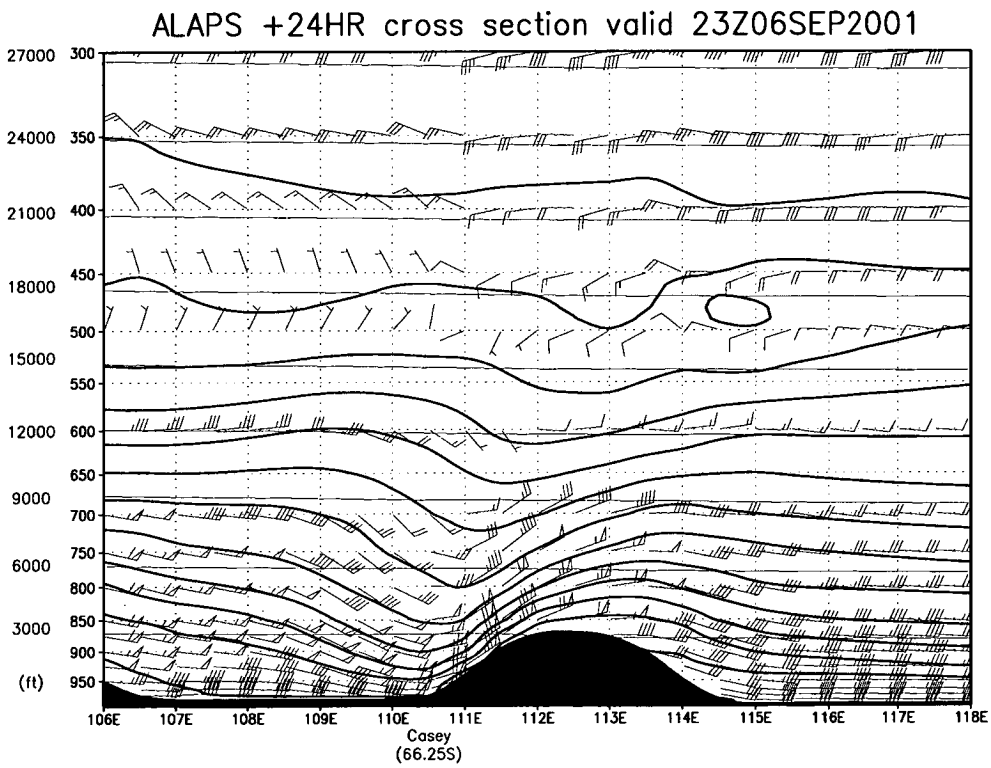

Figure 5.5: Vertical cross-section along the latitude of Casey, showing moist static energy (contours), and air-flow in the vertical plane (wind barbs), from the ALAPS +24 hour forecast valid at 2300UTC 6 September 2001.

flow at Casey was very strong. The accelerated down-slope flow over Casey at 2300UTC 6 September (Figure 5.5) was obvious, as was the emergence of a standing wave in the vertical flow over the Casey area, highlighted in both the moist static energy profile and wind vectors. The modelled surface flow in the Casey area at 0500UTC on 6 September (Figure 5.4), was very light, yet a 45 knot surface wind was evident just up-slope from Casey, providing compelling evidence of an hydraulic jump in the model atmosphere on the lee slope of Law Dome. As mentioned in chapter 3, the ALAPS code invoked the hydrostatic assumption, and with a model resolution of around 27.5 km, an hydraulic jump would not be physically supported by the model code, however, the environment described by the model output was indicative of the flow regime that would support such a phenomenon. Further inferences on the model's ability to capture the dynamics of the storm may be made from comparing the temperature, moisture and wind profiles from the Casey radiosonde flight with +24 hour model output from ALAPS. Figure 5.6 shows the aerological sounding of temperature and dew point from the Casey radiosonde launched at 2300UTC 6 September 2001 (coloured lines), overlaid with the ALAPS +24 hour forecast profiles, valid at the same time (grey lines), with Figure 5.7 showing the Casey observed upper wind profile, at the same time (coloured profiles), overlaid with concurrent +24 hour ALAPS profile data (black, marked, profiles). These two figures highlight both the dynamics of the situation plus some of the model discrepancies. Firstly the model atmosphere was a little too warm in the middle troposphere (Figure 5.6), with the surface temperature inversion layer also modelled as too cool and deep. The model appeared not to adequately capture the moist

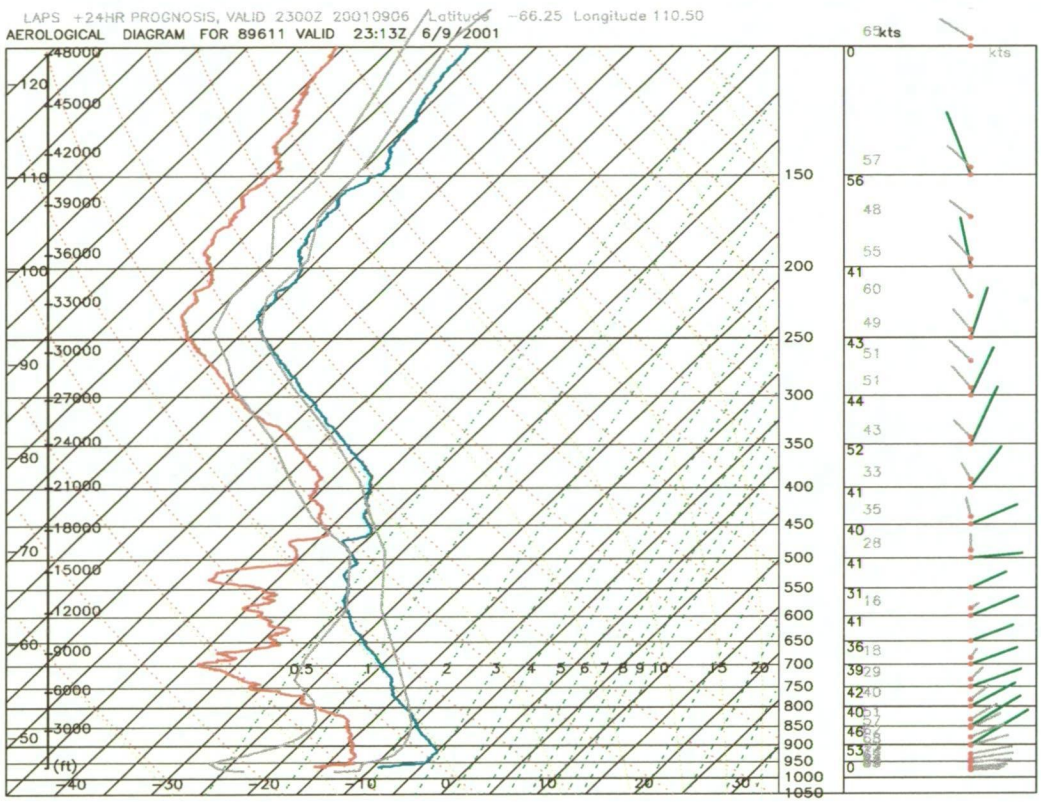

Figure 5.6: Aerological sounding from the Casey radiosonde flight (coloured traces, red dew-point, cyan temperature and green wind), valid at 2313UTC 6 September 2001, overlaid with the ALAPS sounding from the +24 hour forecast valid at 2300UTC 6 September 2001.

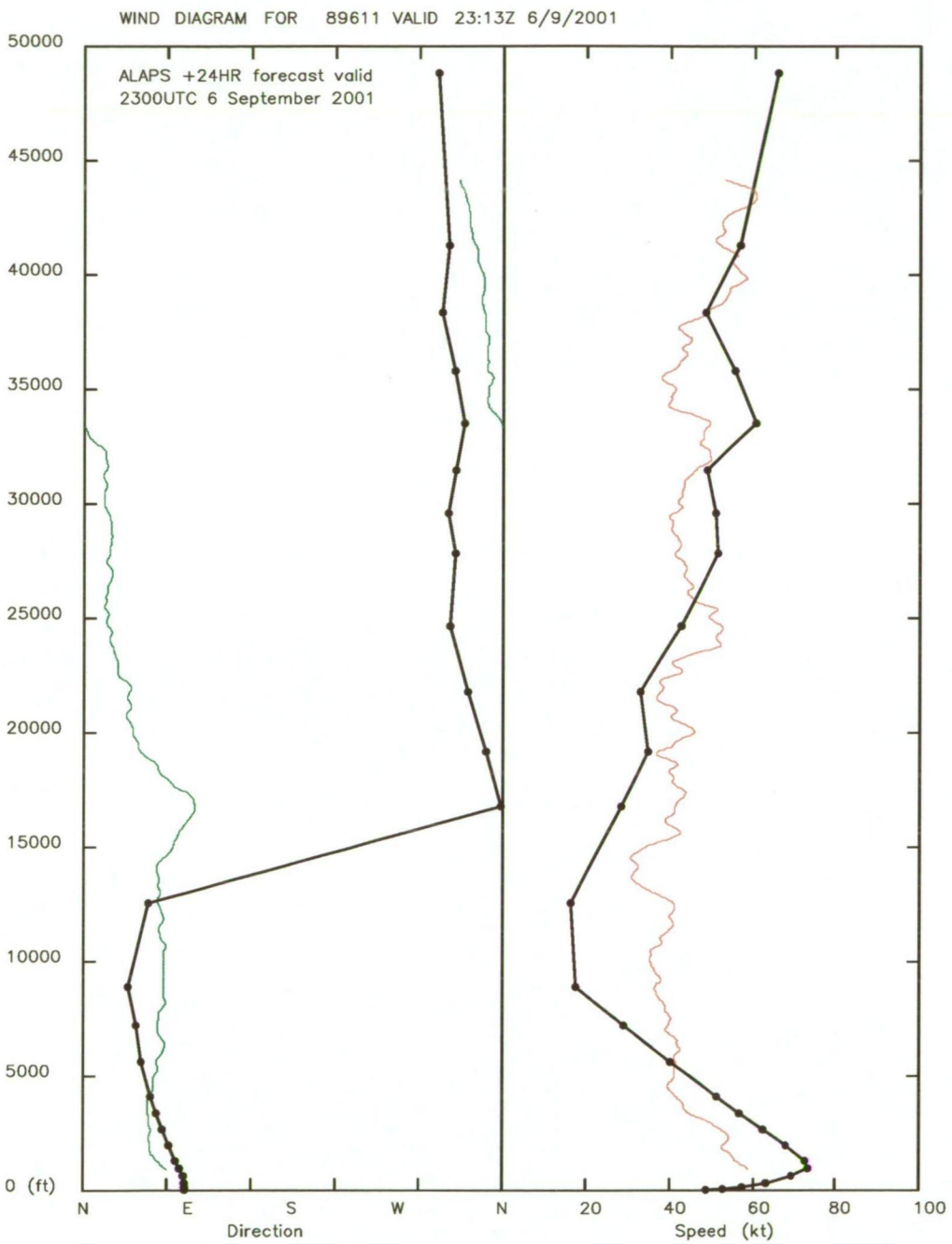

Figure 5.7: Vertical wind profile from the Casey radiosonde flight (coloured traces), valid at 2313UTC 6 September 2001, overlaid with the ALAPS vertical wind profile from the +24 hour forecast valid at 2300UTC 6 September 2001.

adiabatic lapse rate from the top of the surface layer to around 600 hPa, which may have been attributable to the model under-forecasting the wind strength in this layer (Figure 5.7). The radiosonde ascent failed to capture the exact strength of the low level jet, due to problems with the GPS radiosonde technology, and it was possible that the maximum low level wind speed did reach the ALAPS predicted 73.6 knots at 293 m above the surface. Certainly, the maximum recorded wind gust on 6 September 2001 was 71 knots, recorded at 2351UTC, some 38 minutes after the launch of the radiosonde. Given the sharp decrease in wind speed above the surface layer, it would be expected that the gust would have originated very near the surface, and be indicative of the near surface maximum wind speed. However, from Figure 5.7 it was obvious that the depth of the low level wind speed maximum was over-forecast by the model and coupled with the deeper model surface inversion (Figure 5.6). Reasons for these discrepancies have not been fully explored but model diffusion coefficients and the value of the roughness length (0.001 m) may be partly responsible. Of dynamical interest on the aerological sounding at the height of the storm, was the maintenance of a significant temperature inversion (both in reality and modelled), despite the very strong surface wind flow, and expectation of turbulent mixing. Under such strong mixing it would have been expected to see an adiabatic, well mixed, layer, or at least an isothermal layer. Indeed, the observed trace showed an isothermal layer just above 950 hPa, with a moist adiabatic ascent rate above, yet the air below, near the surface, was substantially cooler suggesting strong diabatic effects were still significant, and supporting the Turner et al. (2001) assertion that sources of negative buoyancy due to cool-

ing of the surface air mass by heat flux to the ice surface were adding to the acceleration of the down-slope flow. The modelled +24 hour temperature trace at this time also suggested an isothermal layer over-lying a cooler surface layer, although with the surface layer being too cool and the isothermal region diffuse (Figure 5.6). The wind flow through the troposphere and lower stratosphere was well modelled, although ALAPS did not do well in forecasting the depth of the northeasterly, with the wind shifting into the northwest at around 11000 ft rather than at 35000 ft. By +30 hours the model had veered the wind around into the northeast through the entire troposphere (not shown), in line with the radiosonde observations.

In general, the 2300UTC 5 September 2001 ALAPS forecast did a good job of forecasting the storm, and of defining the dynamics associated with the structure of the storm event. Model output was also consistent with the conceptual model put forward by Turner et al. (2001). Similarly, the ALAPS model run initiated at 2300UTC on 6 September 2001, when the storm was already in full progress, did a good job of forecasting the gradual easing of wind conditions. Figure 5.8 shows a comparison of the observed and modelled surface conditions for the 48 hour period of this model run, with the Casey observations in black, and the ALAPS forecasts in colour. The model missed the minor acceleration in the wind speed early on 7 September but forecast the rise in wind speed during the latter part of 7 September and the gradual decline seen in the wind speed during 8 September. The secondary peak in speed late on 8 September was not faithfully reproduced by the model, however the ALAPS wind speed did rise briefly around 1100UTC on 8 September, consistent with the form of the wind speed trace.

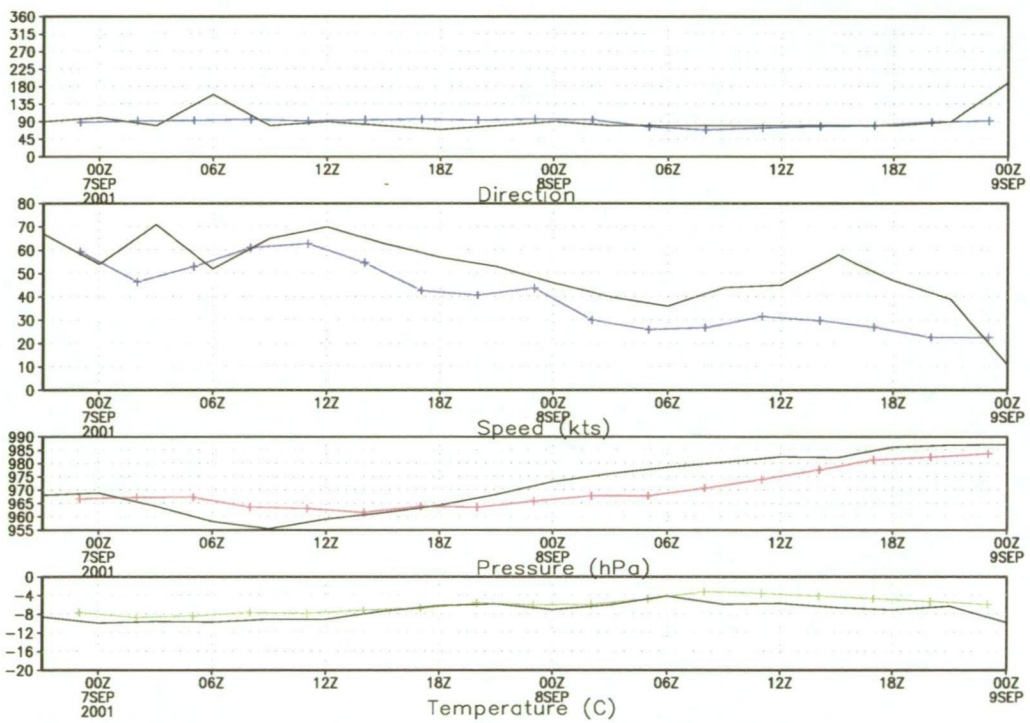

Figure 5.8: Comparison of ALAPS 3 hourly surface data (coloured time-series) with observations from Casey Station (black time-series), for the model run initiated at 2300UTC on 6 September 2001.

5.2 Casey southerly storms

A meteorological event that is poorly forecast in the Casey area is the onset of strong to gale force southerly flow, often accompanied by clear sky conditions. The events have the appearance of a strong katabatic flow moving up the coast from the Vanderford Glacier, situated to the south of Casey (Figure 1.5). However, it is not a common occurrence to see the katabatic pushing as far north as Casey, or of such strength, despite the Vanderford Glacier being only 25 km to the south, and an area that regularly experiences strong katabatic (southerly) flow. Casey generally experiences only light out-flow, and predominantly from the northeast, directed slightly around Law Dome, down from Cape Folger, as evident on the Casey wind rose (Figure 1.6). The katabatic flow off the Vanderford Glacier is often visible from Casey, with a grey "smudge" on the southern horizon, indicative of blowing snow advecting out to sea in the strong south to southeasterly out-flow. Given the common occurrence of the out-flow off the Vanderford glacier, but the rare strong flow at Casey, it has been difficult to identify the ambient conditions that lead to the katabatic reaching as far north as Casey. Simply having a strong flow off the glacier is not enough to predicate the strong flow reaching Casey, casting some doubt as to whether the strong southerly flow at Casey is in fact a true katabatic, given that ambient conditions obviously need to be right for the strong southerly flow to reach as far north as Casey. If the ALAPS dynamics and resolution were sufficient then the model should have captured any such events during the 12 month trial period and so provide a chronology of the developing dynamics associated with the events, and giving valuable clues as to what precursors to the development may be observed in the Casey ob-

servations. During the 12 month verification period of the ALAPS system, 7 strong to gale force south to southeast flows were observed at Casey, with 6 of the 7 events having occurred during periods of ambient light northeast to southeast flow at the station, and with one event directly preceding a gale force easterly storm. Table 17 details the forecast success rate and false

Event	+00HR	+12HR	+24HR	+36HR	+48HR
24 Aug 2001	yes	yes	yes	yes	yes
30 Oct 2001	no	no	no	no	no
29 Nov 2001	yes	yes	yes	yes	yes
14 Dec 2001	yes	yes	yes	yes	yes
19 Mar 2002	yes	yes	yes	yes	yes
2 Apr 2002	yes	yes	no	no	no
5 May 2002	yes	no	no	no	no
False Alarms	0	2	1	1	1

Table 17: Southerly strong wind events at Casey.

alarm statistics for the ALAPS system at varying forecast periods for the 7 storms during the 12 month period, although it should be noted that by +48 hours the model was suffering a lag of between 12 and 18 hours in onset timing of the strong southerly flow.

The third event, around 29 November 2001 was significant, in as much as the wind speed reached during the southerly event was high, and the duration of the gale force wind relatively long, as evident in Figure 5.9, where the surface observational data from Casey are plotted in black. Analysis of the ALAPS model output during this event, (coloured time-series plots in Figure 5.9, highlighted model timing problems, with onset of the strong wind in the model some 20 hours too late. However, the model appeared to perform well in capturing the flow in the Casey area. The direction of the ALAPS modelled surface flow during the strong wind event was slightly

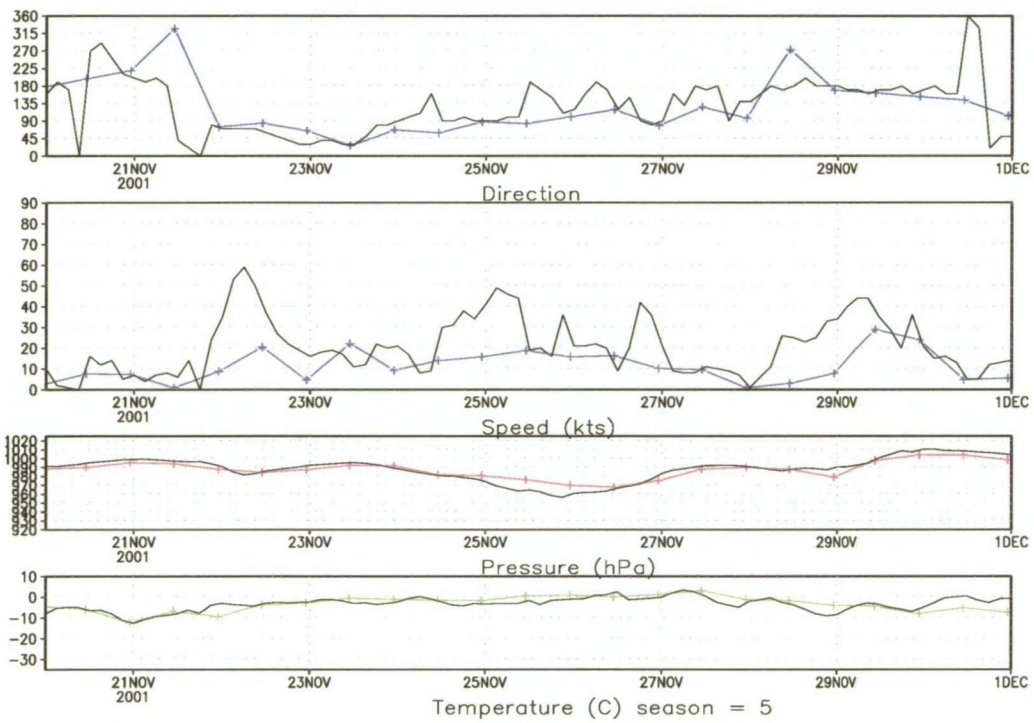

Figure 5.9: Comparison of ALAPS +24 hour surface data (coloured time-series) with observations from Casey Station (black time-series), for the last 10 days of November 2001.

too far into the southeast, from south, however the model tropospheric flow from the +45 hour forecast, valid at 0800UTC on 29 November 2001, agreed well with the profile data (Figure 5.10), measured from the Casey radiosonde flight from early on in the storm, where the surface flow at the Station was still strengthening. The strength of the upper level southwesterly jet was better developed in the model output (Figure 5.10), which was most likely a timing issue, as the ALAPS data shown in the comparison was valid some 21 hours after the radiosonde flight, but valid at a time when the ALAPS southerly storm was also just beginning to develop, and so considered more representative of the flow seen in the Casey observations. The pre-storm environment also seemed to be well captured by the ALAPS model run initiated at 1100UTC on 27 November 2001. A comparison of the radiosonde flight from 2300UTC on 27 November, (Figure 5.11), with the coincident +12 hour ALAPS data showed good agreement, although the model surface flow was a light northeasterly, rather than the observed southeasterly. One problem during strong wind events at Casey, and in particular, strong southerly wind events, is the difficulty in launching radiosondes from the station. It is almost impossible to successfully launch during very strong wind events due to strong eddying of the surface wind around the balloon launch site, and as a result, radiosonde flights are often aborted with a resulting lack of upper air data during these events. On the occasion of the November 2001 storm event, upper wind data were available only during the build up of the storm, with a flight at 1100UTC on 28 November 2001 (Figure 5.10), and as the storm was beginning to ease, with a successful flight at 2343UTC on 29 November 2001 (Figure 5.12). The +48 hour ALAPS profile from the model run initiated

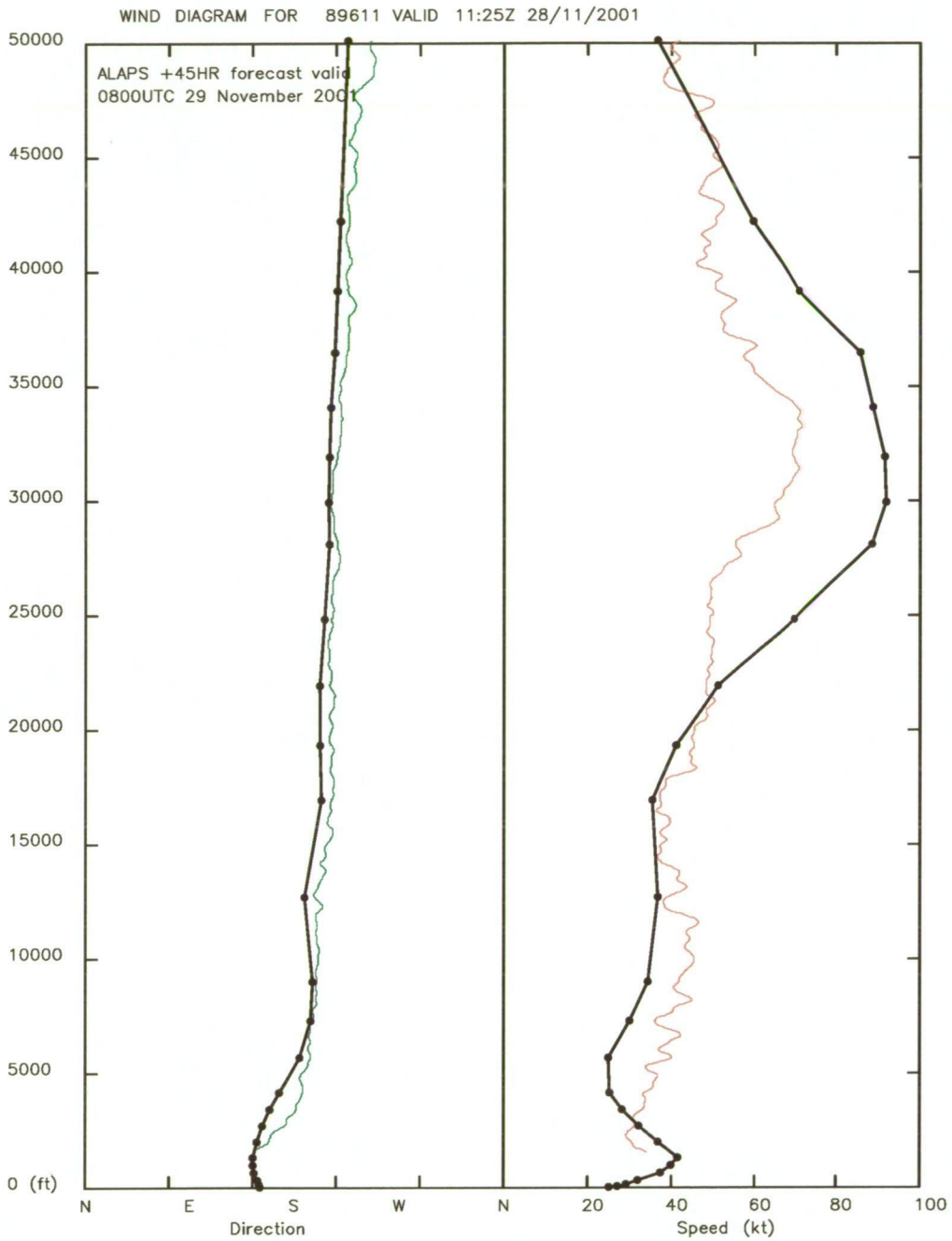

Figure 5.10: Vertical wind profile from the Casey radiosonde flight (coloured traces), valid at 1125UTC 28 November 2001, overlaid with the ALAPS vertical wind profile from the +45 hour forecast valid at 0800UTC 29 November 2001.

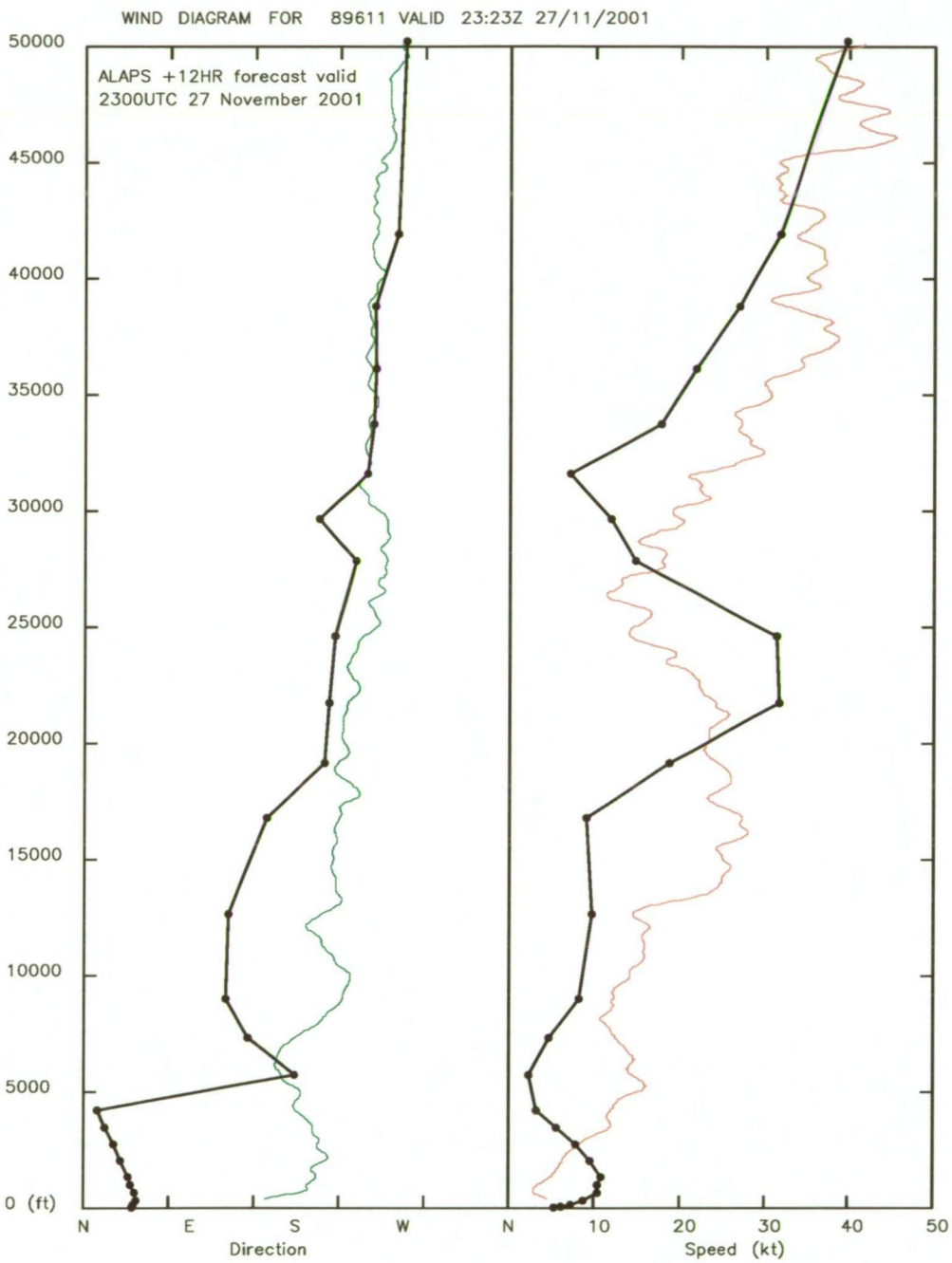

Figure 5.11: Vertical wind profile from the Casey radiosonde flight (coloured traces), valid at 2323UTC 27 November 2001, overlaid with the ALAPS vertical wind profile from the +12 hour forecast valid at 2300UTC 27 November 2001.

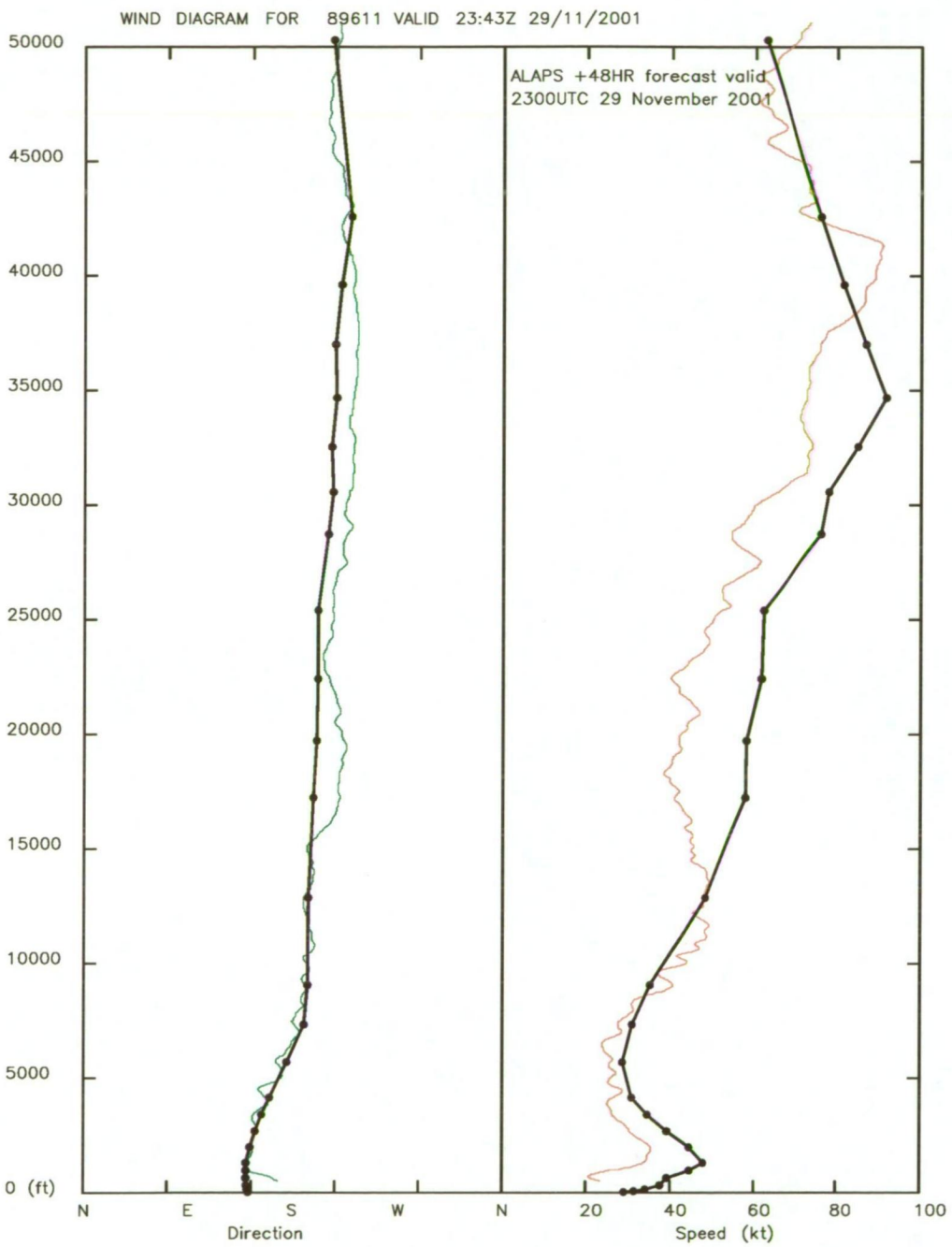

Figure 5.12: Vertical wind profile from the Casey radiosonde flight (coloured traces), valid at 2343UTC 29 November 2001, overlaid with the ALAPS vertical wind profile from the +48 hour forecast valid at 2300UTC 29 November 2001.

at 2300UTC on 27 November 2001, and valid at 2300UTC on 29 November 2001, is also displayed in Figure 5.12, and apart from slight errors in the height and strength of the upper level southwesterly jet, the ALAPS output was in reasonable agreement with the observed flow. So despite the 48 hour ALAPS run initialised at 1100UTC on 27 November 2001 being somewhat late in forecasting the onset of the strong wind, there appeared to be enough similarity in the model output and available observations to warrant using the ALAPS model data from this run to further investigate the development and dynamics of the southerly storm at Casey.

The synoptic situation in the pre-southerly storm environment was dominated by an intense low pressure system, with a central pressure of 953 hPa, located near 60°S, 110°E at 0000UTC on 25 November 2001 (Figure 5.13),

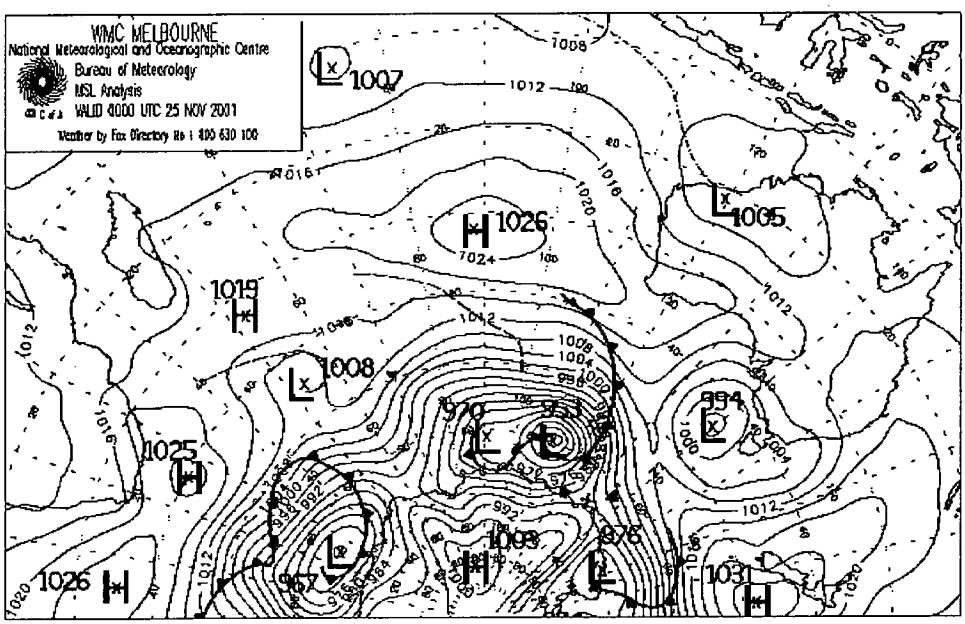

Figure 5.13: MSLP analysis from NMOC, Melbourne, Australia, valid 0000UTC 25 November 2001.

and which was tracking steadily eastward. A ridge of high pressure along 60°E was also evident at this time. By 1200UTC on 27 November, some 12

to 15 hours prior to the onset of the strong southerly, the low had moved away to the east of Casey and weakened to around 982 hPa. The ridge of high pressure had moved into near 95°E, and begun to strengthen (Figure 5.14).

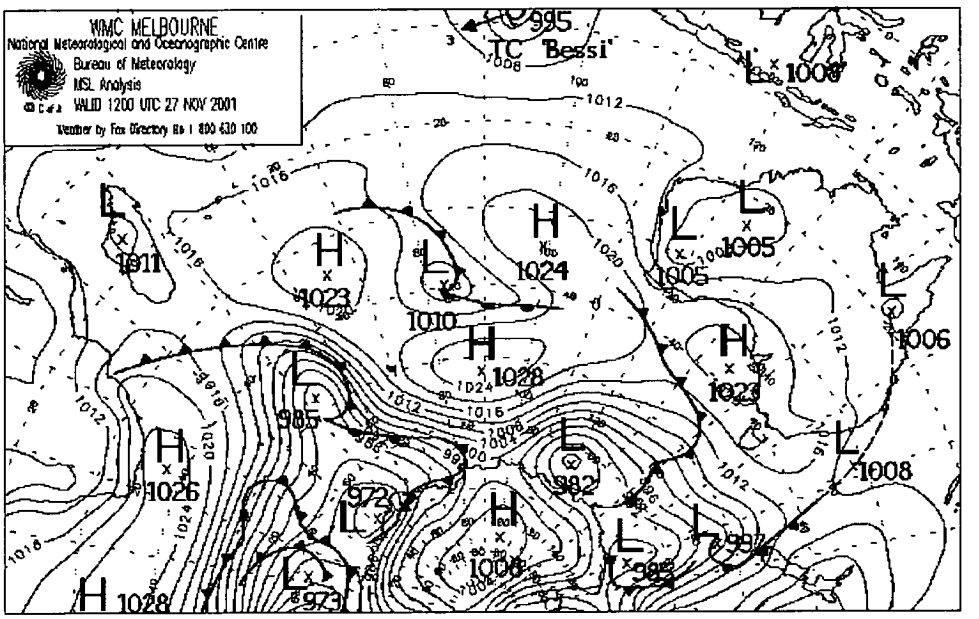

Figure 5.14: MSLP analysis from NMOC, Melbourne, Australia, valid 1200UTC 27 November 2001.

By 1200UTC on 29 November 2001, at the height of the southerly storm, the low was well to the east of Casey, with the ridge of high pressure having moved to 100°E and strengthened substantially, directing a strong southerly air-stream over Casey (Figure 5.15). In the mid-levels, at 500 hPa, there was strong support for both the low pressure system and developing high pressure ridge. No NMOC 500 hPa analyses were available, however 0000UTC analyses from the NCEP AVN model run were available during November 2001, providing an independent data source for the mid-level analyses. At 0000UTC on 27 November 2001 the 500 hPa geopotential height analysis from the NCEP AVN run (Figure 5.16) had a 5000 m minimum located near 65°S, 120°E, to the east-northeast of Casey, supporting the surface low in

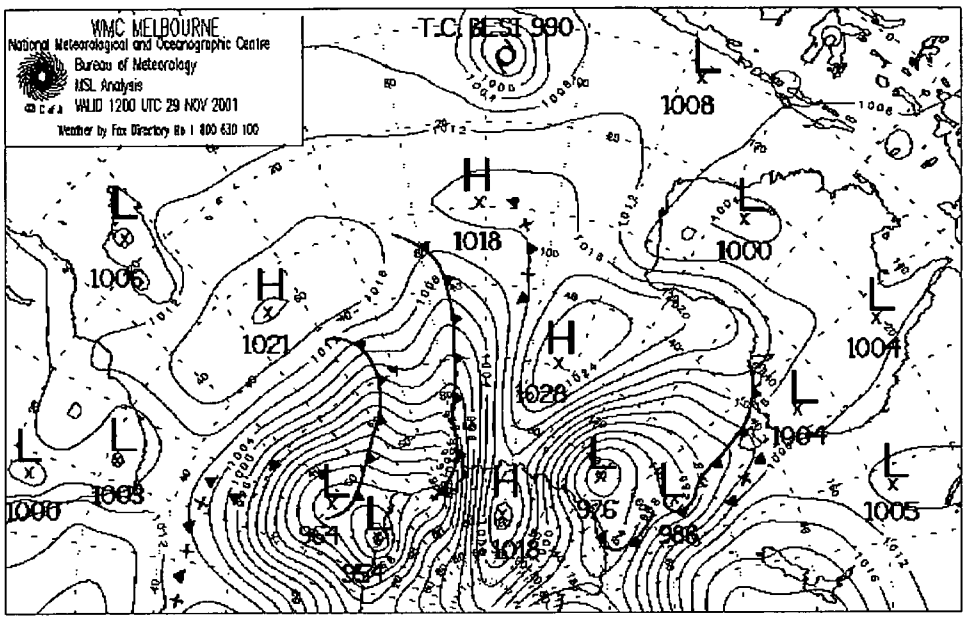

Figure 5.15: MSLP analysis from NMOC, Melbourne, Australia, valid 1200UTC 29 November 2001.

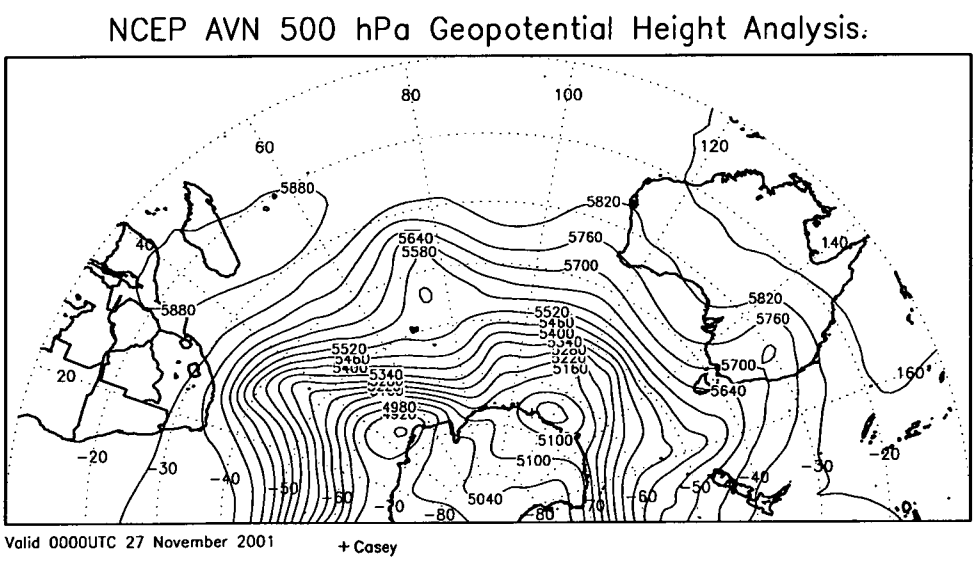

Figure 5.16: 500 hPa geopotential height (m), from the NCEP AVN analysis, valid at 0000UTC 27 November 2001.

that area, with a weak 500 hPa geopotential height ridge evident along 80°E. By 0000UTC on 29 November 2001 (Figure 5.17), the 500 hPa minimum had

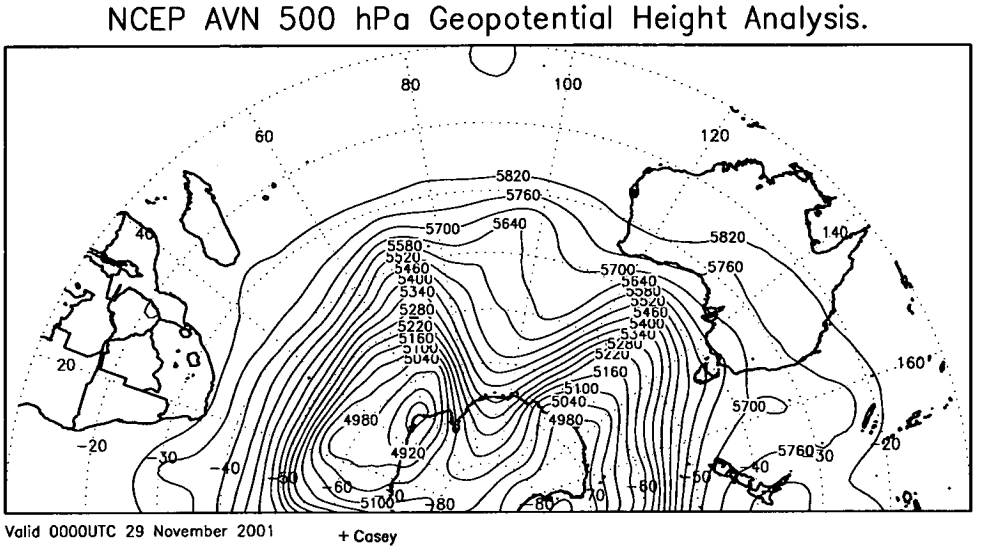

Figure 5.17: 500 hPa geopotential height (m), from the NCEP AVN analysis, valid at 0000UTC 29 November 2001.

tracked inland to near 70°S, 140°E, and deepened to around 4950 m, while the 500 hPa ridge had sharpened and moved to near 90°E, significantly tightening the mid-level gradient over Casey.

Cross-sections from the ALAPS model data were constructed in an attempt to define the time evolution of the three-dimensional wind flow in the Casey area, with cross-sections taken along 109.0°E, some 65 km to the west of Casey, and over the western side of the orographic basin carrying the Vanderford and Adams Glaciers, and along a southeast-northwest transect running through Casey Station, from 70°S, 116.4°E to 61°S, 104.9°E. The pre-storm environment in the Casey area was dominated by very light flow at all levels over the continent, with the receding low pressure system having advected warm maritime air well up onto the plateau (top panel Figure 5.18), and decaying the normal low level temperature inversion found over the con-

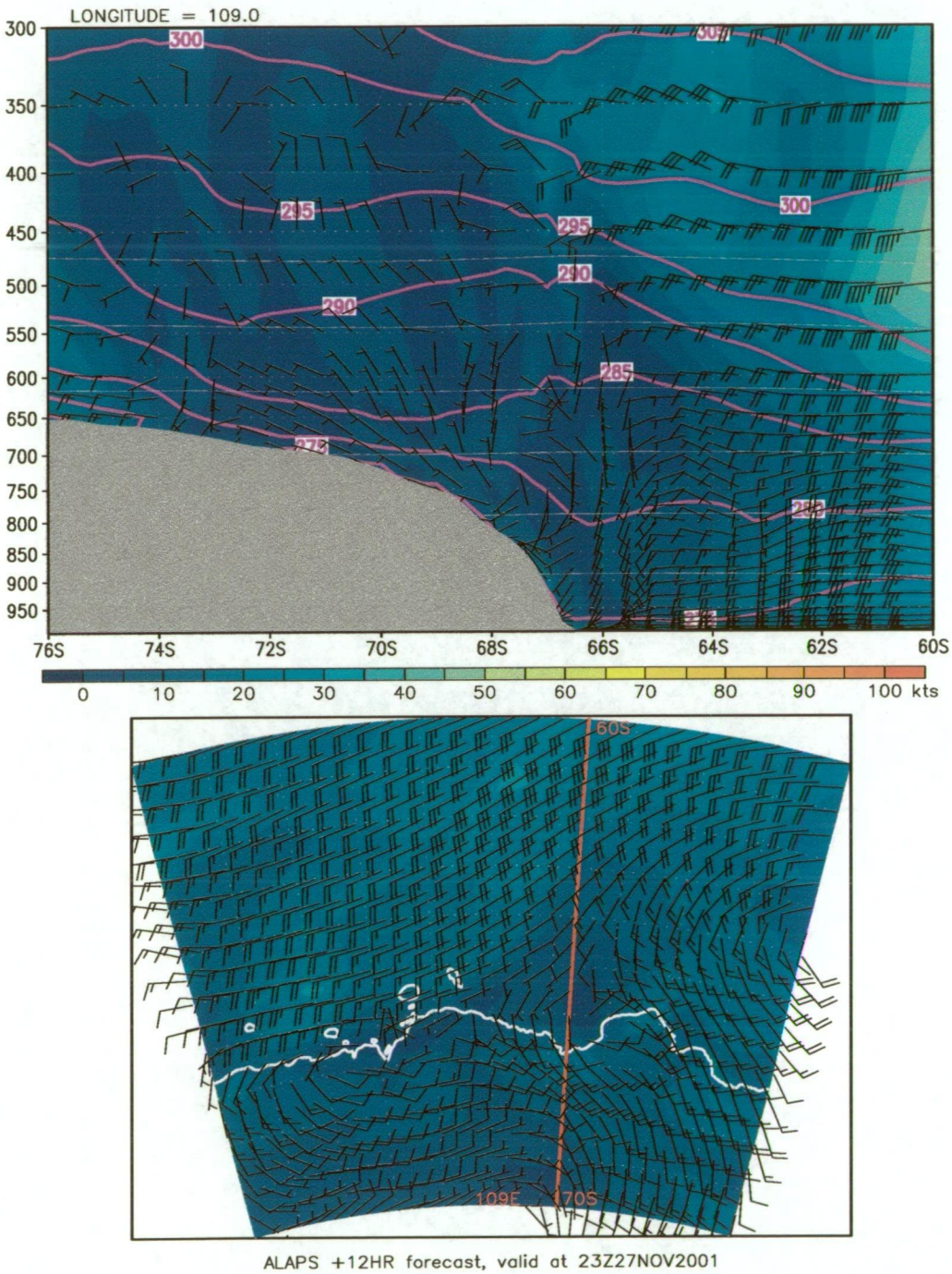

Figure 5.18: North-south cross-section along 109^{O}E showing wind speed (colour shading), wind vectors and potential temperature (contours) - top panel. The lower panel shows the near surface wind speed (colour shading) and wind vectors, with the red line marking the location of the vertical cross-section. From ALAPS +12 hour data, valid at 2300UTC 27 November 2001.

tinent. Figure 5.18 was derived from the ALAPS +12 hour model data, and valid some 24 hours prior to the onset of the strong southerly flow. The top panel shows the cross-section along 109.0^{o}E, from 76^{o}S to 60^{o}S, including the two-dimensional wind flow in the vertical plane, comprised of wind barbs and a colour shaded plot of the wind speed (derived from the meridional flow and vertical motion field), accompanied by a contour analysis of potential temperature (purple). The lower panel shows the near surface wind pattern in the Casey area, highlighting the low pressure system on the eastern boundary, and the very light wind regime in Vincennes Bay. As the low further receded to the east, radiative cooling of the Continent gradually returned the surface inversion to it's more normal state, highlighted by the tightening vertical gradient of potential temperature by +24 hours into the model run (Figure 5.19). Associated with the re-development of the surface inversion was the developing low level katabatic flow, over the steep escarpment to the west of Casey, near 68.0^{o}S (top panel Figure 5.19). A low level synoptic scale southwesterly flow was also developing well to the west of Casey, with the approaching high pressure ridge (lower panel of Figure 5.19). The very dry nature of the stream, and associated clear skies, enhanced the radiative cooling of the Antarctic boundary layer such that by +36 hours the developing surface katabatic flow over the continent had rapidly became more pronounced on the steep coastal escarpment (top panel Figure 5.20). By this stage (2300UTC on 28 November), the approaching pressure ridge was evident, with deep and strong southerly out-flow evident over the continental interior (top panel Figure 5.20), although the very strong, low level flow over the steep escarpment to the west of Casey, was still confined to the lowest

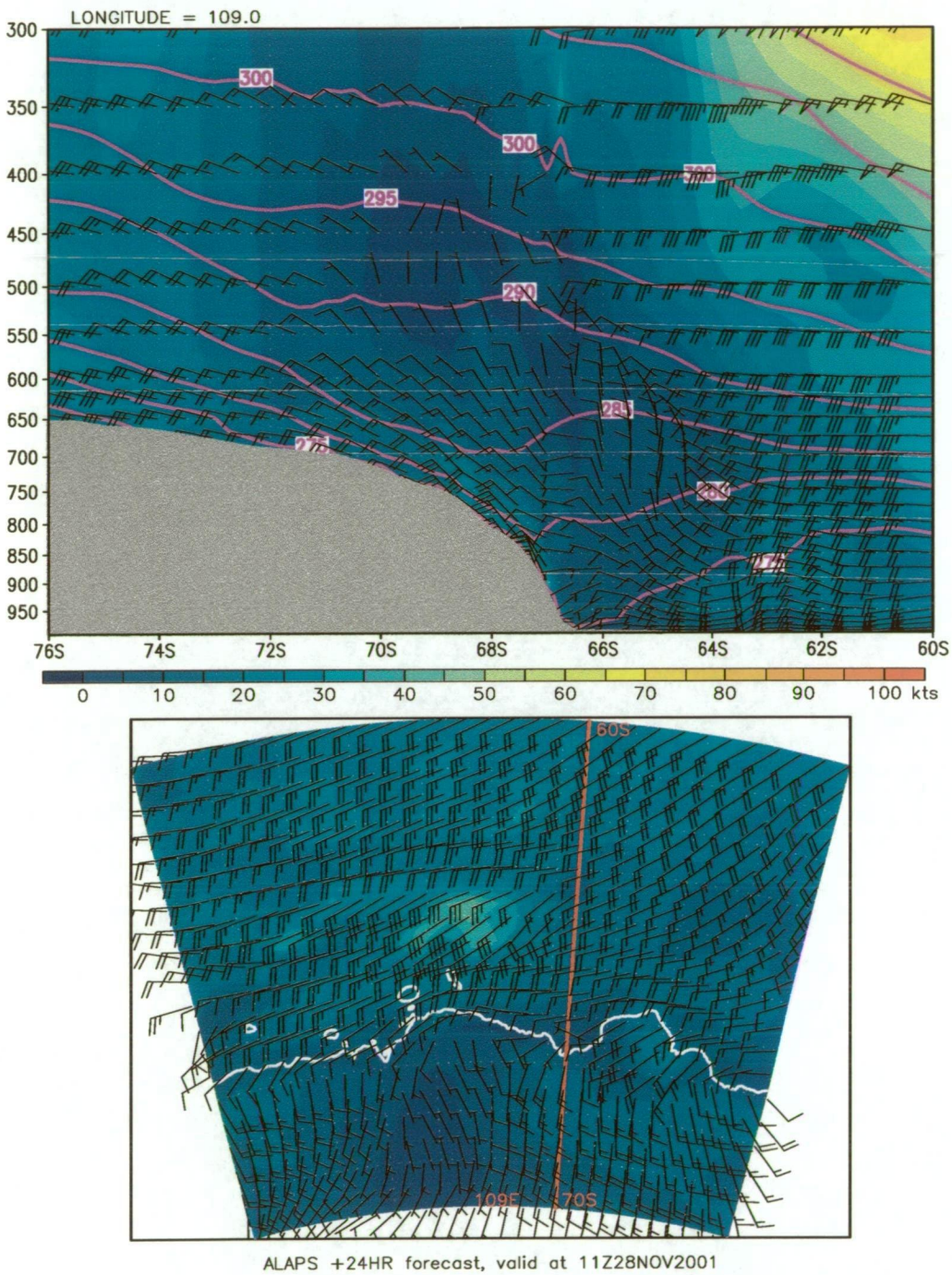

Figure 5.19: North-south cross-section along 109^{O}E showing wind speed (colour shading), wind vectors and potential temperature (contours) - top panel. The lower panel shows the near surface wind speed (colour shading) and wind vectors, with the red line marking the location of the vertical cross-section. From ALAPS +24 hour data, valid at 1100UTC 28 November 2001.

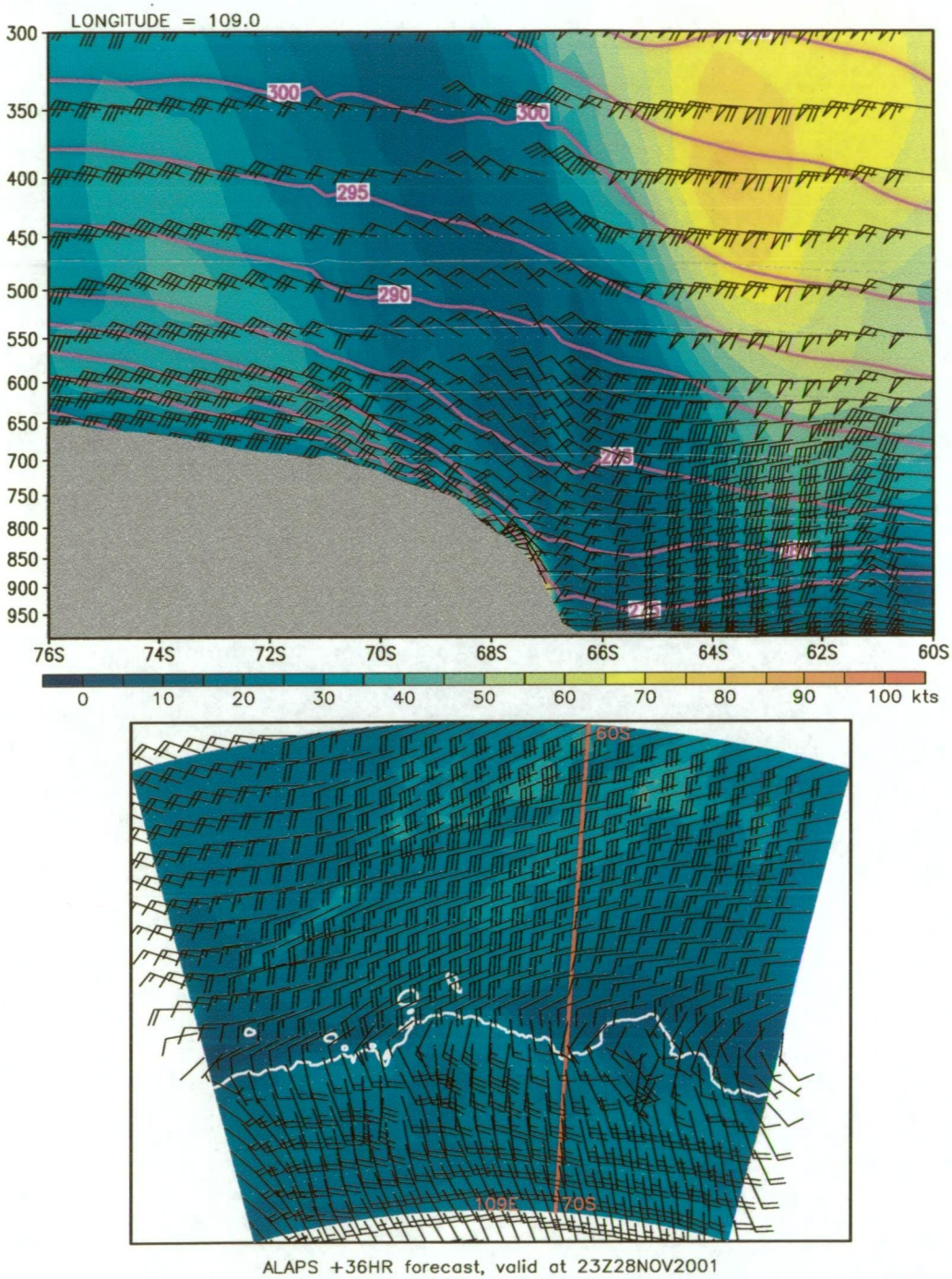

Figure 5.20: North-south cross-section along 109^{o}E showing wind speed (colour shading), wind vectors and potential temperature (contours) - top panel. The lower panel shows the near surface wind speed (colour shading) and wind vectors, with the red line marking the location of the vertical cross-section. From ALAPS +36 hour data, valid at 2300UTC 28 November 2001.

few hundred metres. Low level wind in the Casey area was still very light at this stage. By +39 hours into the model run the very strong surface wind, that had been confined to the steep coastal escarpment, was beginning to push out to sea (bottom panel Figure 5.21), although the flow was no longer pure katabatic, as strong upper level southerly flow was developing at all levels over the continent, and moving northward toward the coast. What was also significant was the maintenance of an area of very light surface flow over Casey Station and to the northeast. During the development of the surface katabatic over the steep escarpment to the west of Casey, a similar development was occurring on the escarpment inland of Casey, although the flow was no where near as well developed at +39 hours (top panel Figure 5.22), with the strongest surface flow remaining well inland, despite the fact that by this time the katabatic flow at 109^{o}E had already moved offshore (Figure 5.21). The cross-section in Figure 5.22 was oriented northwest-southeast, to highlight the development of the inland surface flow directly up-wind of Casey Station. As the intensifying ridge of high pressure approached Casey the southerly flow strengthened throughout the troposphere, with the low level wind maxima also strengthening appreciably, and by +48 hours the low level maxima had moved down off the escarpment, over the station, and out into Vincennes Bay (top panel Figure 5.23). The surface wind at +48 hours (lower panel Figure 5.23), showed a "channel" of stronger wind blowing down the valley carrying the Vanderford and Adams Glaciers, and extending an appreciable distance out off the coast, with a light wind area still evident to the northeast of Casey. A comparison of the cross-section along 109^{o}E at +48 hours, (Figure 5.24), and near Casey, (Figure 5.23), showed significant

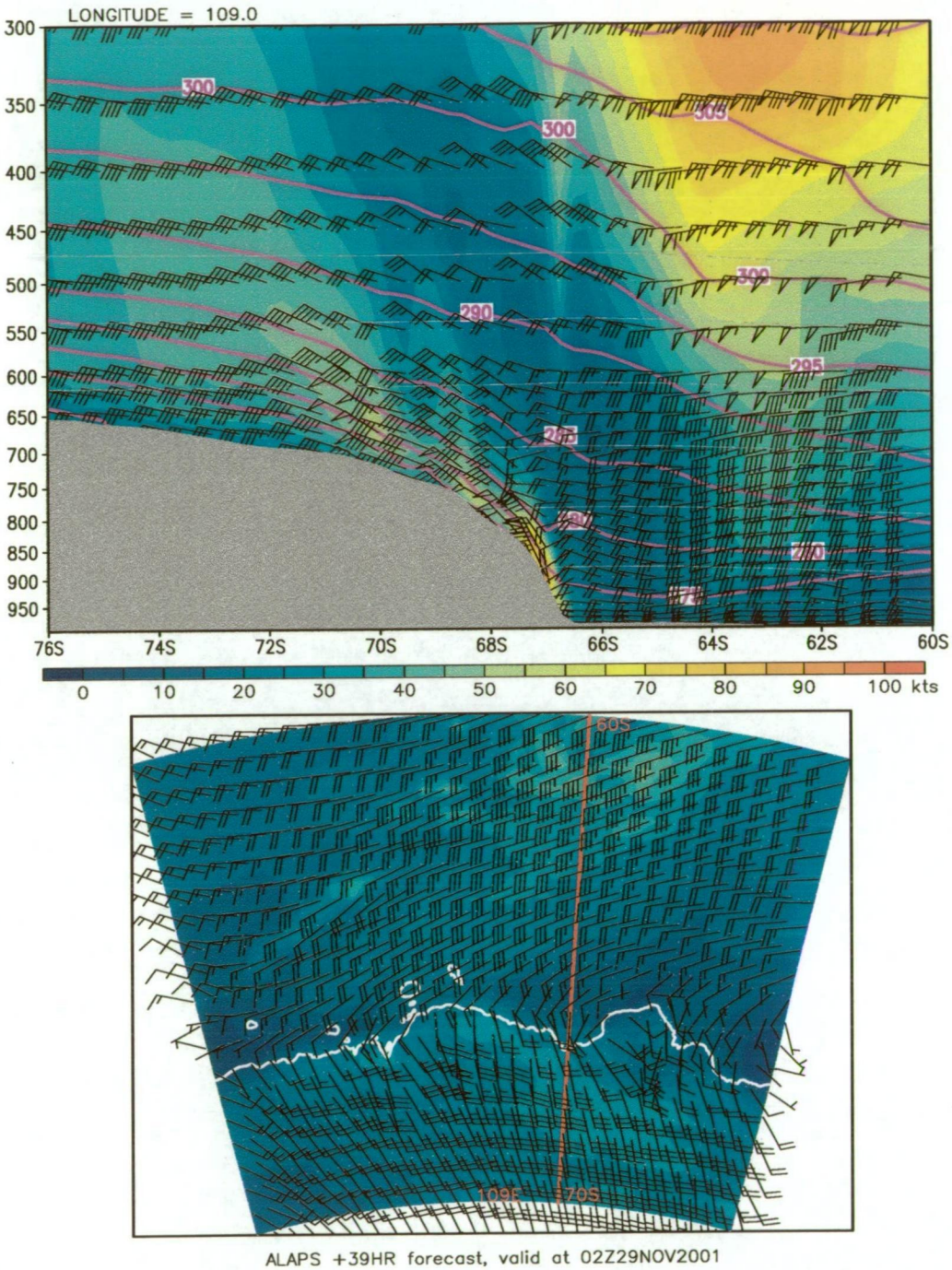

Figure 5.21: North-south cross-section along 109^{o}E showing wind speed (colour shading), wind vectors and potential temperature (contours) - top panel. The lower panel shows the near surface wind speed (colour shading) and wind vectors, with the red line marking the location of the vertical cross-section. From ALAPS +39 hour data, valid at 0200UTC 29 November 2001.

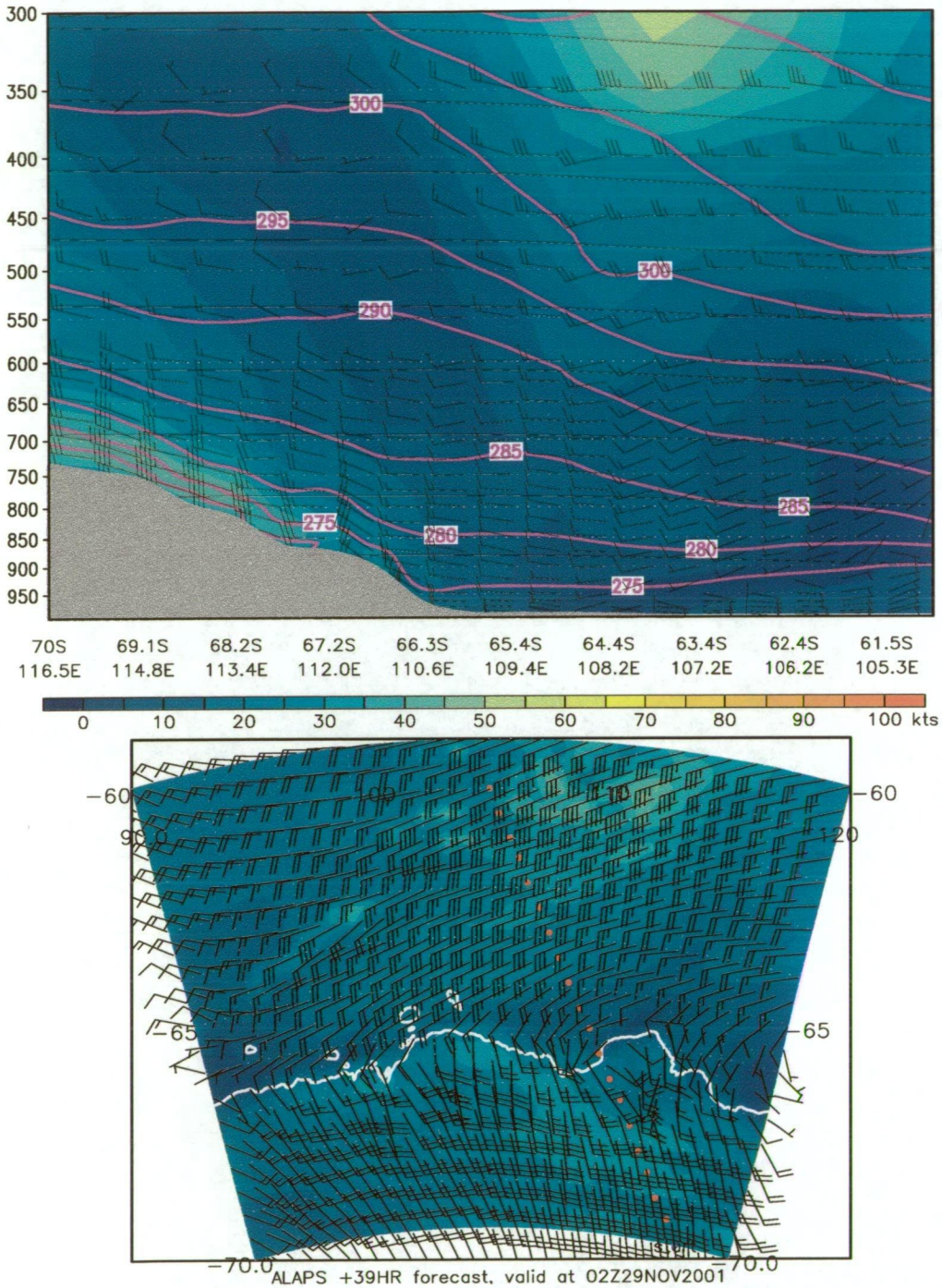

Figure 5.22: Northwest-southeast cross-section through Casey showing wind speed (colour shading), wind vectors and potential temperature (contours) - top panel. The lower panel shows the near surface wind speed (colour shading) and wind vectors, with the red dotted line marking the location of the vertical cross-section. From ALAPS +39 hour data, valid at 0200UTC 29 November 2001.

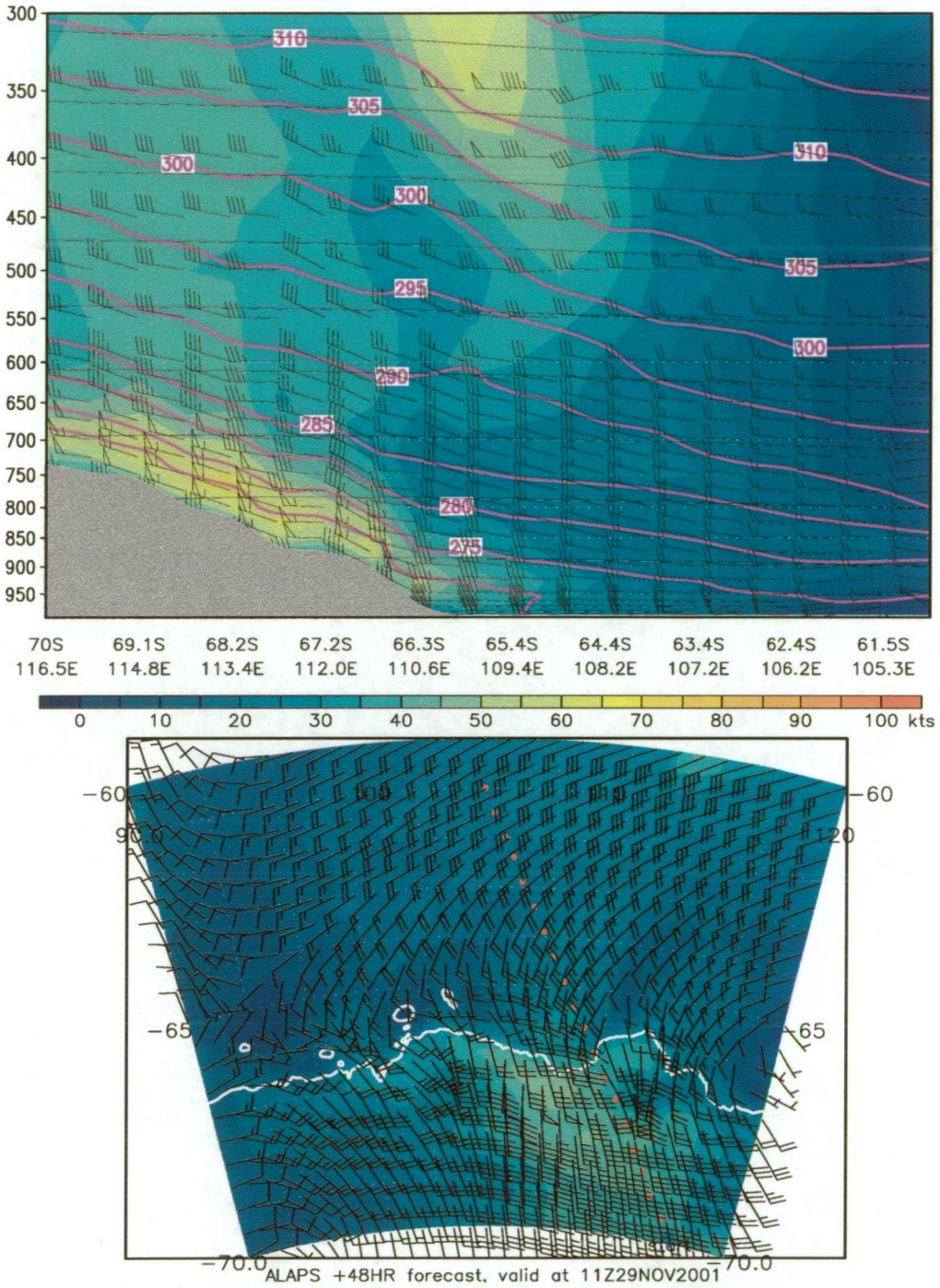

Figure 5.23: Northwest-southeast cross-section through Casey showing wind speed (colour shading), wind vectors and potential temperature (contours) - top panel. The lower panel shows the near surface wind speed (colour shading) and wind vectors, with the red dotted line marking the location of the vertical cross-section. From ALAPS +48 hour data, valid at 1100UTC 29 November 2001.

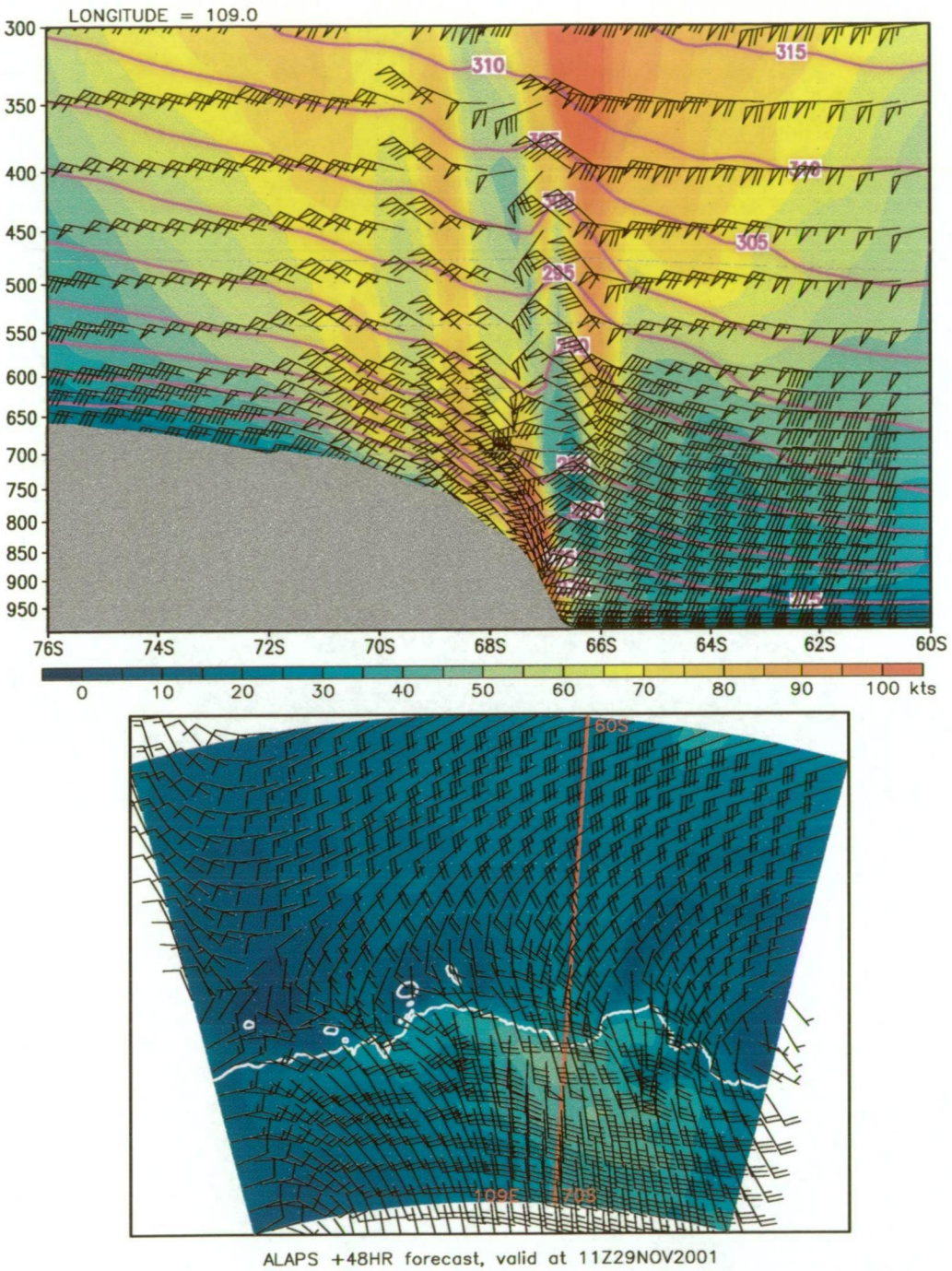

Figure 5.24: North-south cross-section along 109^{o}E showing wind speed (colour shading), wind vectors and potential temperature (contours) - top panel. The lower panel shows the near surface wind speed (colour shading) and wind vectors, with the red line marking the location of the vertical cross-section. From ALAPS +48 hour data, valid at 1100UTC 29 November 2001.

differences in flow strength, with the low level flow to the west appreciably stronger than near Casey. Comparison of the Casey radiosonde flight with the ALAPS +48HR forecast flow, at the height of the strong wind (Figure 5.12), showed excellent model performance but also highlighted the fact that the wind profile was not indicative of a pure katabatic, as the background flow in the lowest few thousand feet of atmosphere was of the order of 30 knots. However, the rather distinct low level jet had it's development in the surface layer, with the development dominated by the radiative cooling of the surface in the post low pressure system environment. The potential temperature in the early cross sections was dominated by slack gradients, but as the surface cooled, and the northward flowing air off the continent compressed, through vorticity constraints, the potential temperature gradient near the surface increased rapidly with a resulting increase in near surface wind speed on the steep slopes (Ball 1960). The development of the strong near surface flow preceded the developing upper level jet. However the strong surface flow was confined to the steep coastal escarpments, under the very strong surface inversion, and strongest on the western side of the broad valley carrying the Adams and Vanderford glaciers. The stronger flow to the west of Casey would have been partially due to the steeper orography in that area, but also in response to general orographic forcing, where out-flow off the continent is channeled to the western side of orographic depressions, in a similar fashion to barrier winds, resulting in a low level jet generally confined on the steep slopes of the western side of valleys (Ball 1960). The strong southerly flow, that generally does not reach Casey, appeared to develop in this case because of the strength of the upper level south to southwest jet, and the developing

southerly flow through the depth of the troposphere advected the surface jet northward and over Casey.

Also of interest was the quite dramatic change in the depth of the surface inversion layer near the coast west of Casey throughout the development of the southerly storm. At +24 hours the strong surface inversion was well developed inland, south of 67^{o}S (top panel Figure 5.19), with a strong wind evident under the inversion and indicative of an hydraulic jump sitting well inland on the steep coastal escarpment. By +48 hours the surface inversion had not only strengthened, but it had also moved down off the plateau and onto the coast (top panel Figure 5.24), suggestive of the hydraulic jump having moved to be on the coast.

In summary, during the event of late November, Casey experienced a dramatic increase in surface southerly flow, which in essence was a katabatic signature, but the flow was in a regime of developing deep southerly flow, with the approach of an intensifying ridge of high pressure, and it was the deep, synoptic scale, southerly flow that caused the katabatic that had developed upstream and inland of Casey to advect off the escarpment and over the station.

The major ALAPS forecast failure during the 12 month trial period occurred late in October 2001 when Casey had been experiencing an almost continuous period of southerly flow, from late on 28 October until early on 31 October 2001. Although, during this period the southerly wind was only strong (around 30 knots) for about 12 hours, from the middle of 30 October 2001. Data from the radiosonde flight, launched just at the onset of the storm (Figure 5.25) show a reasonably deep layer of southwesterly flow, con-

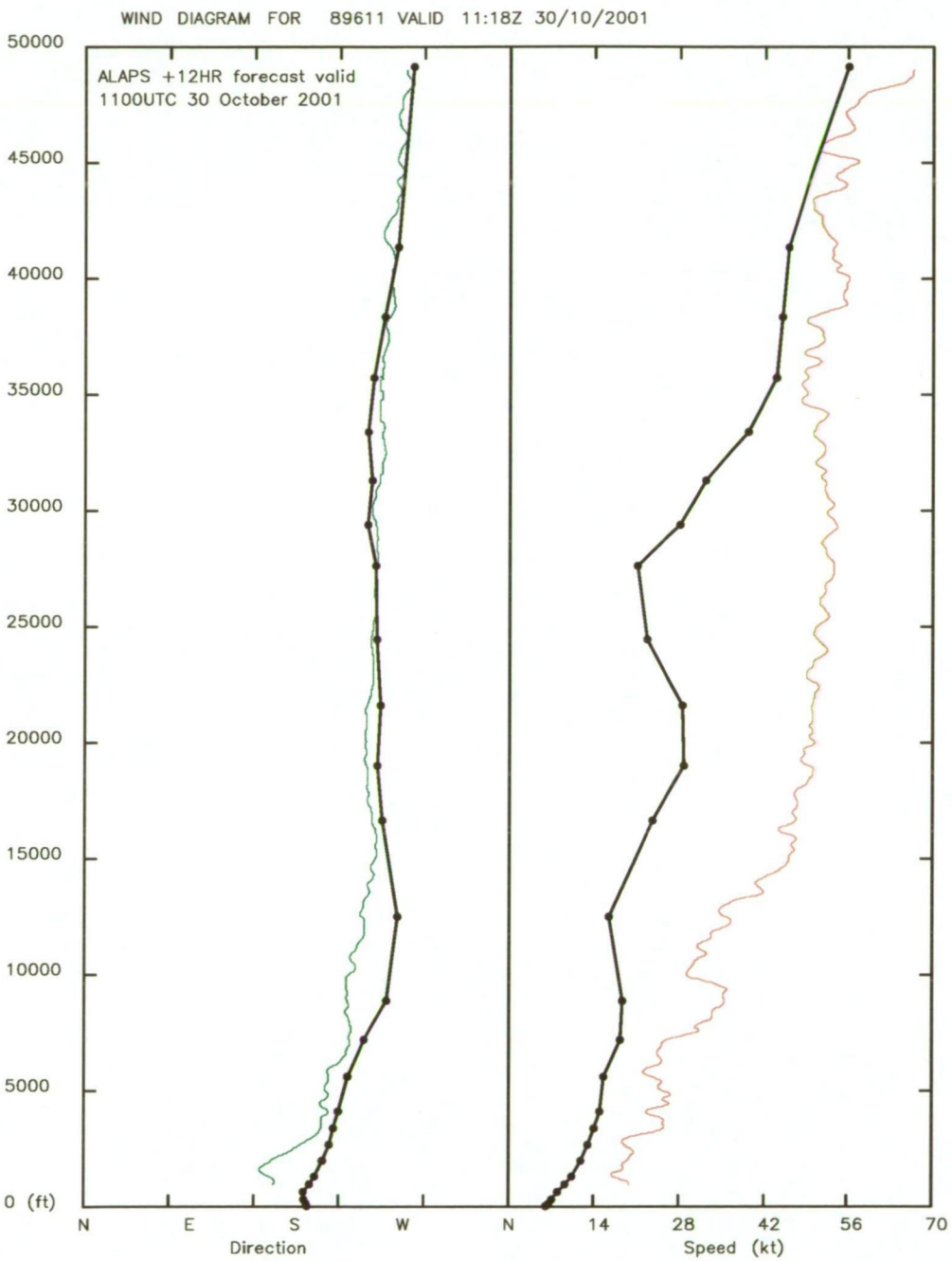

Figure 5.25: Vertical wind profile from the Casey radiosonde flight (coloured traces), valid at 1118UTC 30 October 2001, overlaid with the ALAPS vertical wind profile from the +12 hour forecast valid at 1100UTC 30 October 2001.

sistent with the Casey observations, however the model wind strength was too low right throughout the lowest 35000 ft of atmosphere. At the height of the storm, the model maintained a light surface southwesterly flow, with the southwesterly wind gradually increasing to around 85 knots by 27000 ft (Figure 5.26). Unfortunately the GPS radiosonde launched from Casey at this time was unable to fully sample the atmospheric winds, although what data were available showed the model slightly under-forecasting the low to mid-tropospheric winds, and completely missing the surface wind maxima. Also of note is the fact the modelled flow in the profile is more westerly than occurred during the November 2001 storm (Figure 5.12). Perusal of the model surface flow and cross sections during this event showed, in the initial instant, quite similar development, with a light wind area over Casey and to the north and northeast, and a strengthening low level flow over the steep coastal escarpment to the west and southwest. The model did develop a substantial surface jet some 60 km southwest of Casey at 66.75^{o}S, 110.0^{o}E (Figure 5.27), but the low level jet never advected off the plateau and over Casey during the November 2001 model run. The most significant difference in this case appeared to be the subtle difference in the orientation of the upper jet and broad-scale tropospheric flow, with the model run that failed having more of a westerly component to the tropospheric flow than was observed in the Casey wind profiles, and also more westerly that in the November 2001 case, where the model was successful in predicting the low level southerly wind maxima over Casey. Also, in the November 2001 event, where the model was successful, the upper southwesterly flow was slightly stronger than the October 2001 case, and the ALAPS forecasts of wind speed

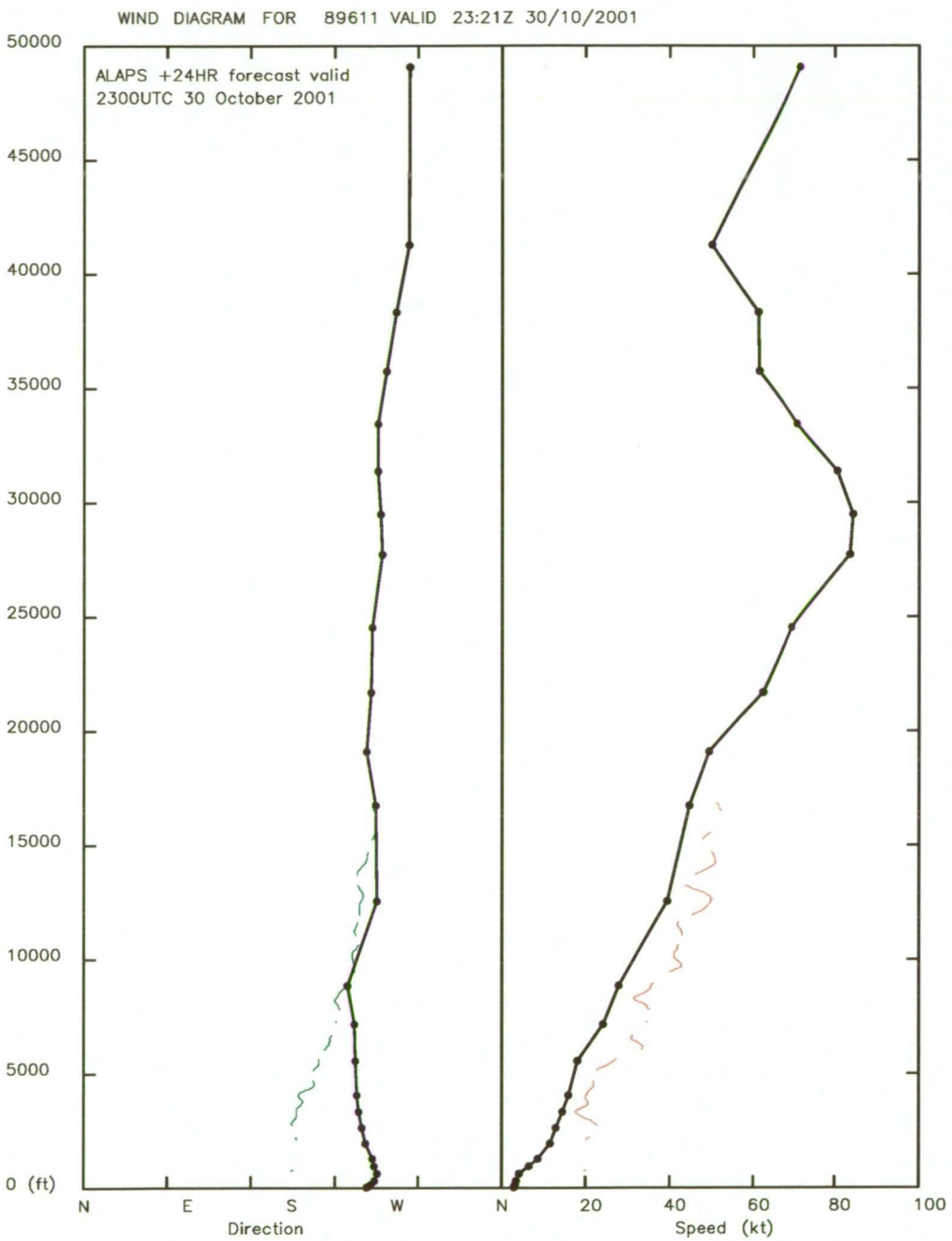

Figure 5.26: Vertical wind profile from the Casey radiosonde flight (coloured traces), valid at 2321UTC 30 October 2001, overlaid with the ALAPS vertical wind profile from the +24 hour forecast valid at 2300UTC 30 October 2001.

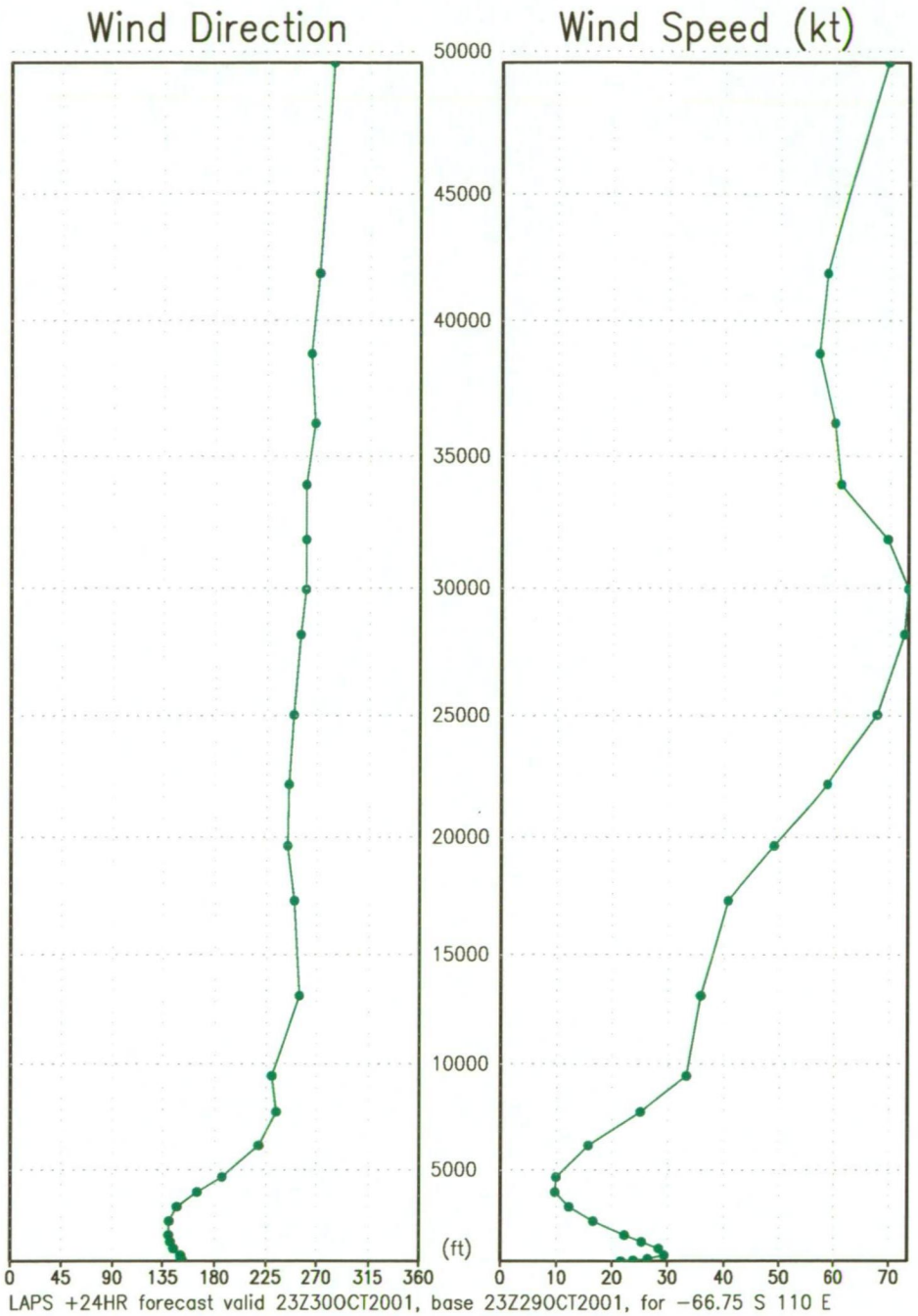

Figure 5.27: Vertical wind profile from the ALAPS +24 hour forecast valid at 2300UTC 30 October 2001 to the southwest of Casey at 66.75^{o}S, 110.0^{o}E.

in fact, exceeded the observed values (Figure 5.12). During the October 2001 case the ALAPS forecasts of tropospheric wind speed were lower than observed (Figure 5.25), so it would seem that the model atmosphere required a substantial synoptic-scale south to southwesterly flow to assist in advecting the low level wind maxima off the steep escarpment inland of Casey, which was present in the November 2001 run of the model, but not in the October 2001 example.

It could be argued that Casey station never experiences a true, strong southerly katabatic flow, as strong surface southerlies appear to be associated with a strong upper south to southwesterly jet, maintaining a wind profile that is not simply katabatic flow. Also the main plateau slope is tho the east of Casey. However, the sequence of north-south cross sections through the Vanderford-Adams Glacier region, detailed here, do show the low level development of a katabatic flow on the steep escarpment prior to the upper southwesterly jet development, with the advection of the katabatic off the glaciers and out over Vincennes Bay appearing to be triggered by the development of the upper southwesterly jet and general increasing of south to southwesterly flow through the entire troposphere.

5.3 Mawson katabatic flow

The local climate of Mawson is dominated by a persistent southeasterly flow, of which a significant component is the katabatic flow off Dome A and the very steep coastal escarpment leading down to the station. Mean wind speeds at Mawson are significantly higher than at both Casey and Davis and the almost uni-directional (southeasterly) nature of the wind prominent. In many

situations the uniformity of the air-stream at Mawson simplifies the forecast process, however during summer there is a strong diurnal signal in the wind flow and occasions where the katabatic breaks down entirely. Attempting to forecast these situations is problematic and a better understanding of the atmospheric dynamics around Mawson essential. Figure 1.4 shows the wind rose for Mawson, composed from all observations over the last 48 years, and highlighting the persistent nature of the Mawson near-surface wind direction where a significant percentage of wind observations are from the southeast, and in excess of 10 ms^{-1} (~20 knots). During the summer months, when the wind speed generally eases, there is often a strong diurnal signal in the wind speed and direction that suggests the local topography also has a strong influence on the katabatic flow. If the dominant drainage flow was entirely off the high plateau then the large body of available cold air would lead to the expectation of a steady flow at Mawson, with little or no diurnal signal. This is indeed what was seen over most of the year, except during the summer months, where the wind speed tended to fall away to around 15 knots or less. Figure 5.28 shows the surface observations from Mawson (solid black lines), for the period 0000UTC 1 January 2002 through until 0000UTC 1 February 2002, where a strong diurnal signal was evident in the wind direction, speed, and temperature data, with little or no background, or geostrophic, flow evident over the first few days of January. If the ALAPS model was performing adequately in capturing the dynamics of the flow then the model should not only capture the essence of the broad scale flow, but should be capable of modelling the mesoscale features such as the diurnal signals evident in Figure 5.28. The coloured time series plots in Figure 5.28

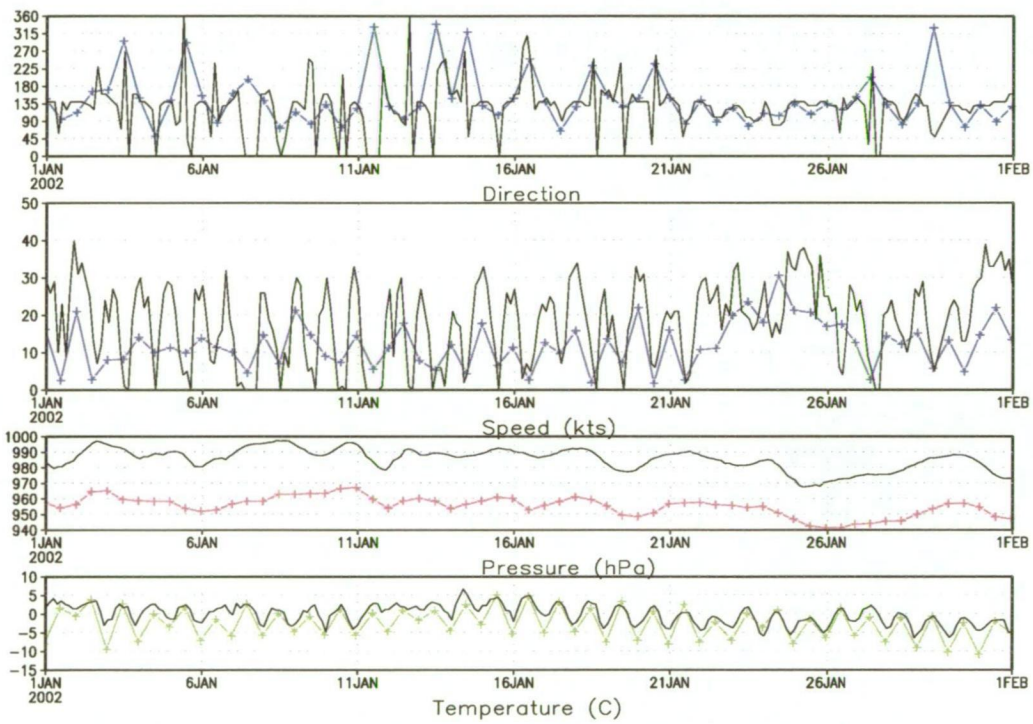

Figure 5.28: Comparison of ALAPS +24 hour surface data (coloured time-series) with observations from Mawson Station (black time-series) , for January 2002.

are from the ALAPS 0.9988 σ-level +24 hour forecast, and as can be seen from the graph, there was a very good agreement between the model and observed diurnal temperature signal, suggesting the model physics was capturing the situation well, although the amplitude of the model temperature variations did appear somewhat too large during the middle of the month. The amplitude of the modelled wind speed oscillation did not fit the observed diurnal wind speed variations particularly well. However, the model did manage to adequately forecast the phase of the oscillation. As will be argued, it was most likely a function of the model resolution and the definition of the terrain slope that led to the lack of wind speed amplitude in the modelled katabatic signal. The top 2 panels of Figure 5.29 show the orography around Mawson, along with terrain slope details from the 30 second topographic data set, with the lower 2 panels in Figure 5.29 showing the same details but from the smoothed topographic data set used in the current ALAPS model run. The colour shading highlights the slope around Mawson (top left Figure 5.29), as compared to the slope used by the model (bottom left Figure 5.29). The actual topographic height is also shown as a contour plot overlaying the shaded graphs. The model grid point closest to Mawson was at -67.5^{o}S, 63.0^{o}E (cross hatched circle in lower left panel of Figure 5.29), which was 6.0 nm to the north and 2.9 nm east of Mawson, with the next closest point to the southwest (cross hatched square in lower left panel of Figure 5.29). The line graphs, to the right in Figure 5.29, detail the orographic slope (open circles) and topographic height (closed circles) along a north-south cross-section through Mawson, from the high resolution orographic data-set (top right panel of Figure 5.29), and from the ALAPS

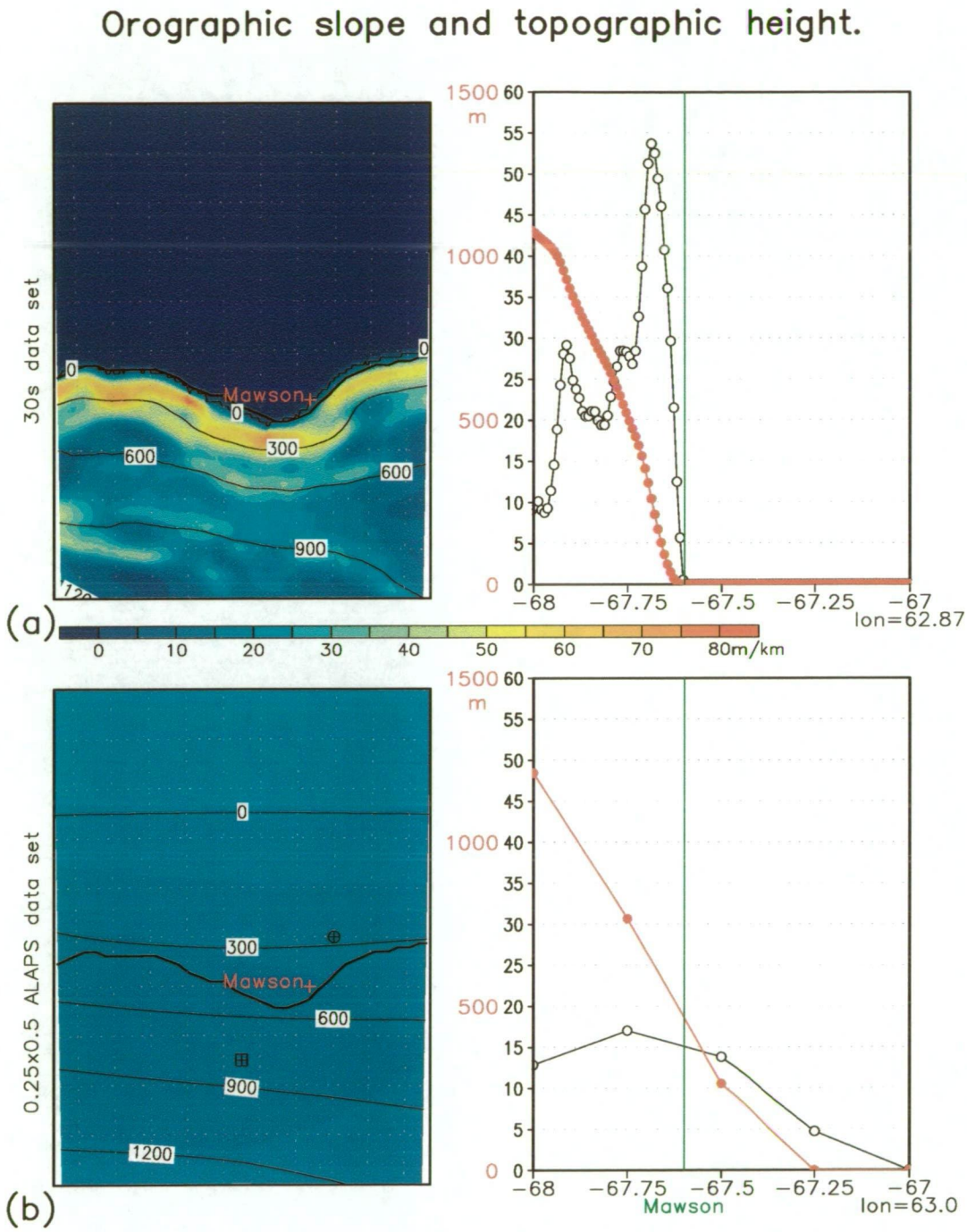

Figure 5.29: Orographic slope and height around Mawson, from a 30 second of arc data-set (top panel, left), and as defined in the ALAPS model (lower panel, left). Cross-sections of the orography (red) and orographic slope (black) along the longitude of Mawson are shown to the right.

model (lower right panel of Figure 5.29). Differences between the model and reality were obvious from Figure 5.29, with significant differences including the fact that the model orographic slope at the point closest to Mawson was 14 m/km, with a maximum slope of only 17 m/km one model grid point to the south. In reality, the slope at Mawson is very near zero, with the station on the coast, and with the slope reaching a maximum of near 55 m/km just to the south of the station. Also, the model version of reality placed Mawson some distance from the model coast, and at an elevation higher than in reality. Both these factors were likely responsible for the weaker katabatic signature in the model wind field, and for the fact that the underlying, background, flow in the model was not zero, as observed.

Ball (1960) presented one of the earliest theoretical studies of the Antarctic katabatic wind using a simple two-layer model in which the stratification of the surface layer was crudely defined to be of depth h with a layer potential temperature of θ - $\Delta\theta$, lying under an infinitely deep layer of potential temperature θ. Following the formulation of King and Turner (1997) the Ball model of the katabatic flow has the solution shown in Equations 2 and 3,

$$V^2 = \frac{\sqrt{f^4 + 4k'^2[(F - fv_g)^2 + f^2u_g^2} - f^2}{2k'^2} \tag{2}$$

$$cos\phi = \frac{u_g f^2 + k'V\sqrt{k'^2V^4 + f^2(V^2 - u_g^2)}}{f^2V + k'^2V^3} \tag{3}$$

where $V = (u,v)$ is the flow in the lower layer, f the Coriolis parameter,

$F = g\alpha\Delta\theta/\theta$, with α the slope angle, g gravity and $k' = k/h$, where k is the drag coefficient and ϕ the cross slope flow angle. The Ball model gives a relatively simple way of testing the impact of the differences between the real slope at Mawson and that prescribed in the model. Figure 5.30 shows

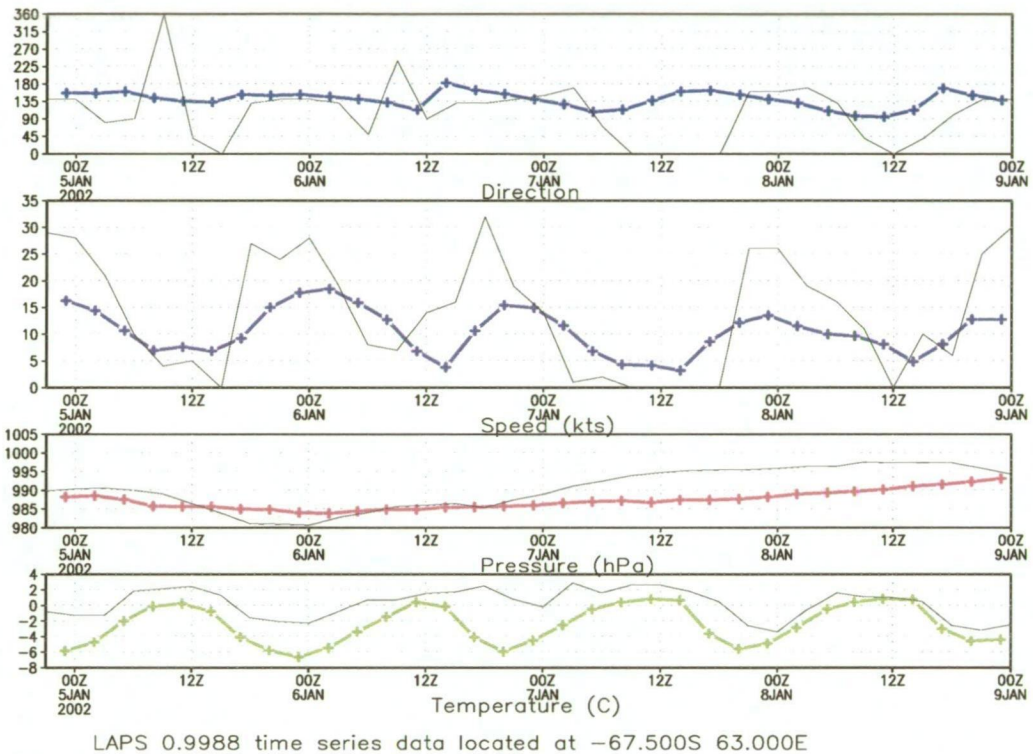

Figure 5.30: Comparison of ALAPS 3 hourly surface data (coloured time-series) with observations from Mawson Station (black time-series) , for the model run initiated at 2300UTC on 4 January 2002.

a comparison of the ALAPS near surface model data (coloured time series plots) from a 96 hour model run initiated at 2300UTC 4 January 2002, with the surface observational data from Mawson (black time series plots). The ALAPS model run had forecast the diurnal signal in both the temperature and wind speed through the 4 day integration, but again, showed a weaker amplitude in the model wind speed signal. From the Mawson temperature sounding of 2300UTC on 5 January 2002 the inversion height was estimated

at 150 m with a mean potential temperature of 272 K in the upper layer, and a potential temperature difference between the surface and upper layer of 2 K. The topographic slope just inland of Mawson, at -67.7^{o}S, from the 30 second data set (top panels Figure 5.29), was 0.055 m/m and taking Ball's assumption of a drag coefficient of 0.005, gave a katabatic flow of 10.54 ms^{-1}, with an angle of 21^{o} to the fall line. From the top panel of Figure 5.29, the fall line at Mawson is approximately 160^{o} giving a katabatic flow of 140^{o} at 20 knots which fits well with the observed surface wind of 135^{o} at 27 knots. Now, using the same meteorological parameters, but applying them to the model domain, where the inland slope only reached 0.017 m/m (lower panel of Figure 5.29) gave a katabatic flow of 5.43 ms^{-1} at 37^{o} to the fall line. The fall line in the model domain (lower panel Figure 5.29) was estimated at approximately 180^{o}, giving a katabatic flow of 143^{o} at 10.5 knots. The actual ALAPS modelled wind at 2300UTC 5 January 2002, was in fact, 145^{o} at 18 knots. However, the model atmosphere appeared to have a background flow, as the modelled wind at 1400UTC was 135^{o} at 7 knots where in fact the true wind was calm. The background geostrophic flow at 1400UTC, estimated from the model mean sea level pressure field, was given by u_g = -5.5 ms^{-1} and v_g = 6.3 ms^{-1}, with the Ball equation then giving a modified katabatic flow of 7.64 ms^{-1} at 47.5^{o} to the fall line, or 132.5^{o} at 14.9 knots, giving better agreement with the modelled wind of 145^{o} at 18 knots. Only one example of a katabatic signature at Mawson has been examined, so categorising the the underlying dynamics is not conclusive, but the simple application of Ball's theory on katabatic flow does appear to agree well with both the observed wind and the modelled wind at 2300UTC on 5 January

2002, suggesting that the ALAPS model was indeed forecasting a diurnal katabatic signature, although under-estimating the true wind as a result of the smoothed, shallower, model topography.

5.4 Oceanic route forecasting

A significant proportion of Australia's involvement in high latitude scientific research has occurred on the high seas, with oceanographic cruises plying the Southern Ocean measuring ocean currents, salinity and marine ecological systems, along with cruises within the latent heat polynya found in the winter-time sea ice zone off the Mertz Glacier. The provision of accurate and timely weather forecasts to support such oceanic cruises, and the resupply voyages to the Australian Antarctic stations, has been reliant on quality numerical model output. Observational data across the Southern Ocean is extremely sparse and sporadic. Macquarie Island (Figure 1.1), has a surface synoptic observations program and has traditionally performed two upper air soundings per day. However, Heard Island, to the north of Mawson, (Figure 1.1) has been limited to a simple automatic weather station, reporting only temperature and pressure, and also reliant on polar orbiting satellites for the transmission of observations back to Australia. At the time of writing (2003), there were only around 6 floating buoys reporting temperature and pressure south of 50°S in the eastern sector of the Southern Ocean. In all, only a very limited data set has been available for analysis and forecasting purposes, forcing a significant reliance on the availability of a robust NWP system to provide weather data over the oceanic regions. Quantifying the veracity of such models in providing useful forecast guidance has become more

important as marine users place more reliance on weather forecast information, but without permanent oceanic observing platforms, single station verification of model data, as described above, has not been possible. However, the Australian research vessel *Aurora Australis,* has been fitted with a comprehensive suite of meteorological sensors recording temperature, pressure, humidity, wind speed and wind direction at 10 second intervals, on both the port and starboard sides of the ship. Pressure, humidity and temperature sensors were at around 20 m above sea level, with the anemometer sensors near 31.6 m, depending on vessel loading. To facilitate a comparison of *Aurora Australis* meteorological data with output from the ALAPS model, temperature and humidity data from the ALAPS 0.9974 σ-level (typically between 19 and 22 m above the Southern Ocean surface) were extracted for comparison with the instantaneous hourly data from the *Aurora Australis* AWS. The one minute wind data from the *Aurora Australis* AWS were used to construct an hourly observational data set of 10 minute average wind for comparison with a composite ALAPS surface wind, taken as the mean of the wind at the 0.9974 σ-level and the 0.9943 σ-level (typically 42 to 48 m above the surface over the Southern Ocean). The constructed mean ALAPS wind was assumed to be representative of the model wind near 30 m and comparable with the *Aurora Australis* observations taken at 31.6 m.

5.4.1 A Southern Ocean cruise.

Voyage 3 of the *Aurora Australis,* undertaken late in 2001, was part of the Climate Variability and Predictability Program (CLIVAR), with the cruise completing a repeat of the SR3 north-south transect, and conducting suspended

and sinking particle studies, iron distribution and phyto-plankton response experiments amongst other marine science duties. The voyage departed Hobart, Tasmania, on 29 October 2001 and reached it's most southerly latitude on the cruise at 67°11'S, 144°52'E at 1700UTC 29 November 2001, before heading north for Hobart, returning on 12 December 2001 (Figure 5.31).

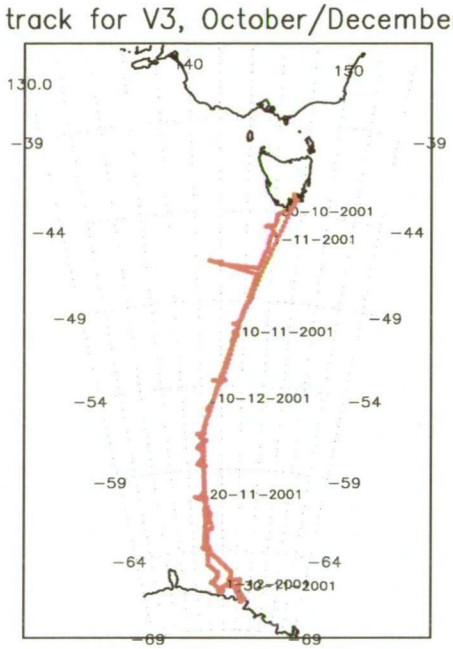

Figure 5.31: Track of the Aurora Australis during voyage 3 of the 2001-02 summer season (October to December 2001).

The time series data from the cruise are shown Figure 5.32, where observations from the *Aurora Australis* are plotted in black, and forecast data from the +48 hour ALAPS forecast, interpolated to the *Aurora Australis* track, shown in colour. *Aurora Australis* wind speed observations were compared with both the ALAPS composite, 30 m, wind (blue time series plot on panel 2 of Figure 5.32) and the ALAPS estimate of the potential wind gust strength (plotted in red on panel 2 of Figure 5.32). The potential gust strength was estimated following the work of Brasseur (2001), on using turbulent kinetic

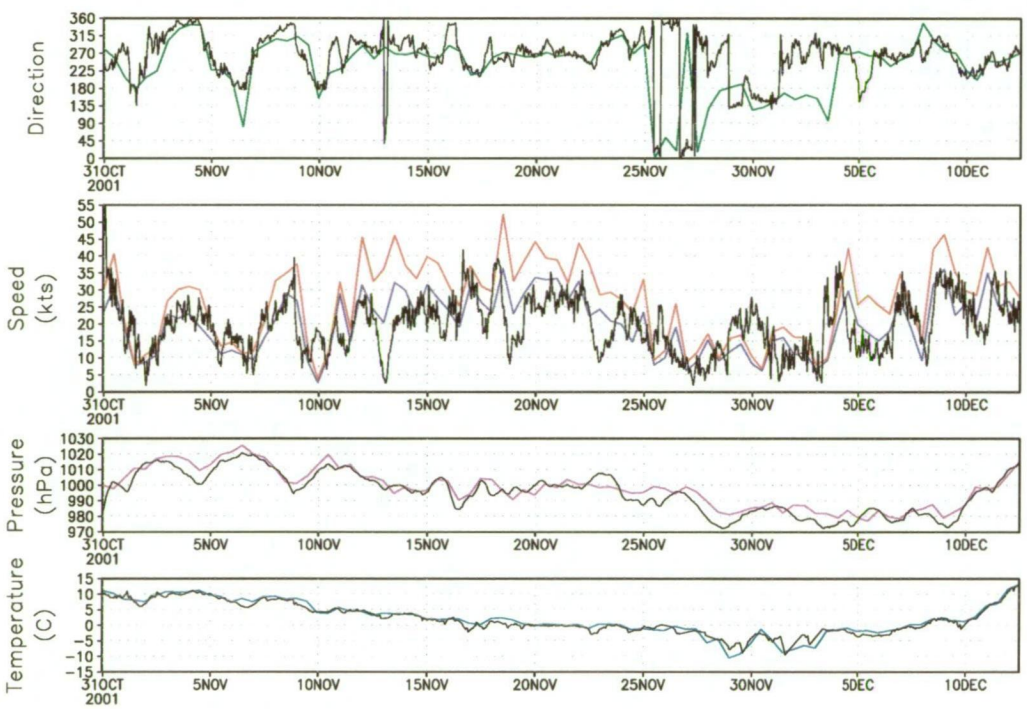

Figure 5.32: Comparison of ALAPS +48 hour surface data (coloured time-series) with observations taken from the Aurora Australis (black time-series), during the voyage 3 cruise.

energy to define the depth of the surface layer through which wind could potentially mix to the surface. The ALAPS implementation was somewhat simplified, whereby the Froude Number profile at each model grid point was used to estimate the depth of the turbulent surface layer, and the maximum model wind speed within this layer was used as the potential gust strength estimate. A more complete discussion of the technique is given in chapter 7 on forecast systems. During the voyage, 8 gale force wind events were encountered where wind speeds reached, or exceeded, 34 knots. Table 18 highlights

Time-step	Successes	Failures	False Alarms
analysis	5	3	3
analysis*	8	0	7
+24 hours	2	6	1
+24 hours*	8	0	5
+48 hours	2	6	0
+48 hours*	8	0	5

Table 18: ALAPS forecast successes and failures over the Southern Ocean.
***Using potential gust strength as a proxy for surface wind.**

the effectiveness of the ALAPS analyses and prognoses in forecasting the gale force wind events, and although it appears that the ALAPS composite surface wind didn't perform particularly well in forecasting gale strength events, the potential gust strength estimate performed very well, although with a poor (high) false alarm ratio. However, a closer inspection of the time series data (Figure 5.32) highlighted the fact that even at +48 hours, ALAPS went very close to achieving a high success rate, with 5 of the 6 recorded forecast "failures" being within 5 knots of gale strength, and so still provided very useful guidance. The potential gust strength forecast appeared to lead to too many false alarms, but, in fact, was also far more useful than this statistic suggested. Of the 5 false alarm events recorded at +48 hours,

the actual reported wind speed was equal to, or in excess of 30 knots on 4 of these occasions and so very nearly reported as a gale and, as such, a potential forecast success. By allowing for small errors in ALAPS forecast wind speeds and potential gust strengths the model actually provided exceedingly good forecast guidance.

Shifts in wind direction were also well modelled at +48 hours with the wind direction time series showing good agreement with the reported wind direction. There was only one period over the first 2 to 3 days of December where the +48 hour forecast persisted in modelling a south to southeast stream where in fact the observations reported a due westerly. It should be noted, however, that the wind speed during the period was generally less than 15 knots, and for a good part of the period less than 10 knots. The timing of significant wind events was also modelled well at +48 hours, although occasional events were forecast with timing errors of up to 6 to 12 hours, with some forecasts early, and others late.

It should be noted that the three hourly synoptic observations from the *Aurora Australis* were assimilated by ALAPS in the above model runs, and so had some impact on the model performance. However, the forecast data described above were at the +48-hour model time-step, by which time the influence of the single ship observation on the forecast would be expected to be small, particularly given that the ship was continually on the move, and at times, covering upwards of 150 km, in 48 hours.

The performance of the ALAPS forecasts over the Southern Ocean in the above case study were remarkably good, giving a very high level of confidence in the model dynamics and physics over oceanic areas.

6 Sensitivity studies

With the move to higher resolution numerics in NWP systems not only do the topographic influences become more significant but the interactions between ocean, sea-ice and atmosphere may also begin to play a significant role in the development of local weather systems. Features such as polynyas, and leads in the sea-ice zone, are not generally resolved at the resolutions employed by the current global models. However, significant gradients in albedo, heat and moisture fluxes that are observed, in reality, across such regions of open water or low ice concentration areas within the sea-ice zone, and are likely to have a large impact on the heat and moisture fluxes in the local area and thus possibly on the development of meso-scale weather systems. With the resolutions now possible with limited area grid point models, polynyas and large leads within the sea-ice zone can be resolved and the gradients in albedo, heat and moisture fluxes associated with these features may very well impact on the short to medium term forecast period. Albedo values across the sea-ice zone can vary from as high as 80% over high concentration sea-ice (Weller 1980), or higher where significant snow cover is present, to as little as 10% over open water leads or polynyas. Weller (1980) has also made estimates of mean upward fluxes of sensible and latent heat with winter values of sensible heat varying from 89 Wm^{-2} in the inner sea-ice zone (ice concentrations $> 85\%$) to 152 Wm^{-2} in the outer pack (ice concentrations in the range 15 - 85%) and winter-time latent heat fluxes varying from 28 Wm^{-2} in the inner pack to 37 Wm^{-2} in the outer pack. Although other studies (Andreas et al. 1985) suggest these values may be too high, considerable variability is observed depending on the synoptic situation. During winter,

values may be exceptionally high over coastal polynyas where the strong katabatic flow is continually removing sea-ice and advecting cold continental air over the relatively warm exposed ocean. Kurtz and Bromwich (1985), in a study of the Terra Nova Bay polynya, cite a net surface energy flux of 861 Wm^{-2} (positive being up and away from the surface) during August to -145 Wm^{-2} during December, where the net surface flux is the residual from the balance between the net radiation, sensible heat flux and the latent heat flux. Budd et al. (1997) in a modelling and observational study of the physical characteristics of the Antarctic sea-ice zone also highlighted the dependence of fluxes on sea-ice concentrations.

The NCEP sea ice data imported into the model was relatively coarse with a resolution of only 0.5x0.5 degrees of longitude by latitude. However, even at such low resolutions some of the polynyas found around East Antarctica are readily evident in the sea ice data and subsequently in the land-sea-ocean mask, surface temperature field, and albedo prescribed within the initial and nesting condition files used by ALAPS. Consequently, the gradients of albedo and heat and moisture fluxes across these areas of open water within the sea ice zone were resolved by the model, making it necessary to ascertain the sensitivity of the model to errors in the prescription of these surface fields. The model employed a fixed ocean and sea ice surface at the model lower boundary, with ice concentration values not changing throughout the 48 hour model integration time. However, if the model output was very sensitive to either over-prescribing or under-prescribing sea ice cover, through the inherent errors in the prescription of the initial surface temperature and albedo values, and resulting errors in fluxes of heat and moisture, then it

may be necessary to either find a more accurate sea ice analysis, or more importantly move toward coupling the atmospheric model to a dynamic sea-ice model to adequately define the surface type within the model domain, and over the 48 hour model integration period.

As discussed in chapter 3, surface roughness over the Antarctic continent was set to a fixed value of 0.001 m (1 mm), for the 12 month trial period of the ALAPS system, as a conservative estimate, but may have been too high for the smooth gentle slopes of the Antarctic interior when compared to some of the observational studies cited in chapter 3. However, the value of 1 mm was considered a reasonable value for the steep coastal escarpment of East Antarctica, where sastrugi and snow dunes are common, and the Australian Antarctic stations are located.

The sensitivity studies detailed below, were limited by computer resources and so, by no means, are considered an exhaustive study of ALAPS sensitivities to altered physical parameters. Sensitivity to altered sea-ice conditions was limited to re-running the model over the first 19 days of January 2002, (37 model runs), with the sea-ice cover and sea surface temperatures taken from a winter data set, and to complement the excess sea-ice study, a second re-run of the model, over the first 22 days of September 2001, (42 model runs), was performed with low sea-ice concentrations,and warm sea surface temperatures, taken from a summer time data set. The sensitivity of the model to altered albedo conditions was very limited, with the study looking at only one model run with continental and sea-ice albedo values increased substantially, and one run with the albedo values decreased significantly. The sensitivity study of the ALAPS model to altered surface roughness was lim-

ited to the study of 2 events, the first a strong wind event recorded at Casey, and the second a strong katabatic signal reported at Mawson. Although a very limited study, it was considered that any sensitivity in the model would be highlighted by these events, where local topographic forcing of the wind was considered to be highly likely. This study also looked at the effects of altering the horizontal diffusion coefficient used by the model. The diffusion term is typically tuned to the conditions being modelled and so it was considered prudent to look at how significant the term was in defining surface flow at Mawson and Casey during the 2 events.

6.1 Excess summer-time sea-ice.

In this sensitivity study 37 runs of the ALAPS model were performed over the first 19 days of January 2002 where the sea-ice concentration and SST data used by the model were taken from a winter-time data-set. Figure 6.1 shows a comparison of the actual sea-ice concentration data from 1 January 2002 with the excessive sea-ice concentration data used for the 37 model runs. Sea surface temperature data from the same winter data-set were also used in the 37 model runs. A comparison of model output between the two runs showed only small differences in S1 skill scores (Figure 6.2), with the excessive sea-ice cover run during January 2002 degrading the model performance over the 19 days by an average of 1 to 2 skill score points. A comparison of time series surface data at Casey from both model runs showed only subtle differences in forecasts of wind speed and direction, surface temperature and pressure (not shown). However, where significant differences were apparent, were in the cloudiness around the coastal fringe of Antarctica. In the Casey area

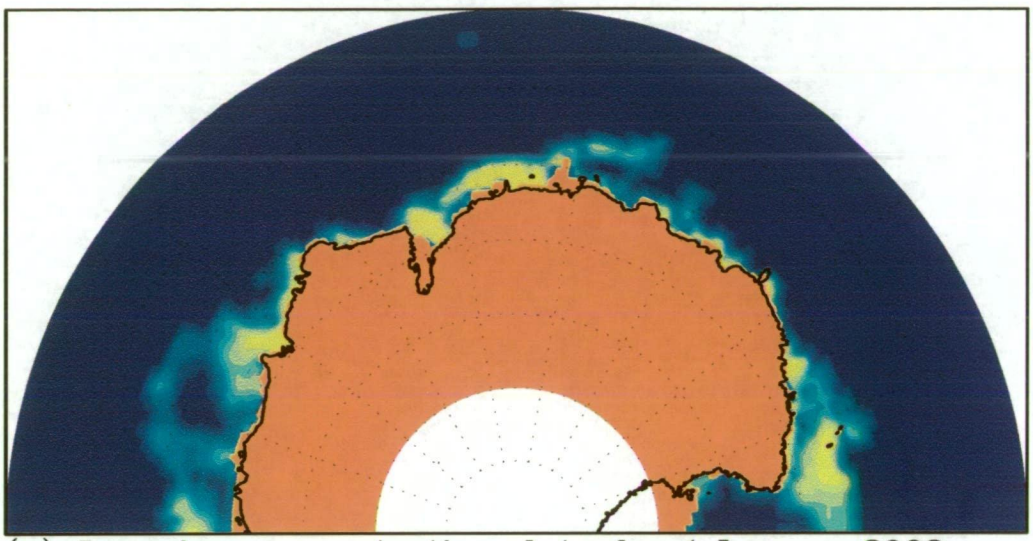

(a) Sea −ice concentration data for 1 January 2002.

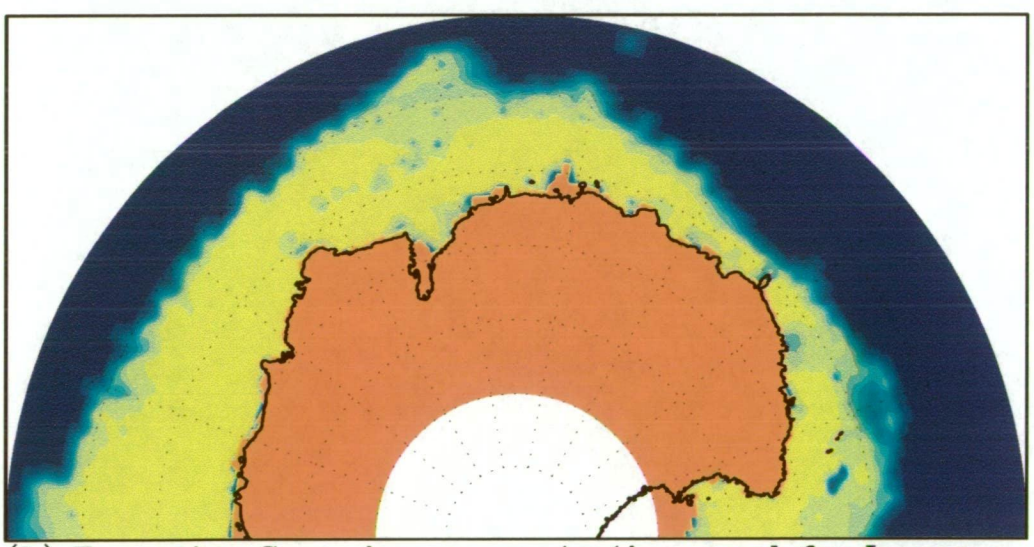

(b) Excessive Sea −ice concentration used for January.

Figure 6.1: Sea-ice concentration as measured on 1 January 2002 (top panel), and as used in the excessive January sea-ice sensitivity study (lower panel).

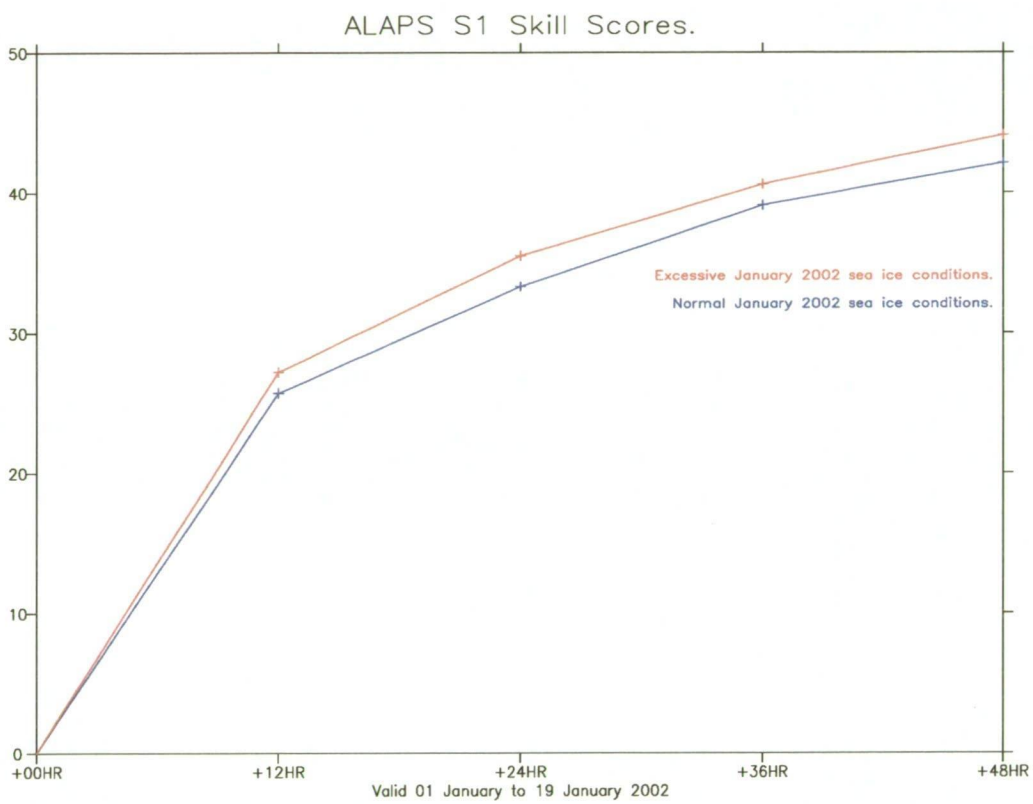

Figure 6.2: Comparison of S1 skill scores for the first 3 weeks of January 2002, with normal sea-ice conditions (blue), and excessive sea-ice (red) over the domain 70^{o}S to 50^{o}S and 80^{o}E to 160^{o}E.

the number of cloud days was reduced by around 5 to 10% (top 2 panels of Figure 6.3). The number of days with a cloud base below 5000 ft was also, in general reduced (middle 2 panels of Figure 6.3), although the low cloud area over Casey, and along the coast to the immediate southwest, wasn't reduced significantly in the excess-ice cover runs. However, the number of days with very low cloud base (less than 500 ft), reduced by about 10 to 15% over the entire area, with Casey, and the proposed runway site, seeing little or no very low cloud days during January in the scenario with excess ice (bottom 2 panels of Figure 6.3). The reduction in very low cloud had an obvious link with a reduction in available low level moisture, with an extensive area of ocean to the north of Casey covered in sea-ice, where normally fluxes of moisture from an open ocean would have been available for condensation into low cloud. The changes in the precipitation field between the normal and excessive ice runs were to be expected, with a reduction in the average 24 hour precipitation totals over the eastern side of Law Dome, and a slight reduction along the coast to the west of Casey (Figure 6.4) for the excess sea-ice runs. This reduction was expected, as a component of the precipitation in these areas would be as a result of topographic up-slide and low level moisture convergence. However, the areas off-shore of Casey, (lower panel of Figure 6.4) experienced slightly higher average precipitation in the case of excess sea-ice, which was unexpected. Closer examination of the model data highlighted the fact that in the case of the excess ice runs the mean surface and near surface temperatures off the Casey coast were warmer than in the normal sea-ice case, because of the absorbed incoming solar radiation by the sea-ice. With concentrations greater than 95% treated as land, significant

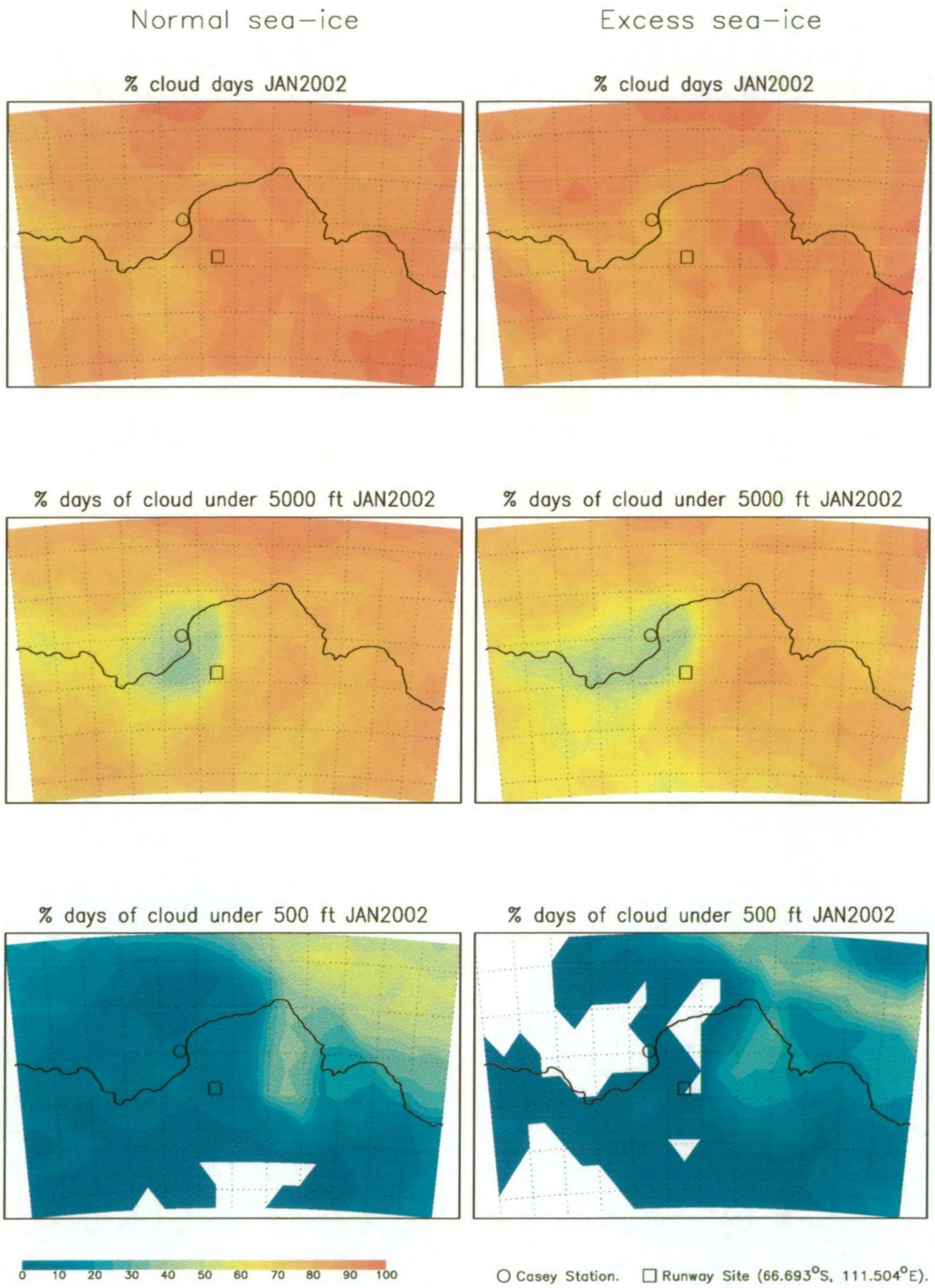

Figure 6.3: A comparison of percentage number of cloudy days (top 2 panels), percentage number of days with cloud below 5000 ft (middle 2 panels), and percentage number of days with cloud below 500 ft (lowest 2 panels), for normal sea-ice conditions (left hand panels) and excess sea-ice conditions (right hand panels) from the ALAPS +24 hour forecasts.

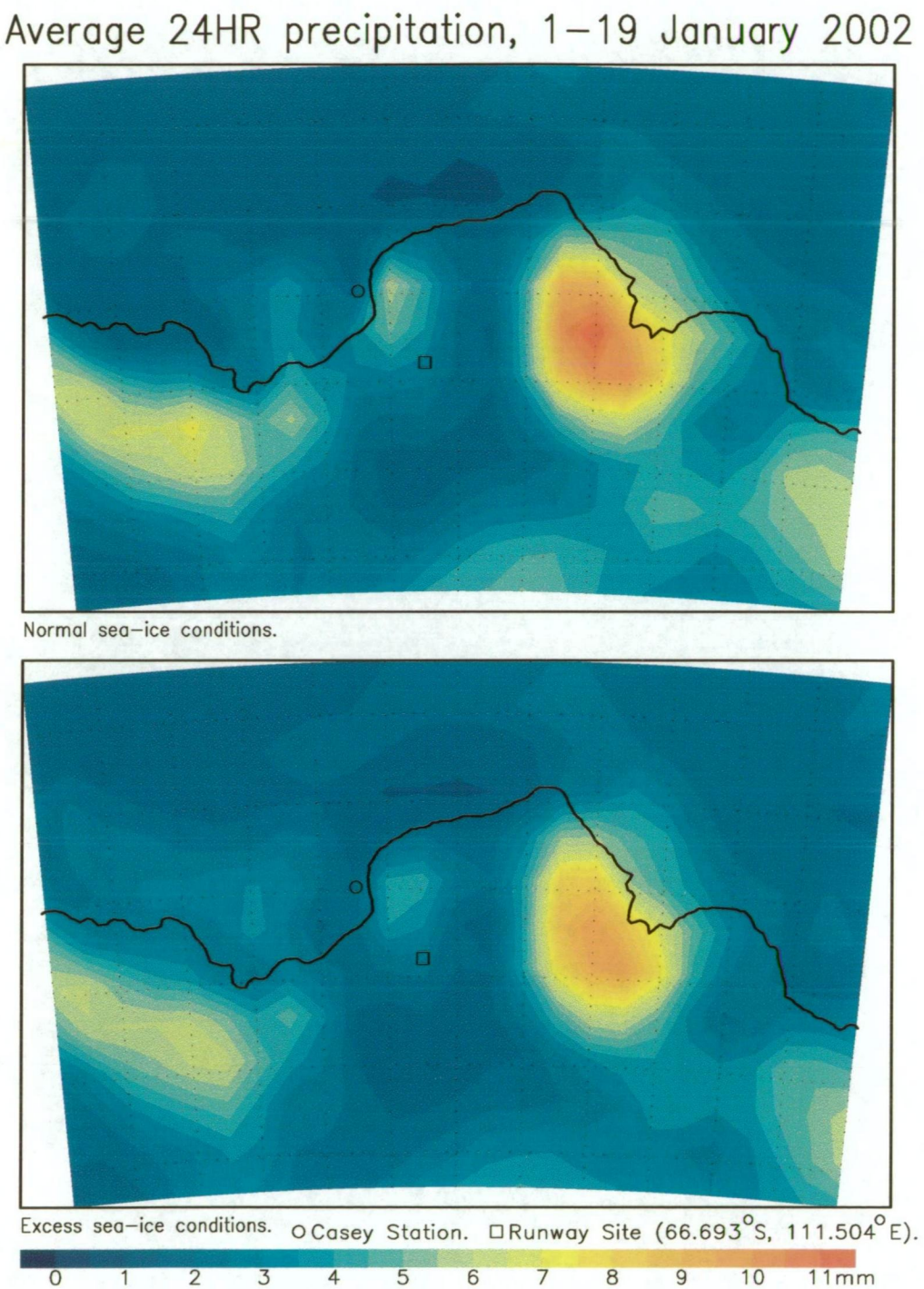

Figure 6.4: Average ALAPS 24 hour precipitation (mm) over the January 2002 sensitivity study, with normal sea-ice conditions (top panel), and excess sea-ice conditions (lower panel).

areas off the coast continued to warm in the excess sea-ice case, leading to relatively high near surface temperatures. The change in near surface temperature gradients resulted in a change in the mean surface pressure pattern, with the observed mean low pressure system off the Casey coast in the normal run (top panel of Figure 6.5) having shifted both southward and to the east when the excess sea-ice was introduced (lower panel of Figure 6.5). Pressure gradients were also slightly tighter in the flow around the low, with a stronger north to northeast inflow onto the Casey coast, resulting in higher precipitation rates, in general along the coast, although still lower on the eastern side of Law Dome, for reasons cited above. In reality the significantly warmer low level temperatures would have lead to a significant decrease in the sea-ice with, a negative feedback on the excess ice case, which highlights the problem of having only a prescribed sea-ice surface and no atmosphere-ocean feed back in which sea-ice is allowed to decay or grow.

6.2 Reduced winter-time sea-ice.

In this study 42 model runs were made from 2300UTC on 2 September 2001 with little, or no, sea-ice around the coast of Antarctica and summer-time SST values. The upper panel of Figure 6.6 highlights the sea-ice concentration data used in the standard model run on 15 September 2001, with the lower panel showing the sea-ice used in the low-ice sensitivity run. A comparison of S1 scores for the 22 day period between the control run and the low-ice run are shown in Figure 6.7, where S1 scores are in fact better for the low-ice run than the control run, but only by between 1 and 2 skill score points. The time-series profiles of surface variables compared against observations from

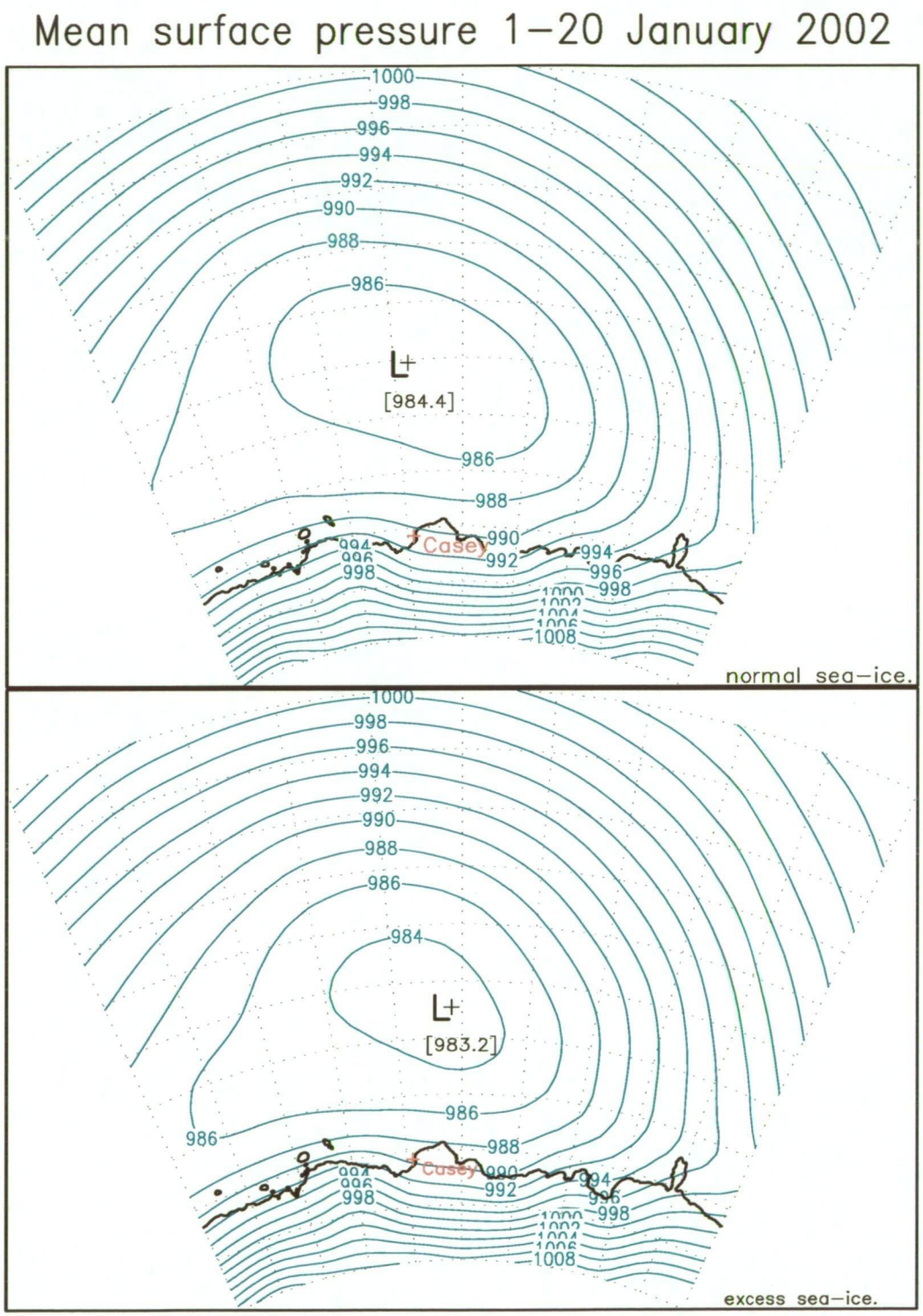

Figure 6.5: Mean surface level pressure (hPa) over the January 2002 sensitivity study, with normal sea-ice conditions (top panel), and excess sea-ice conditions (lower panel).

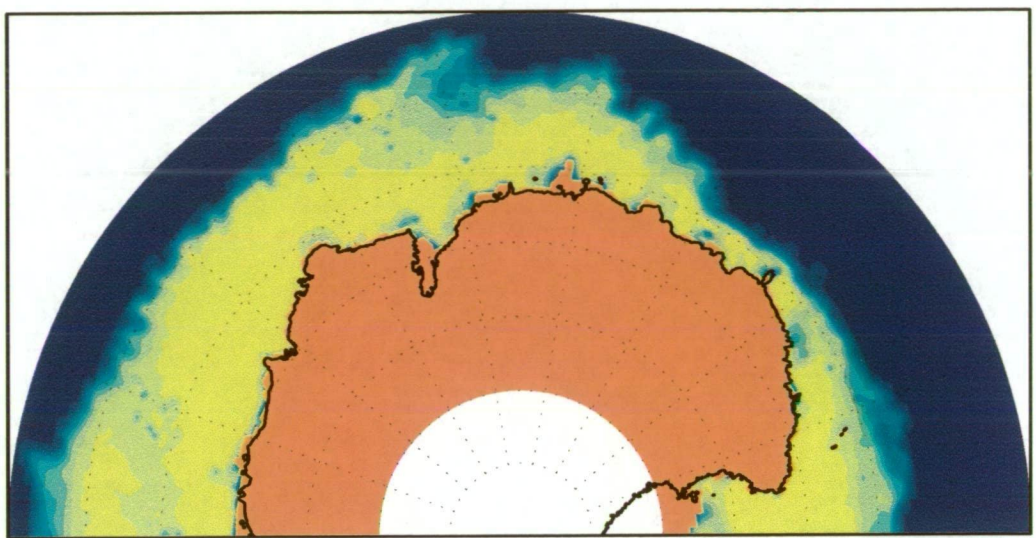

(a) Sea -ice concentration data for 15 September 2001.

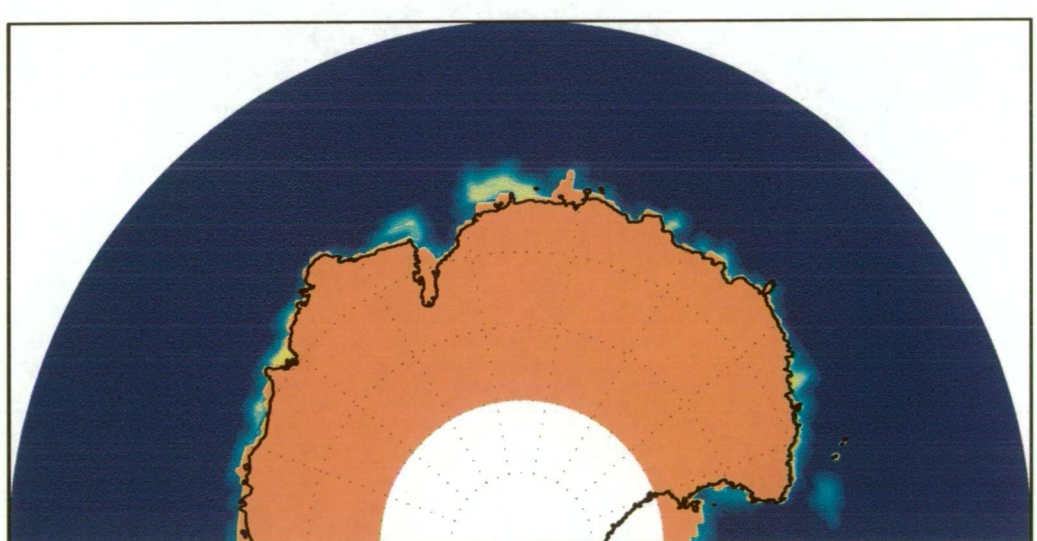

(b) Low Sea -ice concentration used for September.

Figure 6.6: Sea-ice concentration as measured on 15 September 2001 (top panel), and as used in the reduced September sea-ice sensitivity study (lower panel).

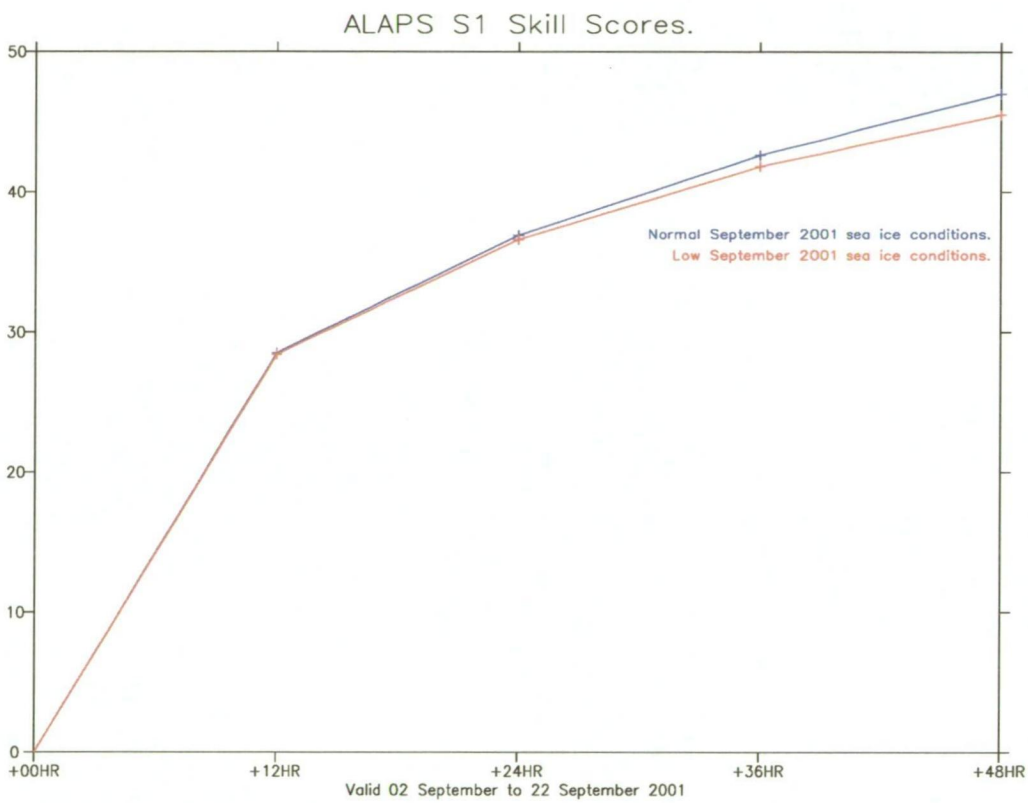

Figure 6.7: Comparison of S1 skill scores for the first 3 weeks of September 2001, with normal sea-ice conditions (blue), reduced sea-ice (red) over the domain 70°S to 50°S and 80°E to 160°E.

Casey (not shown), showed only subtle differences between the standard and low-ice runs, with the control run performing slightly better on wind speed and direction at +24 and +48 hours. As with the excess-ice summer-time ice run, significant changes were observed in the cloud and precipitation output from the model. With the extensive area of open water off the Casey coast, the increased flux of moisture appeared to be responsible for increased cloud at all levels and over much of the Casey area. The top 2 panels of Figure 6.8 show the changes in the percentage number of cloudy days, the middle 2 panels the changes in percentage number of days with cloud below 5000 ft and the bottom 2 panels the changes in number of days with cloud below 500 ft. The increase in low level moisture would directly affect low level cloud, with the extensive area of open water and warmer SST's leading to a build up of moisture at all levels. However, one interesting feature to note is that the cloudiness over, and just to the southwest of, Casey showed little change with the reduced sea-ice cover and, in fact, further to the west, over Prydz Bay, the number of low level cloudy days actually reduced with the reduction in sea-ice cover (Figure 6.9). The reduction in relative humidity over this area was as a result of the significant warming due to the large area of open water offsetting any increased availability of low level moisture. Figure 6.10 shows the differences in low level moisture (mixing ratio) and the surface and near surface temperatures between the normal sea-ice conditions (left hand panels) and low-ice conditions (right hand panels). Over the ocean to the north of Prydz Bay the increase in low level moisture was not as marked as in the Casey area (top 2 panels Figure 6.10), however increases in low level temperatures were marked, resulting in reduced relative humidities

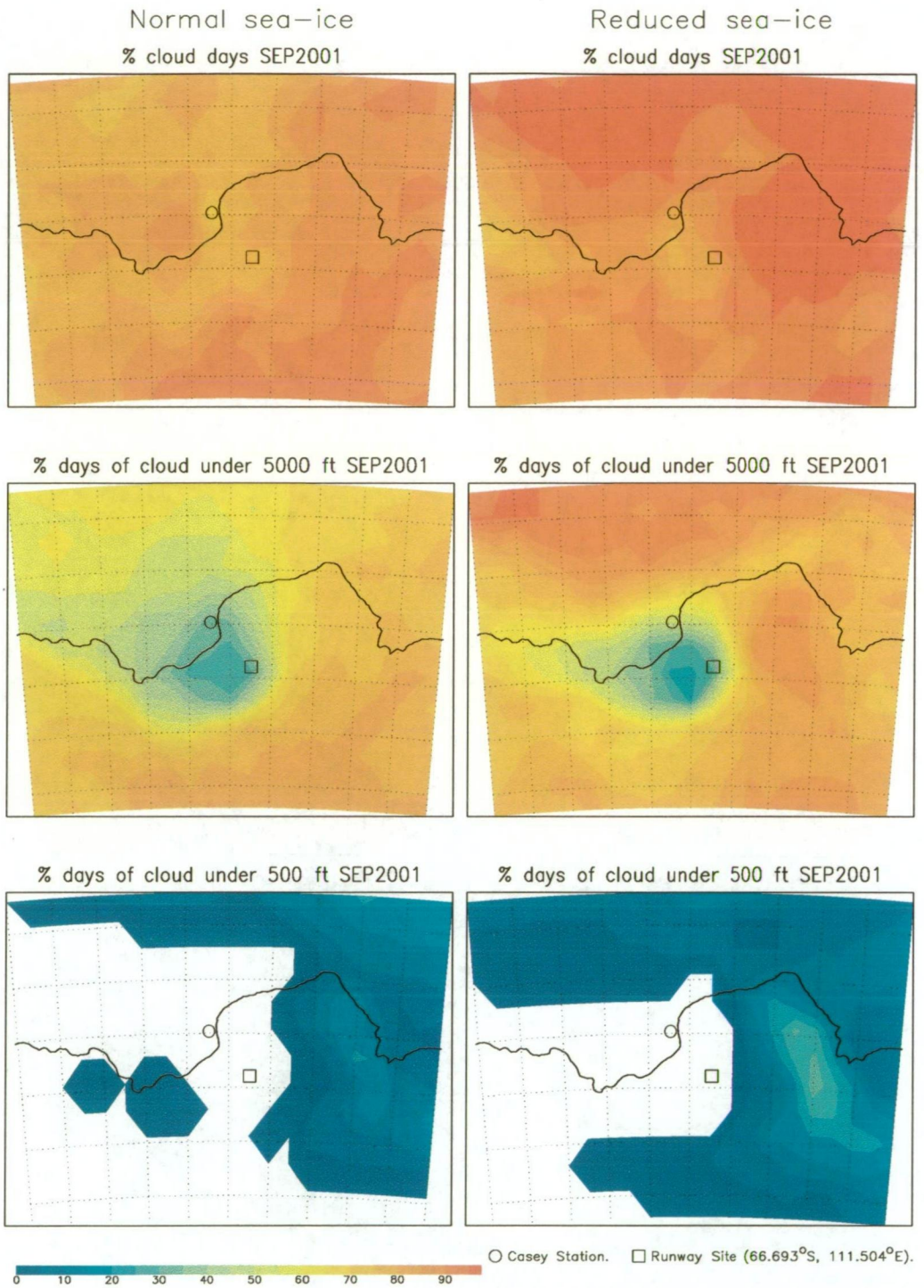

Figure 6.8: A comparison of percentage number of cloudy days (top 2 panels), percentage number of days with cloud below 5000 ft (middle 2 panels), and percentage number of days with cloud below 500 ft (lowest 2 panels), for normal sea-ice conditions (left hand panels) and reduced sea-ice conditions (right hand panels) from the ALAPS +24 hour forecasts.

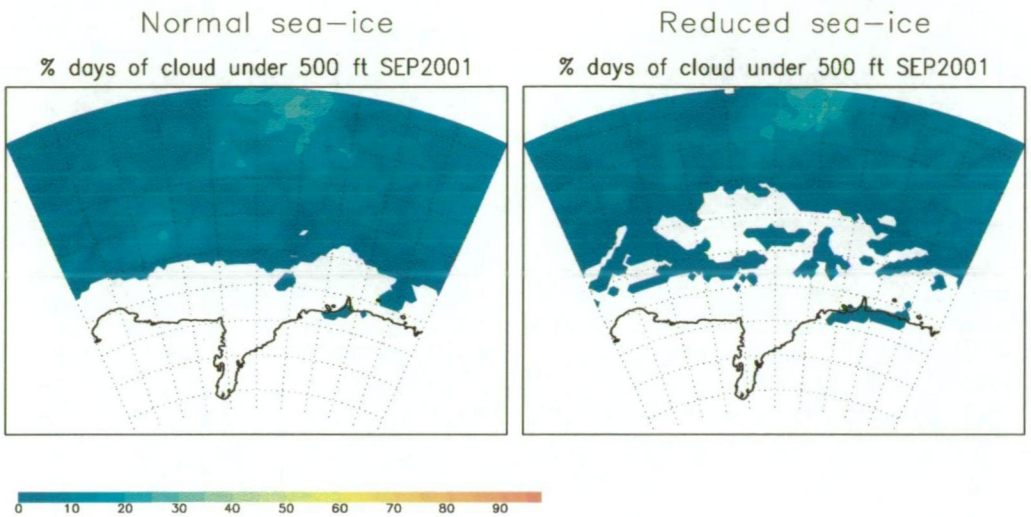

Figure 6.9: A comparison of percentage number of days with cloud below 500 ft, for normal sea-ice conditions (left hand panel) and reduced sea-ice conditions (right hand panel), in the Prydz Bay region from the ALAPS +24 hour forecasts.

and a lower number of low level cloud days.

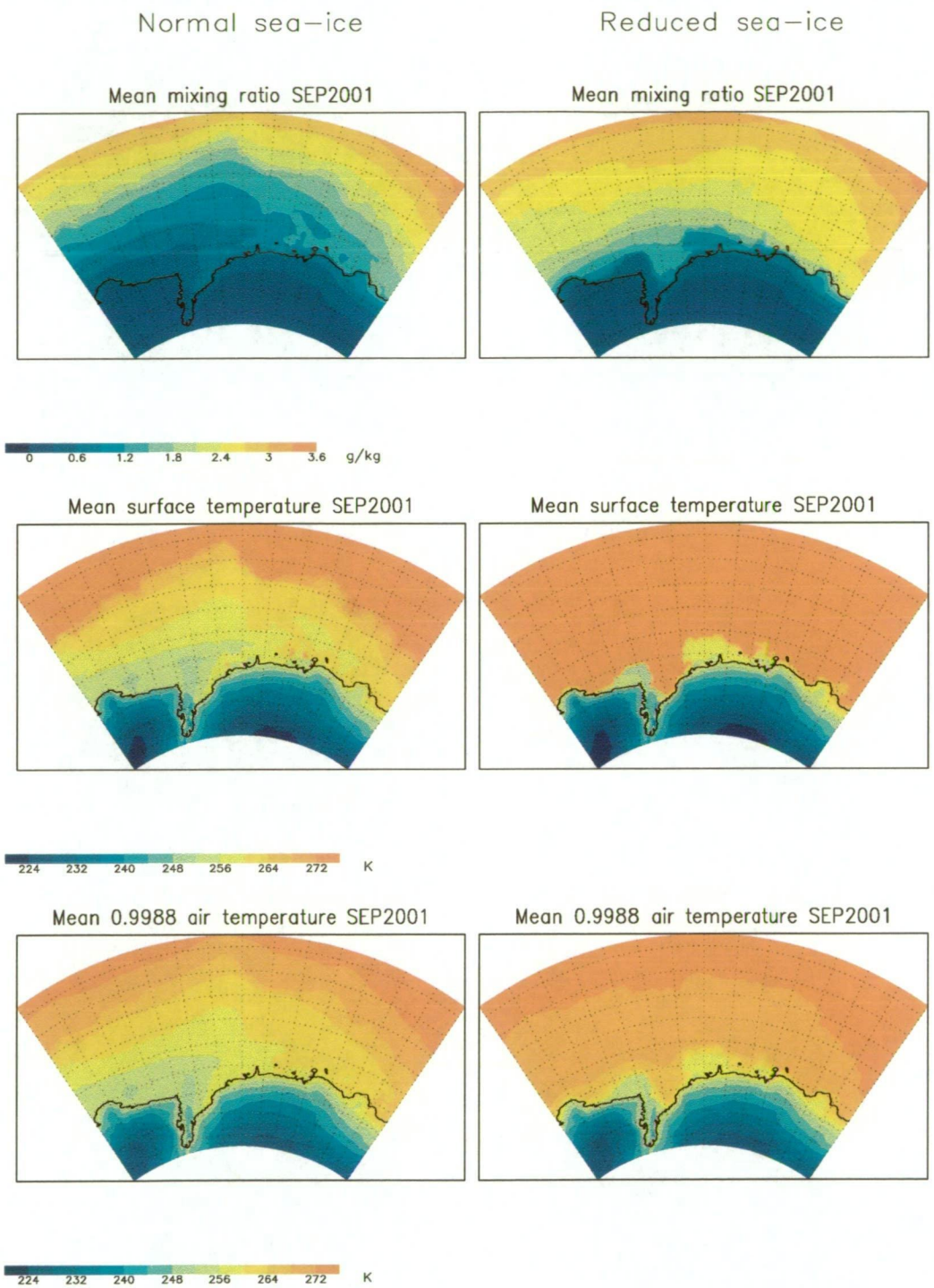

Figure 6.10: A comparison of mean near surface mixing ratio (g/kg) (top 2 panels), surface temperature (K) (middle 2 panels), and near surface temperature (K) (lowest 2 panels), for normal sea-ice conditions (left hand panels) and reduced sea-ice conditions (right hand panels) from ALAPS +24 hour forecasts.

6.3 Altered Antarctic and sea-ice albedos.

During the analysis of the performance of ALAPS (Chapter 4), around both Mawson and Dome C, it became apparent that the ability of ALAPS to model the diurnal variations seen in the skin, and near surface, temperatures was deficient. ALAPS performed well in modelling the phase of the temperature variations, however the amplitude of the model summer-time temperature signal was too low over the high plateau at Dome_C (Figure 4.23), and marginally too large on the coastal fringe, at Mawson (Figure 4.24). It was assumed that the reason behind the errors in the amplitude of the diurnal temperature signal was linked with the radiation balance, and errors in the assumed albedos used, both over the plateau and over the coast. To test the hypothesis the ALAPS model was re-run for 1100UTC on 26 January 2002, where a strong diurnal signal was evident in the observed Dome C temperature data (Figure 4.27), but with a much reduced amplitude in the model data. During this particular model run the modelled temperature variations for Mawson were good, with the modelled skin temperature having an amplitude some 4.5^{o}C larger than the amplitude observed in the 2 m, near surface temperature, and the modelled 8 m diurnal variation in temperature an amplitude around 0.5^{o}C less than the observed 2 m temperature amplitude (Figure 6.11), giving a reduced model 2 m air temperature signal very close to that observed. However, as evident from Figure 4.24, on occasions the modelled Mawson temperature data showed a significantly larger diurnal variation in temperature than observed.

The model run from which Figures 4.27 and 6.11 were generated had a summer-time albedo value for Mawson set at 68.4% and for Dome C at

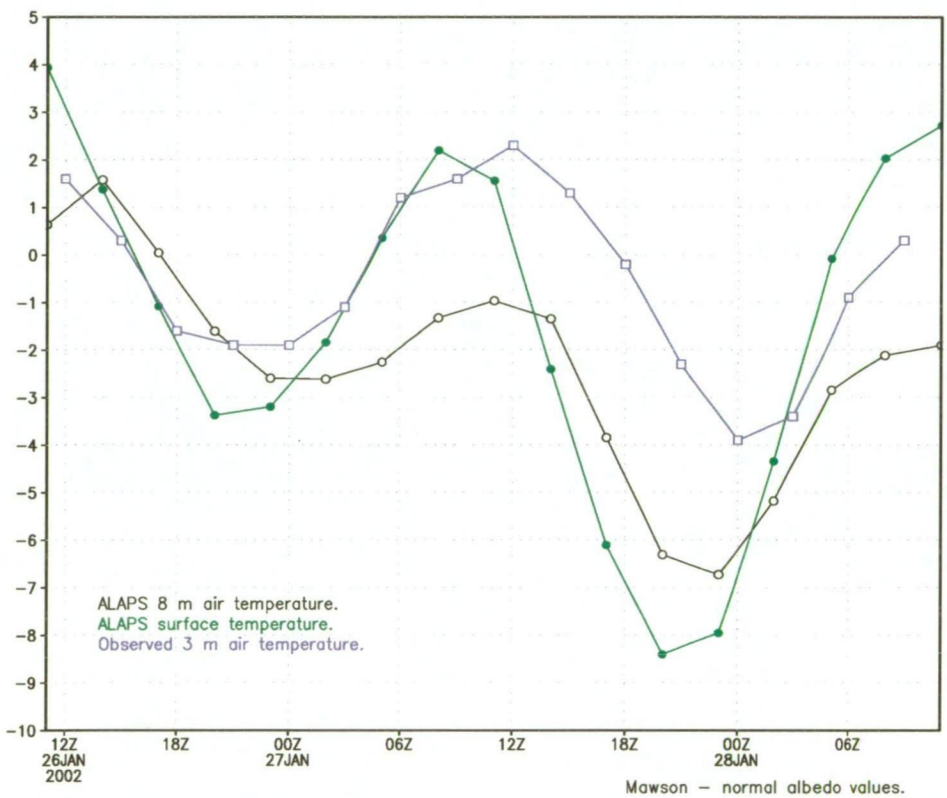

Figure 6.11: ALAPS 3 hourly output of surface (green) and near surface (black) temperature from the model run initiated at 1100UTC 25 January 2002, compared with observations from Mawson (blue).

82%. The sensitivity run was constructed with the albedo values over the Antarctic continent reduced to 75%, and with the coastal minima of 65% raised to 70%. This decreased the albedo at Dome C from 82% to 75% and increased the albedo at Mawson from 68.4% to 71%. Figure 6.12 shows the

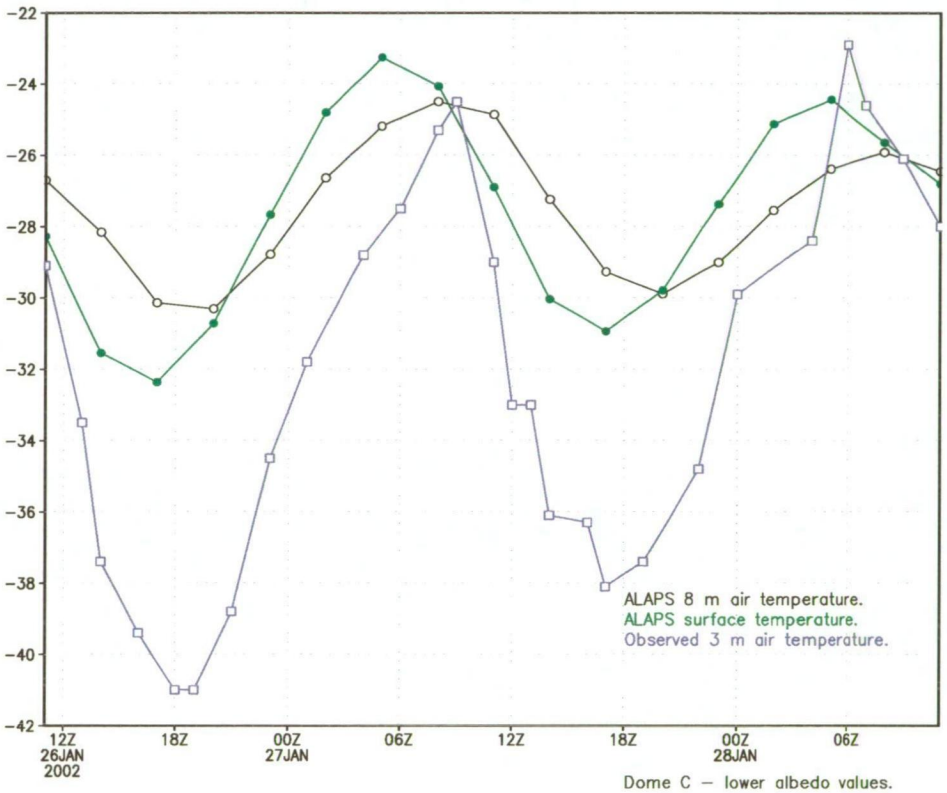

Figure 6.12: ALAPS 3 hourly output of surface (green) and near surface (black) temperature from the model run initiated at 1100UTC 25 January 2002, with a lower albedo, compared with observations from the Dome C AWS (blue).

48 hour modelled temperature data from Dome C with the reduced albedo values, and, as would be expected, the diurnal variation in the 8 m modelled air temperature has increased by around 1^{o}C, and with the the overall mean temperature also increasing by around 1^{o}C. However, despite day-time maximum temperatures being modelled more accurately the night time minimum

temperatures were still too warm. Figure 6.13 shows the temperature traces

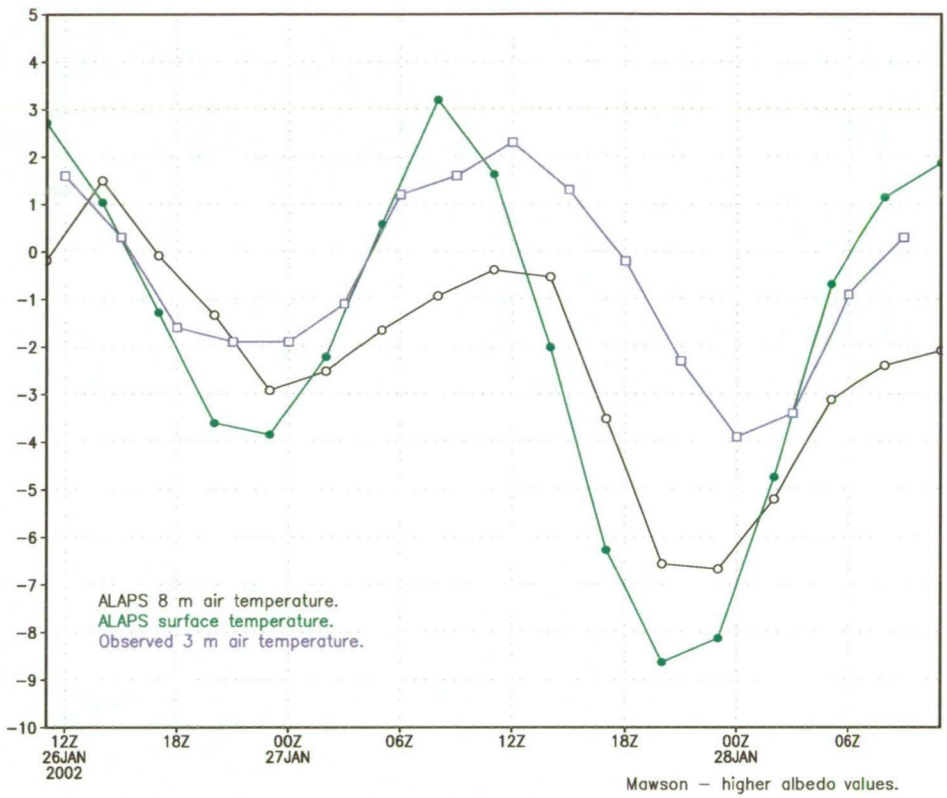

Figure 6.13: ALAPS 3 hourly output of surface (green) and near surface (black) temperature from the model run initiated at 1100UTC 25 January 2002, with higher albedo, compared with observations from Mawson (blue).

for Mawson within the new model run, where local albedo values were in fact increased. However, Mawson modelled temperatures also experienced an increase in the amplitude of the diurnal variation in surface and 8 m temperatures. The amplitude of the variation in 8 m air temperature increased by around 1^{o}C, whereas a slight decrease in amplitude, and mean temperature, was expected with the increased albedo, through greater reflection of incoming solar radiation back into space. The most likely reason for the increase would have been as a result of advection of warmer air off the plateau, where reduced albedo values over the entire continent would have led to a

large body of slightly warmer air , as in the case of Dome C.

Despite the changes in albedo having a positive affect on the diurnal variation seen in the model forecasts of air temperature at Dome C, the model still didn't fully replicate the amplitude seen in the AWS observations of 3 m air temperature. Another possible contribution to the reduced amplitude in the model near surface temperature signal may have been the reflection, or absorption, of radiation by atmospheric moisture, with excess cloudiness in the model reflecting incoming solar radiation back into space, and also inhibiting outgoing long wave radiation, and so damping the amplitude of the diurnal temperature signal.

6.4 Reduced upper atmospheric moisture.

During the precipitation study in Chapter 4 mixing ratio data from the stations of Mawson, Davis and Casey were compared with the ALAPS model output, with the model appearing too dry in the lower troposphere. However, in the upper levels, above around 200 hPa, mixing ratios in the model were in fact too high, of the order of around 5% near 200 hPa, and rising steadily to around 75% by the model upper boundary, near 50 hPa. To assess whether upper level moisture over the continental interior was having a significant impact on the diurnal variation in surface temperature observed in the model near Dome C, the ALAPS model was re-run on 1100UTC, 26 January 2002, with mixing ratio values south of 65.0^{o}S, and above 200 hPa reduced on a sliding scale from 5% at 200 hPa to 75% at the upper boundary. Upper level moisture was reduced in both the initial condition file and the nesting files used for the model run. However, the impact on the Dome C model temper-

atures was only very slight, with an increase in diurnal amplitude of the 8 m air temperature of only 0.2°C, and a 0.4°C increase in the amplitude of the surface temperature diurnal variation. Variations in upper level moisture appeared to have only a minor impact on this model run. However, if moisture in middle levels was also reduced then the impact on the model temperature signals was more pronounced. Figure 6.14 shows the ALAPS modelled sur-

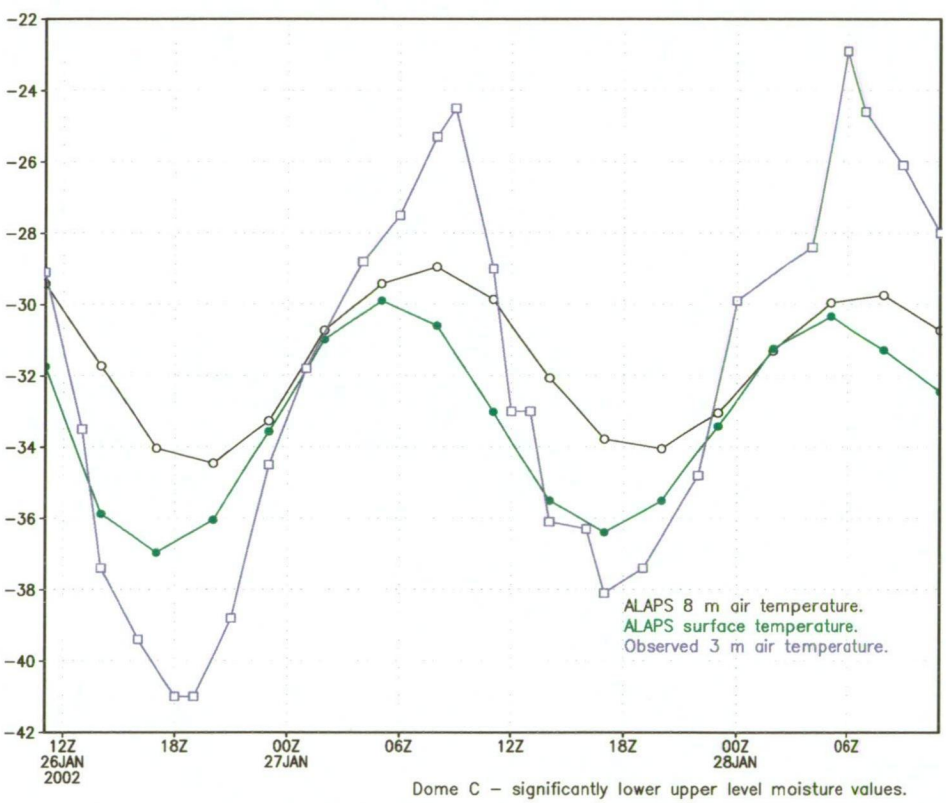

Figure 6.14: ALAPS 3 hourly output of surface (green) and near surface (black) temperature from the model run initiated at 1100UTC 25 January 2002, with reduced upper level moisture, compared with observations from the Dome C AWS (blue).

face and 8 m air temperatures, with the observed 3 m air temperature, for a run in which the mixing ratio was reduced on an increasing scale from 10% at 400 hPa to 85% by the model upper boundary. Major differences between

Figure 6.14 and the base run shown in Figure 4.27, are the increased diurnal variations of model temperatures with the reduced moisture and the colder mean temperatures in the low moisture run. The colder temperatures were as a result of out-going long-wave radiation being increased through the reduction of atmospheric moisture. This also allowed the overnight temperatures to fall to lower values than observed in the original run. Incoming short-wave radiation was little affected because moisture values in both model runs were too low for there to be cloud present, so the solar radiation reaching the surface was unaltered. Overnight minimum temperatures were far better modelled in the low moisture run, however they were still some 3 to 6^{o}C too warm, and with day-time temperatures still some 4 to 6^{o}C too cold.

Low level atmospheric moisture values would need to be reduced even further to force the ALAPS temperatures to better model the overnight minimum temperatures observed at Dome C, which would then require a decrease in the model albedo values to force the day-time warming to increase and better model the full extent of the diurnal signal observed. It is probable that other processes within the model physics were having an effect on the high plateau diurnal temperature variations, with the most likely process being sub-soil temperature profiles and fluxes of heat within the surface layer. ALAPS carries 4 sub-soil temperatures, with the first level at 0.07 m and the deepest at 1.89 m. The model used a local implementation of the ECMWF land scheme, which carries a deep-soil temperature, but one that is set as a constant for the entire Antarctic continent. All the model runs were made with the default ECMWF Antarctic deep-soil temperature of 280K. However, this temperature was considered highly inappropriate for inland

Antarctic areas such as around Dome C and a sensitivity run made with the value reduced to 220K. The resulting time-series temperature profile from the 48 hour run show a mean temperature depressed by 2^{o}C, with overnight minimum temperatures closer to those observed, however the diurnal temperature variation was suppressed, with day-time maximum temperatures also reduced. No modifications were made to the ALAPS physics in regard of terrain type so the model would still have been handling heat fluxes and conductivity over the continental ice sheet of Antarctica in the same manner as over the rocky outcrops of Mawson, or the deserts of Australia. It was not within the scope of this study to re-work, entirely the ALAPS physics, however the case studies and sensitivity studies have highlighted the fact that significant work on the ALAPS physics is necessary.

6.5 Surface roughness and diffusion.

Employing a single, fixed, roughness length to the entire Antarctic continent was, potentially, a significant restriction on the model surface layer physics, as values of roughness length over Antarctica are known to vary by an order of magnitude or more, as discussed in the opening section of the chapter. To assess the sensitivity of the ALAPS system to roughness length, two model runs were made where the roughness length was reduced from 1 mm to 0.5 mm. It was decided to reduce the roughness length in the sensitivity study since the value of 1 mm was considered at the upper end of the range of valid Antarctic roughness lengths, with perhaps a lower value being more realistic over extended areas of the continent. The first of the two model runs was initiated at 2300UTC on 5 September 2001, to assess the model

performance during the storm event observed at Casey early in September 2001, and discussed in detail in the first case study in Chapter 5. The second model run was initiated at 2300UTC on 4 January 2002 and coincided with the strong summer-time katabatic signature observed at Mawson, and also discussed in detail in the third case study in Chapter 5.

The reduced roughness length model run initiated at 2300UTC on 5 September 2001 showed some significant differences in near surface variables from the control run, that used a roughness length of 1 mm. Figure 6.15 shows a

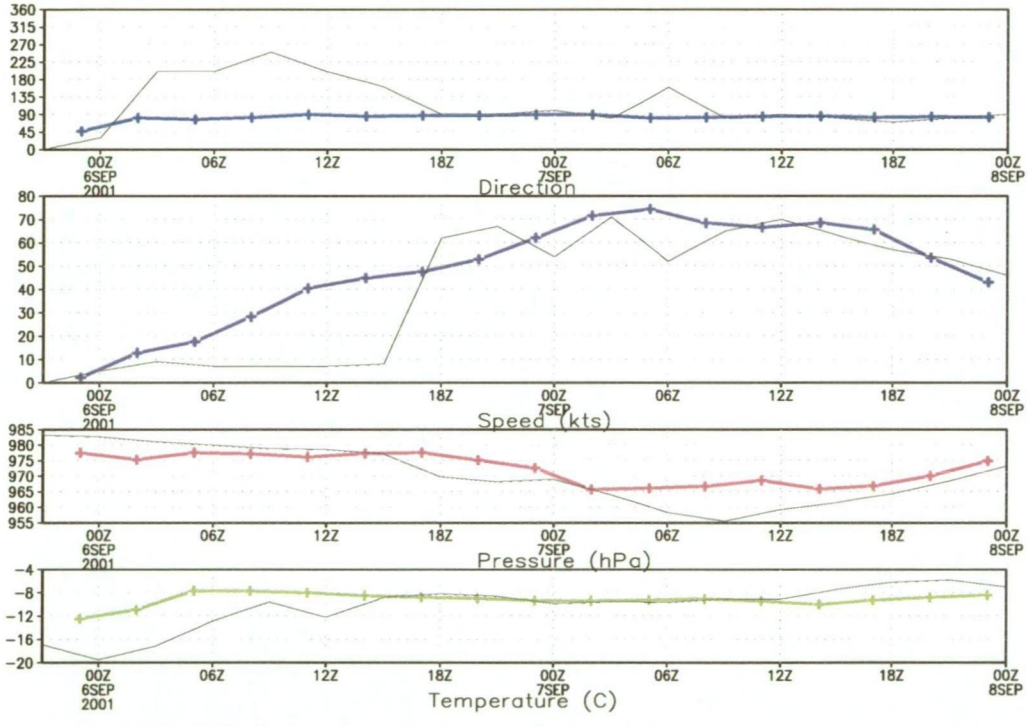

Figure 6.15: Comparison of ALAPS 3 hourly surface data (coloured time-series) with observations from Casey Station (black time-series), for the model run initiated at 2300UTC on 5 September 2001, with a reduced surface roughness length.

comparison of the results from the sensitivity run with the observed surface data from Casey station through the 48 hour model integration. When com-

pared to the results from the control run (Figure 5.2), it became apparent that the reduced roughness length resulted in an increase in near surface wind speed ($\sigma = 0.9988$), during the storm event, with the model actually over-forecasting the wind maxima, with a peak of 73 knots at 0500UTC on 7 September, where in fact the observed peak was 70 knots at 0300UTC. The model also had the wind speed at Casey increasing too early, which resulted in the modelled near surface temperature being too warm in the early part of the model run. One interesting affect of lowering the roughness length was the improvement in the modelling of the drop in surface pressure during the storm development (panel 3, Figure 6.15). The model still under-estimated the drop in surface pressure but did appreciably better than when the roughness length was set at 1 mm (panel 3, Figure 5.2). However, perusal of the vertical structure of temperature and wind showed significant problems with the low roughness length model run. Figure 6.16 shows a comparison of the observed temperature and dew-point profiles, (colour plots), with the ALAPS +24 hour forecast of temperature and dew-point, (grey profiles). The reduction in roughness length resulted in a significant warming of the model atmosphere between 850 hPa and 450 hPa, when compared to the original model run (Figure 5.6). In affect the reduced roughness length appeared to have deepened the surface layer, which was even more pronounced in the profile of wind from the new model (Figure 6.17). Although the maximum in wind speed was still at 961 ft (293 m) above the surface, the magnitude was significantly stronger at 92 kt (47 ms^{-1}), as opposed to 73.6 kt in the original model run (Figure 5.7), and the depth of gale force wind (> 48 kt) some 1500 ft deeper. Decreasing the roughness length from 1 mm to 0.5 mm

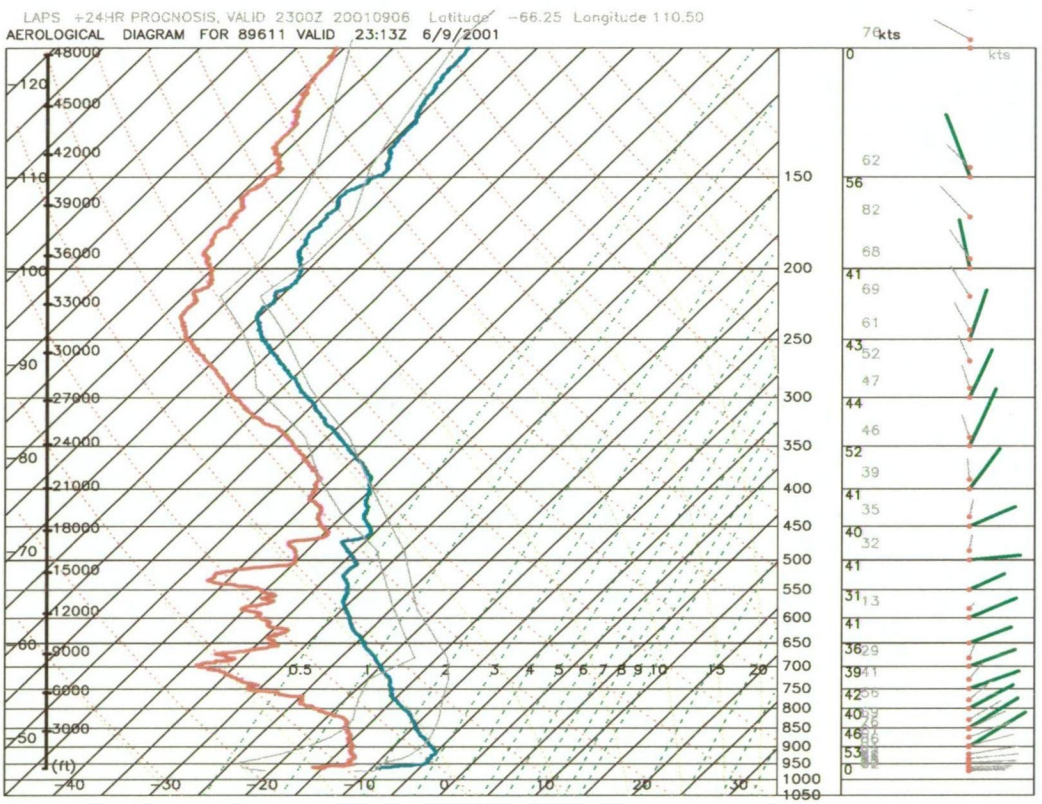

Figure 6.16: Aerological sounding from the Casey radiosonde flight (coloured traces, red dew-point, cyan temperature and green wind), valid at 2313UTC 6 September 2001, overlaid with the ALAPS sounding from the +24 hour forecast valid at 2300UTC 6 September 2001, with a reduced surface roughness length.

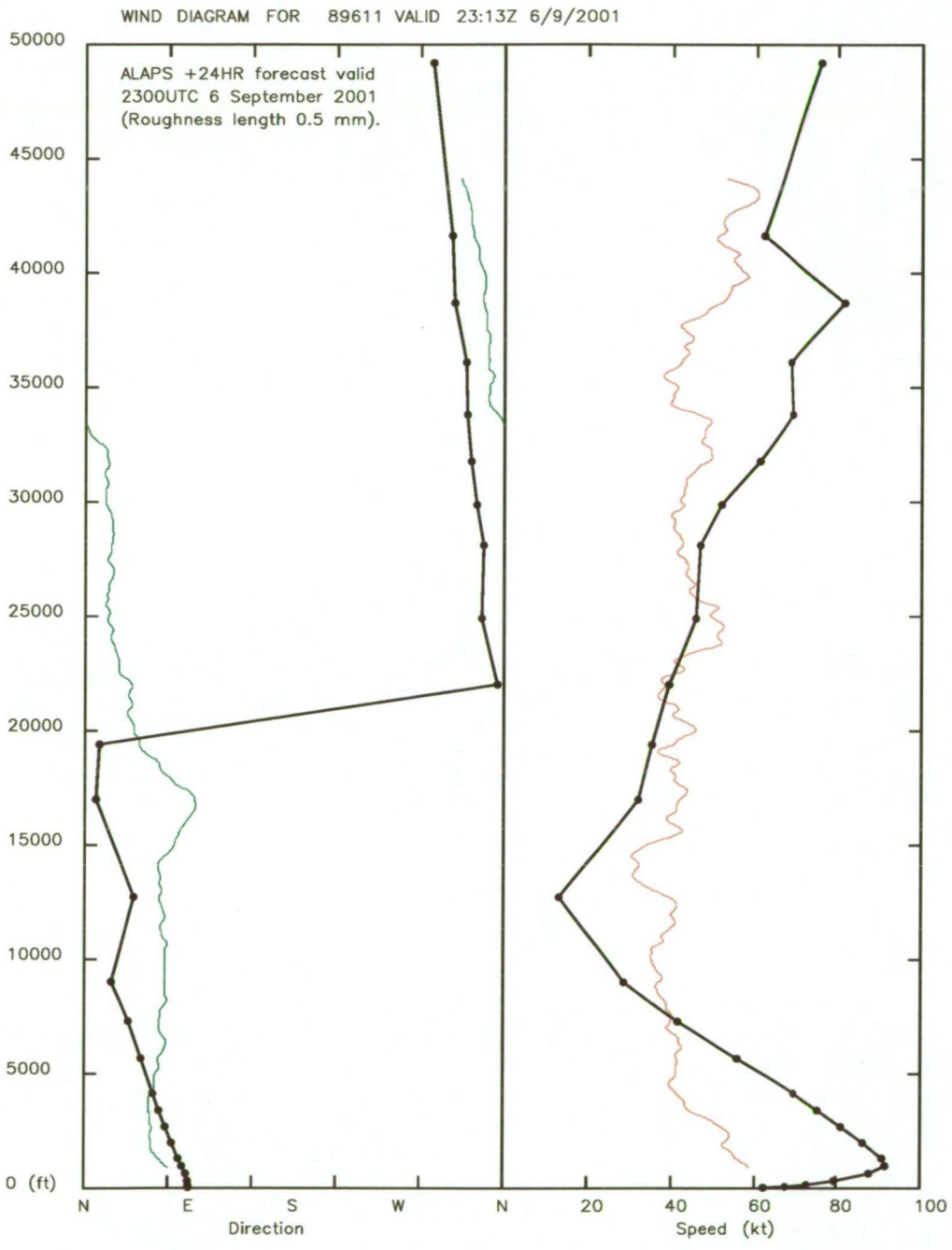

Figure 6.17: Vertical wind profile from the Casey radiosonde flight (coloured traces), valid at 2313UTC 6 September 2001, overlaid with the ALAPS vertical wind profile from the +24 hour forecast valid at 2300UTC 6 September 2001, with reduced surface roughness length.

in this case degraded, significantly, the ALAPS forecast of the Casey storm, generating near surface wind speeds well in excess of those observed, and causing the onset time of the storm to be adversely affected.

The second study involved assessing how sensitive the modelled katabatic flow at Mawson was to changes in the roughness length. The 96 hour period from 2300UTC on 4 January 2002, at Mawson, was dominated by a significant diurnal variation in the near surface wind speed, drawn in black on the second panel of Figure 5.30. The ALAPS model did well at modelling the diurnal variations in near surface wind (coloured plot in Figure 5.30), although under-estimated the peak strength of the katabatic flow. It was argued in Chapter 5 that the ALAPS deficiency in modelling the absolute strength of the katabatic was as a result of the model orography not being as steep as in reality. It was also possible that the surface roughness value of 1 mm may have been too high, so the model was re-run with a roughness length of 0.5 mm to test the sensitivity of the ALAPS flow at this time to surface roughness. Figure 6.18 shows the 96 hour time-series output from the sensitivity run, showing only subtle differences in the near surface model variables. Differences in temperature and pressure were negligible, as were the changes in wind direction. The sensitivity run did perform slightly better in forecasting the katabatic wind speed maximum, with the maximum at 0200UTC on 6 January 2002 increasing from 18 kt in the original run (Figure 5.30), to 22 kt, (Figure 6.18), although still below the observed 27 kt maxima at 0000UTC on 6 January 2002. Subsequent maxima in the 96 hour forecast period were either equal to or only marginally stronger than those peaks in the original run with a roughness length of 1 mm. It would ap-

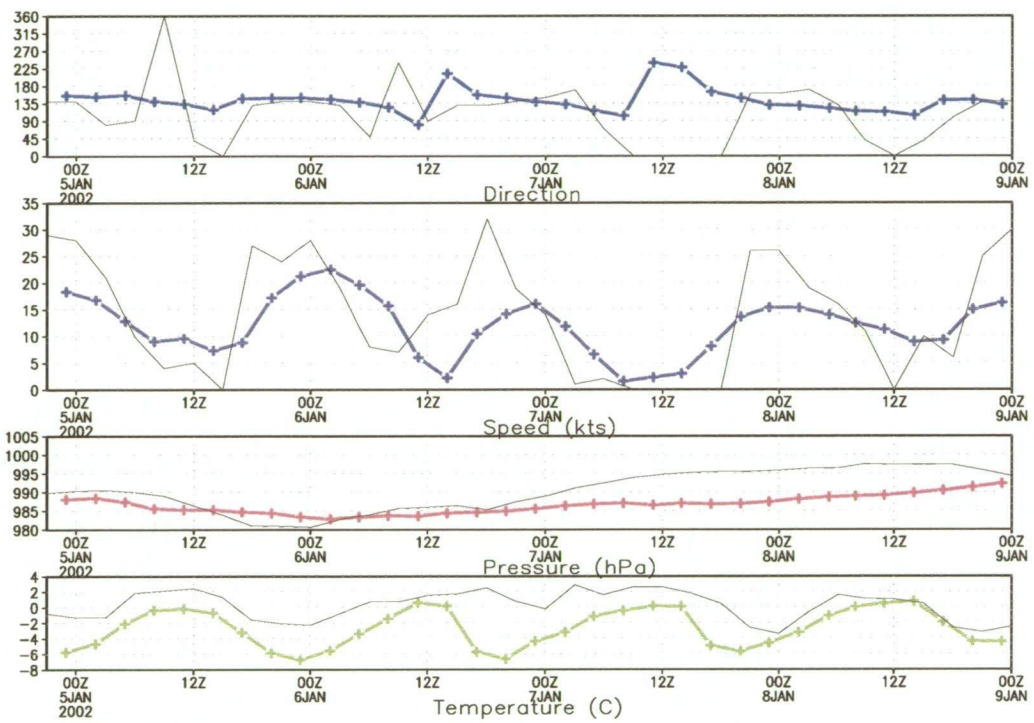

Figure 6.18: Comparison of ALAPS 3 hourly surface data (coloured time-series) with observations from Mawson Station (black time-series) , for the model run initiated at 2300UTC on 4 January 2002, with reduced surface roughness length.

pear that the ALAPS model sensitivity to the roughness length was not a dominating influence in the forecasting of the katabatic flow at this time.

The horizontal diffusion coefficient used within ALAPS is a tune-able parameter and at the start of the ALAPS trials the value was set at 15000 m^2s^{-1}, as was used in the operational model runs over Australia, with the LAPS system. The sensitivity study, again focused on the strong wind event at Casey during September of 2001, and the katabatic flow observed at Mawson during January of 2002. Three model runs were made, with two runs during the Casey storm, both with the horizontal diffusion set at 500 m^2s^{-1}, but with the first run using a roughness length of 1 mm, and the second with a roughness length of 0.5 mm. The third run was during the Mawson katabatic episode where the roughness length was left at 0.5 mm.

The Casey strong wind event proved interesting in that the warm run start with the horizontal diffusion set at 500 m^2s^{-1} and the roughness length set at 1 mm failed during the model integration, with the system reverting to a cold start where current GASP model data were used to initialise the ALAPS run, rather than ALAPS data from the previous forecast. This made a direct comparison with the warm start ALAPS run, with the diffusion set at 15000 m^2s^{-1}, difficult. To assess the impact of the cold start a cold run start was forced with the diffusion set at 15000 m^2s^{-1}. Figure 6.19 shows a comparison of the Casey radiosonde flight, (wind direction in green and speed in red), with the warm start run with diffusion set at 15000 m^2s^{-1} (black traces), a cold start with diffusion set at 15000 m^2s^{-1} (blue traces), and a cold start with the diffusion lowered to 500 m^2s^{-1}. Within the surface layer there are few differences between the 3 model runs, with the cold start forecasting

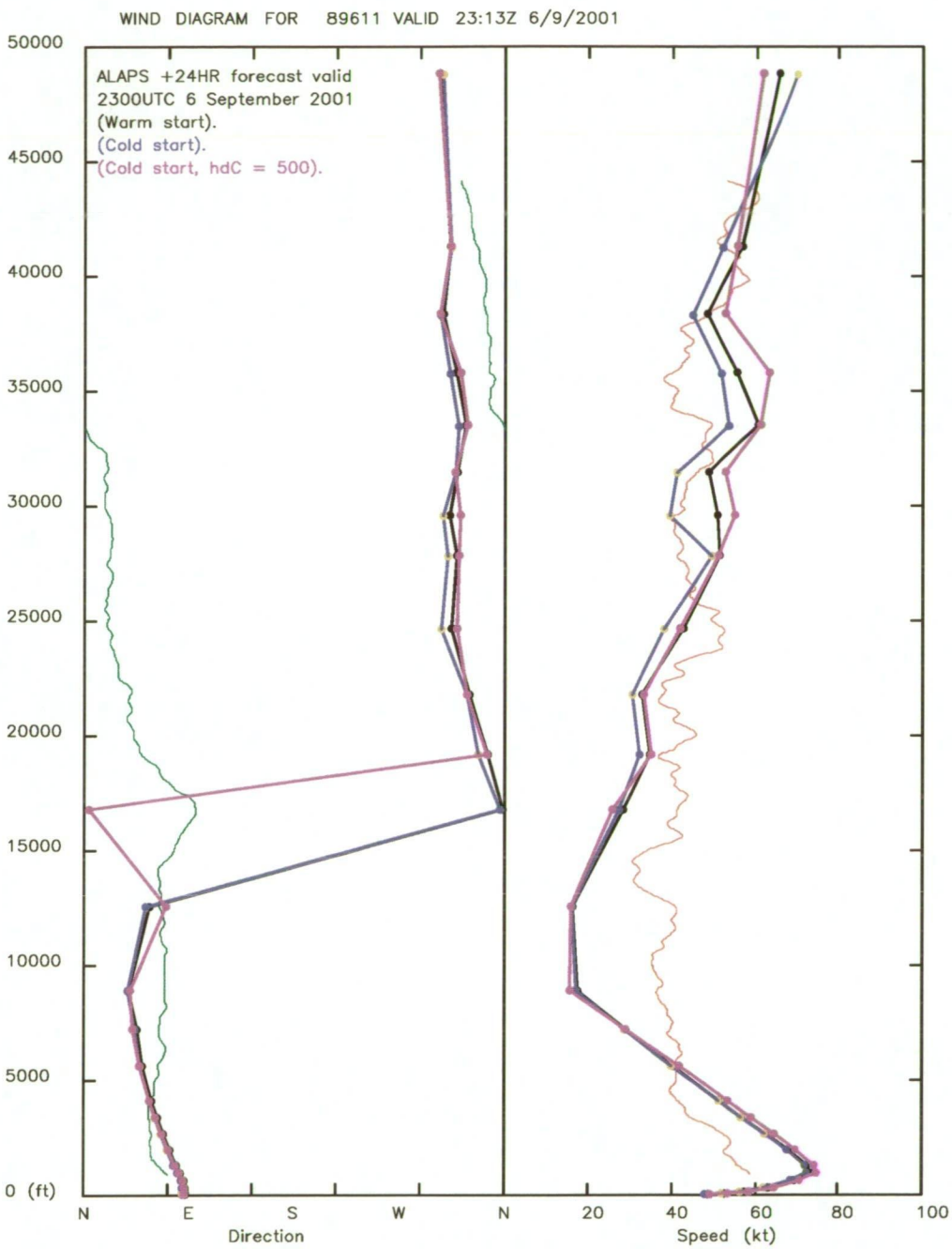

Figure 6.19: Vertical wind profile from the Casey radiosonde flight (green - direction, red - speed), valid at 2313UTC 6 September 2001, overlaid with the ALAPS vertical wind profile from the +24 hour forecast valid at 2300UTC 6 September 2001, black - warm start, blue - cold start, purple - cold start with reduced horizontal diffusion.

marginally lower wind speeds, (by about 1 knot), over the warm start, and the reduced diffusion run forecasting marginally stronger wind speeds, by around 2 knots, over the cold start run with diffusion set at 15000 m^2s^{-1}. The most significant differences between the 3 model runs occurred in the forecast wind speeds between 27000 ft and 37000 ft, with speeds varying by around 5 to 10 knots. With respect to forecasting tropospheric wind, and in particular near surface wind, the model appeared insensitive to the horizontal diffusion. However, in the case where the roughness length was set at 0.5 mm, the reduction in horizontal diffusion showed more of a response in the low level wind speed. Figure 6.20 shows a comparison between the Casey observations, the original warm start run (black traces), the run with roughness length reduced to 0.5 mm (blue traces), and the run where the roughness length is set at 0.5 m and the diffusion has been reduced to 500 (purple traces). In this comparison the reduction in diffusion has had a positive impact on the low roughness length run, with both the excessive low level, and the depth of the strong wind layer being reduced. However, as would be expected, the low diffusion run still showed low level wind speeds in excess of those observed.

The strong katabatic signature in the flow at Mawson during January at 2002 was also adversely affected by reducing the horizontal diffusion. Figure 6.21 shows the 96 hour time series data from the ALAPS model run, with the reduced diffusion, (colour), overlaid with the observations from Mawson. Clearly, the low level wind speeds have increased, with the model forecasting the wind speed peaks far more accurately, but poorly representing the diurnal minima in wind speed.

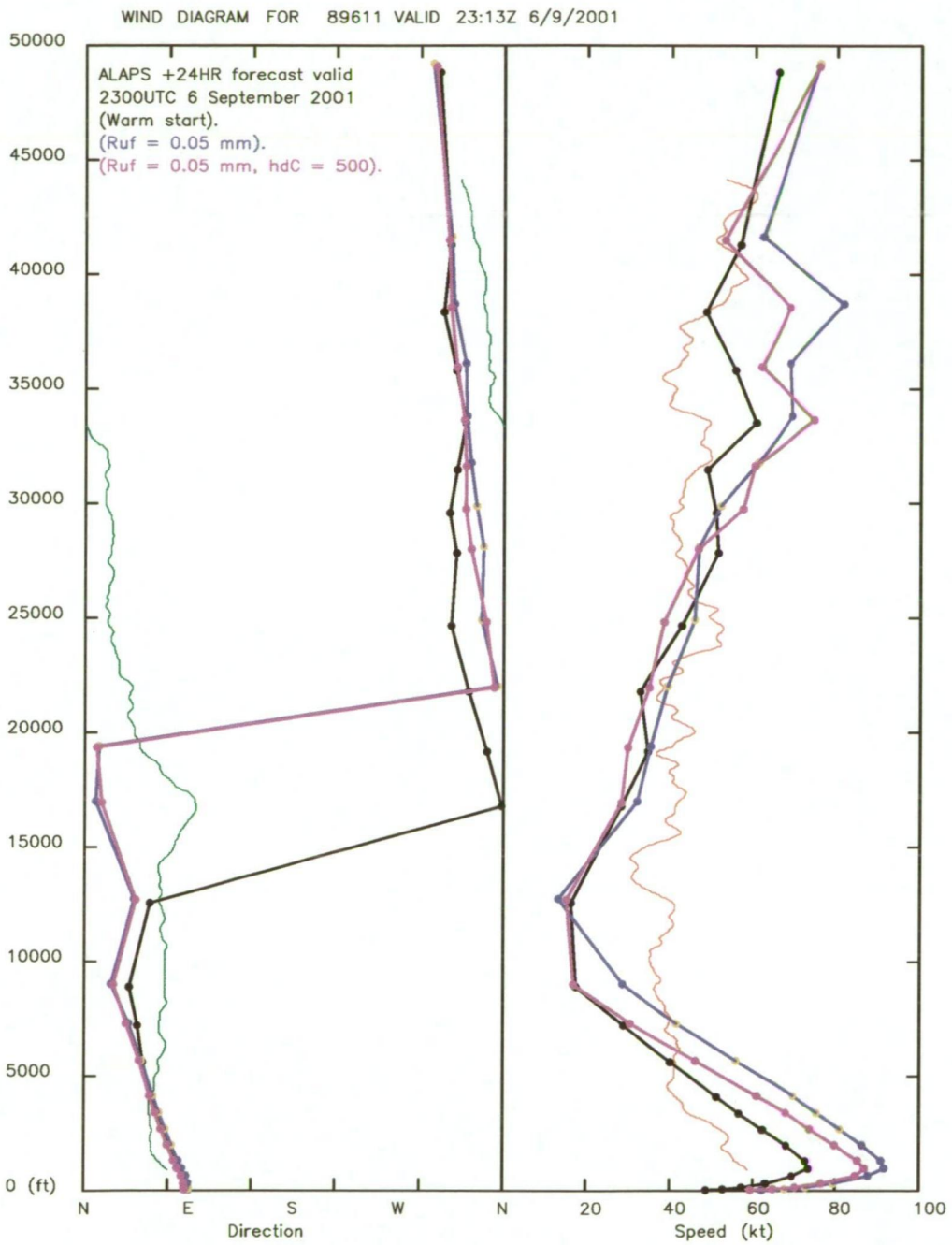

Figure 6.20: Vertical wind profile from the Casey radiosonde flight (green - direction, red - speed), valid at 2313UTC 6 September 2001, overlaid with the ALAPS vertical wind profile from the +24 hour forecast valid at 2300UTC 6 September 2001, black - warm start, blue - low roughness length, purple - low roughness length and reduced horizontal diffusion.

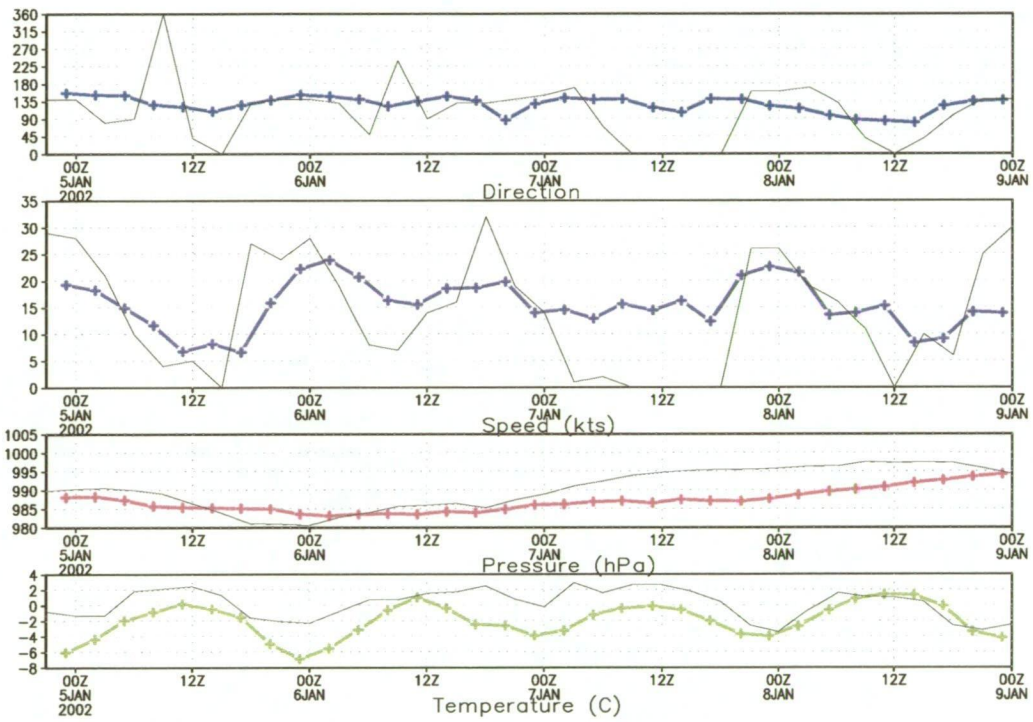

Figure 6.21: Comparison of ALAPS 3 hourly surface data (coloured time-series) with observations from Mawson Station (black time-series) , for the model run initiated at 2300UTC on 4 January 2002, with reduced horizontal diffusion.

Although only a few sensitivity runs were made with varying roughness lengths and horizontal diffusion coefficients, it would appear that the first guess at 1 mm for roughness length, and 15000 for the horizontal diffusion coefficient were reasonable figures. However, a move to spatially varying roughness lengths is one area of research that may prove fruitful.

7 Forecast systems

The primary focus of the NWP research in this thesis has been to advance the science of weather forecasting, and in particular improve the forecasting ability of operational centres at high southern latitudes. Considerable progress has been made in NWP around the globe (Pendlebury et al. 2003) and of concern has been the ability to present the ever increasing wealth of numerical data in such a manner as to not overwhelm the forecaster, yet provide the data in a coherent and logical fashion (Adams 2002). During the progress of this thesis display systems have been developed, along with novel means of post-processing model data, that not only assist in assimilating the NWP output for research purposes, but also provide a useful interface for weather forecasters, providing meteorological support for Antarctic and Southern Ocean operations. This chapter describes the systems that have been developed by the author over the course of the thesis to assist the meteorologist in assimilating the wealth of data now available from high resolution numerical model systems. The systems have been designed for use by both operational meteorologists, tasked with providing weather forecasts to marine, aviation and terrestrial users, and for use in meteorological research, and in particular applied meteorological research aimed at improving weather forecasts in the Antarctic environment. Details on the systems may also be found in Adams (2002).

The availability of high resolution, 4-dimensional, numerical model datasets introduces a challenge for computer systems designers to best present the data in a timely and efficient manner, and in a way that best represents the information required by the meteorologist in issuing weather forecasts. Sev-

eral systems have been developed for displaying the model data, ranging from standard output displays as shown in Figure 7.1, where MSLP is displayed

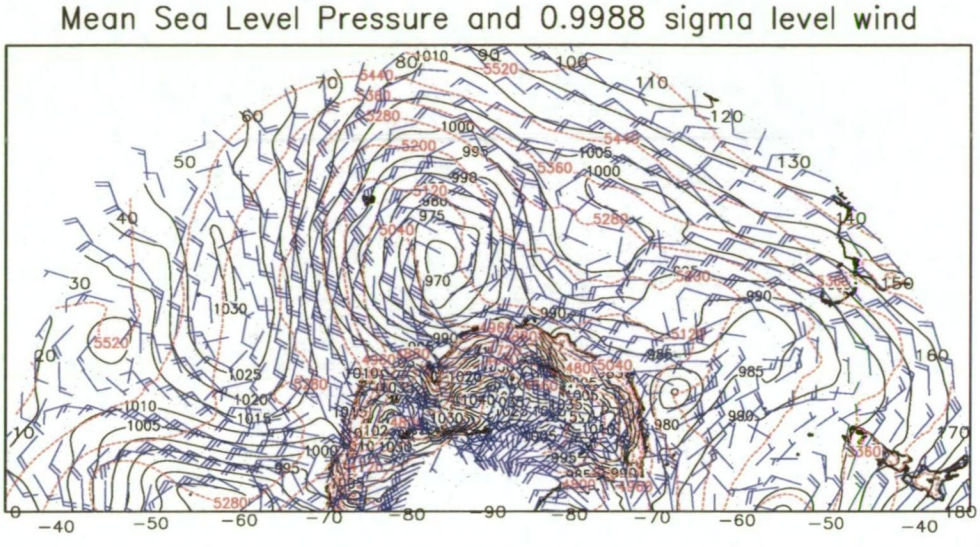

Figure 7.1: Mean Sea Level pressure (hPa), - black contours, with 1000-500 hPa thickness (m) - red contours, and near surface wind barbs (kt) - blue. from ALAPS +24 hour forecast valid 2300UTC 30 October 2001.

(black solid contours), along with the 1000-500 hPa thickness (brown dashed lines), and the first σ-level wind barbs, to single station forecasting aids, such as model aerological diagrams (Figure 7.2), showing temperature, dew-point and wind on a standard skew_T-log_P chart, time-series displays of forecast surface parameters (eg. Figure 5.2), and time-height cross-sections of temperature and wind (not shown), relative humidity (Figure 7.3) and vertical velocity (not shown). These single station displays have proved invaluable in providing the forecaster with model data appropriate to forecasting at both staffed and remote locations around Antarctica and the Southern Ocean. More complex 4-dimensional cross sections, tracking through the model domain, in both space and time, are also readily available, in real-time, for

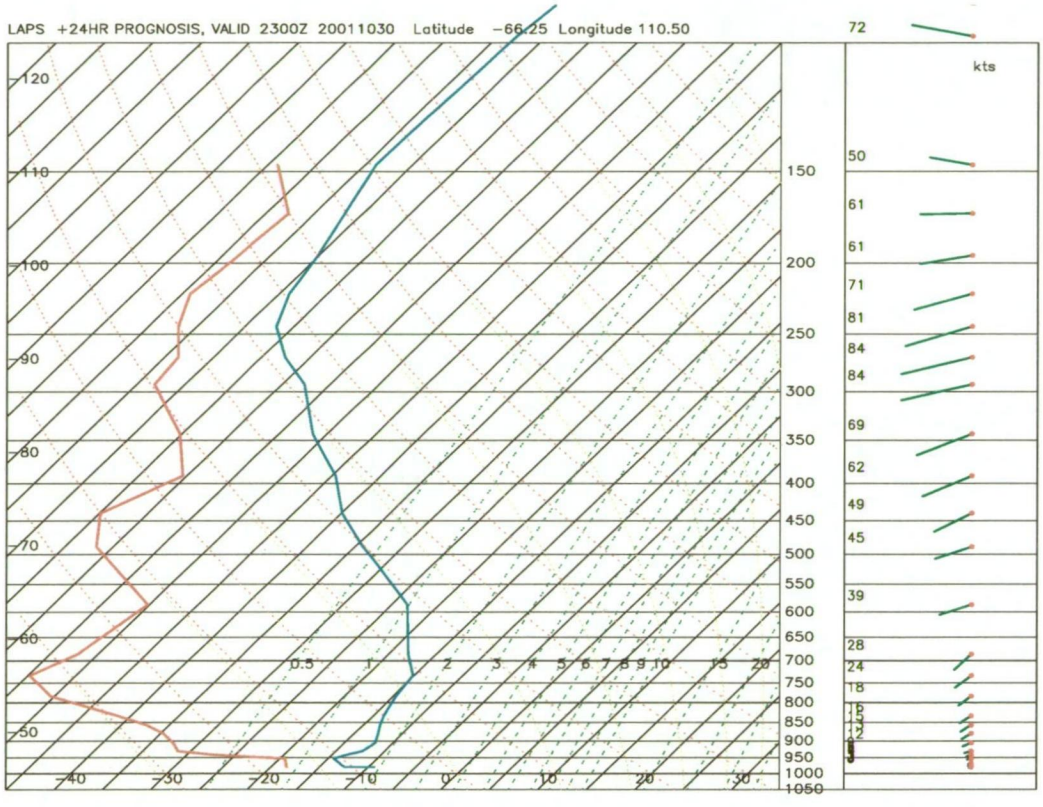

Figure 7.2: Aerological diagram showing profiles of temperature (cyan), dew-point (red), and wind (green), from the ALAPS +24 hour forecast, valid 2300UTC 30 October 2001.

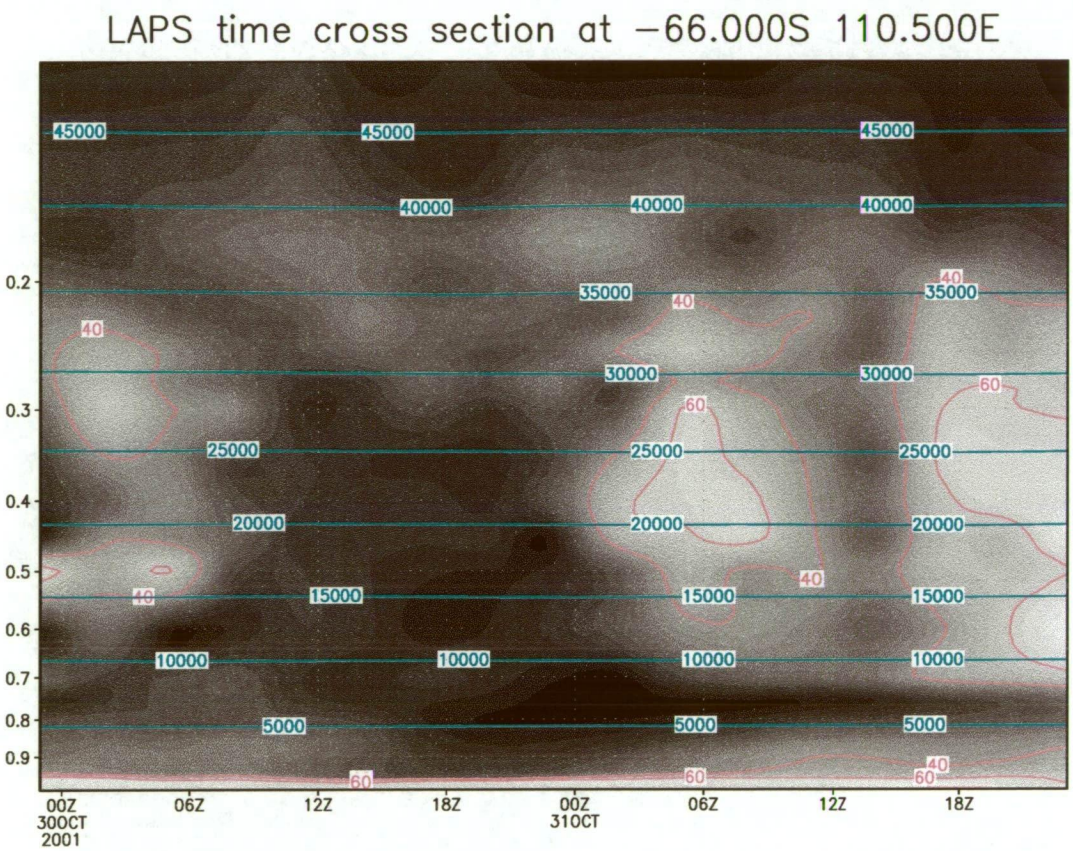

Figure 7.3: 48 hour time-height cross-section of relative humidity (%) from the ALAPS forecast initiated at 2300UTC 30 October 2001.

supporting such operations as the QANTAS Antarctic tourist flights, long range helicopter flights and route forecasting for shipping across the Southern Ocean (Adams 2002). Figure 7.4 shows a typical cross-section display for the

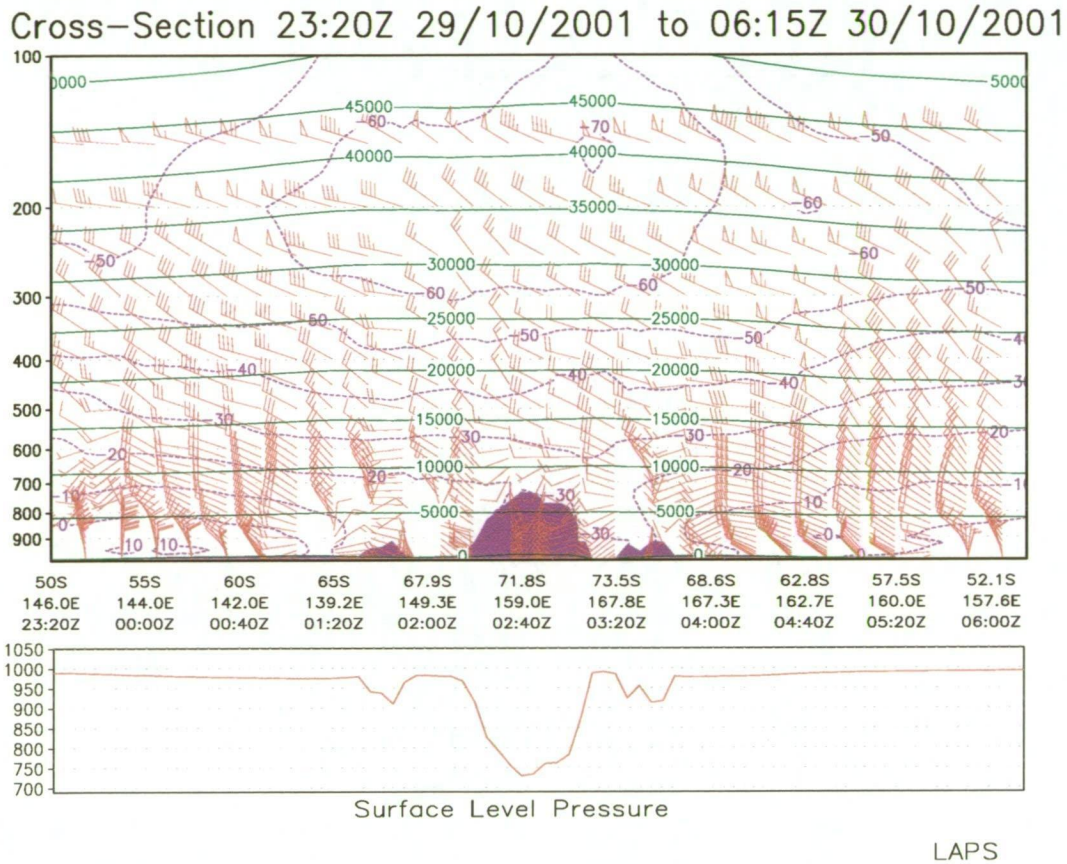

Figure 7.4: Space-time-height cross-section of temperature (purple contours), height (green contours) and wind (red vectors), with orography, shown in shaded purple relief. The lower panel shows the variation in surface level pressure through the cross-section.

QANTAS flight plan detailed in Figure 7.5. These products have provided the backbone of the Antarctic forecasting service provide to QANTAS over the last several years. Other useful post-processed model products include model synthetic cloud, generated through vertical integration of threshold relative humidity values, as described in Chapter 4, and potential wind gust

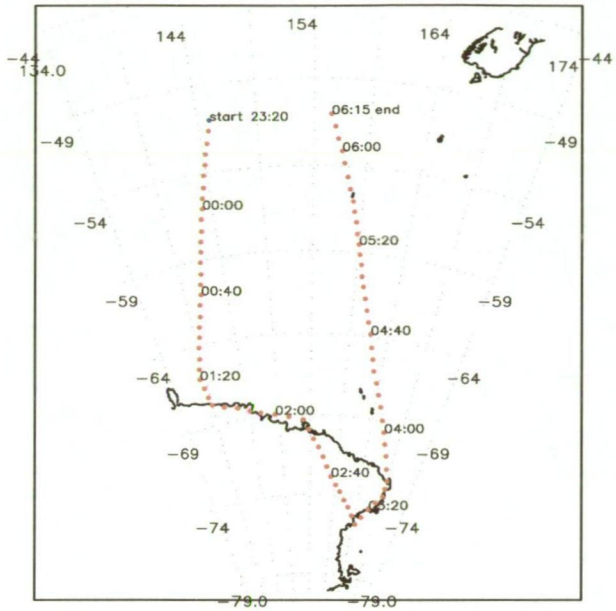

Figure 7.5: Flight plan track used to generate the cross-section shown in the previous diagram.

strength estimations, described below.

Having rapid access to all fields and time-steps within a numerical model, and being able to view these data over different geographical areas, and scales, is an important facility in forecasting, and one that traditionally has not been available to the Antarctic forecaster. With the advent of fast computing, and high resolution graphics systems, programs have been developed to address the issue of displaying numerical model data, in polar stereographic projection, and with fast access to the types of displays mentioned above. The core graphics engine used to develop these displays has been the Grid Analysis and Display System (GrADS) from the University of Maryland (Doty 1995). The scripting language provided with this system has allowed for the rapid development of flexible display systems and a suite of products allowing access to all available numerical model data from GASP, ECMWF,

NCEP and more recently from the newly developed ALAPS. Within the display system the forecaster can easily loop a chosen field through time, have multiple display systems running for inter-comparison of different models, and easily select either a spot aerological diagram (Figure 7.2), or time series profiles (eg Figure 7.3), for a single station forecast from the currently displayed model. The variety of output styles available from the GrADS package has allowed for a comprehensive display system that has provided both Antarctic and Australian forecasters with a powerful and easily implemented tool for assisting in the forecast process. Figure 7.6 shows a screen

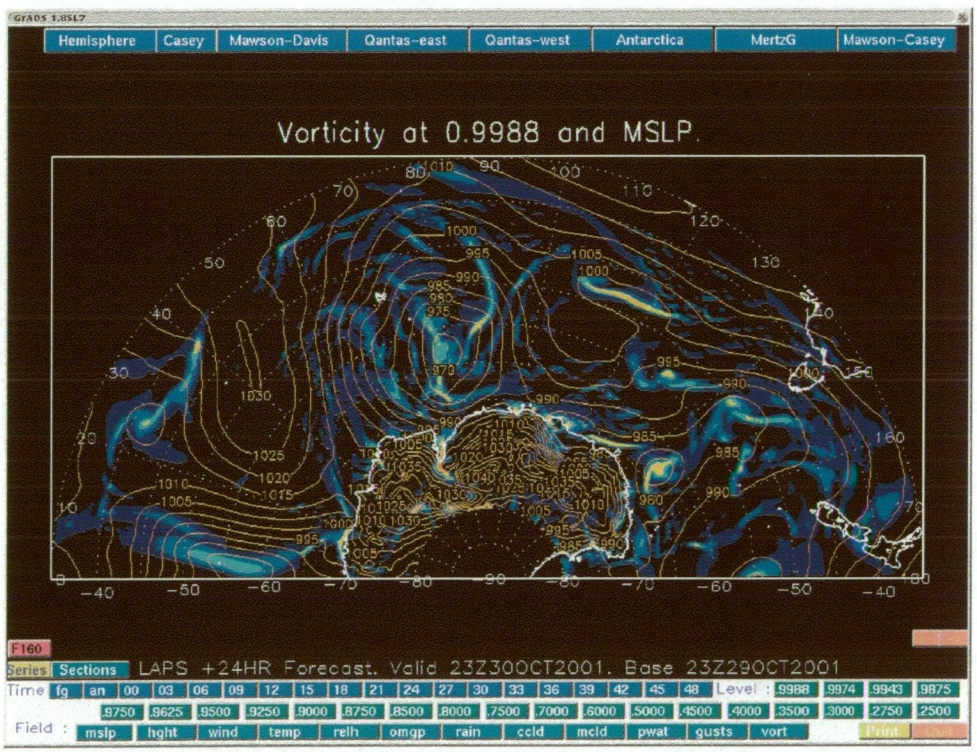

Figure 7.6: Screen snap-shot of the ALAPS model display system, showing the graphical user interface, and an example of the near surface vorticity chart.

shot of the current ALAPS display system, detailing available time-steps, views, and model fields accessible through the system.

7.1 Post-processed numerical model data.

7.1.1 Model cloud fields.

In addition to basic displays of the type shown in the above figures, the system has been extended to provide the forecaster with additional information that may not be readily assimilated from the wealth of basic model fields. Two fields of integrated relative humidity, both displayed in a format analogous to an infrared satellite image, are available through the display system. The first of the "cloud" fields was generated by starting with the model surface temperature field, then, for each grid point, moving up from the first σ-level, and assessing the presence of cloud using the relative humidity threshold values as described in Chapter 4, and if cloud was deemed present then the grid point entry was updated with the model air temperature at that σ-level. By integrating vertically in this manner the temperature at any grid point would equal the air temperature at the highest level where cloud was diagnosed, and by employing a suitable grey-scale the display of the resulting field would be analogous to an infrared satellite image (Figure 7.7). The second cloud image was created in an identical fashion, but rather than assigning an air temperature to the field, a simple level value was assigned to the grid point, such that zero was assigned if no cloud was detected at all, 1 if cloud was detected only at the first σ-level, and 21 if the highest cloud detected was at the 21^{st} σ-level (σ=0.275 was deemed the cut-off level for detecting cloud due to the spurious gravity wave like features seen in the stratosphere, and described in Chapter 4). With the display of this product, the highest cloud number was assigned the brightest value and cloud free areas set to black (Figure 7.8). These two images (Figures 7.7

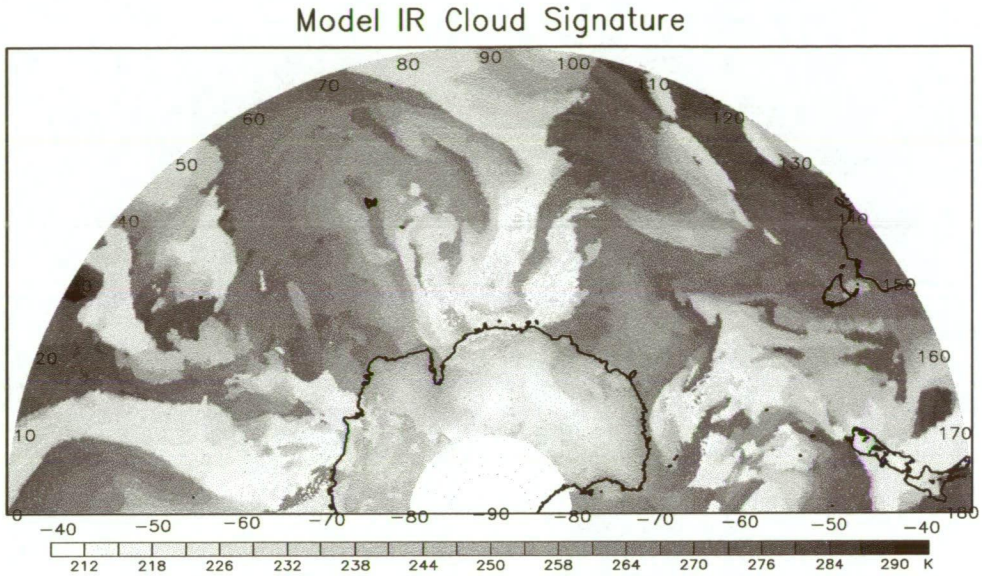

Figure 7.7: Model synthetic cloud (K), from the +24 hour ALAPS run valid at 2300UTC 30 October 2001.

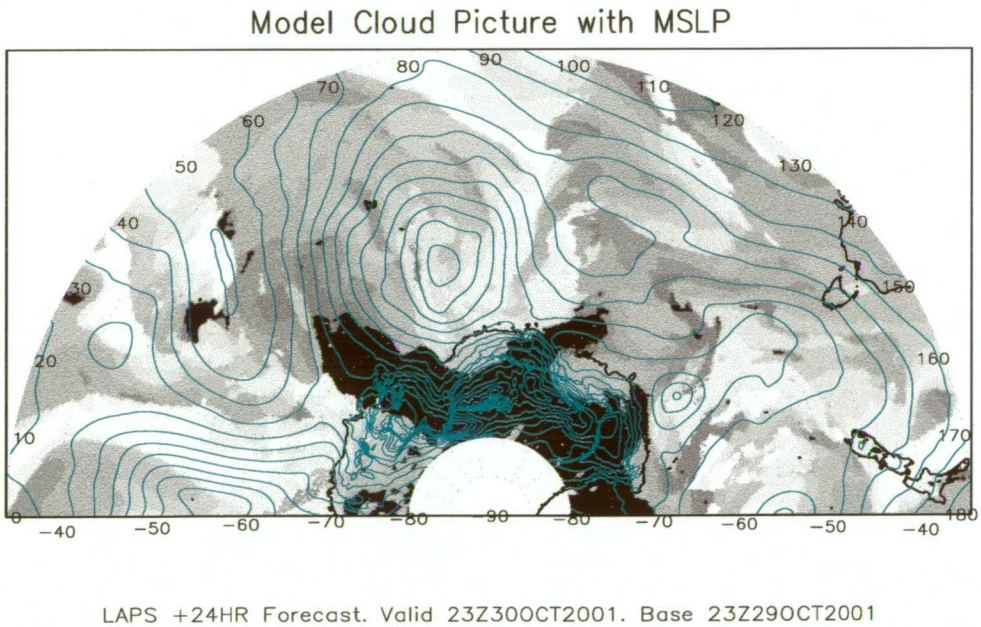

Figure 7.8: Model cloud image and MSLP (cyan), from the +24 hour ALAPS run valid at 2300UTC 30 October 2001.

and 7.8) appear similar, however, the cloud level image has the advantage of better defining cloud free areas, since such areas will always appear black on the display. Over Antarctica, where low cloud is often close in temperature to the surface value, infra-red images offer poor resolution of low cloud areas and this second style of cloud image becomes quite useful.

7.1.2 Potential wind gust strength.

The potential wind gust strength calculation followed the work of Brasseur (2001), where the surface wind gust was assumed to result from the deflection of air parcels aloft, which are brought down to the surface by turbulent eddies. The method Brasseur employed determined the turbulent kinetic energy (TKE), and potential energy of buoyancy (PEB), at each level through the model planetary boundary layer (PBL), and set the potential wind gust strength to the maximum wind speed in the PBL, where the TKE exceeded the PEB. The methodology employed in the ALAPS post-processed field used a calculation of layer mean Froude Number (F, Equation 4), from the surface up through each σ-level of the model atmosphere to ascertain through what depth of the model lower atmosphere there was any potential for mixing of upper level wind to the surface.

$$F = U/Nh \tag{4}$$

where U is the wind speed at the upper boundary of the layer, h the layer depth and N the mean Brunt Vaisala frequency through the layer, where

$$N^2 = \frac{g}{\theta} \cdot \frac{d\theta}{dz}$$

The maximum wind in the defined surface layer was then used as the potential gust strength value. The Froude Number derivation of the potential gust strength was a somewhat simplified calculation in comparison to the TKE method employed by Brasseur (2001), but analogous in concept, as the Froude Number gives a measure of the ratio of kinetic energy to static stability through the layer. When the Froude Number exceeds 1 the kinetic energy is greater than the static stability and the potential exists for mixing of upper level wind to the lower levels. Conversely, if the Froude Number is less than 1 then the static stability will dampen any possible mixing of upper level wind to the lower levels. Within the current derivation of the potential gust strength, once a layer was reached in the model lower atmosphere where the Froude number fell to less than 1, the vertical calculation of F ceased, and the maximum model wind speed in the levels below was considered to be the potential wind gust strength for that grid point. By performing the calculations for all grid points in the model domain a field of potential wind gust strength was generated (Figure 7.9).

7.1.3 Height cross-sections in space and time.

The 4-dimensional cross-sections, mentioned above (Figure 7.4), are available from GASP, NCEP and ALAPS model output, with the products generated in real-time from a user supplied flight-plan of latitude-longitude coordinates, and expected arrival times at each coordinate. The flight plan was then used to convert the 4-dimensional NWP data into a 2-dimensional space-time-height cross-section of wind, temperature and geopotential height, along with a second space-time-height cross section of relative humidity. The system was

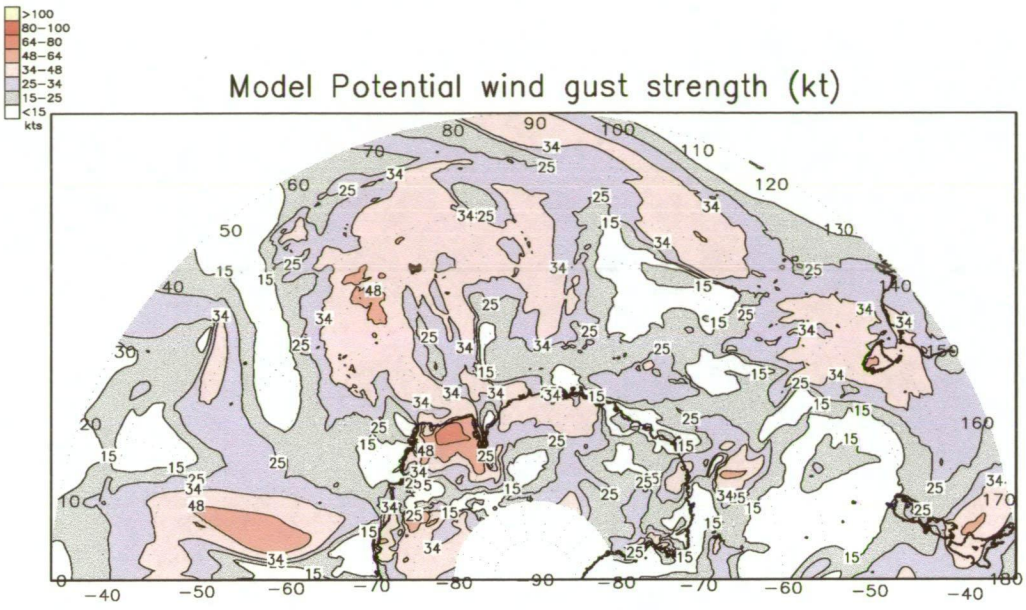

Figure 7.9: Potential gust strength (kt), from the +24 hour ALAPS run valid at 2300UTC 30 October 2001.

designed to be flexible, and depending on how the flight plan was written, several forms of cross-sections may be produced, including pure time cross-sections at a given location, a simple space cross-section at a fixed point in time, or a fully specified time and space varying cross-section. Output from these sections may be displayed with varying height ranges depending on whether a cross section was being provided for high flying aircraft such as the Boeing 747-400 series used on the QANTAS Antarctic tourist flights, or for low flying aircraft such as the helicopters flying between Antarctic stations, which typically remain below 5000ft. The cross-sections may also be displayed with a height range showing only the lowest few pressure or σ-levels from the model to assist in forecasts for surface operations such as shipping.

7.2 Terminal Area Forecasts (TAFS)

As mentioned above, access to high resolution data has now allowed single station forecasting to be attempted directly from the grid-point numerical model output. This opens up the possibility of implementing automated forecasts directly from the model data with little or no intervention from the forecaster. One such system developed for use with ALAPS was the automated Terminal Area Forecast (TAF) system. TAFS are a routine product prepared in support of aviation operations, to provide aircraft pilots with weather information specific to an airstrip. The forecasts are generally valid for a 12 hour period, and encompass an area within a 5 km radius of the airstrip, up to a height of 5000 ft. (Within the aviation community distance is measured in the SI units of metres. However, altitude is still measured in the empirical units of feet where 1 ft = 0.3048 m). TAFS are coded messages providing the pilot with forecasts of wind speed and direction, visibility, significant weather, cloud, temperature and QNH, which is the pressure reduced to mean sea level assuming a standard International Civil Aviation Organisation (ICAO), atmosphere.

Automated TAFS from NWP systems have the potential to significantly improve the forecast service over Antarctica where aircraft are often flying into locations that not only have no observational data but where forecasters have little in the way of local knowledge of prevailing weather conditions. In these situations the NWP systems often provide the only available guidance, and the ability for TAFS to be automatically generated from the model output in a consistent manner may provide the forecaster with a useful product.

Atmospheric fields such as wind speed and direction, temperature and

pressure are directly accessible from the numerical model data and within the ALAPS TAF system wind speed and direction were taken from the 0.9974 (~20m) σ-level, the 2 m screen temperature was approximated by the height weighted mean of the 0.9988 (~10 m) σ-level temperature and surface temperature and the QNH was estimated from the model surface pressure and topographic height using the ICAO approximation of a 1 hPa pressure change per 9.114 m (30 ft) of altitude. Fields such as visibility, weather and cloud are not explicitly carried by the NWP system, and so they were diagnosed from the available numerical model data, using a rules based system. Cloud base height was deduced from threshold relative humidity in the same manner as the cloud field described in the previous section on post-processed numerical model data. However, cloud amount was problematic to deduce, and in the current version of the TAF system was inferred from the cloud layer thickness, with the assumption that thicker cloud is generally more widespread. Cloud layer thickness was calculated by finding cloud top heights through an analogous method to that used in deducing cloud base. This method of cloud amount deduction was neither physical, nor particularly accurate, and was the chief source of TAF error. However, with a model resolution of around 27.5 km it was not possible to deduce cloud cover at a spot location from a comparison of surrounding model grid points. The weather elements that were considered in this system were only those elements relevant to Antarctica, and included fog, precipitation (snow, drizzle and rain showers), blowing or drifting snow, and turbulence. The type of weather was deduced from the model precipitation rate, model air temperature, humidity and wind speed, with the TAF forecast visibility directly linked to the

deduced weather elements.

The creation of a TAF was a three-step process with the user defining a location and TAF starting time. The system first extracted all the basic weather elements from the ALAPS 3-hourly model output data files. These elements included deduced QNH, 2 m screen temperature, low level relative humidity, wind speed and direction, potential gust strength and precipitation rate. Cloud base and cloud top heights were also deduced for the 4 lowest model cloud layers, using the relative humidity threshold method. The second step in the creation of the TAF involved interpolating the data to a one hour interval for the period of the TAF validity, rounding cloud heights to the nearest 100 ft, and deducing visibility, weather and turbulence parameters for each hour of the TAF validity. Visibility and weather components of the TAF were deduced using the same rules, and based on a hierarchical system as described in Table 19. If the final visibility was greater than

Criteria	Weather	Visibility
RH% > 95%, cloud < 100 ft	thick fog	100 m
RH% > 90%, cloud < 200 ft	light fog	500 m
Precip > 2 mm/hr, T < 2^{o}C	heavy intermittent snow	500 m
Precip > 2 mm/hr, T > 2^{o}C	moderate intermittent rain	500 m
Precip > 1 mm/hr, T < 2^{o}C	moderate intermittent snow	1000 m
Precip > 1 mm/hr, T < 2^{o}C	light intermittent rain	1000 m
Precip < 1 mm/hr, T < 2^{o}C	light intermittent snow	5000 m
Precip < 1 mm/hr, T > 2^{o}C	intermittent drizzle	5000 m
Speed > 50 kt, Precip > 0 mm/hr	thick blowing snow	100 m
Speed > 50 kt, Precip = 0 mm/hr	thick drifting snow	500 m
Speed > 35 kt, Precip > 0 mm/hr	thin blowing snow	500 m
Speed > 35 kt, Precip = 0 mm/hr	thin drifting snow	1000 m

Table 19: Weather and visibility criteria.

5000 m and no weather defined yet the cloud base less than 2000 ft then the

visibility was reduced to 5000 m. Turbulence was based on both the absolute wind speed and potential wind gust strength as described in Table 20. The

Criteria	Turbulence
Speed > 30 kt, gust > speed + 20 kt	severe
Speed > 20 kt, gust > speed + 30 kt	severe
Speed > 35 kt, gust > speed + 15 kt	moderate to severe
Speed > 30 kt, gust > speed + 10 kt	moderate
Speed > 15 kt, gust > speed + 10 kt	occasional moderate

Table 20: Turbulence criteria.

final step in the TAF process involved parsing through the hourly data, testing for significant changes, based on TAF amendment criteria found in the Aeronautical Services Handbook, and writing out the coded message. Cloud amount was chosen at this time, based on the cloud layer thickness, with an overcast layer chosen if the cloud layer was greater than 10000 ft, broken cloud if the layer thickness was greater than 5000 ft, scattered cloud for a layer thickness greater than 2000 ft, otherwise a few clouds defined. Surface and horizon definition was also defined on cloud amount, with the surface and horizon definition set to poor in overcast conditions and fair in broken cloud conditions.

Below is an example of a TAF for Casey station valid for the 12 hour period from 1400UTC on 16 August 2000 until 0200UTC 17 August 2000. The model run used for the TAF was initialised at 2300UTC on 15 August 2000.

```
TAF 2000081523Z(16) CASEY 0820 07015G25KT 5000 -SN SCT034 SCT215 OCNL MOD BLW 5000
FM10 08025G35KT 5000 -SN SCT174 OCNL MOD BLW 5000
FM11 08525G40KT 9999 SCT245 OCNL MOD BLW 5000
FM13 08535G50KT 1000 DRSN SCT193 MOD/OCNL SEV TURB BLW 5000
FM15 08540G60KT 500 BLSN OVC130 SEV TURB BLW 5000
FM19 08550G70KT 100 +BLSN OVC056 SEV TURB BLW 5000
T M17 M16 M15 M14 Q 992 991 988 987
```

7.3 Ensemble forecasts.

Although the bulk of this thesis has been based on the implementation of ALAPS to Antarctic forecasting, meteorologists seldom rely exclusively on one numerical model. Australian Antarctic forecasters have had access to ECMWF, GASP and NCEP AVN model data, as well as ALAPS output, and integrating information from all of these models is important in the forecasting process. One such integration method is the ***poor man's*** (Atger 1999) ensemble prediction system (EPS). In this system output of surface variables from all available models are displayed concurrently on a time-series plot for a given point location. At the time of writing model MSLP, near surface air temperature, wind speed and direction and precipitation, were only readily available from GASP, NCEP AVN and the ALAPS system, so to increase the number of ensemble members, output from the previous GASP and ALAPS runs were included in the ensemble, along with the previous 2 NCEP AVN runs, giving a total of 7 ensemble members. The 2 previous NCEP AVN forecasts were included because NCEP model data were available from the 0600UTC and 1800UTC runs, as well as from the standard 0000UTC and 1200UTC times, while the other 2 models only ran at 0000UTC and 1200UTC. The surface pressure and near surface temperature data were bias corrected, using the last 30 forecasts from GASP, ALAPS and NCEP to generate the bias statistics, giving 15 days of bias data for GASP and ALAPS and just over 7 days of bias data for NCEP. Bias data were calculated for each model time (0000UTC, 0600UTC, 1200UTC and 1800UTC for GASP and NCEP and 3 hour steps from 0000UTC for ALAPS), in order to account for diurnal variations that may not have been adequately captured

by the model. Figure 7.10 is an example of a 48 hour ensemble forecast for

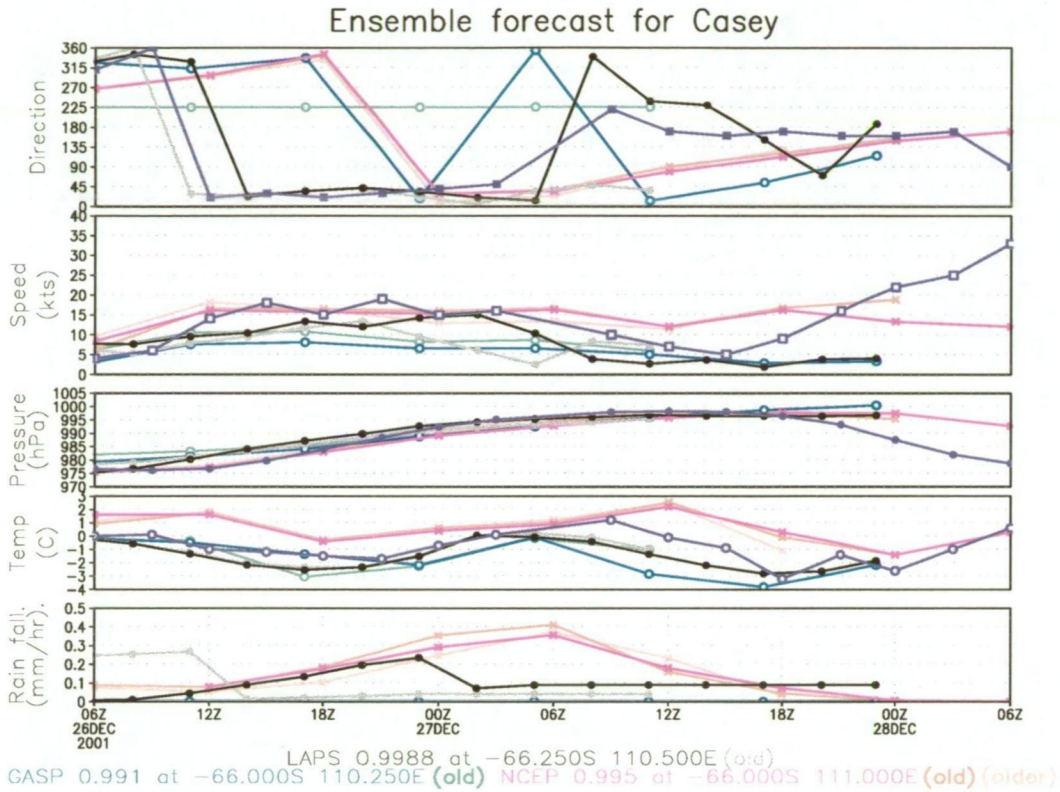

Figure 7.10: 48 hour ensemble forecast for Casey, comprising output from ALAPS, GASP and NCEP, valid from 0600UTC 26 December 2001.

Casey starting at 0600UTC 26 December 2001, with observations (in black) from Casey super-imposed on the ensemble. The bias corrected surface pressure and temperature, (panels 3 and 4, Figure 7.10), ensembles provided very good guidance, with the observations in both panels being close to an average of the ensembles, in the first 24 hours of the forecast. Wind speed and direction do not lend themselves easily to bias corrections, unless a sophisticated bias formulation were to be employed, based on wind speed and direction ranges, requiring a large data-set to provide useful statistics. In the Figure 7.10 example wind direction is reasonable well forecast by the ALAPS ensemble members, where as the observed wind speed was at the upper range

of the ensemble members during the first 24 hours of integration and then significantly under-forecast in the last 6 hours of the integration. The inclusion of ensemble members from a larger set of models, including output from high resolution systems such as AMPS (Figure 7.11) may well improve the

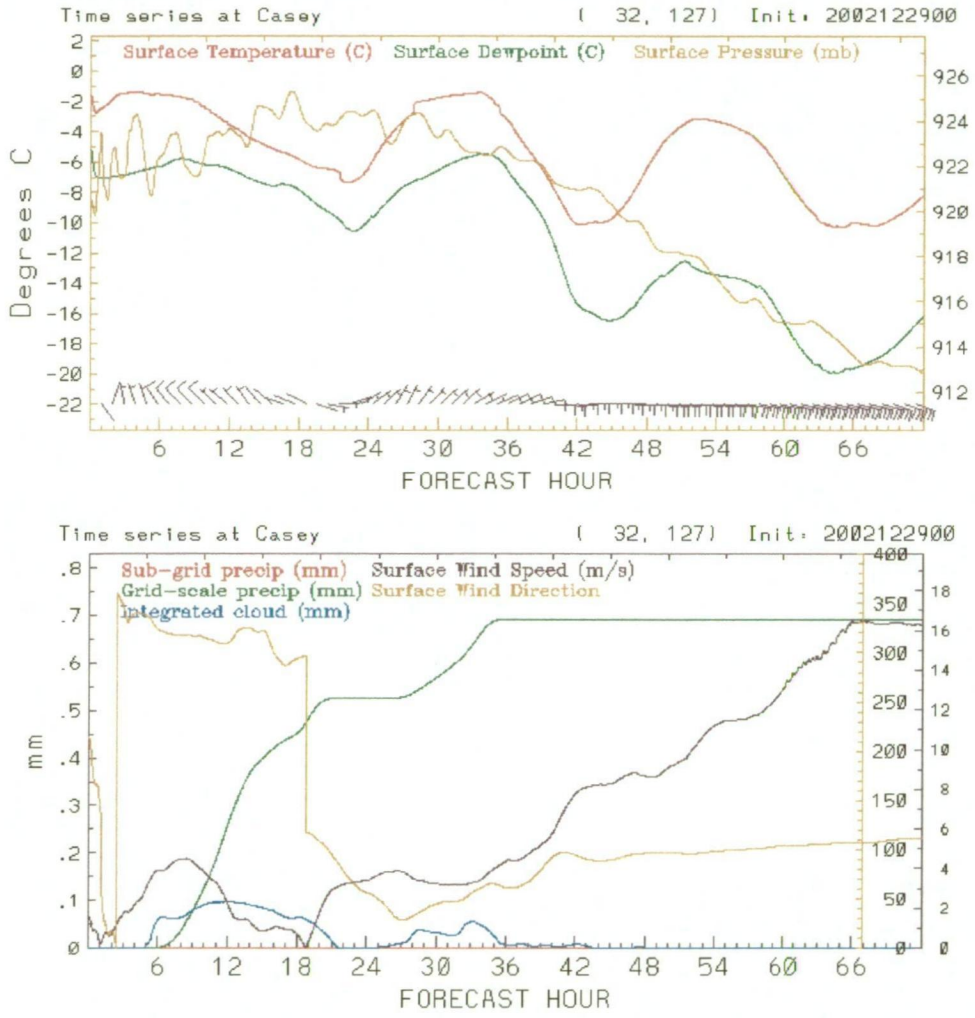

Figure 7.11: Example 72 hour time-series forecast for Casey, from the AMPS web page, courtesy Jordan Powers, MMM, NCAR, Boulder Colorado.

ensemble spread, making the ensemble mean a useful forecasting aid, and a potentially useful field of research. The study on ensemble prediction sys-

tems by Atger (1999) concluded that the 4 member ***poor man's*** ensemble technique, which included the ECMWF control forecast, Deutscher Wetterdienst global model, UK Met. Office global model and the NCEP control forecast, performed better on the probability, or half Brier, score than either the ECMWF single vector EPS (Molteni et al. 1996 and Buizza et al. 1998), with 51 members, or the NCEP breeding method EPS (Toth et al. 1997), with 11 members.

7.4 System Integration.

All the above display and forecast systems, along with programs for monitoring model validity times, and displaying surface and upper air observational data have been integrated into a simple graphical user interface (GUI), so as to that provide the forecaster with easy access to all the required display and forecast systems. These systems sit along side the Bureau forecast preparation system, satellite data display system and alerting system to provide the forecaster with a full suite of products with which to provide meteorological services.

8 Conclusions

The study presented in this thesis was driven both by a user requirement for the provision of detailed, accurate and timely weather forecasts for the support of operations at high latitudes, and a need to better understand the dynamics of the polar atmosphere, and more specifically the meteorological systems affecting Australian stations in East Antarctica. The general meteorology of the high southern latitudes was discussed, along with an assessment of the global model output available for high southern forecasting. The study then focused on the adaptation of the Australian LAPS model to the Antarctic domain (ALAPS), with a verification of the model performance over the July 2001 - June 2002 period, focusing on model performance at key Australian sites and the French-Italian station on Dome C. Along with the assessment of the model veracity as a weather forecasting tool an analysis of the model performance in cloud and precipitation was presented, with the latter study having an important role in both weather forecasting and in assessing the mass balance of the Antarctic ice sheet. Four case studies were presented, to highlight the ability of the ALAPS system to provide insights into the dynamics associated with high latitude weather systems. The sensitivity studies focused on the surface characteristics within the model, and their importance in modulating the model output, and highlighted areas where further model development is required. Finally, a description was given of forecasting systems now in place as a result of the work undertaken during this thesis, and being used both in Australian Antarctic forecasting offices and also in forecasting offices within Australia.

Several key issues within the model development arose from the study,

with the most significant being in the area of data assimilation. The scheme, as described in chapter 3, generated an initial conditions file for the model integration that was not in model balance, and hence produced a ***"shock"*** to the model, that took some 3 to 6 hours to dissipate in the model run. The problems with assimilation were not limited to the scheme employed within ALAPS, as AMPS output also displayed characteristics associated with initialisation ***"shock"***. The time-series plot of surface pressure in the top panel of Figure 7.11 showed a large oscillation of nearly 2 hPa that took some 6 to 10 hours to dampen out. Developing more sophisticated assimilation schemes that maintain model balance is an area requiring further work. As is the area of physical parameterisation schemes and, in particular, a more physical surface scheme that better handles heat and moisture fluxes in the sea-ice zone. In this regard the scheme employed by AMPS (Bromwich et al. 2001), where heat and moisture fluxes are partitioned within a grid box based on the sea-ice concentration would be a useful addition to the ALAPS scheme. Further investigative work on the handling of sub-snow and deep-snow temperatures within the physics scheme is also warranted, following the problems encountered in the Dome C case and sensitivity studies. A scheme for better defining surface roughness lengths over the continent, where surface types can vary widely, from the steep coast escarpments, to the flatter inland slopes, is also another field in need of investigation.

The introduction of meso-scale models to the Antarctic, such as ALAPS and AMPS, have demonstrated the usefulness of such models in supporting weather forecasting services. However, on their own, there are still issues of adequately analysing and assimilating data, and forecast errors in the

timing, or indeed capturing, of major weather events. In this regard, the field of ensemble forecasting, and the maintenance of several Antarctic models, has the potential to improve significantly the usefulness of NWP output in support of weather forecasting services.

9 References

Adams N. 1996. The detection and analysis of a gravity wave observed over Casey in East Antarctica using radiosonde data. *Aust. Met. Mag.*, 45, 219-232.

Adams N. 1997. Model prediction performance over the Southern Ocean and coastal region around East Antarctica. *Aust. Met. Mag.*, **46**, 287-296.

Adams N. 2002. Advances in forecasting systems at the Antarctic Meteorological Centre, Casey. *Meteorol. Appl.*, **9**, 335-343.

Adams N. 2004a. Precipitation Forecasting at High latitudes. *Weather and Forecasting*, **9**, 456-472.

Adams N. 2004b. A numerical modeling study of the weather in East Antarctica and the surrounding Southern Ocean. *Weather and Forecasting*, **In press**.

Allison I., Wendler G. and Radok U. 1993. Climatology of the East Antarctic Ice Sheet (100^{o}E to 140^{o}E) derived from automatic weather stations. *J. Geophys. Res. - Atmos.* **98**, 8815-8823.

Allison I. 2000. Seasonal and short-term variability of East Antarctic snow accumulation. *SCAR Working Groups on Glaciology and Physics and Chemistry of the Atmosphere, Symposium on Antarctic Precipitation and Mass Balance, Tokyo, 13 July.*

Andreas E. L. and Makshtas A. P. 1985. Energy exchange over Antarctic sea-ice in the spring. *J. Geophys. Rev.*, **90**, 7199-7212.

Atger F. 1999. The Skill of Ensemble Prediction Systems. *Mon. Wea. Rev.*, **127**, 1941-1953.

Ball F. K. 1960. Winds on the ice slopes of Antarctica. In: *Antarctic Meteorology*, Pergamon Press, London, 9-16.

Bintanja R. and van den Broeke M. R. 1995. Momentum and scalar transfer coefficients over aerodynamically smooth Antarctic surfaces. *Bound.-Layer meteorol.* **74**, 89-111.

Bourke W., Hart T., Steinle P., Seaman R., Embery G., Naughton M. and Rikus L. 1995. Evolution of the Bureau of Meteorology's Global Assimilation and Prediction System. Part 2: resolution enhancements and case studies. Aust. Met. Mag., 44, 19-40.

Bourke W., Embery G., Harris B., Le T., Naughton M., Paevere J., Rikus L., Seaman R., Steinle P., Sun Z. and Xiao Y. 1999. Global Assimilation and Prediction in the Bureau of Meteorology. Eleventh Annual BMRC Modelling Workshop, 9-11 November 1999, *BMRC Research Report no.75*, Bureau of Meteorology Research Centre pp1-7.

Brasseur O. 2001. Development and Application of a Physical Approach to Estimating Wind Gusts. *Mon. Wea. Rev.*, **129**, 5-25.

Bromwich D. H. 1988. Snowfall in high southern latitudes. *Rev. Geophys.*, **26**, 149-168.

Bromwich D. H. 1989. Satellite Analyses of Antarctic Katabatic Wind Behaviour. *Bull. Amer. Meteor. Soc.*, **70**, 738-749.

Bromwich D. H. and Liu Z. 1996. An Observational Study of the Katabatic Wind Confluence Zone near Siple Coast, West Antarctica. *Mon. Wea. Rev.*, **124**, 462-477.

Bromwich D. H., Cassano J. J., Klien T., Heinemann G., Hines K. M., Steffen K. and Box J. E. 2001. Mesoscale modelling of katabatic winds over Greenland with the Polar MM5. *Mon. Wea. Rev.* **129**, 2290-2309.

Bromwich D. H., Monaghan A. J., Powers J. G., Cassano J. J., Wei H. L., Kuo Y. H. and Pellegrini A. 2003. Antarctic Mesoscale Prediction System (AMPS): A case study from the 2000-01 field season. *Mon. Wea. Rev.*, **131**, 412-434.

Budd W. F., Dingle W. R. J. and Radok I. 1964. The Byrd snow drift project: outline and basic results. *University of Melbourne, Department of Meteorology.* Publication no. 6. Parkville Victoria, Australia.

Budd W. F., Reid P. A. and Minty L. J. 1995. Antarctic moisture flux and net accumulation from global atmospheric analyses. *Annals of Glaciology*, **21**, 149-156.

Budd W. F., Wu X. and Reid P. A. 1997. Physical characteristics of the Antarctic sea-ice zone derived from modelling and observations. *Anals of Glaciology*, **25**, 1-7.

Buizza R. 1997. Potential forecast skill of ensemble prediction, and spread and skill distributions of the ECMWF Ensemble Prediction System. *Mon. Wea. Rev.*, **125**, 99-19.

Cassano J. J., Box J. E., Bromwich D. H., Li L. and Steffen K. 2001. Verification of Polar MM5 simulations of Greenland's atmospheric circulation. *J. Geophys. Res.*, **106**, 33 867-33 890.

Cullather R. I., Bromwich D. H. and Van Woert M. L. 1998. Spatial and Temporal Variability of Antarctic Precipitation from Atmospheric methods. *Journ. Climate,* **11**, 334-367.

Dalrymple P. C., Lettau H. and Wollaston S. 1966. South Pole Micrometeorology Program. In: *Studies in Antarctic Meteorology;Antarctic Research Series,* **Vol. 9**, M. J. Rubin, editor, American Geophysical Union, Washington, pp. 13-57.

Dare R. A. and Budd W. F. 2001. Analysis of Surface Winds at Mawson, Antarctica. *Weather and Forecasting*, **16**, 416-431.

Doty B. 1995. The Grid Analysis and Display System, GrADS. *Center for Ocean-Land-Atmosphere Studies*, 4041 Powder Mill Road, Suite 302, Calverton, Maryland, USA 20705-3106.

Dudhia J. 1993. A nonhyrostatic version of the Penn State-NCAR mesoscale model: Validation tests and simulation of an Atlantic cyclone and cold front. *Mon. Wea. Rev.* **121**, 1493-1513.

Ėgger J. 1985. Slope winds and the axisymmetric circulation over Antarctica. *J. Atmos. Sci.*, **42**, 1859-1867.

Egger J. 1992. Topographic wave modification and the angular momentum balance of the Antarctic troposphere. *J. Atmos. Sci.*, **49**, 327-334.

Gallee H. and Pettre P. 1998. Dynamical Constraints on Katabatic Cessation in Adelie Land, Antarctica. *J. Atmos. Sci.*, **55**, 1755-1770.

Garrat J. R. 1992. The Atmospheric Boundary Layer. Cambridge Atmospheric and Space Science Series. *Cambridge University Press*, 10 Stamford Road, Oakleigh, Melbourne 3166, Australia.

Giovinetto M. B. and Bentley C. R. 1985. Surface balance in ice drainage systems of Antarctica. *Antarct. J. U.S.*, **20**, 6-13.

Grell G. L., Dudhia J. and Stauffer D. R. 1994. A description of the fifth-generation Penn State/NCAR Mesoscale Model (MM5). *NCAR Tech. Note* NCAR/TN-398+STR, 117 pp.

Guo Z., Bromwich D. H. and Cassano J. J. 2003. Evaluation of Polar MM5 Simulations of Antarctic Atmospheric Circulation. *Mon. Wea. Rev.*, **131**, 384-411.

Hart T. L., Bourke W., McAvaney B. J., Forgan B. W. 1990. Atmospheric General Circulation Simulations with the BMRC Global Spectral Model: The Impact of Revised Physical Parameterisations. *Journ. Climate,* **3**, 436-59.

Hummel, J. R., and Reck, R. A. 1979. A global Surface Albedo Model. *Journal of Applied Meteorology*, 18, 239-253.

Jones D. A. and Simmonds I. 1993. A climatology of Southern Hemisphere extratropical cyclones. *Climate Dynamics*, **9**, 131-145.

King J. C. and Turner J. 1997. Antarctic Meteorology and Climatology. *Cambridge Atmosphere and Space Science Series.* Cambridge University Press. Press Syndicate of the University of Cambridge, The Pitt Building, Trumington Street, Cambridge, CB2 IRP, UK.

Krishnamurti T. N. and Bounoua L. 1996. An Introduction to Numerical Weather Prediction Techniques. *CRC Press Inc.* 2000 Corporate Blvd., N. W., Boca Raton, Florida 33431.

Kurtz D. D. and Bromwich D. H. 1985. A recurring, atmospherically forced polynya in Terra Nova Bay. *Oceanology of the Antarctic Continental Shelf, Antarctic Research Series*, **43**, 177-201.

Lynch P. and Huang X. Y. 1992. Initialization of the HIRLAM model using a digital filter. *Mon. Wea. Rev.*, **120**, 1019-1034.

Molteni F., Buizza R., Palmer T. N. and Petroliagis T. 1996. The ECMWF ensemble prediction system: Methodology and validation. *Quart. J. Roy. Meteor. Soc.*, **122**, 73-119.

Murphy B. F. and Simmonds I. 1993. An analysis of strong wind events simulated in a GCM near Casey in the Antarctic. *Mon. Wea. Rev.*, **121**, 522-534.

Murphy B. F. 2003. Prediction of Severe Synoptic Events in Coastal East Antarctica. *Mon. Wea. Rev.*, **131**, 354-370.

Parish T. R. 1982. Surface Airflow Over East Antarctica. *Mon. Wea, Rev.*, **110**, 84-90.

Parish T. R. 1984. A Numerical Study of Strong Katabatic Winds over Antarctica. *Mon. Wea. Rev.*, **112**, 545-554.

Parish T R. and Bromwich D. H. 1987. The surface wind field over the Antarctic ice sheets. *Nature*, **328**, 51-54.

Parish T. R. 1992. On the Role of Antarctic Katabatic Winds in Forcing large-Scale Tropospheric Motions. *J. Atmos. Sci.*, **49**, 1374-1385.

Parish T. R. 1994. On the Role of the Antarctic Continent in Forcing large-Scale Circulations in the High Southern Latitudes. *J. Atmos. Sci.*, **51**, 3566-3579.

Parish T. R. and Bromwich D. H. 1998. A Case Study of Antarctic Katabatic Wind Interaction with Large-Scale Forcing. *Mon. Wea. Rev.*, **126**, 199-209.

Pendlebury S. F., Adams N. D., Hart T. L. and Turner J. 2003. Numerical Weather Prediction Model Performance over High Southern Latitudes. *Mon. Wea. Rev.*, **131**, 335-353.

Phillpot H. R. and Zillman J. W. 1970. The surface temperature inversion over the Antarctic continent. *J. Geophys. Res.*, **75**, 4161-4169.

Phillpot H. R. 1991. The derivation of 500hPa height from automatic weather station surface observations in the Antarctic continental interior. *Aust. Met. Mag.*, **39**, 79-86.

Pook M. 1995. Atmospheric blocking in the Australasian region in the southern hemisphere winter. PhD thesis. *Institute of Antarctic and Southern Ocean Sciences, University of Tasmania*, Sandy Bay, Hobart, Tasmania, Australia.

Powers J G, Monaghan A. J., Cayette A. M., Bromwich D. H., Kuo Y. H. and Manning K. W. 2003. Real-time mesoscale modeling over Antarctica: The Antarctic Mesoscale Prediciton System. *Bull. Amer. Meteor. Soc.*, **84**, 1533-1545.

Puri K., Dietachmayer G. S., Mills G. A., Davidson N. E., Bowen R. A. and Logan L. W. 1998. The new BMRC Limited Area Prediction System, LAPS. *Aust. Met. Mag.*, **47**, 203-223.

Radok U. and Brown T. J. 1996. Antarctic 500hPa heights and surface temperatures. *Aust. Met. Mag.*, **45**, 55-58.

Reeder M. J. and Smith R. K. 1998. Mesoscale Meteorology. Meteorology of the Southern Hemisphere, edited by Karoly D.J. and Vincent D. G. *American Meteorological Society*, 45 Beacon St., Boston, MA 02108.

Rintoul S. 2001. Antarctic Science Project No. 1335. *Australian Antarctic Division.* Channel Highway Kingston, Tasmania, Australia, 7050.

Schwerdtfeger W. 1984. Weather and Climate of the Antarctic. Developments in Atmospheric Science, 15. *Elsevier Science Publishing*

B. V. Molenwerf 1, P.O. Box 211, 1000 AE Amsterdam, The Netherlands.

Seaman R., Bourke W., Steinle P., Hart T., Embery G., Naughton M. and Rikus L. 1995. Evolution of the Bureau of Meteorology's Global Assimilation and Prediction System. Part 1: analysis and initialisation. Aust. Met. Mag., **44**, 1-18.

Shepherd D. 1999. Aviation Climatology of Australia's Antarctic Stations. I*nternal memo,* Tasmania and Antarctic Regional Office, Australian Bureau of Meteorology.

Skinner W. 1995. Numerical prediction model performance summary April to June 1995. *Aust. Met. Mag.*, **44**, 309-312.

Skinner W. and Hart T. 1995. Numerical prediction model performance summary October to December 1995. *Aust. Met. Mag.*, **45**, 131-135.

Skinner W. and Hart T. 1996. Numerical prediction model performance summary April to June 1996. *Aust. Met. Mag.*, **45**, 261-265.

Skinner W. and Hart T. 2000. Numerical prediction model performance summary April to June 2000. *Aust. Met. Mag.*, **49**, 343-350.

Skinner W. and Hart T. 2001. Numerical prediction model performance summary July to September 2000. *Aust. Met. Mag.*, **50**, 77-86.

Schwerdtfeger W. 1984. Weather and Climate of the Antarctic. Developments in Atmospheric Science, 15. *Elsevier Science Publishers*

B. V. Molenwerf 1, P.O. Box 211, 1000 AE Amsterdam, The Netherlands.

Stearns C. R., Keller L. M., Weidner G. A. and Sievers M. 1993. Monthly mean climatic data for Antarctic automatic weather stations. *Antarctic Meteorology and Climatology: Studies based on Automatic weather stations, Antarctic Research Series, Vol. 61.*The American Geophysical Union, 2000 Florida Avenue, N. W., Washington, DC 20009.

Taljaard J. J. and van Loon H. 1964. Southern Hemisphere weather maps for the I.G.Y. *Bull. Am. Meteor. Soc.*, **45**, 88-95.

Taljaard J. J. 1967. Development, distribution and movement of cyclones and anticyclones in the Southern Hemisphere during the IGY. *J. Appl. Met.*, **6**, 973-987.

Targett P. S. 1998. Katabatic winds, hydraulic jumps and wind flow over the Vestfold Hills, East Antarctica. *Antarctic Science*, **10(4)**, 502-506

Teweles S. and Wobus H. B. 1954. Verification of prognostic charts. *Bull. Am. Met. Soc.*, **35**, 455-464.

Tiedtke M. 1989. A comprehensive mass flux scheme for cumulus parameterisation in large-scale models. *Mon. Weath. Rev.*, **117**, 1780-1800.

Toth Z and Kalnay E. 1997. Ensemble forecasting at NCEP and the breeding method. *Mon Wea. Rev.*, **125**, 3297-3319.

Turner J., Pendlebury S., Cowled L., Jacka K., Jones M. and Targett P. 2000. Report on the First International Symposium on Operational Weather Forecasting in Antarctica. *Bull. Am. Met. Soc.*, **81**, 75-94

Turner J., Lachlan-Cope T. A., Marshall G. J., Pendlebury S. and Adams N. 2001. An extreme wind event at Casey Station, Antarctica. *JGR-Atmosphere*, **106**, No. D7, 7291-7311.

van den Broeke M. R., van de Wal R. S. and Wild M. 1997. Representation of Antarctic Katabatic Winds in a High-Resolution GCM and a Note on Their Climate Sensitivity. *J. Clim.*, **10**, 3111-3130.

Vaughan D. G., Bamber J. L., Giovinetto M., Russell J. and Cooper A. P. R. 1999. Reassessment of net surface mass balance in Antarctica. *Journ. Climate*, **12**, 933-46.

Weller G. 1968. The Heat Budget and Heat Transfer Processes in Antarctic Plateau Ice and Sea Ice. Australian Antarctic Research Expedition (ANARE), *Scientific Report 4A*, **No 102**, Australian National Antarctic Research Expedition, Melbourne, 155p.

Weller G. 1980. Spatial and temporal variations in the South Polar surface energy balance. *Mon. Wea. Rev.*, **108**, 2006-14

Wilson J. C. 1992. Wind flow around Law Dome, East Antarctica. Minor MSc thesis. *Dept. Math., Monash Univ.*, Clayton, Victoria, Australia.

Wood N. and Mason, P. 1993. The pressure force induced by neutral, turbulent flow over hills. *Quart. Journ. Roy. Met. Soc.*, **119** 1233-1267.